AN EXPERIMENTAL INVESTIGATION INTO CLUSTER FORMATION TOWARDS MODELLING THERMAL CONDUCTIVITY OF NANOFLUIDS

A thesis submitted in partial fulfillment of the requirements for the award of the degree of

Doctor of Philosophy

Submitted by

Kundan Lal

Regn. No. 951008005

Under the supervision of

Dr. S. S. Mallick
Associate Professor, Mechanical Engineering Department

THAPAR INSTITUTE
OF ENGINEERING & TECHNOLOGY
(Deemed to be University)

Mechanical Engineering Department

Thapar Institute of Engineering & Technology, Patiala-147004

(Declared as Deemed-to-be University u/s of the UGC Act, 1956 Vide Notification No. F9-12-84-U.3 of G.O.I)

July 2018

CERTIFICATE

I, **Kundan Lal** hereby certify that the work presented in this thesis report entitled "**An Experimental Investigation into Cluster Formation towards Modelling Thermal Conductivity of Nanofluids**" in fulfillment of requirement for the award of degree of **DOCTOR OF PHILOSOPHY**, submitted in Mechanical Engineering Department, Thapar Institute of Engineering & Technology, Patiala is an authentic record of my research work carried out under the supervision of **Dr. S. S. Mallick** (Associate Professor, Mechanical Engineering Department, Thapar Institute of Engineering & Technology, Patiala) from January 2011 to July 2018. The results embodied in the thesis have not been submitted in part or full to any other University or Institute for the award of any degree or diploma.

(Kundan Lal)

Registration No.: 951008005 Date: 23rd July, 2018

It is certified that the above statement made by the student is correct to the best of my knowledge and belief.

(Dr. S. S. Mallick)

Associate Professor, Mechanical Engineering Department,

Thapar Institute of Engineering & Technology, Patiala, Punjab, India

Supervisor

ACKNOWLEDGEMENT

Paying thanks is the remembrance of God. Quantum of someone's help cannot be evaluated at the end of our achievement. At the time, when we need someone's help, one's little direction in the right way can lead to a great success. For me, submitting a doctoral thesis is a stepping-stone to start research with the cooperation of all the persons, I have interacted during my research.

From the bottom of my heart, I would like to express my sincere gratitude to my thesis supervisor Dr. S.S. Mallick, Associate Professor, Department of Mechanical Engineering, TIET, Patiala, for his invaluable guidance, enthusiasm, and insight in supervising the thesis. His keen observations and support have provided an incredible contribution to this thesis. Moral support, encouragement, useful criticism and constant invigilation extended by him in the hours of need cannot be accounted. The knowledge that I gained during his inspiring guidance would be valuable to me for all my future endeavors.

I am thankful to Dr. Prakash Gopalan, Director, Thapar Institute of Engineering & Technology Patiala, for his generous financial assistance and facilitation of my research work. I would like to take this opportunity to put on record my respect to Dr. T.P. Singh, Professor and Head Mechanical Engineering Department, TIET Patiala for his support and encouragement.

My sincere grateful thanks to Dr. S.K. Mohapatra, Sr. Professor and Dr. Ajay Batish, Professor, the former Heads, Mechanical Engineering Department, TIET Patiala, for their constant support and encouragement. A sincere thanks also to Dr. Gangacharyaullu, Professor, CHED, Dr. Tarun Nanda, Dr. Madhup Kumar Mittal, members of the doctoral committee for their technical as well as moral support during my research. I am also very thankful to Dr. Bonamali Pal, Professor, SCBC, for their constant support and encouragement and especially allowing me to use his laboratory as when needed to conduct my experiments. I am very thankful to all the faculty of mechanical engineering department especially Mr. Devender Kumar, Mr. Bikramjit Sharma, Mr. Kishore Khanna, Mr. Daljeet Singh for their continuous support in the department. Words are inadequate to say thanks for the invaluable technical support from Dr. Kulvir Singh (Professor, SPMS), Dr. B.N. Chudasama (Associate. Professor, SPMS), Dr. Vikas Sangal (Associate

Professor, CHED), Dr. Alok Garg (Assistant Professor, CHED), I owe my grateful thanks to my friends, especially Dr. Shakti Singh (Assistant Professor, EED), Dr. Bhupender Pal (Research Scholar SCBC, TU), Mr. Mukesh Aggarwal (SAI Lab), and many others who generously helped and encouraged me during my research work. I am also thankful to the technical and non-technical staff of the department who helped me during the course of my research work. I pay my thanks to Mr. Pardeep Singla, Ms. Promila, Mr. Sohan Lal, Mr. Sukhbir Singh, Mr. Charanjit Singh, Mr. Bipan Kumar and Harbhajan Singh for their kind hearted support. I am extremely grateful to the celebrated authors whose research work freely consulted and referred in my research work. I am also thankful to the Organizing Secretary of PGBSIA-1 (2003), TIET Patiala, for providing financial support in research work. I will never forget the support of my research colleagues, in the labs I have worked with. My sincere thanks to Dr. Bhupender Pal, and others (SCBC, TU), who has provided me with all kind of support, during my research. Group discussions to elaborate on the technical problems were always a source of my energy during my research work.

In the journey of research, sacrifice and support of family members have no compensation. I wish to express my indebtedness to my wife Mrs. Sunita Rana and my loving daughter and son Yashika Rana and Dhruvyansh Rana, who have been always a source of strength and whose affection and patience enabled me to complete this thesis. My thesis was made possible with the support of my brother Mr. Ashok Kumar.

Last but not least, my parents are always two strong pillars of my life. My father Mr. Kaur Chand Rana and my mother Mrs. Swarna Devi have always nurtured my life with values of humanity and to follow the ethics in research. They have always been a massive source of motivation and inspiration for me to focus on my research for the betterment of society.

Cooperation of every single person during research work is much more than saying formal words of gratitude. In true sense, taking the oath for willingness and courtesy to spread knowledge is the real acknowledgment to everyone, who have helped me directly or indirectly for the completion of this thesis.

(Kundan Lal) Date: 23rd July, 2018

ABSTRACT

The structural appearance and growth of nanoparticles in the form of nanoclusters have a considerable effect on the thermal conductivity enhancement of nanofluids. The growth of nanoclusters of Al_2O_3 and TiO_2 nanoparticles (size 25-30 nm) in water (DI) (along with suitable surfactants) has been investigated. A comprehensive study on the size distribution of the particles while in suspension at different pH values at their respective zeta potentials along with the stability ratio of suspensions have been carried out. Experiments were performed to observe the effect of various surfactants on stability, nanocluster formation and on the thermal conductivity of Al_2O_3-H_2O nanofluid, which was found to be getting improved significantly with SDS surfactant. The prolonged sonication was not adequate to break the clusters of Al_2O_3 nanoparticles into an average size of less than 163 nm, indicating the tendency of Al_2O_3 nanoparticles to remain in the form of clusters instead of individual nanoparticles of the initial size of 20 nm. The stability, thermal conductivity of Al_2O_3-H_2O nanofluid and also the average nanocluster size is found to reduce to less than 200 nm from 1,602, 1,827, 1,069, and 922 nm by using sodium dodecyl sulfate (NaDS) (SDS) as an affecting surfactant out of several other surfactants. A consistent enhancement in the thermal conductivity (i.e., 0.70 W/mK over a period of 3 hours) was observed. The Box Behnken Design (BBD) under Response Surface Mythology (RSM) has been used to model the thermal conductivity of Al_2O_3-H_2O nanofluid by taking volumetric concentration, temperature, and surfactant as the affecting parameters. The developed model is validated against the experimental data of thermal conductivity of Al_2O_3-H_2O nanofluid and with the other existing models. The results confirmed that the model could predict the experimental results with a high accuracy level ($R^2 = 0.98$). The model can be used to obtain various combinations of these parameters (volumetric concentration, surfactant amount, and temperature) to achieve a significant enhancement in the thermal conductivity of Al_2O_3-H_2O nanofluids. It is also emphasized that dispersion quality and stability are the key factors required to predict the thermal conductivity enhancement for a particular type of nanofluid accurately in addition to some other well-established affecting parameters. A quantitative analysis on the thermal conductivity enhancement of nanofluids, along with investigations on the role of nanoparticles present in the form of dead-ends and backbone chains in aggregates have been carried out. In suspensions, the concentration of nanoparticles changes with elapsed time depending on the morphological properties of the nanoclusters and the

nature of nanoparticles and base fluids. The experimental investigations carried out in this thesis represent a quantitative analysis of the effect of time, temperature, and instantaneous volume fractions on perikinetic heat conduction and Brownian motion induced micro-convection mechanisms. The investigations show that the zeta potential is proportional to stability ratio and inversely proportional to the hydrodynamic size of the nanoparticles while in suspension. The stabilities of various samples of nanofluids are found to be decreasing with increase in the size of nanoclusters and temperature (20 to 50°C). The aggregation time constant and stability ratio are found to be directly proportional. The effect of static and dynamic heat transport parameters on the overall thermal conductivity of Al_2O_3-H_2O and TiO_2-H_2O nanofluids have been investigated. The structural models and Brownian motion based convection models of thermal conductivity for the varying concentration of the nanoparticles in the respective suspensions have been developed to predict the thermal conductivity enhancements. In addition to the suspensions' stability parameters, these models also take into account the effect of nanocluster growth, temperature, thermal interfacial resistance and liquid layering in the nanoclusters. At the lower working temperature, i.e., from 20 to 30°C, the Brownian motion based induced convection effects are found to be negligible compared to the perikinetic conduction effects. The phenomenon was observed to be getting reversed with an increase in temperature i.e. from 30 to 50°C. Both the mechanisms were found to be responsible for the heat transport through the nanofluids, although their magnitudes vary depending on the nature, size, temperature, and properties of nanoclusters and base fluids. The effect of base fluid layering around the nanoparticles in an aggregate has also been highlighted to include the effect of liquid layering on the thermal conductivity of the water present in an aggregate compared to the bulk water present outside the nanocluster or an aggregate. The thermal conductivity measuring equipment becomes more prone to the convection effects above 50°C when water is the working medium. Thermal Property Analyzer gives fairly good results (till 50°C) of thermal conductivity measurements within accuracy and precision of ± 5%. In KD2 Pro, by maintaining the sensor needle in inverted position and angle within 5° (with vertical) while measuring the thermal conductivity, has been found to be a useful way to control its accuracy and precision within the limit. While developing models, more focus has been laid to the average hydrodynamic size of the nanoparticles while in suspensions rather than the individual particle size. The modified models give fairly a good prediction of the thermal conductivity enhancement for the nanofluids. The error involved in experimental and theoretical results of the

overall thermal conductivities varies from 8 to 13% for Al_2O_3-H_2O nanofluid and from 4 to 7% for TiO_2-H_2O nanofluid, in the temperature range from 20-50°C. Thus, in the study undertaken the error between the experimental and the theoretical values of the overall thermal conductivities is observed varies from 4-12% at temperature from 20-50 °C. While taking the measurements of the thermal conductivity of nanofluids, it is observed that thermal property analyzer (KD2 Pro) becomes more prone to the convection effects especially, when water is used as working medium beyond 50°C. It gives fairly good results (up to 50°C) of thermal conductivity measurements within accuracy and precision of ± 5%.

Keywords: Nanofluid, Perikinteic, Induced micro-convection, Brownian number, Thermal conductivity

TABLE OF CONTENTS

LIST OF PUBLICATIONS (SCI)

1. Lal Kundan, Soumya Suddha Mallick, 2018, Effect of time dependent morphological parameters of nanoclusters on perikinetic heat conduction and induced micro-convection mechanisms of oxide based nanofluids, *Experimental Heat Transfer (Taylor and Francis)*, Vol. 31(3), pp. 251-274. IF 1.687

2. Lal Kundan, Soumya Suddha Mallick & Bonamali Pal, 2017, An investigation into the effect of nanoclusters growth on perikinetic heat conduction mechanism in an oxide based nanofluid, *Powder Technology (Elsevier)*, Vol. 311, pp. 273-286. IF 3.230.

3. Lal Kundan, Soumya Suddha Mallick & Bonamali Pal, 2017, Effect of time dependent nanoclusters morphology on the thermal conductivity and heat transport mechanism of TiO_2 based nanofluid, *Heat and Mass Transfer (Springer)*, Vol. 53, pp. 1873-1892. IF 1.494.

4. Lal Kundan, Soumya Suddha Mallick & Bonamali Pal, 2017, Prediction and optimization of nanoclusters based thermal conductivity of nanofluids: Application of Box-Behnken Design (BBD), *Particulate Science and Technology (Taylor and Francis)*, Vol. 35 (3), pp. 265-276. IF 1.081.

5. Mishra A., Kundan L. & Mallick S.S., Modelling thermal conductivity for alumina-water nanofluid, *Particulate Science and Technology (Taylor and Francis)*, Vol. 32 (3), pp. 319-326. IF 1.081.

6. S.S. Mallick, A. Mishra & L. Kundan, 2013, An investigation into modelling thermal conductivity for alumina-water nanofluids, *Powder Technology (Elsevier)*, Vol. 233, pp. 234-244. IF 3.230.

ABBREVIATIONS AND SYMBOLS

Nomenclature

$\Delta k_{overall}$	Overall gain in the thermal conductivity of a nanofluid (W/mK)
Δk_{eff}	Thermal conductivity gain of a nanofluid for perikinetic heat conduction (W/m K)
Δk_{exp}	Experimental thermal conductivity (W/mK)
k_l	Thermal conductivity of the bulk base fluid (W/mK)
k_p	Thermal conductivity of nanopowder (W/mK)
k_f	Thermal conductivity of the fluid present inside the nanocluster (W/mK)
k_{f1}	Thermal conductivity enhancement of the fluid present inside the nanocluster characteristic dimension (W/mK)
k_{db}	Thermal conductivity enhancement inside a nanocluster due to dead-end nanoparticles (W/mK)
k_{adb}	Cluster thermal conductivity gain due to presence of nanoparticles as dead-ends and backbone chains (W/mK)
k_{eff}	Effective thermal conductivity of nanofluid (W/mK)
k_{nf}	Thermal conductivity of nanofluid (w/mK)
R_g	Cluster characteristic dimension (nm)
R_{eB}	Brownian Reynolds number
P_r	Prandtl number of nanofluid
P_{rp}	Prandtl number of nanoparticle
P_{rf}	Prandtl number of basefluid
R_e	Reynolds number of flow for single fluid
R_{ep}	Particle Reynolds number
R_{ef}	Reynolds number of base fluid (for local micro-convection)
k_m	Thermal conductivity due to Brownian motion induced convection (W/m K)
h	Convective heat transfer coefficient (W/m^2 K) and hour
c_p	Specific heat of liquid (J/kg K)
d_f	Fractal dimension of a nanocluster (dimensionless constant)
d_l	Chemical dimension of a nanocluster (dimensionless constant)

t_p	Aggregation time constant (s)
a	Average hydrodynamic size (diameter) of the particle (nm)
N	Average number of nanoparticles in a nanocluster
N_b	Number of nanoparticles in a nanocluster which belongs to backbone chains
W	Stability ratio
T	Temperature (º C)
E_R	Electrostatic repulsion (J)
E_A	Van der Waals attraction (J)
E_{tot}	Total interaction energy (J)
Wt.	Weight (mg)
C_f	Specific heat of base fluid (J/kg K)
C_p	Specific heat of base fluid (J/kg K)
K_B	Boltzmann constant (1.3807×10^{-23} J/K)
x	Particle surface to surface distance (nm)
pH	pH level of nanofluid
A_{132}	Hamaker's constant (J)
$B(x)$	Parameter representing the hydration interaction
V_a	Volume of a nanocluster (nm^3)
V_{na}	Volume of the nanoparticles per cluster (nm^3)
r_p	Average radius of a nanoparticle (nm)
p	Aspect ratio (dimensionless)
R_{BL}	Resistance due to thermal boundary layer (m^2 K/W)
F Val.	F distribution-a mathematical function
Prob >	P value-a mathematical function
R^2	Correlation coefficient
Adj.^{2}	Correlation coefficient
Pred.	Correlation coefficient
C_f	Specific heat of base fluid (J/kg K)
C_p	Specific heat of nanoparticle (J/kg K)
d_p	Nanoparticle diameter (nm)
R_e	Reynolds number of flow for single fluid

R_{ep}	Particle Reynolds number
R_{ef}	Base fluid Reynolds number (for local micro-convection)
P_r	Prandtl number for nanofluid
t	Elapsed time (h)

Abbreviations

DI	De-ionized water
DLS	Dynamic light scattering
XRD	X-rays diffraction
TEM	Transmission electronic microscope
SDB	Sodium dodecyl benzene sulphonate
M-G	Maxwell Garnet Model
DF	Degree of freedom
hcp	Hexagonal close packing
fcc	Face centered cubic
Prob	Probability
ANOVA	Analysis of variances
C.V.	Coefficient of variation
3D	Three dimensional
BBD	Box Behenkin design
RSM	Response surface methodology
Std.	Standard deviation
PRES	Prediction error of sum of squares
TEM	Transmission electronic microscope
DOE	Design of experiment
CTAB	Cetyltrimethyl ammonium bromide
SDS	Sodium dodecyl sulfate
PVP	Poly-vinyl pyrrolidone

Greek Symbols

φ, φ_p	Volume fraction of the primary nanoparticles in the base fluid (%)
Φ_{pc}	Volume fraction of the nanoparticles in an aggregate
φ_{bp}	Volume fraction of backbone particles in the aggregate
φ_{dp}	Volume fraction of the particles belonging to dead-ends
φ_{f1}	Volume fraction of fluid elements present in the aggregate
φ_{at}	Total Volume fraction of the aggregates present in the base fluid (%)
ε_r	Relative dielectric constant of the liquid
ε_0	Dielectric constant of free space ($8.854X10^{-12}$ $CV^{-1}M^{-1}$)
ζ	Zeta Potential (mV)
ρ_{nc}	Nanocluster density (g/cm^3)
ρ_f	Density of base fluid (g/cm^3)
ρ_{nf}	Density of nanofluid (g/cm^3)
μ	Viscosity of base fluid(Pas)
μ_{nf}	Viscosity of nanofluid (Pas)
α_{nf}	Thermal diffusivity (m^2/s)
α	Ratio of thermal conductivity of particle to that of base fluid
β	$(\alpha-1)/(\alpha+2)$
δ	Nanolayer (interfacial) thickness (nm)
ω	Weight fraction (%)

LIST OF FIGURES

LIST OF TABLES

Chapter 1

Introduction and Objectives

1.1 Introduction

The key challenge of today's fast growing technology of heat transport is to develop an efficient, high performance, economically viable, and environmentally friendly cooling systems. The conventional coolants, commonly used in many cooling applications suffer from their poor inherited thermal conductivity responses, and efforts to increase heat transportation by creating turbulence or by increasing the surface area, etc. have already been saturated (Das *et al.*, 2007). Therefore, there is a need to develop new alternatives for cooling and stable cooling mediums too, with their improved thermal characteristics especially with higher thermal conductivities. In the recent years, an innovative concept of 'Nanofluid' has been proposed as a potential solution to meet these key challenges (Das *et al.*, 2007). To achieve thermal transport by using colloidal suspensions have been of little interest in the scientific world until the advent of nanotechnology (Hunter, 2001). Nanofluid, an innovative class of heat transfer fluids, represents a rapidly emerging field where Nanoscience and Thermal Engineering coexist. This idea of nanofluid was firstly coined by Choi and Eastman (Choi and Eastman, 1995). Over the past few years, nanofluids have attracted significant interests because of their improved thermophysical properties over the conventional fluids (Buongiorno *et al.*, 2009; Palabiyik *et al.*, 2011). Various researchers working in the area of microfluidics and nanofluids have already emphasized on their much needed potential applications (Das *et al.*, 2007; Mitra and Chakarborty, 2011). The idea of using the suspension of solids in liquids was exercised more than a century ago when Maxwell (a pioneer in this area) presented a theoretical basis to calculate the effective thermal conductivity of suspensions (Maxwell, 1873). Later on, his efforts were conceived and followed with other theoretical and experimental studies (Hamilton and Crosser, 1962; Jeffery, 1973). However, these studies were limited to the suspensions of micro to mm-sized particles only and found to bear drawbacks, such as; rapid particles settling, forming a layer on the surface of the nanoparticle and reducing the heat transfer capacity of the fluid, erosion of the heat transfer devices and clogging of the flow channels (Das *et al.*, 2007). However, due to the potential features of nanofluids, notably higher thermal conductivity, the emergence of nanofluids has drawn the attentions of research community to stimulate and re-examine the option of cooling using solid-liquid mixtures (Das *et al.*, 2007). Researchers have also been found studying the numerical modeling of nanofluid flows in complex geometries which has its relevance to the many scientific and industrial

applications (Takabatake *et al.*, 2016). The detailed numerical modeling of these complex systems is essential for better understanding and optimizing the industrial designs (Sun and Sakai, 2016).

The thermophysical properties of nanofluids, such as thermal conductivity, viscosity, density, and specific heat play a prominent role as far as the development of energy efficient and effective heat transfer fluids are concerned. Primarily, due to the smaller size and higher surface area of nanoparticles, their suspensions are found to be more stable over prolonged time periods as compared to microparticles based suspensions. The higher specific surface area (SSA) of particles increases heat conduction capabilities of nanofluids as the heat exchange takes place predominantly through the surface of the particles (Das *et al.*, 2007). The nanophase materials are made of nanometer-sized substances. These materials are engineered on their atomic or molecular scale to produce solids with improved properties, such as mechanical, magnetic, optical, and electrical, etc. The nanoparticles used in nanofluids are generally oxide ceramics (Al_2O_3, CuO, and TiO_2), nitride ceramics (AIN, SiN), carbide ceramics (SiC, TiC), metals (Cu, Ag, and Au), semiconductors (TiO_2, SiC), and carbon nanotubes (CNT), composite materials ($Al_{70}Cu_{30}$) and polymer composites (Das *et al.*, 2007). The fluids, such as water, glycols, oils, etc. are being used worldwide as the host or base fluids in nanofluid (Hunter, 2001; Das *et al.*, 2007). There are two ways to produce stable suspensions of nanoparticles: single-step and two-step method. In both the cases, homogeneous and uniformly dispersed nanofluid suspensions are always desirable for practical applications. Preparing stable and well-dispersed nanofluid using Two-Step Method is a major challenge, as the individual particles quickly adhere to each other and form agglomerates before dispersing. The agglomerates have high tendency to settle down quickly and thus makes the suspension highly unstable (Prasher *et al.*, 2006). The surface modification and de-agglomeration via rapid expansion of high pressure or supercritical suspensions (REHPS) of nanoparticle aggregates are shown to be highly effective for their dispersion. In this technique, the size distribution of fragmented nano-powders is characterized by scanning mobility particle spectrometer (SMPS) and by offline scanning electron microscopy (SEM) (Ghoroi *et al.*, 2013). The surface modification of particles is also done to mitigate the disadvantages of agglomeration and poor flowability, followed by characterization using SEM, XRD and laser scattering (Han *et al.*, 2011). The light emitting diode (LED) filled with Al_2O_3 nanofluid was experimentally investigated for its high power thermal performance with the vapour chamber plate (Wang *et al.*, 2013). On the other hand, nanofluid preparation by using One-Step Method has its own

complications (Das *et al.*, 2007). The success to achieve a significant augmentation in the thermophysical properties of nanofluids lies in producing and suspending the nearly monodispersed and non-agglomerated nanoparticles in their respective base fluids.

The various research groups emphasize that the mechanism of enhancement of thermal conductivity of nanofluids is influenced by the following factors, such as (a) Brownian motion of the particles develops a micro-convection effect in fluids that increases energy transport; (b) cluster formation of particles within the nanofluid and heat percolates preferentially along such clusters; (c) base fluid molecules form a highly ordered layer of high thermal conductivity around the particles thus increasing the effective volumetric fraction of the particles (Chandrasekar and Suresh, 2009). Few other researchers have stressed upon the fact that clustering of nanoparticles will enhance the thermal conductivity only up to a certain level and this behavior of nanofluids is observed because of percolation effects in aggregates (Prasher *et al.*, 2006; Gao *et al.*, 2009; Özerinç and Yazıcıoğlu, 2010). However, this augmentation will decrease if clusters remain to continue to form bigger size aggregates, which ultimately results into sedimentation (Prasher *et al.*, 2006; Gao *et al.*, 2009). In a benchmark study on the thermal conductivity measurement of nanofluids, four different set of samples (alumina nano-rods in de-ionized water, gold nanoparticles in deionized water and stabilizer, silica monodispersed spherical nanoparticles and stabilizer in de-ionized water and Mn\Zn ferrite particles in a solution of stabilizer and water) were analyzed (Buongiorno *et al.*, 2009). It was observed that the data from most organizations lie within a relatively narrow band; the thermal conductivity of the nanofluids was found to be increasing with an increase in particle concentration and aspect ratio of nanoparticles. Ganguly and Chakraborty (2009) also emphasized that the physics of interparticle interaction mechanisms is essential to characterize the behavior features of a suspension (nanofluid). Clarke *et al.*, (1997) established the effective medium theory for colloidal suspensions and found that it was following the experimental data very closely. Furthermore, they also emphasized that nanoparticles' clustering phenomenon had played the main role in the enhancement of the thermal conductivity of such colloids (Clarke *et al.*, 1997). The effect of clustering has been further emphasized for alumina-based nanofluid, where the dry nanopowder size (obtained using TEM image) was 44-58 nm, while the in-situ size of particles present in nanofluid (measured using DLS technique) was 110 nm, thus indicating the cluster formation (Jie and Bo-Ming, 2006; Longo and Zilio, 2011; Longo *et al.*, 2012). It was also found that while the actual size of the nanopowders was 30±10

nm, the size present in nanofluid suspension was 165 nm even after 48 h of sonication (Longo and Zilio, 2011). This again indicates towards cluster formation and makes it quite evident that the actual size of nanoparticles while in suspension is more than their size in dry powdered form. This gives us the reason to shift our analysis on nanofluids from particle to cluster based and emphasizes that the cluster size should be included in modelling of thermal conductivity of nanofluids. The nominal or average diameter of the nanoparticles in their dry powdered state may not be a real or actual depiction of nanopowder size compared to that in suspension. However, the information on cluster size and their associated effects is generally missing from the literature. The clustering and structural arrangement of the suspended nanoparticles and time-dependent volume concentration of nanoparticles are the main factors affecting the thermodynamic properties and performance of nanofluids apart from the nanoparticle diameter, primary volume fraction, pH, temperature, etc. Therefore, a thorough investigation is required into the existing relevant classical/structural models for thermal conductivity with suitable amendments based on the nanocluster morphology and their associated effects. Different theories have been projected by various research groups to understand the thermal conductivity augmentation due to the Brownian motion of nanoparticles (Chon *et al.*, 2005; Xie *et al.*, 2005; Teng *et al.*, 2010). Similar investigations have been conducted to observe the effect of the presence of interfacial layers on the thermal conductivity (Keblinski *et al.*, 2002; Murshed *et al.*, 2006). However, there appears wide discrepancies among these different postulates in terms of agreement.

At present a variety of colloidal solutions with nanoparticles i.e. 'Nanofluids' with improved thermal properties (i.e. k, μ, C_p, ρ) are being produced and tested for their potential heat transfer applications such as micro-channel heat exchangers, high energy density engine cooling, heat pipes, oscillating heat pipe (OHP) (Chien *et al.*, 2003; Zhou, 2004; Ma *et al.*, 2006). Palm *et al.* (2006) showed experimentally an enhancement in the heat transfer capabilities of a radial flow impingement jet cooling systems by using nanofluids (Palm *et al.*, 2006). By using 1 to 4% volume fraction of Al_2O_3 nanoparticles, an average heat transfer coefficient was observed to be increased to double, whereas the wall shear stress was decreased to half. The use of CuO and Al_2O_3 based nanofluids in an automatic power transmission system lowers down the temperature distribution at both high and low rotating speeds and helps to achieve the better heat transfer effect (Tzeng *et al.*, 2005). Lin *et al.* (2011) prepared Al_2O_3 based nanofluids by using a surfactant as a dispersant and evaluated their suspension and heat transfer characteristics (Lin *et al.*, 2011). The ever-

growing demand to generate more electricity require the up-gradation of the transformers cooling systems, which can be achieved with nanofluids (Ramires *et al.*, 1995; Xuan and Li, 2000; Yu *et al*., 2007). Nanofluids find their prominent applications in pool boiling heat transfer and in tribological applications (Que *et al*., 1997; Li *et al.*, 2004). The experiments performed on lubricant based nanofluids (comprising of IrO_2 and ZrO_2 nanoparticles) showed that nanoparticles reduce the friction on the surface of 100 C6 steel remarkably. At the beginning of the advent of nanofluids, the use of nanofluids was thought of primarily for thermal management applications. However, nanofluids are also being developed for medical applications, such as cancer therapy and drug delivery (Jordan *et al.*, 1999). Nanofluids such as ferrofluids find their promising potential for heat transfer applications in the biomedical field, which can help to destroy cancer cells by heating a Ferrofluid-impregnated malignant tissue and thereby causing a minimal damage to the surrounding healthy tissues (Ganguly *et al.*, 2004). The relationship between an imposed magnetic field of Ferrofluid and the temperature distribution helps in designing and implementation of applications (Kappiyoor *et al.*, 2010).

In spite of the potential benefits of nanofluids, the nanofluid technology and its applications are still limited for commercial use as there are no well-established, precise and accurate standardized techniques available, which can predict the heat transport capabilities of nanofluids. The difficulties lie in understanding the behavior of thermophysical properties of nanofluids, mechanism of heat transport through nanofluids and in developing efficient heat transfer models, which might predict their performance with higher accuracy. Thus, in order to bring more understanding and clarity about the functioning of nanofluids, investigation into its thermophysical is required, especially on the thermal conductivity of nanofluids. Over the years, various researchers have been trying to model the thermal conductivity of solid-liquid mixtures and nanofluids by using certain existing models. However, most of the time researchers have been evaluating the different models mainly on their own produced data, but not for a broad range of other experimental conditions. Thus, the accuracy of these models is not a certainty and they cannot be reliably applied to commercial and industrial systems with confidence as yet. The measurement techniques used for the thermal conductivity of nanofluids are highly sensitive to surrounding environment/laboratory conditions (Zhang, 2010). It has also been observed that the measured values obtained for thermal conductivity beyond 50^oC temperature using a commercially available thermal property tester are very much prone to inaccuracy and instability. It has also been

experienced during the experimentations that the errors are likely to arise even with the slightest of air flow, temperature variation, inclination and position of the sensor needle, vibration of the floor, etc. Such a susceptible measurement procedure may provide data that is less likely to be reproduced or repeated. Moreover, there is no standardized configuration suggested in the literature which could enhance the accuracy and precision of the instruments. Therefore, standardizing the thermal conductivity measuring procedure using thermal property tester is also of prime importance. In view of above-presented facts, following thesis objectives have been drafted, as given below:

1.2 Objectives

The following are the objectives:

(1) To investigate experimentally the effects of size distribution and volume fraction of nanoparticle in base fluid, temperature, sonication parameters, surfactants and pH on cluster formation in Al_2O_3 and TiO_2 based nanofluids within 5% volumetric condition as upper limit, range of pH being 2 to 12, sonication and settling times are limited to the maximum of 3 and 240 hours, respectively, temperature range of 50 to 60°C and using surfactants, such as; Cetyl trimethyl ammonium bromide (CTAB), Sodium dodecyl sulfate (SDS), Poly-vinyl pyrolidone (PVP), Triton X100 and Oleic acid.

(2) To model the thermal conductivity of nanofluid by taking into account the clustering phenomenon.

(3) To predict the thermal conductivity enhancement of nanofluid using design and analysis of experiments.

(4) To evaluate the different measuring configurations used for the thermal conductivity measurement of nanofluids and accuracy and reproducibility.

Although, there are various types of materials which can be used to prepare nanofluids, such as oxide ceramics (Al_2O_3, CuO), carbide ceramics (SiC, TiC), metals (Cu, Ag, Au), semiconductors (TiO2, SiC) and carbon nanotubes etc. However, it was decided to work with Al_2O_3, and TiO_2 nanoparticles in the present thesis keeping in view the following:

(i) The quantity and cost to prepare nanofluid would be significantly high if it is to be used in high energy density flux heat exchangers. Therefore, the choice of oxide based nanoparticles would help to minimize the preparation cost of nanofluids.

(ii) The oxide based nanoparticles are lighter compared to metal nanoparticles (e.g. density of TiO_2 is 4.07 g/cm^3 and density of Ti is 4.57 g/cm^3). As a result of this, the suspension containing oxide based nanoparticles are likely to be stable over a longer period of time. This also provide the ease of preparation of nanofluids using Two Step method.

The potential application of such nanofluids (Al_2O_3 and TiO_2 based) are is in large thermal systems, such as; radiators, solar systems, heat exchangers used to transfer nuclear energy, refrigeration systems, cooling jet etc. (Wen and Ding, 2004; Kim *et al.*, 2005; Tzeng et al., 2005; Palm *et al*., 2006; Das *et al.*, 2007; Bi *et al.*, 2011).

.

Chapter 2

Literature Review

Researchers have been engaged worldwide to investigate into the thermos-physical behaviour of the nanofluids and their potential to perform in a variety of applications. The work titled, "*An Experimental Investigation into Cluster Formation towards Modelling Thermal Conductivity of Nanofluids*" has been undertaken to report a deeper understanding of the thermal conductivity of nanofluids and heat transport mechanisms, such as heat transport through nanoclusters, perikinetic conduction and through the induced micro-convection. A detailed discussion of literature has been given in this section which has helped to build up the foundation to carry out the necessary investigations.

2.1 Parameters Affecting the Thermal Conductivity of Nanofluids

There are many parameters which influence the thermal conductivity of nanofluids, such as the size and shape of nanoparticles, the concentration of nanoparticles, temperature, thermophysical properties of nanoparticles and base fluids, morphological characteristics of particles, particle motions, nature and time of sonication, pH and additives (Das *et al.*, 2007). In the subsequent sections, these parameters and their effect on the enhancement of thermal conductivity of nanofluids have been discussed in detail. The experimental results published before the year 2005 indicate an anomalous enhancement of the thermal conductivities of various nanofluids, assuming well-dispersed suspensions of nanoparticles. However, more recent efforts with refined transient hot wire and optical methods have spawned a controversy on whether the anomalous enhancement beyond the mean field theory is real or not. To provide some physical insight into these facts, a benchmark experimental data sets of thermal conductivities obtained in 2010 and before 2010 were reviewed by Kleinstreuer and Feng (2011). However, some fundamental questions remain unanswered, such as the best nanoparticle and liquid pairing and reliable measurements of thermal conductivity and the ease to use. It has been found that the interactive mechanisms, such as the Brownian motion of nanoparticles, induced micro-convection, conduction, clustering, etc. are mainly responsible for the heat transfer in nanofluids. Brownian motion-induced micro-mixing has been arguably the most important one (Shukla and Dhir, 2008; Malvandi and Ganji, 2014). Out of the various thermophysical properties of nanofluids, the thermal conductivity is a very prominent parameter which affects the performance of nanofluids. It was also shown that thermal

conductivity of nanofluids increases with an increase in nanofluid bulk temperature (Kumar *et al.*, 2004; Mukherjee *et al.*, 2016). A benchmark study, namely "*International Nanofluid Property Benchmark Exercise (INPBE)"* was conducted where the thermal conductivity of identical samples of colloidally stable dispersions of nanoparticles was measured by over 30 organizations worldwide. The various experimental approaches including transient hot wire method, steady-state method and optical method were used to collect the data on thermal conductivities (Buongiorno *et al.*, 2009). The nanofluids were comprised of aqueous and non-aqueous base fluids, metal and metal oxide particles, near-spherical and elongated particles and with low and high particle concentrations. The main objective was to compare the thermal conductivity data obtained by different organizations for the same samples of nanofluids. This study showed that the choice of measurement technique could affect the measured value of thermal conductivity within ± 5% in temperature range from 20-30°C. Therefore, to ensure an accurate determination of the thermal conductivity enhancement, it is important to measure both the base fluid and nanofluid's thermal conductivities at the same temperature using the same technique.

2.1.1 Morphology

Morphology is defined as the study of shape, size, texture, and phase distribution of a physical material. The investigations show that the thermal conductivity enhancement in nanofluids is an active function of the shape, size, and arrangement of particles (Chon *et al.*, 2005; Chopkar *et al.*, 2006). Minsta *et al.* (2009) conducted the experiments with different sizes of Al_2O_3 nanoparticles (36 and 47 nm) and found that nanofluids with smaller nanoparticles are showing a higher enhancement in the thermal conductivity (Mintsa *et al.*, 2009). Xie *et al.* (2002) performed investigations to study the effect of the shape of the nanoparticles, i.e., spherical and cylindrical (SiC) on the thermal conductivity enhancement of nanofluids (Xie *et al.*, 2002). Murshed *et al.* (2005) investigated the effect of particle shape on the thermal conductivity of nanofluids by considering the spherical (15 and 10 nm) and rod-shaped (40 nm) nanoparticles of TiO_2. Finally, it was reported that the nanofluid with rod-shaped nanoparticles possess higher thermal conductivity (Murshed *et al.*, 2005). Results were also reported on the thermal conductivity enhancement for Cu nanoparticles (size 50 nm, shape: needle and square) dispersed in water (Liu *et al.*, 2006). Xie *et al.* (2002) showed that the increase in the specific surface area (SSA) of nanoparticles leads to an enhancement in the thermal conductivity (Xie *et al.*, 2002). Choi and

Eastman (1995) investigated Al_2O_3 (size: 28 nm) and CuO (size: 23 nm) dispersing in water, vacuum pump fluid, engine oil, and ethylene glycol. They observed that the thermal conductivity of nanoparticle-fluid mixtures increases with a decrease in the particle size, but the increase also depends on the dispersion technique (Choi and Eastman, 1995). Yoo *et al.* (2007) investigated TiO_2, Al_2O_3, Fe, and WO_3 (25 nm, 48 nm, 10 nm, and 38 nm,) based nanofluids where, a cell disrupter was used for improving the dispersion quality of nanoparticles. This was also followed by the thermal conductivity measurements using a transient hot wire method (Yoo *et al*., 2007). The thermal conductivity got increased by 4% when 1.0% volume fraction of Al_2O_3 nanoparticles was used, whereas, TiO_2 based nanofluid containing 1.0% volume fraction of nanoparticles exhibited a 14.4% enhancement in the thermal conductivity for the same base fluid. Timofeeva *et al.* (2007) reported that nanofluids with elongated and dendritic structures of nanoparticles are more efficient in enhancing the thermal conductivity than the compact spherical structures of the nanoparticles of same volume fractions. The nanoparticles used in this work were Al_2O_3 with a nominal diameter of 11, 20, and 40 nm and the volume fraction was varied between 3.6 and 13% (Timofeeva *et al.*, 2007). It was shown that the geometry, agglomeration state and their interconnectivity, surface resistance of nanoparticles are the primary variables which control the thermal conductivity enhancement of nanofluids. The results also emphasized that the nanoparticle motion did not make any considerable contribution to thermal transport as compared to the diffusion of heat through static composites of nanoparticles and fluid.

2.1.2 Nanomaterial and concentration of nanoparticles

There are various physical and chemical processes available to produce variety of nanoparticles (Kimoto *et al.*, 1963; Gleiter, 1989). The physical processes typically involve the phenomenon of inert gas condensation and mechanical grinding (Granqvist and Buhrman, 1976). On the other hand, the chemical methods include the chemical vapour deposition, microemulsion, chemical precipitation, spray pyrolysis, and thermal spray. A similar process was exercised to develop the iron nanoparticles based suspensions by using an oleic acid as a stabilizer (Suslick *et al*., 1996). The ball milling technique has been also employed successfully to produce the alloyed nanoparticles of $Al_{70}Cu_{30}$ (Chopkar *et al*., 2006). In the ball milling process, the balls impart lots of mechanical energy into the slurry based powders whose nanoparticle are to be produced. During this process, chemicals are also used to bring out the required physical and chemical changes in

the nanomaterials under process. Hence, by using these techniques, nanosized nanoparticles are produced, which are generally in the powdered form. Various researchers have performed the experiments with a variety of nanofluids and showed that a nonlinear relationship exists between nanofluid concentration and thermal conductivity enhancement (Choi and Eastman, 2001). The same is also supported by the Hong *et al.* (2005) for Fe-ethylene glycol nanofluids (Hong *et al*., 2005). Nowadays, it has been well established through the different models/experiments that the volume concentration of nanoparticles and thermal conductivity enhancement has a nonlinear, but a direct relationship. Yu *et al.* (2009) also studied and modelled the results of the thermal conductivity augmentation by taking into account the volume concentration of nanoparticles of ZnO in ethylene glycol (Yu *et al.,* 2009). Wie *et al.* (2009) studied the effect of molar concentration on the thermal conductivity of nanofluid (Wei *et al.,* 2009). Duangthongsuk and Wongwises (2009) were other researchers who also studied the effect of nanoparticle volume fractions on nanofluids' thermal conductivity. They observed an enhancement in the thermal conductivity up to 9.5% for TiO_2 nanoparticles in a base fluid with different volume fractions of nanoparticles ranging from 0.2% to 2% at a temperature of 25^{o}C (Duangthongsuk and Wongwises, 2009). Furthermore, they also compared their experimental results with H-C model (Hamilton and Crosser, 1962), Bruggeman model (Bruggeman, 1935), Wasp model (Wasp, 1977), Yu and Choi model (Yu *et al.,* 2003) and observed that the test results are following the model predictions with the accuracy of 8 to 10%.

2.1.3. Temperature

Literature survey on the thermal conductivity enhancements of nanofluids reveals its strong dependence on working temperature. Das *et al.* (2003) reported their investigations on water-based nanofluids containing nanoparticles of CuO and Al_2O_3 in the range of 20 to 50^{o}C. They debated on the effect of temperature and random motion of particles on the thermal conductivity of nanofluids. At higher temperature, the nanoparticles have the tendency to exhibit higher Brownian motion, which leads to the thermal conductivity enhancements of nanofluids (Das *et al.*, 2003). The thermal conductivity measurements were recorded by an instrument working on the basis of temperature oscillation method and a 2 to 4 fold increase was observed in the thermal conductivity of nanofluid over a temperature range of 21°C to 51°C. Ding *et al.* (2006) studied the CNT-water based nanofluids and reported an increase in the thermal conductivity of nanofluid with the rise in

temperature (Ding *et al.*, 2006). Furthermore, it has also been observed that temperature and thermal conductivity have a direct relationship, i.e., when temperature increases, the thermal conductivity of nanofluid also rises. Yu *et al.* (2011) have also confirmed the same facts after carrying out investigation with aluminum nitride nanofluid (Yu *et al.*, 2011).

2.1.4 Thermal conductivity of base materials (nanoparticles)

The thermal conductivity of nanoparticles also influences the thermal conductivity of nanofluids. In general, higher the thermal conductivity of nanoparticles, larger is the thermal conductivity enhancement for the same base fluids (Li and Peterson, 2006). Li and Peterson (2006) tested two water-based nanofluids in which CuO and Al_2O_3 were suspended with almost the same dispersion quality. They found that the nanofluid with CuO solid nanoparticles was showing a higher thermal conductivity than that with Al_2O_3 nanoparticles. The experiments were conducted under the same conditions for both the nanofluid samples and by using the same volume fraction of nanoparticles (Li and Peterson, 2006). Chopkar *et al.* (2008) also carried out investigations about the effect of nanoparticle materials on the thermal conductivity of nanofluids (Al_2Cu and Ag_2Al, suspended in water and ethylene glycol mixture). As the thermal conductivity of Ag_2Al is more than Al_2Cu, therefore nanofluids containing these also responded accordingly for the thermal conductivity enhancements (Chopkar *et al.*, 2008).

2.1.5 Thermal conductivity and viscosity of base fluid

The motion of particles especially, Brownian motion too has a deeper effect on the thermal conductivity of nanofluids. Apart from many other factors, such as; temperature and size of the particle, the Brownian motion of nanoparticles is too influenced by the viscosity of base fluid (Malvandi and Ganji, 2014). The electric double layer around nanoparticles could be considered as one important parameter affecting the thermal conductivity of nanofluids (Lee, 2007). Wang *et al.* (1999), tested several nanofluids containing Al_2O_3 and CuO as nanoparticles in water, vacuum pump fluid and engine oil as base fluids. The maximum enhancement of 12.23% in thermal conductivity is achieved by a combination of Al_2O_3 and ethylene glycol (Wang *et al.*, 1999). Xie *et al.* (2002) also inspected the effect of various base fluids such as water, glycerols, oils and

mixture of ethylene glycol and water with different volume fractions on the thermal conductivity of nanofluids (Xie *et al.*, 2002).

2.1.6 The pH Level of nanofluids

There are various reports, which relate to the investigations about the impact of pH of base fluids on the thermal conductivity (Fovet *et al.*, 2001; Wang and Li, 2009; Wang *et al*., 2009; Goudarzi *et al.,* 2015). Xie *et al.* (2002) made the investigations about Al_2O_3-H_2O nanofluid and observed that the increase in pH value decreases the thermal conductivity of nanofluid (Xie *et al.*, 2002). Furthermore, they also reported that thermal conductivity of Al_2O_3-H_2O nanofluid varies from 23% to 19% when pH changes from 2 to 11.5. Lee *et al.* (2006) also investigated and advocated for the strong dependency of nanofluids' thermal conductivity on its pH value (Lee *et al.*, 2006). Wang *et al.* (2009) too investigated the thermal conductivity of nanofluids under varying pH and attained a maximum gain in the thermal conductivity at optimized pH values (Wang *et al*., 2009). As per their observations, pH around 8 for Al_2O_3-H_2O water and about 9.5 for Cu-H_2O water led to maximum improvements in the thermal conductivity. Murshed *et al.* (2008) reported the thermal conductivity of TiO_2-H_2O nanofluid and found the same to be decreasing with an increase in pH value (Murshed *et al.*, 2008). They tested TiO_2-H_2O nanofluid for their improvements in the thermal conductivity and achieved a reduction of only 2% in the thermal conductivity when pH was changed from 3.4 to 9. The dispersion behavior of two particular water-based nanofluids, namely Al_2O_3-water and water-Cu mixtures were investigated by measuring the absorbency and zeta potential of the nanofluids under different pH values (Huang *et al.*, 2009). The results showed that the stability of nanofluids is highly dependent on the pH values and an optimal pH value results into a higher stability of nanofluids. The greater the zeta potential and absorbency, higher is the particle concentration in the suspension, and hence the more stable the suspension is (Huang *et al.*, 2009). Beck *et al.* (2009), tested nanofluids by dispersing pre-weighed quantities of alumina nanoparticles (8-282 nm) into either de-ionized water or ethylene glycol. The samples were subjected to an ultrasonic processing to obtain uniform dispersions. The isoelectric point of alumina was found to be lying between the pH of 7 and 9 and the acidic pH of nanofluid was adjusted to a value of 4 by adding HCl, just to ensure the electrostatic stabilization of the suspension (Beck *et al.,* 2009). The observations were used to develop a simple relationship for

the thermal conductivity of alumina nanofluids in both water and ethylene glycol (Beck *et al.*, 2009).

2.1.8 Additives/surfactants

The role of additives/ surfactants is to keep the nanoparticles in suspension and to prevent them from agglomeration and settling. Thus, with aid to improve the suspension stability they are also expected to cause the thermal conductivity enhancement of nanofluids. The method of preparation of nanofluids can significantly affect the formation and stability of nanosuspensions and hence their overall performance. Poorly dispersed nanosuspensions can be managed successfully by employing a variety of techniques such as (i) solubilisation in surfactant solutions, (ii) use of antisolvents, (iii) through adjusting pH, (iv) emulsions, and (v) solid dispersions (Filippos *et al.*, 2007). The techniques used to produce nanoparticles can be categorized as top-down methods (such as homogenization and milling) or bottom-up methods (such as spontaneous emulsification or anti-solvent precipitation) (Iris *et al*., 2013). Anti-solvent precipitation is an attractive technology as there is no need for specialized equipment and complex operating conditions. The associated costs are reasonably low, the technique can easily be scaled up and the risk of sample contamination is often significantly less compared to the using of top-down technologies. Anti-solvent processes are already widely used in industry to produce nanoparticles for pharmaceutical purposes (Iris *et al*., 2013). Despite extensive research on nanosuspensions technology, stability remains a limitation for industrial applications of nanosuspensions. Furthermore, the empirical relationship between stabilizer efficacy and nanosuspensions stability has not been well characterized (Wang *et al.*, 2013). On the other hand, cavitation fields developed due to ultra sonication assist in generating nanoparticles in several ways such as (i) creating turbulent flow conditions inside the system ensuring efficient mixing (ii) atomization of organic solutions of the drug, during addition into the aqueous stabilizer solution and precipitation of fine particles and (iii) particle size reduction of the newly formed bigger particles (Verma *et al.*, 2009). Anti-solvent precipitation allows the production of very fine particles with an improved control over particle properties, such as size, morphology and physical state. The investigation on the influence of the supercritical CO_2 processing on the particle size and morphology of puerarin crystals shows that decreasing the antisolvent addition rate, increasing the temperature and the addition volume below 50 ml lead to a decrease in size of the particles (Li *et al.*, 2016). In another study, organic

itraconazole (ITZ) solutions were mixed with aqueous solutions to precipitate sub-300 nm particles over a wide range of energy dissipation rates. The highest nucleation rates and slowest growth rates were found with the stabilizer poloxamer 407 at temperatures below 20°C (Matteucci *et al.*, 2006). Eastman *et al.* (2001), performed some experiments on Cu nanoparticles dispersed in ethylene glycol with and without additives (thioglycolic acid) and concluded that the presence of an additive could strongly affect the thermal conductivity of nanofluid (Eastman *et al.*, 2001). The effect of different types of additives on MWCNT dispersed in water has also been investigated by Assael *et al.* (2005). There are various types of surfactants which can be used to prepare nanofluids, such as; Cetyltrimethyl ammonium bromide (CTAB), Sodium dodecyl sulfate (SDS), Sodium dodecyl benzene sulfonate (SDBS), Poly-vinyl pyrrolidone (PVP), Triton X100 and Oleic acid (Das *et al.*, 2007). Thus, it can be concluded that antisolvents/additives/surfactants could play an important role to improve the thermal conductivity of nanofluids, through ensuring the suspension stability.

2.1.9 Sonication techniques

The preparation of a uniformly dispersed nanofluid is essential for obtaining the stable physical properties or superior characteristics of nanofluids (Das *et al.*, 2007; Zhu *et al.*, 2009; Nasiri *et al.*, 2011; Saterlie *et al.*, 2012; Kundan *et al.*, 2016). Many experimental studies on nanofluid systems have been performed; however, the preparation methods to form stable nanofluids have not been systematically studied as yet (Hwang *et al.*, 2008). Pastoriza-Gallego *et al.* (2009) investigated the dispersion and stability of nanofluid containing Al_2O_3 nanoparticles in water (Pastoriza-Gallego *et al.*, 2009). Li *et al.* (2006) conducted an experimental investigation to examine the effect of variations in the temperature and volume fraction on the steady-state effective thermal conductivity of two different nanoparticle suspensions (Li and Peterson, 2006). The blending of nanoparticles with base fluid was done by immersing the suspension in an ultrasonic bath for 3 hours to breakup any residual agglomerations and ensured that the suspensions were well-dispersed. The suspensions were examined and found to be stable with substantially no sedimentation or stratification over a period of several days. However, practically it has been observed that the suspension quality of nanofluid changes continuously and to achieve a suspension stability of nanofluids over a long time period is a big challenge. Therefore, it is decided to study the formation of nanoclusters and the parameters affecting clustering in nanofluids over a

couple of days only i.e. up to 10 days. The Al_2O_3 and CuO, nanoparticles with area weighted diameters of 36 nm and 29 nm respectively, were blended with distilled water at 2, 4, 6, and 10% of their volume fractions and the resulting suspensions were evaluated at temperatures ranging from 27.5 to 34.7 °C. It was found that the nanoparticle material, diameter, volume fraction, and bulk temperature, all have a significant impact on the effective thermal conductivity of these suspensions (Li and Peterson, 2006). Another study was presented on the dispersion and stability of the nanoparticles in nanofluids where, various physical treatment techniques, including a stirrer (revolution speed: 1500 rpm, revolution time: 120 min), an ultrasonic bath (sonication time: 60 min, frequency: 40 kHz), an ultrasonic disruptor (sonication time: 60 min, frequency: 20 kHz, power: 350 W), a high-pressure homogenizer (number of pass: 3, pressure: 18,000 psi), and a modified magnetron sputtering system (DC power: 0.2 kV, Ar gas mass flow rate: 25 cm^3/min) were used to prepare nanofluids followed by their effect on suspension stability of nanofluids (Hwang *et al.*, 2008). The high-pressure homogenizer was found to be the most effective method to de-agglomerate the nanoparticles in the suspensions. It was believed that the highly agglomerated nanoparticles were able to be quickly and easily broken up by the combination of strong shear force and cavitation generated by the high-pressure homogenizer (Jang *et al.*, 2007).

2.2 Mechanisms of Heat Transport in Nanofluids

In spite of extensive research on the behavior of nanofluids and anomalous increases in the thermal conductivity of particle-fluid suspensions, the fundamental understanding of the mechanisms which create exciting and promising properties is limited and still evolving. The lack of knowledge put the limit on the applicability of nanofluids and ability to model them accurately (Okhio *et al.*, 2010). Their investigation on systematic surveys of experimental and modelling reviews revealed that the most of the models are phenomenological in nature, and addressed the problems partially. They also emphasized on the fact that the effectiveness of nanofluid depends not only on the enhanced thermal conductivity but also on other properties such as; viscosity, density, and specific heat. The benchmark studies conducted by various researchers show that the mechanisms of thermal conductivity enhancement of nanofluids is influenced by the many factors, such as; (i) Brownian motion of the particles which develops a micro-convection effect in fluids and hence increase the energy transport (Prasher *et al.*, 2006) (ii) cluster formation of particles within the

nanofluid and heat percolation through such clusters (Evans *et al.*, 2008), and (iii) base fluid molecules forming a well-ordered layer of comparatively higher thermal conductivity around the particles, (Keblinski *et al.*, 2002; Prasher *et al.*, 2006).

Brownian motion

There are many evidences which emphasize that Brownian motion (BM) as one of the possible origin responsible for thermal conductivity enhancement of nanofluids. This enables direct particle-particle transport of heat from one to another, and induces the surrounding fluid flow, called induced micro-convection (Keblinski *et al.*, 2002; Prasher *et al*., 2006; Evans *et al.*, 2008). It is assumed that in nanofluids, the additional energy transport is because of motion of the number of particles induced by the action of different forces such as; van der Waals forces, the electrostatic forces, the stochastic forces that give rise to the Brownian movement to the particles and the hydrodynamic forces. Jang and Choi (2007) proposed that Brownian movement (BM) based induced nano-convection is a nanoscale mechanism of thermal energy transport which possibly determine the thermal performance of nanofluids (Jang and Choi, 2007). The Brownian motion is also found to be associated with other effects, such as, the collision of base fluid molecules with each other, energy exchange among nanoparticles with each other, and also the energy exchange among the base fluid molecules and nanoparticles because of thermally induced fluctuations (Jang and Choi, 2007). They concluded that convection instigated by the Brownian or stochastic motion of nanoparticles is the primary mechanism that gives rise to the thermal conductivity enhancements. It was also debated that at low temperatures, the Brownian motion is not very significant however, as the temperature increases, it results into more convection effects. The investigations indicate that it is possible to have a threshold temperature corresponding to the nanoparticle/nanocluster size at which the effective thermal conductivity enhancement through Brownian motion of the particles start dominating (Das *et al.*, 2003). The microstructure investigation of nanofluids by rheological techniques showed that the particles do not exist as individual particles and nanofluids of rod-like alumina nanoparticles (Al_2O_3) (50 nm × 10 nm) have a solution of weakly flocculated gel-structure depending upon the particle concentration (up to 3%) (Kim *et al.*, 2011). The thermal conductivity increases at a faster rate in the solution state than in the weakly flocculated gel state where Brownian motion was found to be playing a fundamental role in enhancing the thermal conductivity (Kim *et al.*, 2011). On the other hand,

there are also some contrary opinions, which goes to doubt that the thermal conductivity enhancement of nanofluids is due to the Brownian motion. They are of the view that thermal conductivity variations track the temperature behaviour of base fluids (Kwek, *et al.*, 2010). Evans *et al.* (2006) investigated the effect of the Brownian motion (BM) on the thermal conductivity of stationary nanofluids and reported that that the ratio of Brownian motion to base fluid thermal conductivities is directly proportional to the ratio of nanoparticles diffusivity to the thermal diffusivity of a concerned fluid (Evans *et al.*, 2006). Nie *et al.* (2008) claimed that enhancement in nanofluids' thermal conductivity because of Brownian motion is approximately equal to T/μ, however, this augmentation is minimal and of the order of 10^{-15} W/m K and hence can be neglected (Nie *et al.*, 2008). Similarly, there are other researchers who also expressed their reservations about the improvements in the thermal conductivity because of Brownian motion (Das *et al.*, 2003; Kumar *et al.*, 2004; Keblinski *et al.*, 2005; Chandrasekar and Suresh, 2009; Mostafizur *et al.*, 2015).

Ordered liquid layer (Nanolayer)

The liquid molecules close to the particles form an ordered layer of the solid-like structure, known as a nanolayer. The orientation of the liquid molecules at the solid-liquid interface is well-organized than that of the majority of remaining bulk fluid, called as a nanolayer. This nanolayer performs as a thermal link between nanoparticles and bulk liquid and as a result of this thermal conductivity of nanofluids increases (Keblinski *et al.*, 2002). The interfacial resistance present at the interface is known as Kapitza resistance and due to better solid-liquid interface contact, this Kapitza resistance may not be a prevailing factor affecting the heat transfer. Also, the calculation for the Kapitza resistance per unit area revealed that it is only of the order of 10^{-7} (Jang and Choi, 2007). Hence, it seems not very reasonable to assume that the nanolayer of this order can offer any considerable hindrance to heat transfer. Xie *et al.*(2005) concluded that thermal conductivity follows a linear distribution through the nanolayer. This distribution was assumed to have the thermal conductivity equal to the thermal conductivity of base fluid at one side and on the other side equivalent to nanoparticle thermal conductivity. Researchers also believed that nanofluid is a very complex system where, the overall thermal conductivity may be determined through the thermal conductivities of particles and host fluid (Xue and Xu, 2005). Yu *et al.* (2003) made some modifications to the model given by Maxwell and Hamilton-Crosser (H-C) for suspensions

containing spherical and non-spherical nanoparticles. It was also hypothesized that the presence of nanolayers could increase the volume concentration of nanoparticles (Yu *et al.*, 2003). Murshed *et al.* (2006) suggested another model by assuming the discontinuities among the temperature gradients at the interfacial boundaries. By considering the thickness of the interfacial layer equal to 1 nm and its thermal conductivity equal to two to three times as that of base fluid, thermal conductivity predictions were agreeing well with the experimentally reported results. On the other hand, Evans *et al.*(2008) argued that there will be no increase in the thermal conductivity of nanofluids when the particle radius and Kapitza radius are equal. Nanolayer thickness role becomes necessary for heat transport in nanofluids only at higher volume concentrations (Chandrasekar *et al.*, 2010). Hwang *et al.* (2008) presented an equation for the thickness and thermal conductivity of nanolayer by proposing a formation of an electrical double layer around the nanoparticle surface (Hwang *et al.*, 2008). The increased temperature makes nanolayer thicker and wide which thereby increases the apparent volume concentration. Tillman and Hill (2007) introduced three different and distinct forms for thermal conductivity profiles within a nanolayer to determine its thermal conductivity, where it was concluded that the nanolayer thickness is almost equal to 19% to 22% of the nanoparticle radius (Tillman and Hill, 2007). Thus, both the experimental and theoretical studies have reported the existence of an ordered liquid layer near the solid surface. As a result of this, the molecular structures of liquid layers are significantly more ordered and well defined than that of the bulk liquid. As of now, sufficient research has not been conducted on the formation of these ordered liquid layers and their associated effects. A detailed examination of the properties of these layers is still required. Since the ordered crystalline solids normally possess much higher thermal conductivity than liquids, the thermal conductivity of such liquid layers is also believed to be better than that of the bulk liquid present.

Nanoclusters

The clustering or aggregation of nanoparticles while in suspension results into the enhancement of thermal conductivity of colloidal suspensions (Keblinski *et al.*, 2002). This clustering of nanoparticles results in the formation of a better network of nanoparticles which thereby reduces the thermal resistance to heat flow. Nanoclusters comprising of comparatively larger masses may have a tendency to settle down and thus creating a particle-free regions within the suspension which may results into a decrease in the thermal heat exchange. Thus, clustering phenomenon may

offer both desirable and undesirable effects on the nanofluids' thermal conductivity. The nano-suspensions with higher concentrations are more prone to the clustering effect because of decreased inter-particle distance. Karthikeyan *et al.* (2008) made time dependent microscopic observations about the formation of nanoclusters in CuO-water nanofluid, where the measured time-dependent thermal conductivity was found to be decreasing with elapsed time. This is attributed due to the formation of excessive clusters of nanoparticles. The structural arrangement of nanoparticles within nanoclusters is expected to be made up of the linear chains of nanoparticles that spread throughout the cluster and others which are not forming the chain type arrangement, called backbones and dead ends (Shih *et al.*, 1990). The effective thermal conductivity of nanofluids is found to be increasing with the early formation of nanoclusters and then it becomes almost constant and remains constant without a much significant increase (Evans *et al.*, 2008). Xuan *et al.* (2003) proposed a theoretical model for the thermal conductivity of nanofluids on the basis of physical properties of base fluid and nanoparticles and their structural arrangements in aggregates. The distribution and arrangement of the nanoparticles while in suspension too affect the thermodynamic and thermos-physical properties of nanofluids beside other primary parameters, such as the shape and size and volume fraction of nanoparticles. In addition to this, the properties of host fluid such as density, viscosity, specific heat and its own thermal conductivity also pays a significant role in determining the thermosphysical properties of nanofluids. Philip *et al*. (2008) also observed a significant augmentation in the thermal conductivity of nanofluids when nanoparticles suspensions were found with chain-like aggregates of magnetite (Fe_3O_4) nanoparticles. They also hypothesized the fact that nanofluids containing well-dispersed nanoparticles (without aggregates) do not exhibit a significant enhancement in thermal conductivity. Therefore, further modifications to the theoretical models are very much required to study the heat conduction through the arrangement of nanoparticles of larger aspect ratios. The effect of clustering has been further emphasized for alumina-based nanofluids where, the dry nanopowder size was 44-58 nm, while the size of particles present in nanofluid was found to be 110 nm, thus indicating a cluster formation (Longo and Zilio, 2011; Longo *et al.*, 2012).

Thermophoresis

Thermophoresis and osmophores are the well-ordered movements of the particles in the direction of temperature gradient and pressure gradient. Their effects are unlike the Brownian motion. The

Brownian diffusion and diffusion-phoresis are the important slip mechanisms where, particles might generate a slip velocity with regard to base fluid. This information might be useful in developing the model for the transport phenomena of nanofluids (Buongiorno, 2005). Fu and Gao (2012) employed a two-step method to investigate the thermophoretic mobility of nanoparticles in nanofluids. In general, thermophoresis and Brownian motion result in an enhancement in heat transfer at any volume fraction of nanoparticles. On the other hand, heat transfer gets deteriorated if the role of thermophoresis and Brownian motion is neglected. This deterioration gets elevated with an increase in the volume fraction of nanoparticles (Haddad *et al.*, 2012). The nanoparticles migrate from the heated walls (nanoparticles depletion) towards the core region of the microchannel (nanoparticles accumulation) and construct a non-uniform nanoparticles distribution. The ratio of the Brownian to thermophoretic diffusivities (NBT) has relatively significant effects, both on the distribution of the nanoparticles and the convective heat transfer coefficient of nanofluids (Malvandi and Ganji, 2014). It was further observed that for smaller nanoparticles, the nanoparticle volume fraction is more uniform and the abnormal variations in the heat transfer rate vanishes. The transport equations used in the analysis took into account the effects of Brownian motion and thermophoresis parameters. The results indicated that Nusselt number is an increasing function of the buoyancy ratio number, but it is a decreasing function of Lewis number and Hartmann number (Sheikholeslami *et al.*, 2014). Although, Brownian motion and thermophoresis parameters seem to be playing an important role in the heat transport mechanisms of nanofluids, however further investigations are to be conducted to bring out more facts about these phenomena.

Diffusive and ballistic nature

Generally in many theoretical and fundamental approaches of nanofluids, a diffusive mode of heat transportation has been acknowledged and explored. However, this is also true that phonons are responsible for the heat conduction in many crystalline solids. It has been observed that the formation, propagation and scattering of such phonons takes place in random directions. This whole phenomenon leads to the macroscopic description of heat transport. Researchers believed that the diffusion of the phonon is not possible if particle size is less than 35 nm. Therefore, the hypothesis of the diffusive mode of heat transportation especially, in nanofluids is not valid. However, a ballistic phonon can transport heat more efficiently than the very fast diffusion phonon

transport (Keblinski *et al.*, 2002). The ballistic mode of heat transport problem can be studied by applying any one of the following methods, such as (i) irreversible thermodynamics, (ii) the universal Boltzmann equation, (iii) time lag equations, and (iii) heat transport using lattice theory. Avsec J. (2008) described how phonon heat transport could be expressed in term of Knudsen number where mean free paths of the particles (electrons) for materials (Copper and aluminum) are found to be 350 and 65 nm, respectively (Avsec, 2008). Hence, it is very difficult for the electrons to diffuse through 10 nm particles, rather than to move ballistically through the particles. This was also endorsing the opinion put forward by Keblinski *et al.* (2002). Hence, there are no general mechanisms to rationalize the strange behaviour of nanofluids for the purpose of modeling of the thermal conductivity of nanofluids accurately.

2.4 Models and Empirical Correlations for Thermal Conductivity of Nanofluids

The majority of the available models which are used to describe the thermal conductivity of microparticles based suspensions cannot be used for nanofluids. The thermal behavior of nanoparticles based suspensions containing dispersed arrangements and motion of nanoscale particles is much more complicated than the conventional suspensions (solid-liquid). Therefore, it is difficult to study such behaviour of nanosuspensions on the basis of diffusive heat transport mechanism alone. The mathematical modelling of the thermal conductivity of nanofluids can be classified into two broad areas: firstly, (i) modification of the existing models and secondly, (ii) the development of new models. Many researchers have recommended and suggested the use of static and dynamic mechanisms-based models to describe the thermal conductivity enhancement of nanofluids.

Static models

The study of the static or structural models is based on some perceptions, such as; nanolayer acts as a thermal link, fractal configuration of agglomerates, percolation across the high aspect ratio nanostructures, thermal resistance at interface and charge on particle surface (Koo and Kleinstreuer, 2005; Prasher *et al.*, 2006; Jang and Choi, 2007; Philip *et al.*, 2007a). Yu *et al.* (2003) modified Maxwell model for the effective thermal conductivity of colloidal suspensions by taking

into consideration the effect of ordered nanolayer. However, the model did not explain the nonlinearity involved in the thermal conductivity of nanofluids. Later on, a model describing the nonlinear behaviour of the thermal conductivity was proposed by taking into account liquid layering effects and polarization theory together (Xue and Xu, 2005). Wang *et al*. (2003) too studied the clustering of particles and their distribution and suggested a fractal model for thermal conductivity of nanofluids (Wang *et al.*, 2003). Xie *et al.* (2002) also reported on the importance of the shape effect of the nanoparticles (spherical and cylindrical) on the thermal conductivity of nanofluids. Yu *et al.* (2003) hypothesized a model for the thermal conductivity on the basis of cubic arrangement of spherical particles (Yu *et al.*, 2003). It has been shown that the relationship between the particle volume fractions and the thermal conductivity of nanofluids is nonlinear. Prashar *et al.* (2006) conducted the experiments to measure the thermal conductivity of alumina-water nanofluids with particle radii of 7.5, 10, 13.5, and 20 nm, with the volume fraction of each equal to 0.5% (Prasher *et al*., 2006). They developed two model equations without considering the effect of thermal boundary resistance between the particles and the fluid. The first one addresses the thermal conductivity of an aggregate (k_a), given as:

$$(1-\varphi_{\text{int}})(k_l-k_a)/k_l+2k_a+\ \varphi_{\text{int}}\,(k_p-k_a)/k_l+2k_a=0 \qquad (2.4.1)$$

Another equation takes into account the aggregation kinetics which is expressed to determine the overall thermal conductivity of an aggregate based nanofluid, given as:

$$k_{eff}/k_l=([k_a+2k_l]+2\varphi_{\text{a}}\,[k_a-k_l\,])/([k_a+2k_l]-\varphi_{\text{a}}[k_a-k_l) \qquad (2.4.2)$$

where, k_{eff} and k_a is the effective and aggregate thermal conductivity of nanofluid, and φ_a is the primary volume fraction of aggregates.

The aggregation phenomenon to determine the enhancement in the thermal conductivity of nanofluids is also found to be associated with high-aspect ratio fillers, including fibers and plates (Evans *et al.*, 2008). Evans *et al.* (2008) used a three-level homogenization theory of heat conduction and model fractal aggregates to study the thermal conductivity enhancement of nanofluid. The thermal conductivity of a composite consisting of randomly oriented cylinders,

fully aggregated systems (for large values of k_p/k_l ranging from 25 to 200) (Evans *et al.*, 2008) is given as:

$$\frac{k_{eff}}{k_l} = 1 + \varphi_p \left({k_p}/{3k_l} \right) \tag{2.4.3}$$

where, all the terms have their usual meanings given in nomenclature.

The interfacial resistance offered at solid-liquid interface is considered as a barrier to the heat flow and might bring down the benefit of adding the conductive filler materials in the composite. Under this condition, for the low volume fractions of well-dispersed spherical nanoparticles, the effective medium theories predicts the following equation for the thermal conductivity enhancement, given as:

$$\frac{k_{eff}}{k_l} = 3f \left[\frac{\left(\frac{r}{A_k} - 1 \right)}{\left(\frac{r}{A_k} + 2 \right)} \right] + 1 \tag{2.4.4}$$

where, '*r*' is the nanoparticle radius and A_k is the Kapitza radius. As per the Eq. (2.4.4), when the particle radius becomes equal to the Kapitza radius, there is no enhancement in the conductivity of nanofluids. For larger values of the interfacial resistance, the addition of nanoparticles decreases the thermal conductivity of the composite.

A model for thermal conductivity enhancement of nanofluids based on the particle size distribution (PSD) of nanofluids is given as (Zhou and Wu, 2014):

$$\frac{k_{nf}}{k_{pm}} = \frac{k_p + (\xi - 1) k_{pm} - (\xi - 1)\varphi_p (k_{pm} - k_p)}{k_p + (\xi - 1) k_{pm} + \varphi_p (k_{pm} - k_p)} \tag{2.4.5}$$

where, ξ is the shape factor given by, $\xi = 3/\psi$, with ψ denotes the sphericity of a nanocluster (i.e., the ratio of the surface area of sphere with the same volume of a cluster to the external surface area of a nanocluster). The k_{pm}, is the thermal conductivity of nanofluid containing only the primary nanoparticles and k_{nf} is the thermal conductivity of the nanofluid consisting of both primary

particles and nanoclusters. All the remaining terms have their usual meaning. More recently, Selvakumar and Dhinakaran (2016) have proposed a multi-level homogenization approach based on the effect of the Brownian motion, interfacial layer formation and particle clustering to predict the thermal conductivity of nanofluids. In their approach, nanofluid is considered to be a complex system which has both primary nanoparticles and particle clusters suspended in base-fluid. The particle size distribution (PSD) analysis has been used to determine the volume fraction and the size of nanoparticles and nanoclusters. The first, second and third level of homogenization approaches were used to express the thermal conductivity of (i) complex primary particles (k_{cpm}), (ii) suspension of complex primary particles in base fluid (k_l) including the effects of nano-scale convection caused by Brownian motion and (iii) the thermal conductivity of complex cluster spheres (k_{cc}). The model to predict the effective thermal conductivity of nanofluids is given as:

$$k_{eff} = \frac{k_{cc}+2k_l+2\varphi_{cc}\,(k_{cc}-k_l)}{k_{cc}+2k_l-\varphi_{cc}(k_{cc}-k_l)} \tag{2.4.6}$$

where, φ_{cc} is the effective volume fraction of complex clusters, given as $\varphi_{cc} = \varphi_p\,(1+\xi)^3$, and ξ are the thickness ratio of interfacial layer to cluster radius.

Dynamic models

It has also been conceptualized and understood that nanofluids' behaviour is dynamic in nature. Therefore, nanoparticles motion and the energy interactions among the moving nanoparticles and base fluid molecules are required to be taken into consideration to develop fundamentally accurate models. The thermal conductivity of aqueous Al_2O_3 nanofluid was investigated and showed as a strong function of the particle size and working temperature (Xie *et al.*, 2002). Xuan *et al*. (2003) was the first group of researchers who developed a dynamic model for the thermal conductivity of nanofluid by considering the Brownian motion (BM) of particles and the fractals (Xuan *et al.*, 2003). The dynamic models showed that the Brownian motion of nanoparticles plays a vital role in enhancing the thermal conductivity of nanofluids (Jang and Choi, 2004; Prasher *et al.*, 2005). However, these models show substantial disagreements amongst themselves and their validity is still a matter of debate and discussion. Yu *et al.* (2003) developed a simplified drift velocity based model for the thermal conductivity of nanofluid, where they assumed that the thermo-phoretically

drifting of nanoparticles is superimposed on their Brownian motion. However, this model could not explain the effect of nanoparticle size on the thermal conductivity of nanofluid. A model based on the nanoscale convection induced by the Brownian motion of nanoparticles was proposed by Jang and Choi (2004), which could explain the enhancement in the thermal conductivity of nanofluid. This new dynamic model was able to define the fundamental role of nano-convection in predicting the temperature and size-dependent thermal conductivity of nanofluids. The empirical Brownian motion based models exclusively assume that the nano-convection is mainly responsible for increased thermal conductivity of nanofluids (Prasher *et al.,* 2006). Kumar *et al.* (2004) developed a nano-convection model based on nano-convection prompted Brownian movements and the SSA of nanoparticles. Koo and Kleinstreuer (2005) extended the convection model of Yu *et al*. (2003) to consider the effect of fluid dragged by pairs of nanoparticles. Furthermore, it was also argued that the role of the Brownian motion is more important than the thermophoretic and osmophoretic motion of the particles and is primarily responsible for the energy interactions among the particles.

2.5 Thermal Conductivity Measurement Methods

Nanofluids have attracted a worldwide attention due to their improved thermophysical properties especially, the thermal conductivity. The measurement of these thermophysical properties is a challenge as the different methods and techniques provide different results (Paul *et al.*, 2010). There is no doubt that the method with significant lower measurement error and uncertainty would be the best one to be used. Following are the primary methods, which are generally recommended and used to measure the thermal conductivity of nanofluids:

1. Transient hot-wire techniques
2. Transient Plane Source (TPS) method
3. Steady-state parallel-plate method
4. Temperature oscillation technique
5. Cylindrical cell method
6. 3ω method
7. Thermal comparator method

Paul *et al.*, (2010) presented a report after reviewing the different methods of measuring thermal conductivity and concluded that the Transient Hot Wire (THW) method is the most reliable and widely accepted method.

Transient hot-wire (THW) method

This is most commonly used method to determine the thermal conductivity of nanofluids. As compared to other methods, it is fast and the conceptual design of the apparatus is simple as well. The quick measurement has the least possibility of natural convection when it is applied to measure the thermal conductivity of fluids (Paul *et al.*, 2010). In general, the transient hot-wire experimental setup consists of a Whetstone bridge circuit, DC power supply, stabilizer, switch, A/D converter and a computer where a platinum wire is used for heating and measuring the temperature. The power is supplied to the platinum wire, which causes an increase in its temperature (Paul *et al.*, 2010). This wire would heat up the material/liquid in contact. Thereafter, the thermal conductivity of a given sample can be determined by knowing the heat flux, temperature difference and some geometric parameters based on Fourier's law of heat conduction. The Transient hot-wire method has been used by many researchers to measure the thermal conductivity of nanofluids (Kwak and Kim, 2005; Murshed *et al.*, 2005; Timofeeva *et al.*, 2007; Zhang *et al.*, 2007). Over the years with some variations, a transient short hot-wire method is being used widely to measure the thermal conductivity of a variety of liquids (Paul *et al.*, 2010). The liquid metal technique, i.e. transient hot-wire technique has been devised especially to measure the thermal conductivity of electrically conducting liquids (Gustafsson, 1990), whereas, transient short hot-wire is a suitable method for measuring the thermal conductivity of corrosive liquids (Xie *et al.*, 2006).

Transient Plane Source (TPS) method

The thermal constant analyzer uses "Transient Plane Source (TPS)" theory to measure the thermal conductivity of liquids. Here, TPS sensor plays a similar role to that of the probe or wire in THW method. It acts as a heating source as well as a temperature sensor. Fast measuring capability, a wide range of thermal conductivity measurements (0.02 to 200 W/m K), no sample preparation and flexible sample size are the advantages of using TPS (Zhu *et al.*, 2009). The main components

of an experimental setup for the transient plane source method are: thermal bath with a thermometer, TPS sensor, sample holder, thermal constants analyzer and a computer. To determine the thermal conductivity of liquids, a probe of the analyzer is immersed into a prepared sample. The sample holder is required to be kept in a thermal bath at a constant temperature and a small amount of power is supplied to the sensor for a short time. The analyzer would be calculating the thermal conductivity later on. It should be noted that convection can cause an error in the results of the thermal conductivity. Therefore, the parameters of an analyzer are required to be controlled accurately. Few researchers have used this method for thermal conductivity measurements of nanofluids (Zhu *et al.*, 2009; Jiang *et al*., 2009).

Steady-state parallel-plate method

An apparatus involving a guarded hot-plate design can also be employed to determine the thermal conductivity of nanofluids. This apparatus consists of parallel plates and works on the principle of steady state heat transfer (Challoner and Powell, 1956). To measure the thermal conductivity, a small and known volume of the fluid/nanofluid sample is placed between two parallel plates, generally round in shape, called sample holder. The sample holder is located in a larger cell made of aluminum. The thermocouples are attached to the top and bottom of the sample holder enabling measurement of the temperature difference across the sample. Then, energy is supplied externally through a heater to warm up the sample. After knowing certain parameters such as heat input, cross-sectional area, total area, temperature difference, the thickness of sample, the heat conduction equation extracted from Fourier's law of heat conduction can be applied to calculate the thermal conductivity. The thermal conductivity measurements have been done successfully for some nanofluids such as Al_2O_3 and CuO dispersed in water, vacuum pump fluid and engine oil (Challoner and Powell, 1956; Das *et al.*, 2007).

Cylindrical cell method

This method is one of the most common steady-state methods used for measuring the thermal conductivity of fluids (Paul *et al.*, 2010). Kurt and Kayfeci (2009) used cylindrical cell method to measure the thermal conductivity of water and ethylene glycols. The results so obtained were compared with the results outcomes of Artificial Neural Networks (ANNs) predictions. This

instrument, i.e., cylindrical cell method consists of two coaxial cylinders, which are named as inner and outer cylinders. Inside the inner cylinder, which is generally made of copper, heater is placed, while the outer cylinder is galvanized. The fluid whose thermal conductivity is to be measured is kept between the gap of the inner and outer cylinder. After applying power from the external source (heater) and maintaining the heat transfer caused by a heater, Fourier's law of conduction heat transfer in coaxial cylinders is used to determine the thermal conductivity of liquid sample placed in a gap.

Temperature Oscillation method

The thermal conductivity by using temperature oscillation method is based on the propagation of a temperature oscillation inside a cylindrical liquid volume. The temperature oscillation method is given by Roetzel *et al.* (2010), where the temperature response of the sample was measured under a varying heat flux (Roetzel *et al*., 1990; Paul *et al.*, 2010). The main components used in a temperature oscillation method are a test cell, cooling water, thermal bath, DC power supply, amplifier and filter, data acquisition system and computer. The sample whose thermal conductivity is to be determined is held inside the test cell and is heated up by means of supplying power from external sources. Thermocouples measured the temperature variations of the sample continuously and at the same time cooling water from water bath was used to maintain the temperature close to the preferred value or set point. Displaying temperature value on a line would provide an assessment of steady oscillation and recording data. Thermocouples' data are amplified by an amplifier with a filter. Through this method, the thermal diffusivity and thermal conductivity of a sample can be measured accurately. This measurement of thermal diffusivity and thermal conductivity is based on the conduction energy equation (Das *et al.*, 2007).

3ω method

In 3ω method, an element acts as a heater and thermometer and possesses the radial flow of heat. When the temperature oscillation is applied, the passing sinusoidal current at a frequency of ω through a metal wire creates a heat wave of frequency 2ω. Afterwards, the voltage components at the frequency 3ω would be reduced (Paul *et al.*, 2010). Few researchers successfully used this

technique to determine the thermal conductivity of various nanofluids, such as; Al_2O_3/DI and Al_2O_3/ethylene glycol (Oh *et al.*, 2008).

Thermal comparator method

As per this method, two metal balls located in a block having thermal insulation are used to measure the thermal conductivity of materials, such as aluminum, iron, alloy steel etc. (Powell, 1957). Afterwards, this method has also been used to measure the thermal conductivity of different materials (Sherif and Mahmoud, 1966; Kreitman, 1976; Nottenburg *et al.*, 1978). This method is composed of mainly a copper probe, sample holder, DC voltmeter, voltage stabilizer and a heater. In this method, unlike few other methods, a probe is required to have only a point contact with the sample. Thermocouples are placed between the sample and the probe, which is supposed to have a constant temperature maintained through the heater. After sensing the temperature by a thermocouple, there should exist a direct relationship between thermal conductivity and observed differential emf. It is to be noted that when this occurs, a probe would be kept in a point contact with the sample. By knowing the different voltages in a circuit and boundary conditions and proper equations, the thermal conductivity of a sample can be calculated (Paul *et al.*, 2010). Some researchers used this method with liquids such as water, ethylene glycol and reported their satisfaction over the obtained results (Das *et al.*, 2007; Paul *et al.*, 2010).

A descriptive literature report on the thermal conductivity of nanofluids, mechanisms, and methods used to measure the thermal conductivity of nanofluids has been presented. A list of important parameters, such as volume concentration of nanoparticles, size and shape of nanoparticles, temperature, surfactant and their bound for the selected experimental conditions have been provided in Table 2.1. Table 2.1 also highlights the nature of nanoparticles, base fluids, sonication time and method used to prepare and measure the thermal conductivity of nanofluids. The corresponding percentage changes reported in the thermal conductivity measurements of nanofluids have been also provided.

Table 2.1: Detail of parameters, methods, sonication time, and thermal conductivity measuring methods

Author	**Base fluid**	**Nano Mat.**	**Shape**	**Size**	**Vol. Conc.**	**Temp.**	**Method**	**pH**	**Additives**	**Sonication time**	**Settling time**	***k*-tester**	**% change in *k***
Xie *et al.* (2003)	Water, EG & DE	MWCNTs	Cylindrical	50-200 nm	0.1% to 1.0%	Room temp.	Two step	2-12	Nitric acid and sulfuric acid mixture	Not studied	5 min. and 1 month	THW	19 % at 1.0 % of vol. conc.
Xie *et al.* (2002)	H_2O & EG	SiC	Spherical & cylindrical	SiC-26 & SiC-600	4.2% max.	Room temp.	Two step	Not studied	Not used	Not studied	Not studied	THW	15.8% for SiC-26 & 22.9% for SiC at 4.2% of vol. conc.
Murshed *et al.* (2005)	H_2O	TiO_2	Cylindrical& spherical	10 nm X 40 nm & 15 nm	5% max.	Room temp.	Two step	6.8 to 6.2	Oleic acid (CTAB) (0.01 to 0.02%)	8 to 10 h	Not studied	THW	33% & close to 30%
Liu *et al.* (2005)	EG & engine oil	CNTs	Fibre like	100:1 aspect ratio	1% for EG & 2% oil	Room temp.	Two step	Not studied	Not used	Not studied	Not studied	THW	12.4% at 0.01% and 30% at 2% of vol. conc.
Jang and Choi (2004)	H_2O	Al_2O_3 & CuO	Spherical	38.4 nm & 6 nm	1 %	25°C to 50°C	Two step	Not studied	Not used	Not studied	Not studied	THW	Up to 20%
Eastman *et al.* (2001)	EG	CuO	Spherical	<10 nm average diameter	Up to 1.0%	Room temp.	Two step	Not studied	thioglyolic acid,<1% vol.	Not studied	Not studied	THW	40% at 0.3% of vol. conc.
Chon *et al.* (2005)	H_2O	Al_2O_3	Spherical	11 nm to 150 nm	1 to 4%	21 ˚C to 71˚C	Two step	Not studied	Not used	Not used	Not studied	THW	3.36% deviation in the results of thermal conductivity
Kwak and Kim (2005)	EG	CuO	Rod like	10 to 30 nm	0.02%	Room temp.	Two step	Not studied	Not used	1 to 30 h	Not studied	THW	6% at 0.02% of vol. conc.
Ying *et al.* (2006)	Poly α-olefins oil(PA06)	CNT MWCNTS	Cylindrical	30-49:1	0.04 to 0.34%	Room temp.	Two step	Not studied	Polyisobutene succinimide (0. 3 to 8 % wt.)	5, 8, 15, 30 min	Not studied	THW	Not studied

Author	Base fluid	Nano Mat.	Shape	Size	Vol. Conc.	Temp.	Method	pH	Additives	Sonication time	Settling time	*k*-tester	% change in *k*
Liu *et al.* (2006)	H_2O	Cu	Spherical and square	30.8 nm and 39.2 nm	Up to 5%	Room temp.	Two step	Not studied	Not used	Not studied	Not studied	THW	18% at 4% and 22.4 % at 5% of vol. conc.
Li and Peterson (2006)	H_2O	Cu & Al_2O_3	Spherical	29 & 36 nm	2% to 10 %	20˚C to 50˚C	Two step	Not studied	Not used	Not studied	Not studied	Transient hot strip	52% at 6% of vol. conc. of CuO and 30 % for Al_2O_3 at 34 ˚C
Ma and Liu (2007)	Hg H_2O EG Ga	CNT, Au, Ag, Cu	Spherical and cylindrical	10 to 100 nm	0 to 0.2 %	Room temp.	Two step	Not studied	Not used	Not studied	Not studied	Not used	k_{eff}/k_f =1.8 and 2.3 at 0.01% and 0.04% of vol. conc.
Karthikeyan *et al.* (2008)	H_2O & EG	CuO	Spherical	8 nm	0.01 to 1%	Room temp.	Two step	6-7	Not used	30 min	Stable up to 3 weeks	THW	31% for water & 54% for EG at 1% of vol. conc.
Philip *et al.* (2007)	Kerosene	Fe	Spherical	6.7 nm	Up to 6.3%	25˚C	Two step	Not studied	oleic acid	Not studied	Not studied	KD2 Pro	300 % at 6.3% of vol. conc.
Amrollahi *et al.* (2007)	H_2O	MCM-41	Spherical	2.8 nm	0.5 to 2.5%	25˚C to 50˚C	Two step	24 h	Not used	1 to 25 h	2 to 18 hr	Steady state concentric cylinder	5 and 7% at 2.5% of vol. conc. and at 25 and 50 ˚C
Prasher *et al*. (2006)	H_2O	Al_2O_3	Spherical	7.5, 10, 13.5, and 20 nm	0.50 %	20-55 ˚C	Two step	2-12	Not used	2-12h	24 h	THW	30-35% at 50 ˚C
Zhu *et al*. (2007)	H_2O	CuO	Shuttle like shape	20-100 nm	0.1 to 10%	Room temp.	Synthesis	Not studied	Ammonium citrate	30 min	stable after long time	THW	18%, 28% &31% & at 1%, 3% ,5% of vol. conc.
Jang and Choi (2007)	H_2O & EG	CuO, Al_2O_3, CNT	Spherical	10, 20, 30 nm	0.5, 1 & 3%	20-50˚C	Two step	Not studied	Not used	Not studied	Not studied	Not used	20% for the 1% vol. con of CNT and 30% at 5% of vol. conc. of CuO in EG
Nnanna and Agwu (2007)	H_2O	Al_2O_3	Spherical	28 nm	0 to 8%	20-80˚C	Two step	Not studied	Not used	Not studied	Not studied	Buoyancy driven set up	30% at 5% of vol. conc.

Author	Base fluid	Nano Mat.	Shape	Size	Vol. Conc.	Temp.	Method	pH	Additives	Sonication time	Settling time	*k*-tester	% change in *k*
Yu *et al.* (2009)	EG	ZnO	Spherical	10 to 20 nm	0.2 to 5%	10 to 60˚C	Two step	Not studied	Not used	2-3 h	Up to 6 h	THW	26.5% at 5% of vol. conc.
Li *et al.* (2009)	H_2O	Cu and Al_2O_3	spherical	29 and 36 mm	5%	27.5 to 34.7 °C.	Two step	Not studied	Not used	Not studied	Not studied	THW	Models are compared
Chandrasekar *et al.* (2010)	H_2O	Al_2O_3	spherical	43nm	0.33 to 5%	Room temp.	Two step	5		6 h	3h	KD2 Pro	1.64, 3.28, 3.43, 7.52 and 9.7%, at vol. conc. of 0.33, 0.75, 1, 2 and 3%.
Sundar *et al.* (2007)	H_2O	Al_2O_3	spherical	47 nm	0.01 to 0.8%	30 to 60 °C.	Two step	5 to 7	Not used	10 h	12 h	Not used	*k* is not studied
Wang *et al.* (2011)	H_2O	TiO_2 and Al_2O_3	Spherical	25-50 nm	0.01 to 0.05%	Room temp.	Two step	2 to 12	SDS 0.10 and 0.14% of vol. conc.	2-3h	Up to 20 h	Not used	*k* is not studied
Akbari *et al*. (2011)	H_2O, EG	Al_2O_3, CuO and Cu	Spherical	10-100 nm	0.011 to 9.6%	Room temp.	Two step	Not studied	Not used	Not studied	Not studied	Model is developed and compared	20-30 %
Gharagozloo and Goodson (2011)	H_2O	Al_2O_3	Spherical	40, 60, 80, and 130 nm	1, 3 and 5%	25 to 50 °C	Two step	5.5	<1% of Nitric acid	3-4 h	10 to 60 min	Numerical models are compared	up to 30%
Teng *et al.* (2010)	H_2O	Al_2O_3	Spherical	20, 50, and 100 nm	0.5, 1.0, 1.5, 2.0 wt.%,	10, 30, 50 °C	Two step	Not studied	Not used	Not studied	Not studied	THW based KD2 Pro	7, 12, and 16%, 2% of vol. conc., and at 10, 30 and 50 °C.
Beck *et al.* (2009)	H_2O, EG	Al_2O_3	Spherical	8-282 nm	2, 3 and 4%	25 °C	Two step	Not studied	Not used	Not studied	Not studied	THW	6, 12, 18%
Duangthongsuk and Wongwises (2009)	H_2O	TiO_2	Spherical	21 nm	0.2–2%	15 to 35°C	Two step	6.5 to 7.5	Not used	Not studied	Not studied	THW	5 to 18%

Author	Base fluid	Nano Mat.	Shape	Size	Vol. Conc.	Temp.	Method	pH	Additives	Sonication time	Settling time	*k*-tester	% change in *k*
Gao *et al.* (2009)	hexadecane and hog fat	Al_2O_3	Spherical	70 nm	0.5 to 2%	5-52 °C	Two step	Not studied	Not used	Not studied	Not studied	THW	2 to 8%
Wang *et al.* (2009)	H_2O	Al_2O_3 and Cu	Spherical	25 nm	0.02, 0.05, 0.1 and 0.15% wt.	Room temp.	Two step	2 to 11.5	SDBS (up to 0.15% wt.)	15-20 min.	Not studied	Transient plane source (TPS)	Up to 15% for Al_2O_3 and 18% for Cu at the 0:8% weight fraction suspension
Yoo *et al.* (2007)	H_2O and EG	TiO_2,Al_2O_3, Fe, and WO_3	Spherical	25, 48, 10 and 38 nm	0.1 to 1%	Room temp.	Two step	Not studied	Not used	Not studied	Not studied	THW	14 and 4 % at 1% of vol. conc. of TiO_2, Al_2O_3 16.5 and 13.8% at 0.3% of vol. conc. of Fe and WO_3
Zhang *et al.* (2007)	H_2O and toluene	Au, Al_2O_3, TiO_2, CuO	Spherical	1.65, 20, 40, 33 nm	0 to 5%	5 to 40 °C	Two step	Not studied	SDS	Not studied	Not studied	THW	8% (for Au/toluene) and maximum up to 20% for others
Das *et al.* (2003)	H_2O	Al_2O_3 and CuO	Spherical	38.4 and 23.6 nm	1 to 5%	21 to 51°C	Two step	Not studied	Not used	12 h	1.5 to 2 h	Energy equation for conduction	5 to 25% for Al_2O_3 and 10 to 40% for CuO
Lee *et al.* (1999)	H_2O and EG	Al_2O_3 and CuO	Spherical	38 and 23 nm	0 to 4%	10 to 35°C	Two step	Not studied	Not used	Not studied	Not studied	THW	20% for CuO in EG and 10% for Al_2O_3 in EG at 4% of vol. conc
Liang and Tsai (2011)	H_2O	Au-Ar	Spherical	30 and 60 nm	0 to 5%	Room temp.	Two step	Not studied	Not used	Not studied	Not studied	Molecular dynamics simulations	29.2% and 31.3% for particles with radius of 30 and 15 nm at 5% of vol. conc.

Author	Base fluid	Nano Mat.	Shape	Size	Vol. Conc.	Temp.	Method	pH	Additives	Sonication time	Settling time	*k*-tester	% change in *k*
Hong *et al.* (2006)	EG	Fe	Spherical	10 nm	0.2 to 0.55%	Room temp.	Two step	Not studied	Not used	10 to 70 min	10 to 60 min	THW	up to 18% at 0.5% of vol. conc.
Philip *et al.* (2008)	Kerosene oil	Fe_3O_4	Spherical	6.7 nm	0 to 8%	Room temp.	Two step	Not studied	Oleic acid and external magnetic field	Not studied	Not studied	THW based KD2 Pro	23% at 7.8% of vol. conc.
Xuan *et al.* (2003)	H_2O	Cu	Spherical	10 nm	0.1 to 0.3%	10 to 80 °C	Two step	Not studied	Not used	Not studied	Not studied	THW	16% at 0.3% of vol. conc., and at 50°C.
Ghadimi and Metselaar (2013)	H_2O	TiO_2	Spherical	25 nm	0.1 wt.%	Room temp.	Two step	5	SDS at @ 0.1 wt.%	3h	1 day to one year	THW	Up to 5%
Wu *et al.* (2010)	H_2O	SiO_2	Spherical	15 nm	0.2%	20°C	Two step	8.5 to 10	Not used	15 min to 3 hrs	Not studied	3ω -wire method	5% at 0.2% of vol. conc.
Chopkar *et al.* (2007)	H_2O and EG	Al_2Cu and Ag_2Al	Spherical	20-80 nm	0.2 to 1.5%	Room temp.	Two step	Not studied	1% vol. of oleic acid	Not studied	Stable colloidal dispersion	Thermal comparator	70 % at 1% of vol. conc. of Al_2Cu in H_2O and 50% for EG 30% at 2.5 % of vol. conc. of Ag_2Al in EG

Chapter 3

Materials and Methods

The outcome of the different experimental investigations have been proved to be a new dimension to look into the phenomena of heat transport in nanofluids. The use of various types of materials and the equipment and instruments have been of a great advent to establish and correlate the facts. A detailed discussion regarding the working of such equipment and instruments, types of nanomaterials used and methods along with their relevance particularly to nanofluids have been presented in subsequent portion of this Chapter.

3.1 Nanomaterials

The nanopowders can be dispersed in the host medium (water, ethylene glycol, oils etc.) to prepare a variety of nanofluids. In the work undertaken, commercial nanopowders of Al_2O_3 (γ) and TiO_2 (anatase + rutile) of an average size of nanoparticles 20-25 nm were procured from Intelligent Material Pvt. Ltd., NANOSHEL, USA. These nanopowders along with water (DI) and suitable surfactants have been used to prepare the various samples of nanofluids.

3.2 Preparation of Nanofluids

The preparation of nanofluids is a major step to carry out the experimental studies on nanofluids. These nanofluids are not simply solid-liquid mixtures, but are processed to acquire some unique features such as uniformity and stability in suspension, minimum agglomeration of nanoparticles and negligible change in the chemical properties of the host fluids. There are mainly two techniques which are used to prepare the variety of nanofluids, discussed as under:

Single Step Method

This technique involves condensation of the nanophase materials (powders) from their vapour phase directly into the low vapour pressure fluids and has a capability to produce the nanoparticles with minimum agglomeration, see Fig. 3.1.

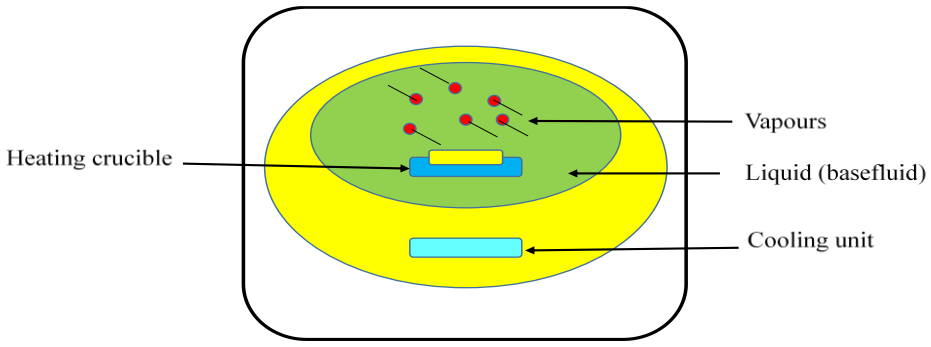

Fig. 3.1: One Step Method of nanofluid preparation

This technique is called vacuum evaporation running oil substrate (VEROS) (Akoh *et al.*, 1978). However, the procedure involved is quite cumbersome as the separation of particles from fluid to dry powdered form is difficult. Later on, a modified VEROS technique was developed where Cu vapours were directly condensed into nanoparticles through contact with a flowing low vapour pressure liquid (ethylene glycol) (Eastman *et al.*, 1997; Wagener et al., 1997). In another method, a vacuum submerged arc nanoparticle synthesis system is also employed to prepare Cu-based nanofluids with some different dielectric liquids especially with de-ionized water. An advantage of the one-step technique is that a minimum agglomeration is achieved, while the disadvantage is that first this it can be employed only with low vapour pressure fluids and secondly it has not been yet scaled up to meet out the large industrial applications/ requirements.

Two- Step Method

In this technique, at the first stage nanoparticles are produced as dry powders, typically through the inert gas condensation process. Then in the second phase, dry nanoparticle powders are dispersed into base fluids, such as water, ethylene glycol, mixtures of water and EG, and oils, etc. (Granqvist and Buhrman, 1976), see Fig. 3.2.

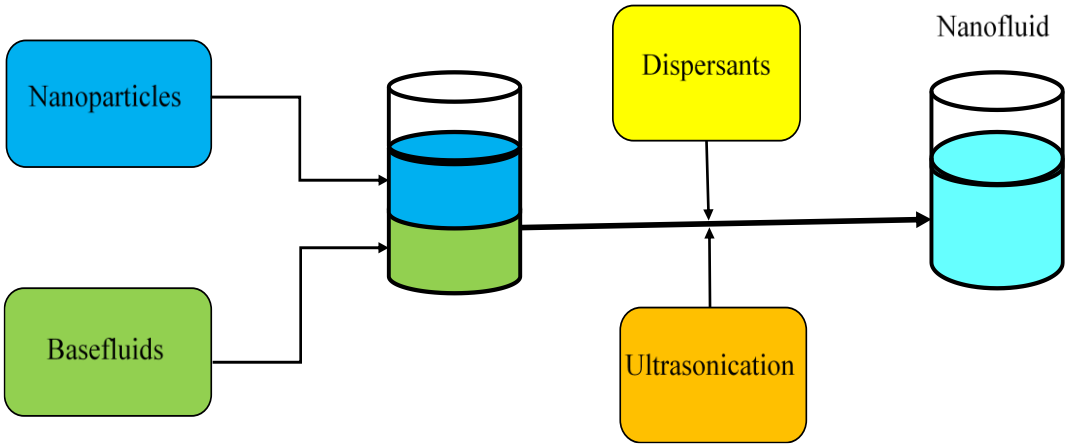

Fig. 3.2: Two Step Method of nanofluid preparation

The advantage of the two-step process is that it has been scaled up to the commercial nanoparticle production. This technique mainly prepares the oxide nanoparticles (Al_2O_3, CuO, TiO_2 etc.) based nanofluids. A main drawback of this method is that the nanoparticles form agglomerates during their storage and dispersion in base fluids, particularly when the particles are heavier and metallic. To overcome this problem use of some surfactants and other surface-stabilization additives are recommended which will help to prepare homogeneous and stable suspensions. In the present work, Two Step Method has been employed to prepare the nanofluids. More details about their preparation, stability and sonication parameters have been provided in the subsequent Chapters 5 and 6.

Sonication and Sonication Time

In the present work, a probe type sonicator has been used to prepare nanofluids. The samples of different volume concentration of nanoparticles in the respective base fluids have been developed by using a probe type ultrasonicator (OSCAR ULTRSONICS, 250 W, 20 ± 3 kHz), see Fig. 3.3.

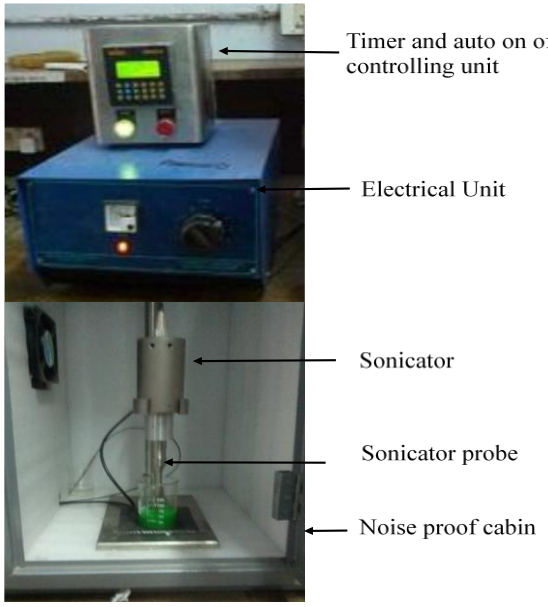

Fig. 3.3: A probe type sonicator

In general, sonication processes can be carried out either by using a probe-type ultrasonic homogenizer or an ultrasonic bath. Although, both the techniques apply ultrasound to the sample, there are significant differences in term of their effectiveness, efficiency and process capabilities (Timofeeva *et al.*, 2007). The various physical treatment techniques based on two-step method, including stirrer, ultrasonic bath, ultrasonic disruptor, and high-pressure homogenizer have been systematically tested to verify their versatility and feasibility to prepare stable nanofluids (Hwang *et al.*, 2008; Huang *et al.*, 2009). During ultra-sonication, the desired effects such as homogenization, dispersion, de-agglomeration, emulsification, disintegration, etc. are caused by cavitation (Ghadimi *et al*., 2011). The high power ultrasound in a liquid medium, create alternating high-pressure (compression) and low-pressure (rarefaction) cycles at different rates depending on the frequency. During the low-pressure reporting period, high-intensity ultrasonic waves create

small vacuum bubbles or voids in the liquid and when these bubbles attain a volume at which they can no longer absorb energy, they collapse violently during a high-pressure cycle. This phenomenon is termed as cavitation. During the implosion a very high temperatures (about 5,000K) and pressures (about 2,000 atm) are reached locally (Li *et al.*, 2009).

Surfactants and additives

The addition of surfactants and pH control are the techniques which are used to prevent the clustering and agglomeration of nanoparticles. The researchers have used these techniques to improve the stability of nanofluid (Zhu *et al.*, 2009; Lin *et al*., 2011). There are several types of surfactants which have been used to prepare different kinds of nanofluids. The important ones are; Sodium dodecyl sulfate (SDS) (Hwang *et al.*, 2008; Chandrasekar *et al.*, 2010; Meibodi *et al.*, 2010), SDBS (Jiang *et al.*, 2003; Zhu *et al.*, 2009), Salt and oleic acid (Hwang *et al.*, 2007, 2008), Cetyltrimethyl ammonium bromide (CTAB) (Jiang *et al*., 2003; Assael *et al.*, 2005), Dodecyl trimethyl ammonium bromide (DTAB) and sodium octanoate (SOCT) (Li *et al.*, 2008), Hexadecyl trimethyl ammonium bromide (HCTAB) (Yu *et al.*, 2010), Polyvinylpyrrolidone (PVP) (Pantzali et al., 2009). The selection of a particular type of a surfactant for a nanofluid depends upon its nature of physical and chemical properties along with their effect on the properties of nanofluid which are to be investigated. In context to the work undertaken initially, surfactants CTAB, SDS, PVP, Triton X 100 and oleic acid were tried to with different samples of Al_2O_3 and TiO_2 based nanofluids. The surfactant, SDS was found to have a significant effect on the thermal conductivity enhancements of Al_2O_3 and TiO_2 based nanofluids and hence in later part of this study, only SDS has been used (discussed in Chapter 5 and 7).

pH Control

The suspension stability of the nanofluids is directly related to their electro-kinetic properties. Therefore, the pH control indicates control on the repulsive forces among the particles, which thereby affect the suspension stability of nanofluids (Zhu *et al.*, 2009). As an example, simple acid treatment done by Xie *et al.* (2009) could cause a significant improvement in the stability of CNT in water (Xie *et al.*, 2009). In general, there are two types of forces which cause the attraction and repulsion among particles i.e. van der Waals and electrostatic forces. It is quite possible to control

these forces through pH control. Li *et al.* (2008) have accomplished their research to study the effect of pH and SDBS surfactant on thermal conductivity of Cu-H_2O nanofluid (Murshed *et al.*, 2008). The role of pH values on suspension quality of Al_2O_3 nanofluid is also investigated by Fovet *et al.* (2001) and a decrease and increase in the agglomeration rate is observed just by changing the pH of nanofluid. The optimized pH value is different and varies from sample to sample. In the study undertaken, the pH value of the various samples prepared through Two Step method followed by sonication has been controlled from 2 to 12. This is achieved by using NaOH and HCl of standard grades. The effect of pH on the hydrodynamic size of the particles while in suspension, suspension stabilities and on the zeta potential of the respective nanofluid, has been discussed in the subsequent chapters, i.e. Chapter 5 and 7.

3.3 Zeta Potential Measurements

Suspension stability plays an important role for the performance of nanofluid. One of the primary requirement to investigate the suspension stability is to measure the zeta potential of the nanofluids samples. This zeta potential is a measure of the magnitude of the electrostatic charge i.e. repulsion/attraction among the particles and is one of the important parameters known to be affecting the stability of nanofluid, Fig. 3.4.

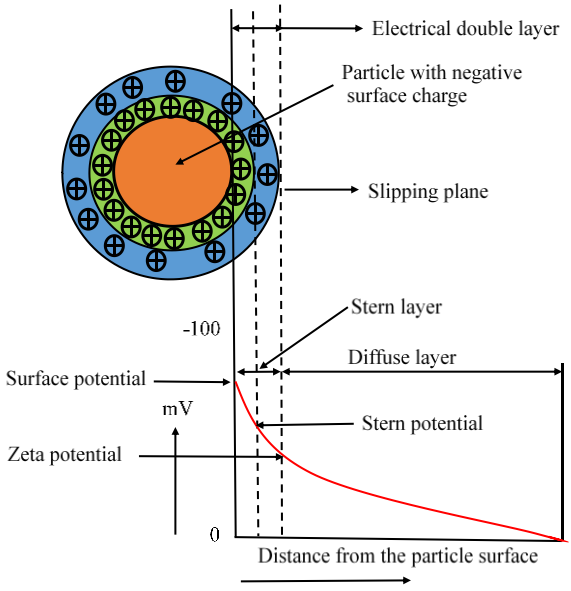

Fig. 3.4: Concept of zeta potential, surface potential and stern potential and their effect on suspension stability

Zeta potential measurement brings detailed insight into the causes of dispersion, aggregation or flocculation and can be applied to improve the formulation of dispersions, emulsions, and suspensions, see Fig. 3.5. In the present work, the pH value of the samples has been varied to investigate into the effect of the zeta potential and pH on the suspension quality and stability of the various samples of Al_2O_3 and TiO_2 based nanofluids. A detailed report regarding the zeta potential and its effect on the suspension stability has been provided in Chapter 5 and 6.

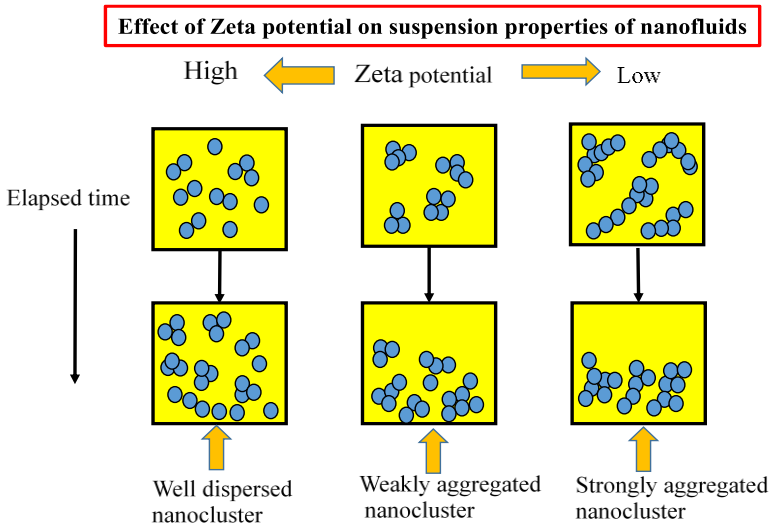

Fig. 3.5: Effect of zeta potential on particle suspension and their associated properties

3.4 Powder X-Ray Diffraction (XRD)

The XRD is a non-destructive testing technique and a powerful tool for analyzing the crystalline structures of the materials. The X-ray has its wavelengths comparable to the crystalline lattice constants, which makes it be used suitably for the accurate measurement of lattice parameter, crystallite size, and lattice strains. X-ray diffraction of the nanopowder samples was performed using the diffractometer system, XPERT-PRO, available in the laboratory, see Fig 3.6. The XRD diffractometer is found to have the automatic divergence slit, an irradiated length of 10.00 nm, anode material Cu, K-Alpha1 of 1.54060 Å and generator settings of 40 mA, 45 kV. During the

process of XRD investigation, the angle was found to be varying from 20.0276 (2θ, start position) to 79.9836 (2θ, end position) with a step size of 0.0130 (2θ).

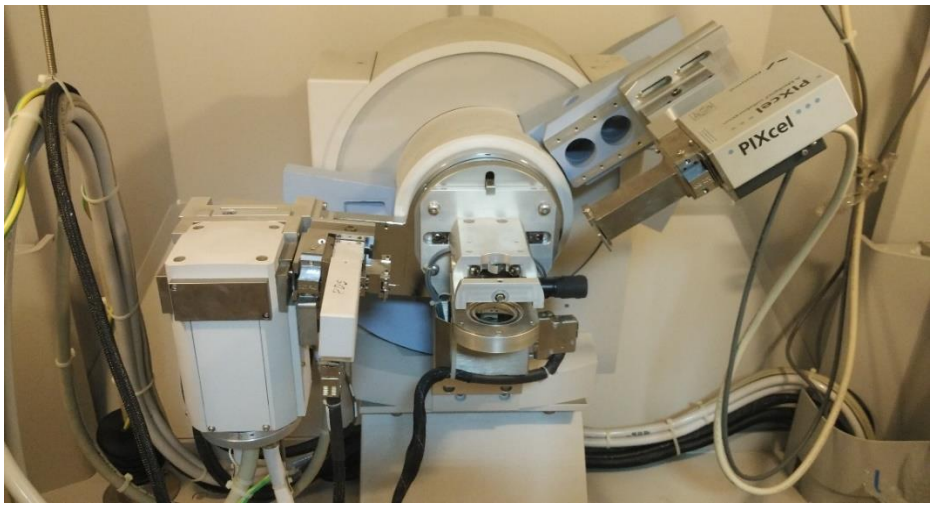

Fig. 3.6: The XRD diffractometer

All the measurements were recorded at 25°C with scan step time of 39.2700 seconds and with the continuous PSD mode of scanning and PSD Length of 3.35 (2θ). The phase and particle size of nanoparticles are crucial parameters that influence the physical properties of materials. The data on particle size and shape has been obtained using X-Ray Diffraction (XRD) technique as the particle size is related to the diffraction peak broadening. Hence, XRD methods allow not only to measure the particle size, but also to identify crystalline phases of nanomaterial.

3.5 Dynamic Light Scattering (DLS)

Dynamic Light Scattering (DLS)/ Photon Correlation Spectroscopy/Quasi-Elastic Light Scattering is a light scattering technique which can allow particle size measurements down to 1 nm diameter. The stability of nanoclusters and suspension quality of the different samples of nanofluids have been studied with Dynamic Light Scattering (DLS, Brookhaven 90 plus instrument), Fig. 3.7. The typical specifications of this model are: range: 0.3 nm to 6 μm, light

scattering at 90°, temperature control -5°C to 110°C, high power 40 mW, 640 nm and temperature controlled semiconductor laser.

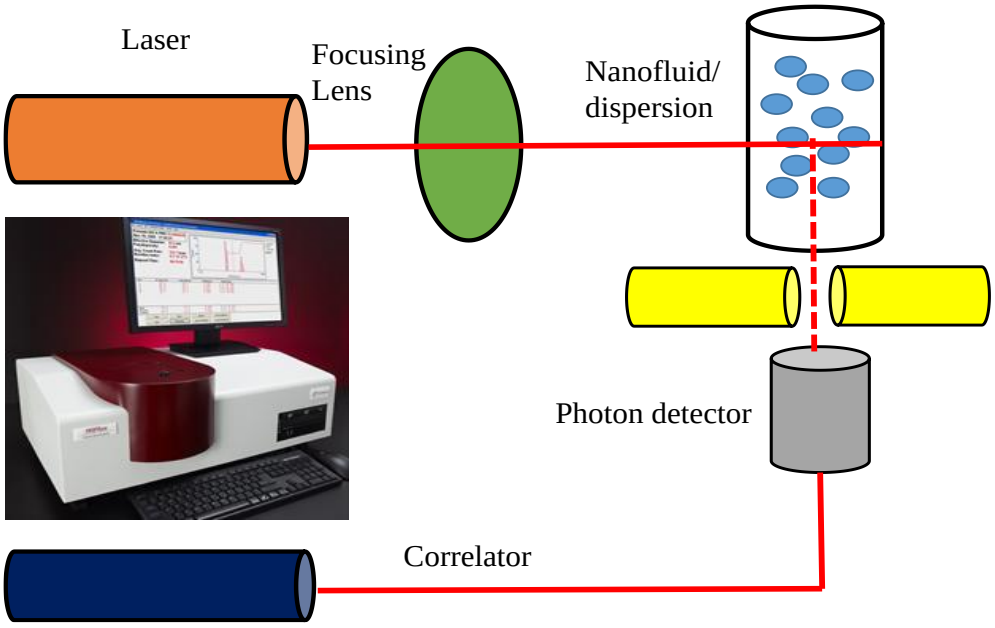

Fig. 3.7: Dynamic Light Scattering (DLS, Brookhaven 90 plus instrument)

In DLS measurements, the speed at which the particles diffuse due to the Brownian motion is measured by recording the rate at which the intensity of the scattered light fluctuates. The fundamental principle is that the sample is illuminated by using a laser beam and then fluctuations of the scattered light are detected by a fast photon detector. The light scattering through the particle imprint information about their motion. Thus, the analysis of the fluctuation of the scattered light gives information about the particles. The particle size is expressed in terms of hydrodynamic radius which is the diameter of a sphere that has the same translational diffusion coefficient as the particle. The translational diffusion coefficient is the measure of the velocity of the Brownian motion of the particles. The hydrodynamic size of the particle is determined by Stokes-Einstein equation, i.e. $(H) = \frac{kT}{3\pi\mu D}$. where, d (H) is the hydrodynamic size of the particle, k is the Boltzmanns' constant, T and μ are sample temperature and viscosity and D is the translational diffusion coefficient. In the study undertaken, a detailed DLS investigations have been done on the various samples of nanofluids (Al_2O_3-H_2O and TiO_2-H_2O) as per the requirements, whose details are provided in chapter 5 and 7.

3.6 Transmission Electron Microscope (TEM)

The transmission electron microscopy (TEM) or scanning electron microscope technique can be used directly to observe the shape and size of the particles. The HR-TEM (NIPER Mohali, India) has been used to examine the particle size, crystallinity and morphology of various samples of nanofluids, shown in Fig. 3.8.

Fig. 3.8: High-Resolution Transmission Electron Microscope (HR-TEM)

Samples are prepared by placing a drop of the nanofluid samples on a copper grid coated with a carbon film and then dried at room temperature. In TEM, the particle size is determined by taking the multiple particle images and then the average particle size (d) and standard deviation (σ) are obtained from the number (n_i) and size (d_i) of particles in those images, as given under:

$$d = \frac{\sum n_i d_i}{\sum n_i}, \ \sigma = \left[\frac{\sum n_i \ (d_i - d)^2}{\sum n_i}\right]^{1/2} \tag{3.1}$$

3.7 Thermal Conductivity Measurements

A Thermal Property Analyzer, KD2 Pro (Decagon Devices, Inc., USA) has been used for measuring the thermal conductivity of nanofluids. Its design follows the ASTM Standard D5334-08 and IEEE Standard 442-1981 and works on the principle of transient hot wire method (TWH). It consists of a microcontroller and a needle sensor such as KS-1, TR-1, and SH-1. Out of these three different needle sensors, the KS-1 is employed to determine the thermal conductivity of liquids and nanofluids, shown in Fig 3.9.

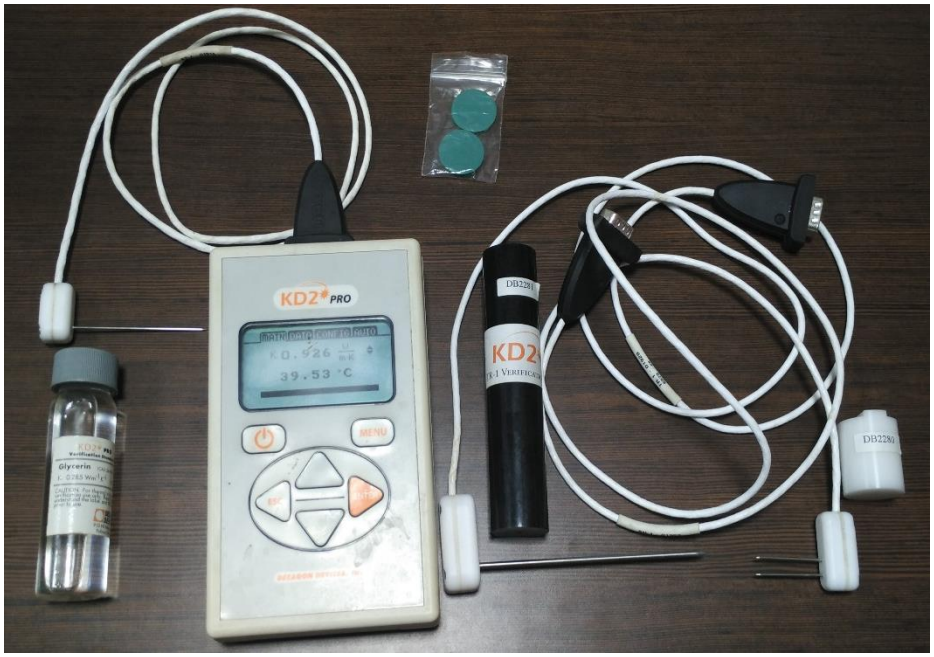

Fig. 3.9: Thermal Property Analyzer, KD2 Pro (Decagon Devices, Inc., USA)

This sensor needle contains both a heating element and a thermistor. The controller unit consists of a battery, a 16-bit microcontroller/AD converter, and a power control circuit. The length of the needle sensor (stainless steel) is 60 mm and diameter is 1.3 mm. While measuring the thermal conductivity, certain assumptions are considered, such as (i) an infinitely long heat source, (ii) medium is homogeneous as well as isotropic, and (iii) uniform initial temperature. Although, practically these assumptions are not very true to be achieved, but these need to be controlled adequately during the measurements. The needle sensor measures the thermal conductivity of

fluids/ nanofluids with an accuracy of ± 5% in the range of 0.2-2 W/mK and ± 0.01% in the range of 0.02-0.2 W/mK. In KD2 Pro, each measurement read cycle consists of 90s. During the first 30s, the sensor needle will equilibrate with surrounding fluid and then it is followed by heating and cooling of a sensor needle for next 30 s each. The equipment, KD2 Pro analyzer collects the data at each one second interval during a heating time of 30 seconds and cooling time of 30 seconds and hence, in total sixty (60) readings are collected. This collected data is used in simultaneous least square computations, which finally determine the thermal conductivity, *k*. The microcontroller calculates the thermal conductivity from the temperature (*T*) versus time (*t*) relationship (Nagasaka and Nagashima, 1981; Codreanu, Codreanu and Obreja, 2007), given as:

$$\Delta T\ (r, t) = \frac{Q}{4\pi K} ln\left(\frac{4\alpha t}{r^2\ C}\right) \tag{3.2}$$

Where, *q* represents a constant heat rate (applied to an infinitely long and small ‘‘line” source), ΔT is the change in the temperature at times t_1 and t_2, α is the thermal diffusivity of the test fluid, and *r* is the radius of the testing needle and *C* is the constant, respectively. The plot of the temperature *T* (*r, t*) on a logarithmic scale of time is linear, with slope, s = q/(4π *k*), from which the thermal conductivity of a liquid sample can be determined as:

$$k = \frac{q}{4\pi s} \tag{3.3}$$

In this study, the thermal conductivity has been measured in the temperatures range from 20 to 80°C (with ± 1°C). A packed water jacket of a water bath has been used to obtain more precise data of thermal conductivity by maintaining the needle at a stable temperature. Water bath has been used to stabilize the temperature of samples through circulating water through the water jacket. To conduct the different experiments for a variety of samples, each experiment was performed at least four times (for one hour) under the given set of conditions. Thus, a data point reported through the study represents an average of four measurements with an estimated repeatability of ± 2 to ± 5%. Before using the KD2 Pro for actual measurements its accuracy and repeatability is ensured through calibration and the right technique used to measure the thermal conductivity of given sample of any liquid or nanofluid.

3.8 Viscosity Measurements

An objective to use any nanofluid in a cooling system is that it should have a significantly high thermal conductivity and thereby it would be helpful in achieving an appreciable heat transfer rate. On the other hand at same time and in the same cooling medium, a minimum increment or at least constant viscosity is required to be maintained. Thus, the higher ratio of thermal conductivity and viscosity is always desirable.

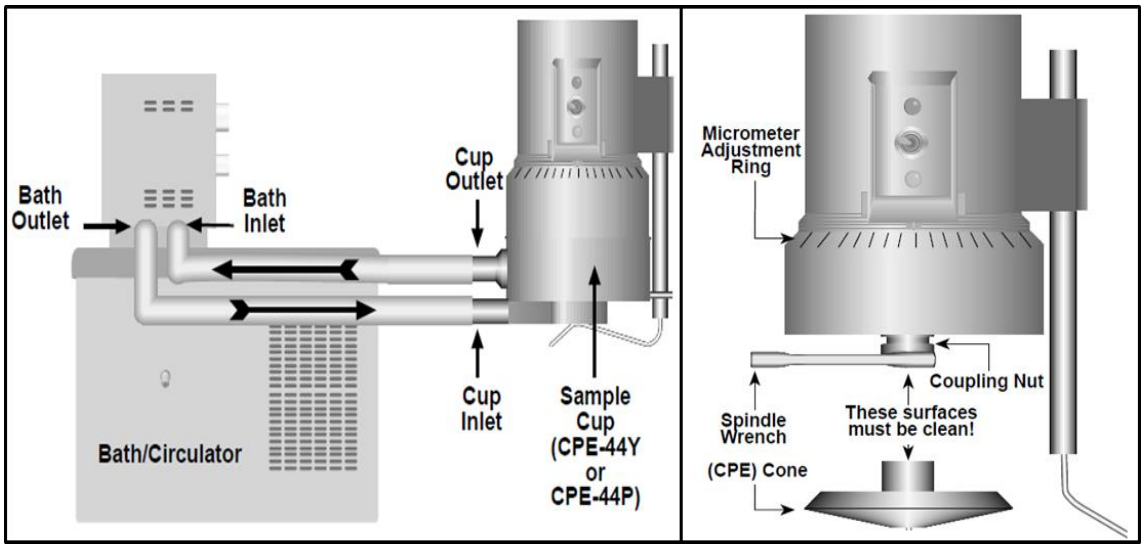

Fig. 3.10: A typical line diagram of LVDV-III Ultra Viscometer

Like thermal conductivity, the various important parameters which influence the viscosity are: temperature, the volume concentration of nanoparticles, the particle size, nanoparticles' morphology, sonication time, suspension stability and shear rate (Li *et al.*, 2009). Therefore, while investigating the thermal conductivity, an investigation into viscosity variation is also required to be carried out. This will help in predicting the overall performance of any nanofluid in a better and effective way. In context to the present work, the viscosity of various samples of nanofluids has been measured using a Brookfield LVDV-III Ultra Viscometer (Cone Spindle CPE-42) available in laboratory, see Fig 3.10 and Fig. 3.11. In this viscometer, a cone is attached to the spindle drive and a plate is mounted in the sample cup. The spindle CPE-42 can be used to measure the viscosity of various samples of fluid/ nanofluids (viscosity range of 0.3-600 cP). With the help of electronic

gap adjustments, a small gap of 0.013 mm between the cone surface and the plate is required to be maintained where the testing fluid is placed. When the spindle rotates, the viscous drag force offered by the fluid against the spindle is measured by the deflection produced in the calibrated spring. In general, the viscometer with cone and plate type geometry requires a small sample volume of fluid/nanofluid (0.5-2 ml) whose viscosity is to be measured. Another advantage of using such small volume of samples is that the equilibrium temperature is achieved rapidly.

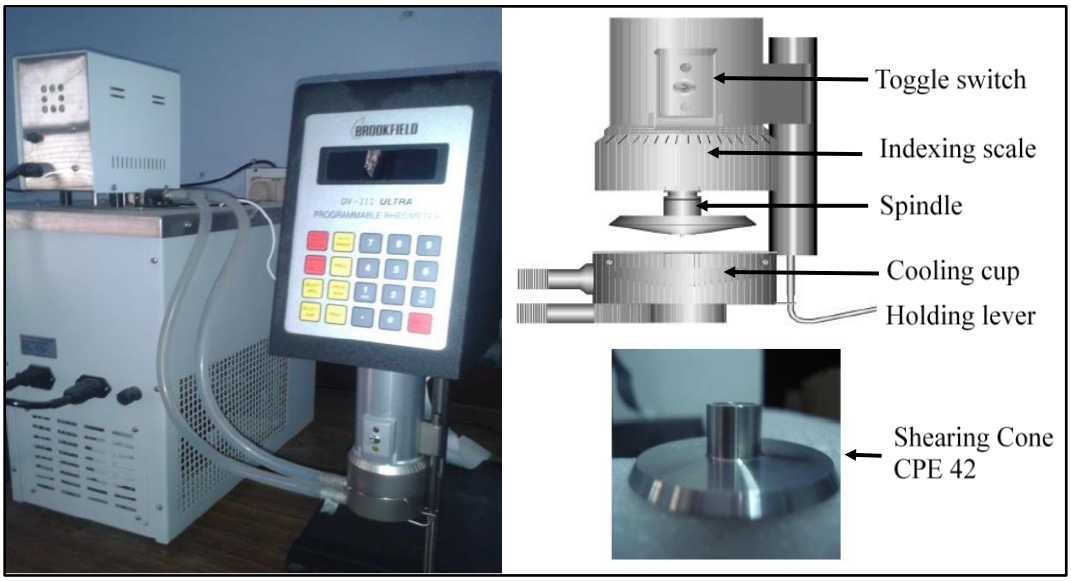

Fig. 3.11: LVDV-III Ultra Viscometer Cone Spindle CPE-42

Chapter-4

Material Characterization and Evaluation of Measuring Equipment

Material characterization and evaluation of the measuring equipment are required to be completed first, before performing the main experimentation. This investigation will help in correlating the results with more precision and accuracy. A detailed study on the time dependent particle size distribution, material characterization and evaluation of measuring instruments and equipment have been presented over here.

4.1 Characterization of Nanomaterials

The commercial nanopowders of Al_2O_3 (γ) and TiO_2 (rutile + anatase), size 20-25 nm were procured from Intelligent Material Pvt. Ltd., NANOSHEL, USA. These nanopowders along with water (DI) and surfactants (Cetyl trimethyl ammonium bromide (CTAB)/ Sodium dodecyl sulfate (SDS)/ Poly-vinyl pyrrolidone (PVP)/ Triton X100/ and Oleic acid) have been used to prepare the various samples of nanofluids whose properties are given in Table 4.1.

Table 4.1: The nanopowder data used to investigate the thermal conductivity of Al_2O_3-H_2O and TiO_2-H_2O nanofluids

Parameter/factor	**Value**	**Al_2O_3 Nanoparticles**	
Relative dielectric constant of the liquid, ε_r	80 for H_2O	Crystal form	Gamma (γ)
Dielectric constant of free space, ε_0	$8.854X10^{-12}$ $CV^{-1}M^{-1}$	Density, ρ_{Al2O3}	3. 88 g /cm^3
Room temperature, T	298 K	Specific surface area (SSA)	15-20 m^2/g
		Thermal conductivity, k_p	35 W/mK
		Appearance	White solid
Resistance due to thermal boundary layer, R_{BL}	1×10^{-9} m^2 K/W	**TiO_2 Nanoparticles**	
A constant, α	$13.58X10^{20}$ s/m^3		

Boltzmann constant (K_B)	1.3807×10^{-23} J/K	Crystal form	Rutile + anatase
Viscosity of base fluid, μ	0.89 mPa-s at 25 ° C	Density, ρ_{TiO2}	4.076 g/cm^3
Specific heat of the base fluid, C_f	4.071KJ/kg K	Specific surface area (SSA)	30-35 m^2/g
Thermal conductivity of base fluid (DI water), k_f	0.6060 W/m K at 25° C	Thermal conductivity, k_p	13.5 W/mK
		Appearance	White solid

Powder X-Ray Diffraction (XRD) analysis

Al_2O_3 (γ) nanopowder XRD

A complete analysis of XRD pattern, including lattice parameters and Bragg profiles, confirmed the existence of Al_2O_3 (γ) with 99.99% purity. The XRD pattern of Al_2O_3 (γ) shows the intense sharp intensity at (2 2 0), (3 1 1), (4 0 0) and at (4 4 0), see Fig. 4.1.

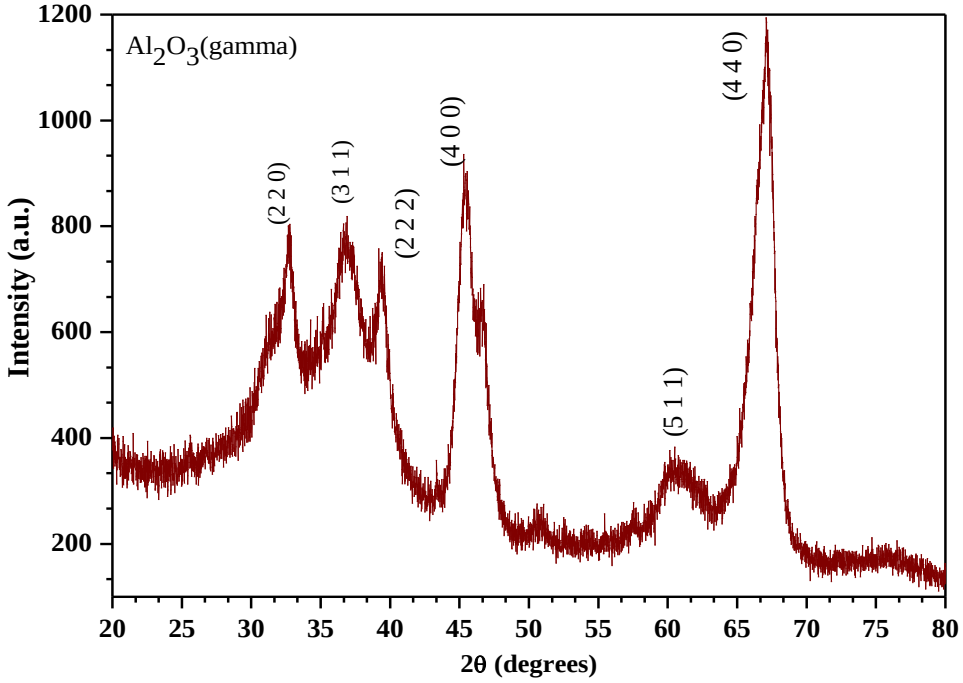

Fig. 4.1: Powder X-ray diffraction (XRD) pattern of Al_2O_3 (γ)

TiO_2 nanopowder XRD

The commercial TiO_2 nanopowder was characterized by X-Ray diffraction (XRD) technique. The XRD patterns of nano-TiO_2 in rutile and anatase phases is shown in Fig. 4.2. The XRD pattern exhibits strong diffraction peaks at 27°, 37° and 56°, thereby indicating that TiO_2 is in the rutile phase. On the other hand, in the same Fig. 4.2, XRD pattern also exhibits strong diffraction peaks at 25°, 48°, and 63° indicating TiO_2 in the anatase phase. The crystals structure of TiO_2 belongs to anatase and rutile (70:30). The TiO_2 exists mostly as rutile and anatase phases and both of them have the tetragonal structures (Kim *et al.*, 2005). In Fig. 4.2, XRD pattern of TiO_2 also indicates that the phases are composed of irregular polycrystalline. Furthermore, the particle size can be identified by the characteristic of XRD pattern; the diffraction pattern peak intensity of TiO_2 increases with increasing particle size.

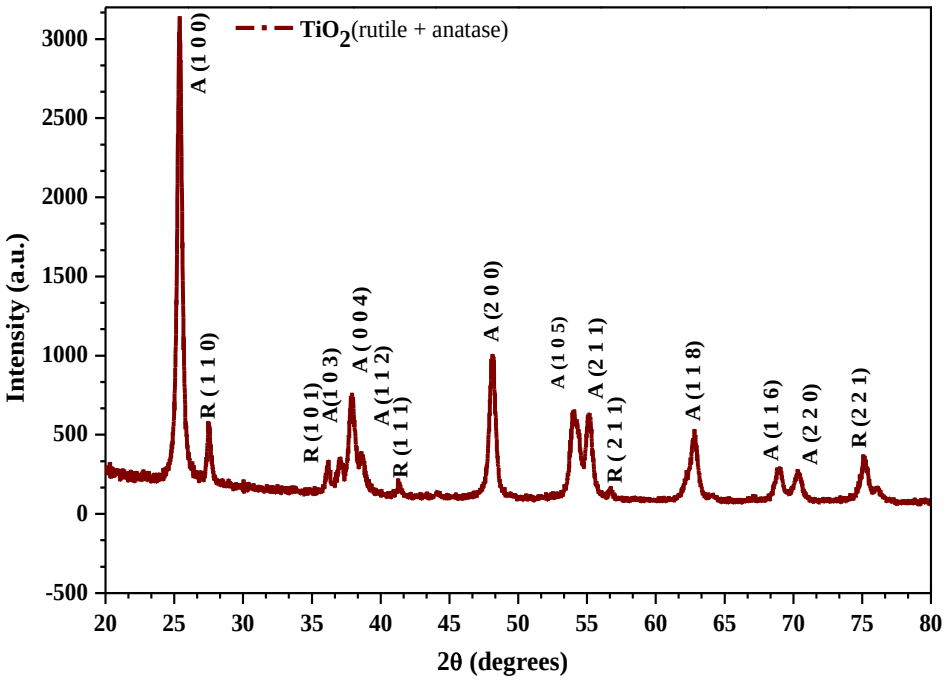

Fig. 4.2: Powder X-ray diffraction (XRD) pattern of TiO_2 (rutile + anatase)

4.2. Particle Size Distribution (PSD)

Dynamic Light Scattering (DLS) of nanofluid samples

DLS is performed to determine the average hydrodynamic size of the nanoparticles while in suspension. The details of the various samples of nanofluids taken under investigation have been provided in Chapter 5 and 7.

Transmission Electron Microscope (TEM) imaging of samples

TEM images of Nanopowders (Al_2O_3 and TiO_2)

The TEM images of Al_2O_3 (γ) and TiO_2 (rutile + anatase) nanopowders confirm their average size around 20-30 nm, see Fig. 4.3 and Fig 4.4. The TEM images of both the nanopowders show that nanoparticles are spherical in shape.

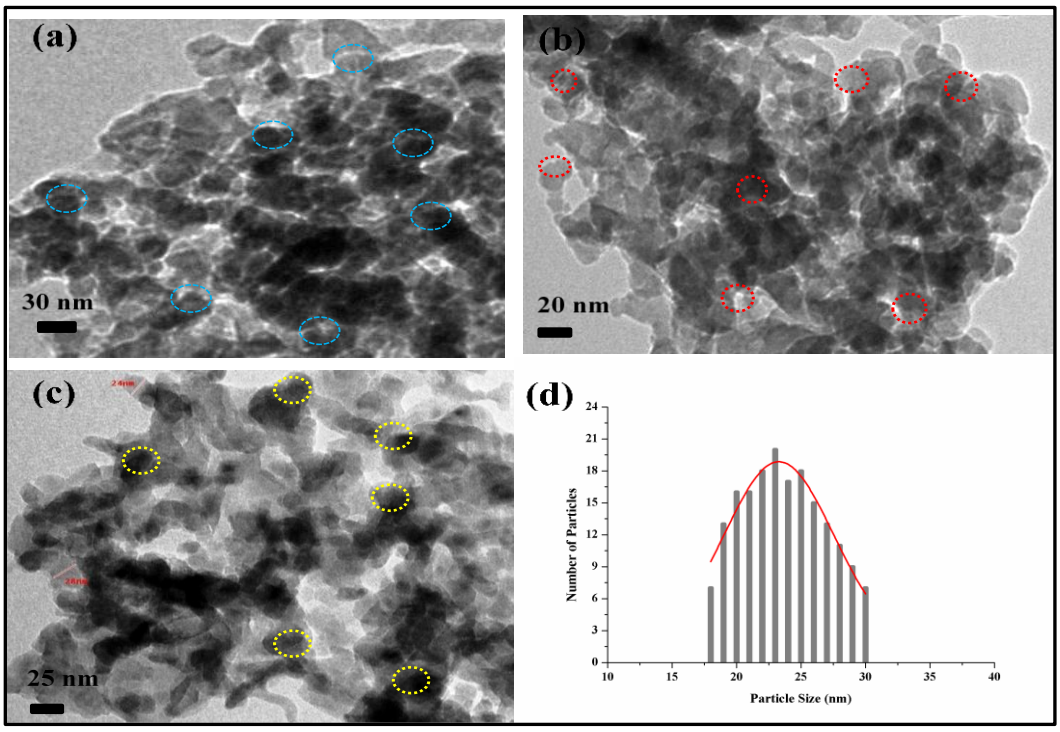

Fig. 4.3: TEM images **(a, b, c)** and **(d)** size distribution of Al_2O_3 nanoparticles

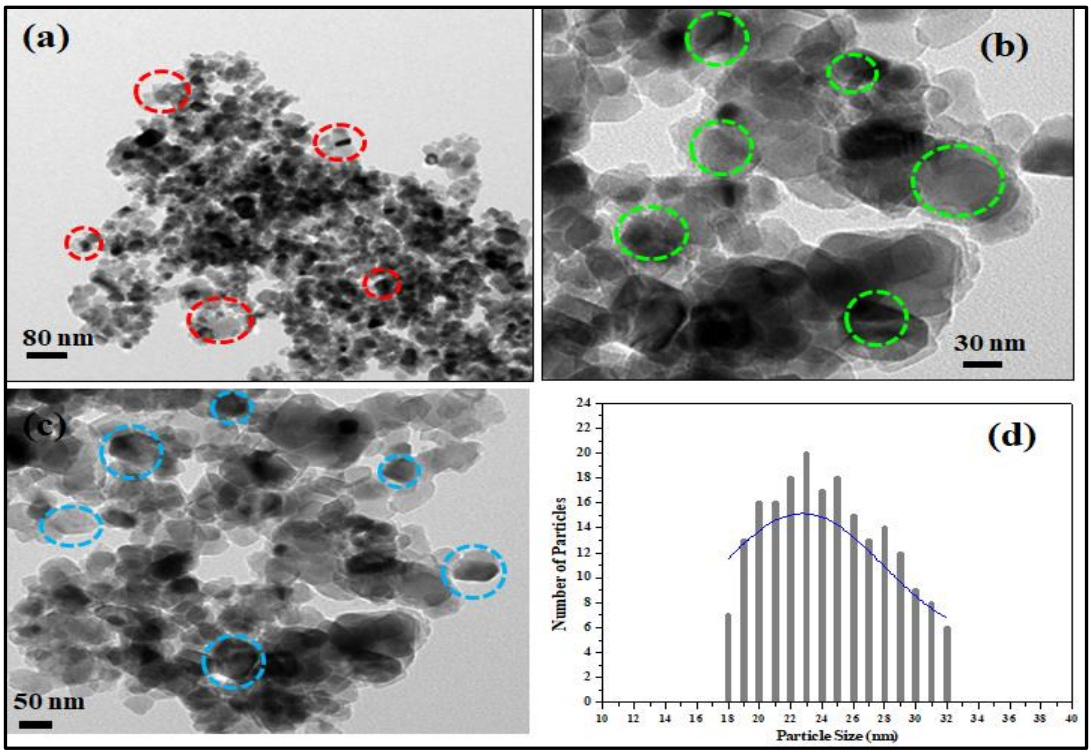

Fig. 4.4: TEM Images **(a, b, c)** and **(d)** size distribution of TiO_2 nanoparticles

TEM images of nanofluid samples

To investigate the stability and morphology of Al_2O_3 and TiO_2 based nanofluids, the various TEM images of the different samples of nanofluids are collected for time ranging from 0 h to 240 h. Samples of Al_2O_3 and TiO_2 based nanofluids are prepared at pH 7.96 and 9.81 and at room temperature and kept under supervision for next 240 hour (240 h). Fig. 4.5 and 4.6 show the average hydrodynamic size of nanocluster just after sonication is turned off (after 3h of sonication). The size of nanocluster is found to be of the order of 50 nm for Al_2O_3-H_2O nanofluid and around 40 nm for TiO_2-H_2O nanofluid. Similarly the size variation of nanoclusters is observed after 120 h and found that nanoclusters have grown from 50 nm to around 250 nm for Al_2O_3-H_2O nanofluid and from 40 nm to around 200 nm for TiO_2-H_2O nanofluid, see Fig 4.7 and 4.8. The same procedure with the same samples of nanofluids was repeated after an elapsed time of 240 h and it is observed that the average size of nanoclusters have become of the order of 320 nm for Al_2O_3-H_2O nanofluids and around 240 nm for TiO_2-H_2O nanofluid, see Fig. 4.9 and 4.10.

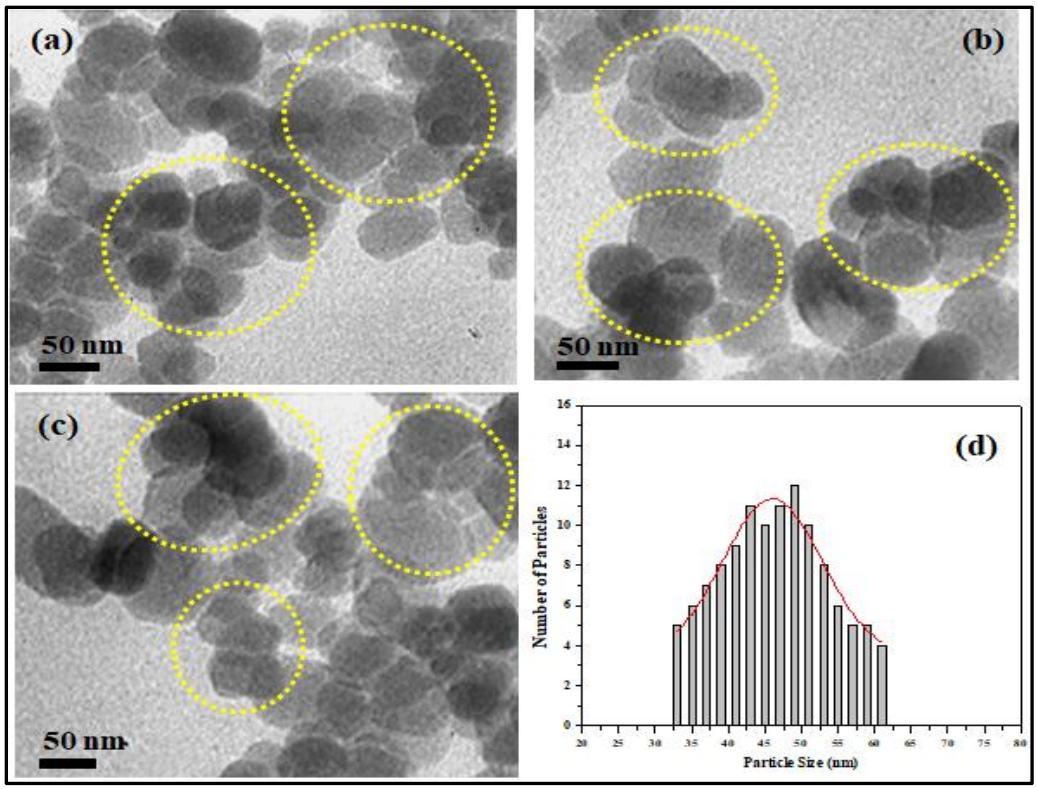

Fig. 4.5: TEM images and size distribution of Al_2O_3-H_2O nanofluid at elapsed time, t = 0 h.

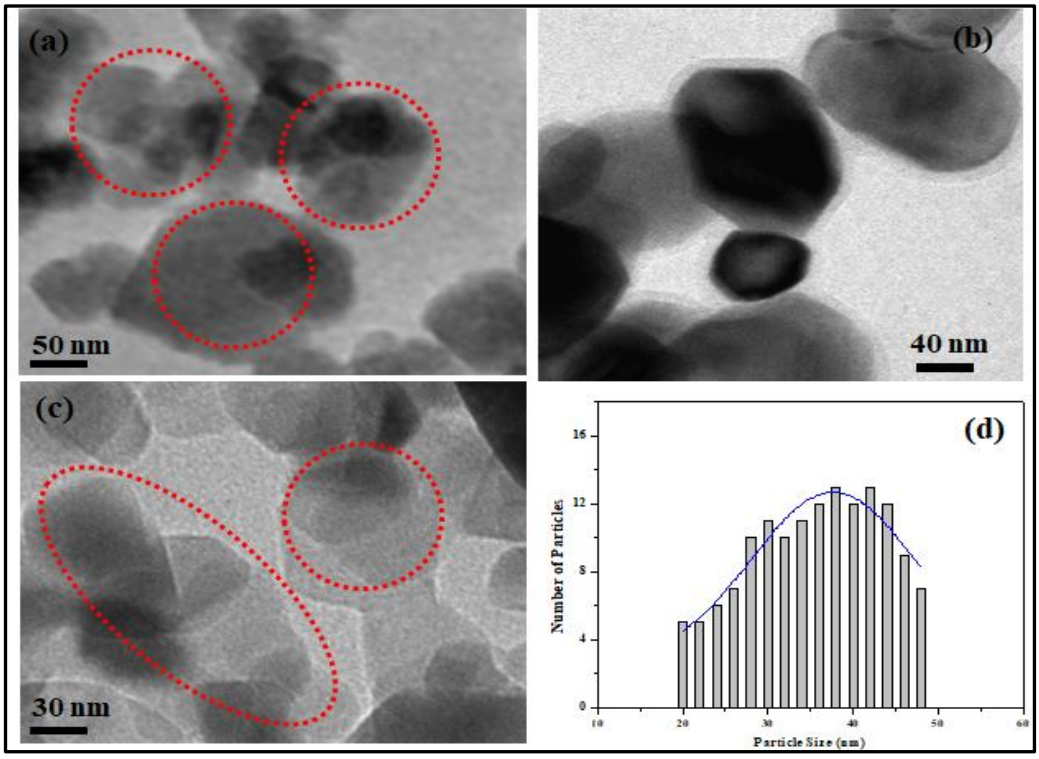

Fig. 4.6: TEM images and size distribution of TiO_2-H_2O nanofluid at elapsed time, t = 0 h.

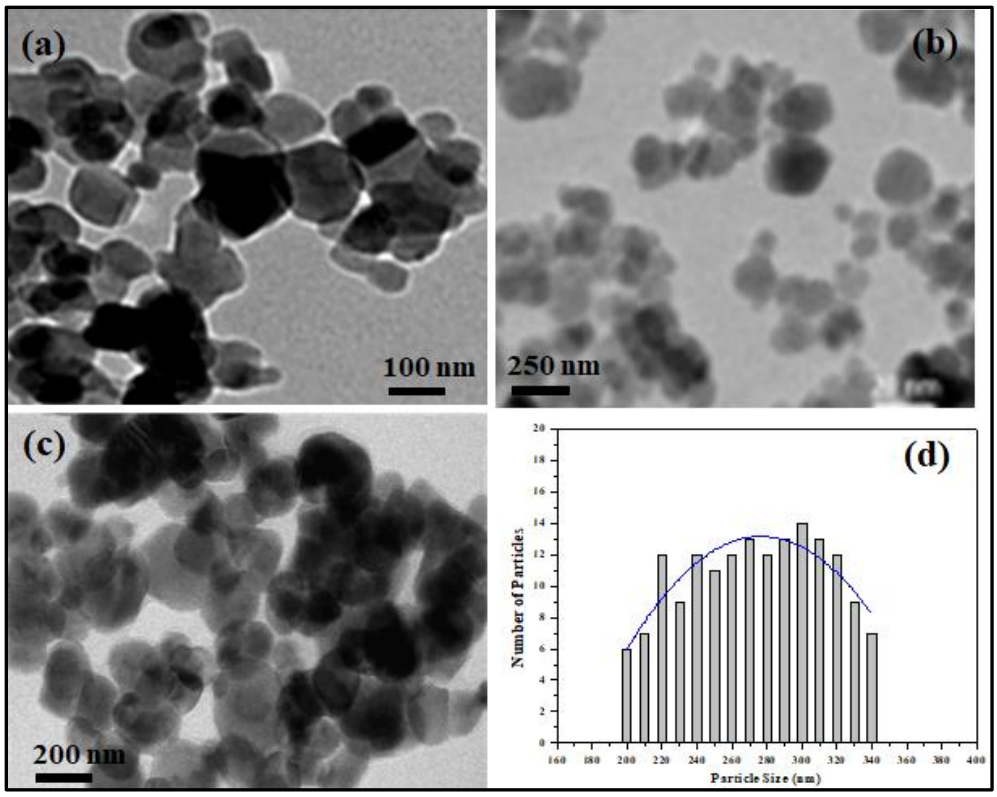

Fig. 4.7: TEM images and size distribution of Al_2O3-H_2O nanofluid at elapsed time, t = 120 h.

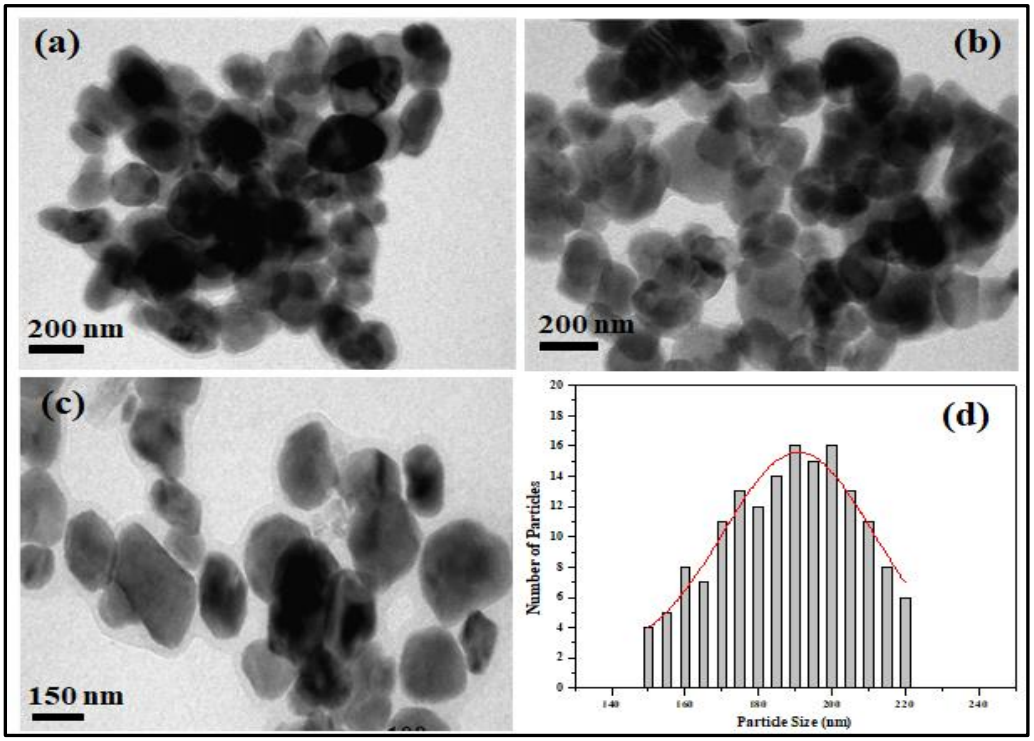

Fig. 4.8: TEM images and size distribution of TiO_2-H_2O nanofluid at elapsed time, t =120 h.

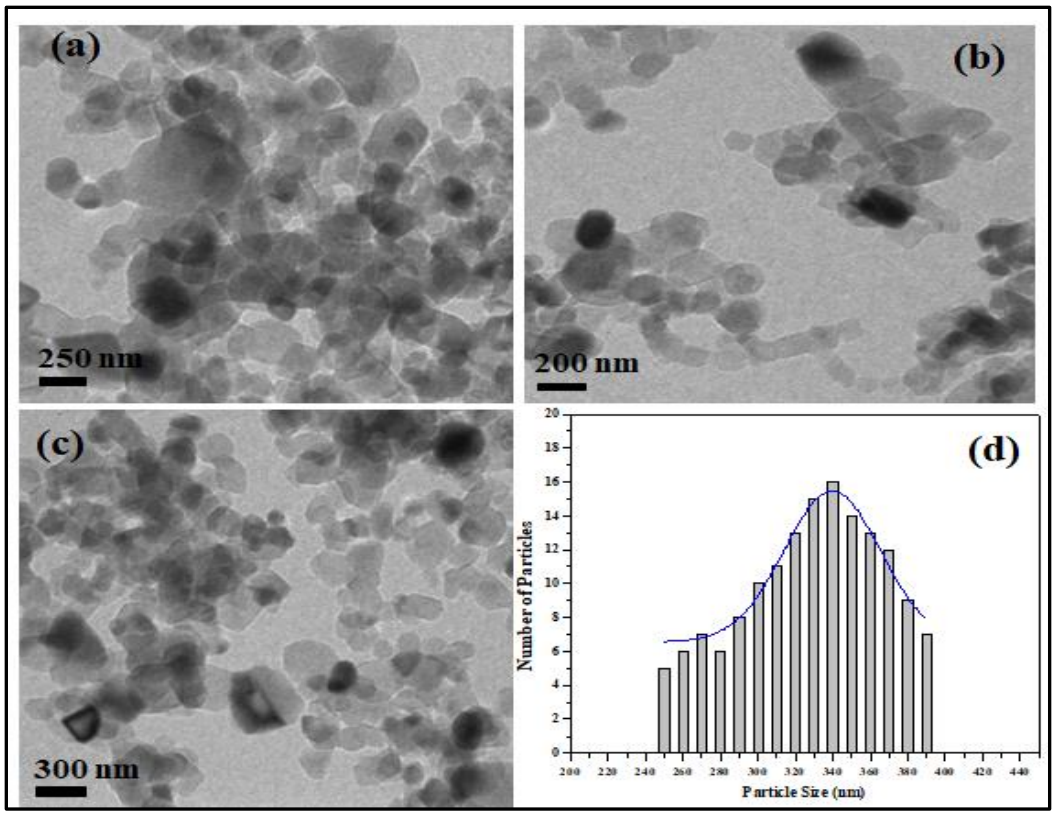

Fig. 4.9: TEM images and size distribution of Al_2O_3-H_2O nanofluid at elapsed time, t = 240 h.

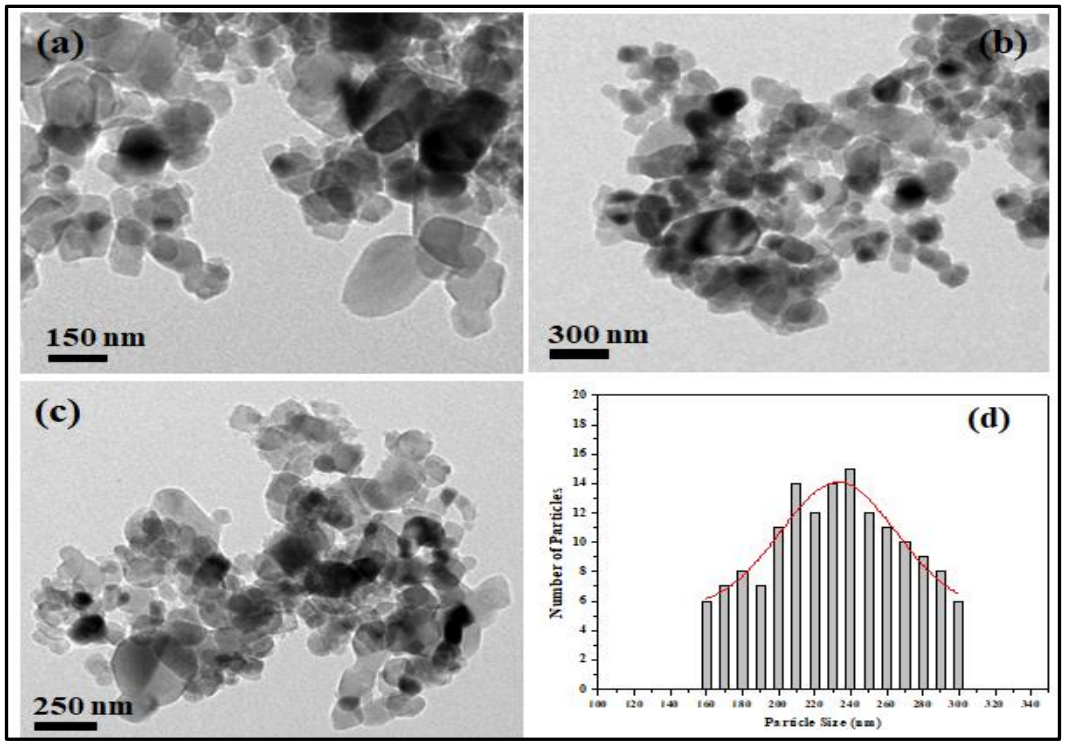

Fig. 4.10: TEM images and size distribution of TiO_2-H_2O nanofluid at elapsed time, t = 240 h.

It is quite evident from the above presented TEM images of Al_2O_3-H_2O and TiO_2-H_2O that nanoparticles do not exist as individual particles (Fig. 4.5 to 4.10). It is very difficult prepare the nanofluids of original nanoparticle size (25 nm). The size of nanoparticles while in suspension is different from the individual particle size. Nanoclusters grow in size with elapsed time, although growth of nanoclusters in Al_2O_3 based nanofluids is comparatively faster compared to their growth in TiO_2 based nanofluids. In other words, nanoclusters of TiO_2 in TiO_2-H_2O nanofluid remain smaller in size and comparatively finer in distribution compared to nanoclusters of Al_2O_3 in Al_2O_3-H_2O. Detail discussion and effect of these nanoclusters on the thermal conductivity enhancement of nanofluids are provided in Chapter 5 and 7.

4.3 Evaluation of Measuring Equipment

4.3.1 Thermal Property Analyzer (KD2 Pro)

Calibration of KD2 Pro has been carried out by measuring the thermal conductivity of two common fluids: (i) distilled water, and (ii) ethylene glycol followed by their comparison with standard data (available literature) (Bohne *et al*., 1984; Ramires *et al.*, 1995; Wagner and Prub, 2002; Beck *et al*., 2007; Fluid Properties, 2011; Pastoriza-gallego *et al.*, 2011). The base fluid samples of 20 ml each were taken in a vial of 20 mm diameter and 70 mm length whose cap was equipped with a septum through which the sensor needle (in an inverted position) could be inserted. The thermal conductivity of water (DI) and EG is found to be increasing with the rise in temperature (10-80°C), see Fig. 4.11 and Fig. 4.12. While working with KD2 Pro (thermal property analyzer), it is observed that the instrument is quite sensitive to the surrounding conditions, vibrations, temperature, position and angle of the sensor needle. With a rise in temperature, the convection effects start dominating and thereby would increase the thermal instability of nanofluid. With the rise in temperature, viscosity of the base fluid drops rapidly. This whole process contributes to a significant rise in the error in measurement of the thermal conductivity. However, the level of accuracy in each case is different and also found to be varying with temperature, see Fig. 4.13 and 4.14. The error between the experimentally measured thermal conductivity for water (DI) and literature data values of thermal conductivities are found to be within ± 5% up to 50°C.

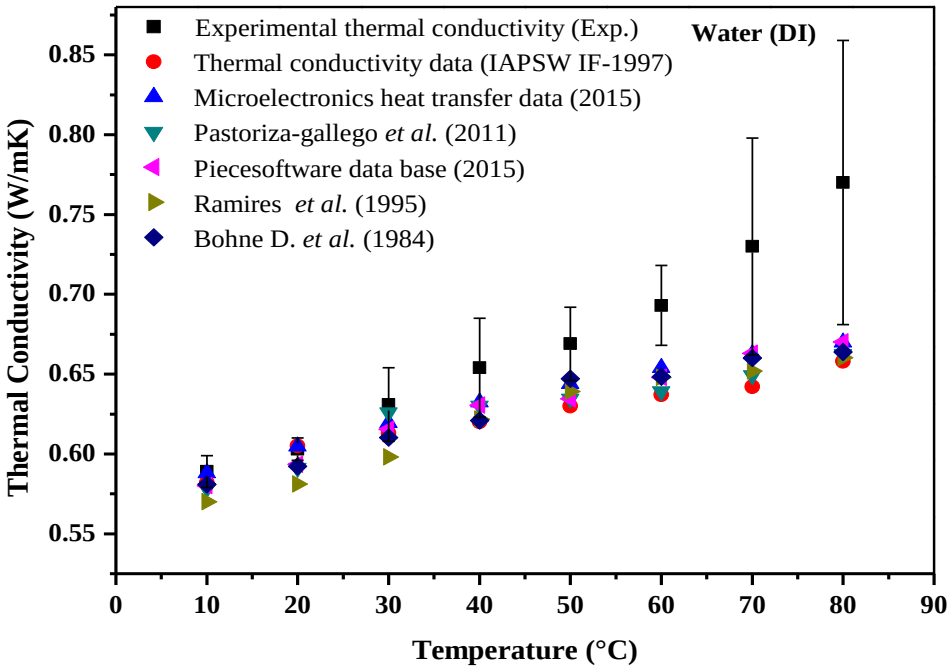

Fig. 4.11: Comparison of thermal conductivity of water (DI) with standard data

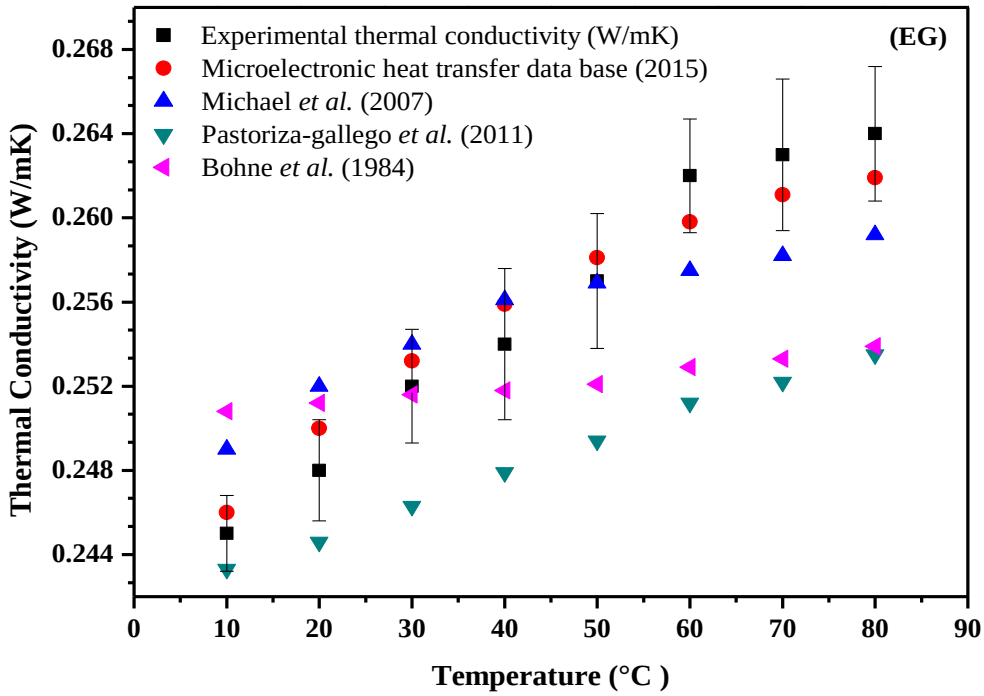

Fig. 4.12: Comparison of thermal conductivity of ethylene glycol (EG) with standard data

This error rises further from 8 to 18%, especially, when water is used as base fluid. Whereas, it remains within ± 5% for EG even up to 80°C. This has also been established by determining the error between the experimental thermal conductivity and the average data value of thermal conductivity (see, Fig. 4.15 and Fig. 4.16). This is because of the higher viscosity of the EG compared to the water which helps to suppress the convection effects and thereby maintains high accuracy (within ± 5%) of thermal conductivity measurements. As a result of this, it can be concluded that the thermal conductivity measurements can be done with reasonable accuracy (± 5%) by maintaining the upper working temperature up to 50°C if the water is chosen as a base fluid. Whereas, in the case of EG as working fluid, readings can be collected even up to 80°C with reasonable accuracy.

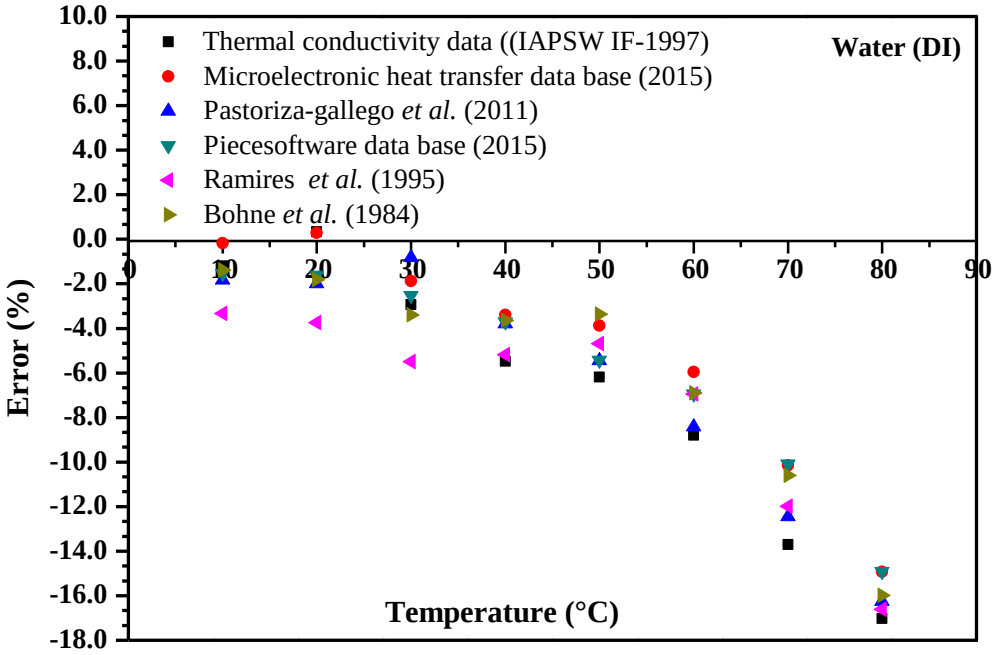

Fig. 4.13: Deviation in the experimentally measured thermal conductivity and the thermal conductivity data available for water (DI) at different temperatures

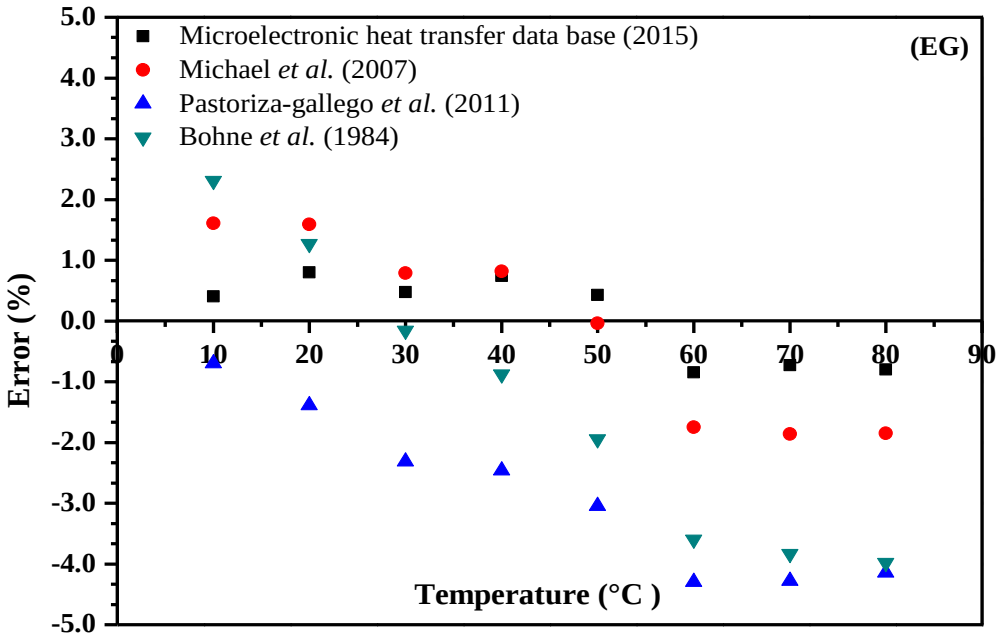

Fig. 4.14: Deviation in the experimentally measured thermal conductivity and the thermal conductivity data available for EG at different temperatures

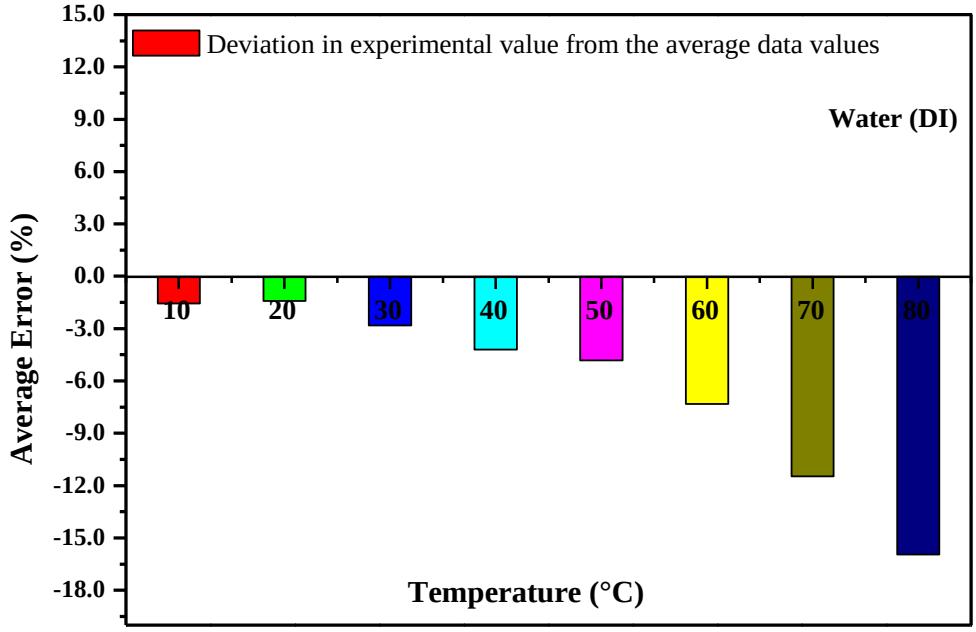

Fig. 4.15: Deviation in the experimental value from the average data value of thermal conductivity available for water (DI)

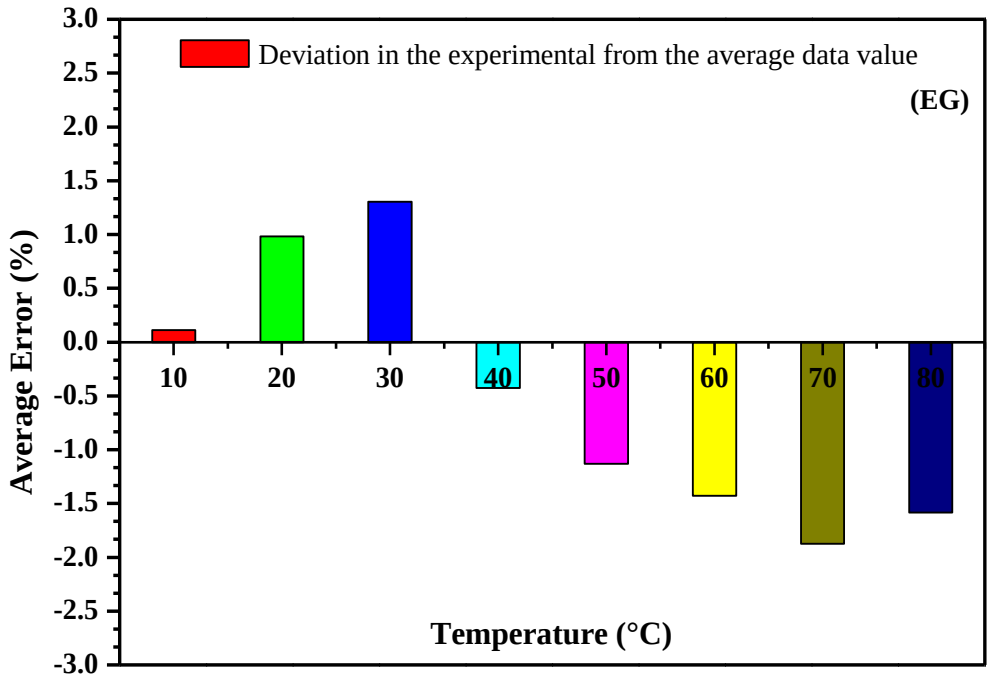

Fig. 4.16: Deviation in the experimental value from the average data value of thermal conductivity available of EG

4.3.2. Thermal Conductivity measuring configurations

While using the KD2 Pro for thermal conductivity measurements, it has been observed that the measurement results depend on the position and measuring angle of its sensor needle. However, the volume of the nanofluid sample, i.e., sample size (length and diameter of the sample) are also required to be optimized as per the KD2 Pro requirements. Nanofluid will be wasted if too large sample size is taken, on the other hand, the accuracy of the instrument will be compromised if too small sample size is chosen. A brief discussion of these issues is as follows.

(i) The selection of the right size of vial (filled with base fluid/ nanofluid), i.e., the effect of length and diameter on thermal conductivity measurements

The vials of different sizes such as 100 × 20, 100 × 30, 100 × 50, 150 × 20, 150 × 30, and 150 × 50 (length × diameter, all in mm) have been investigated to learn the level of accuracy and precision maintained while measuring the thermal conductivity of water (DI).

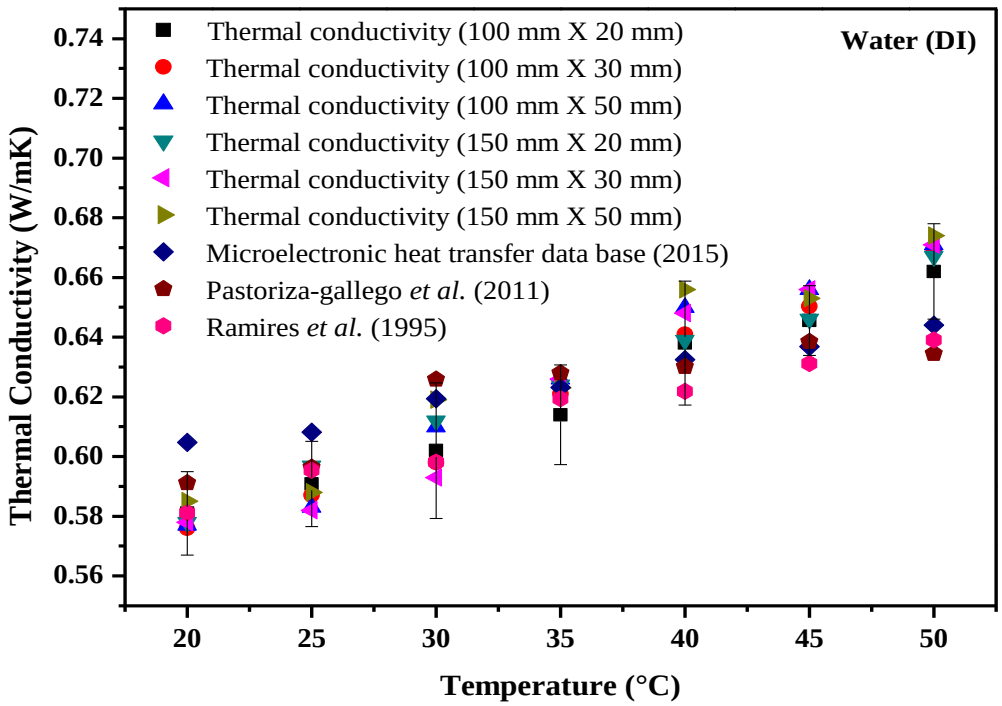

Fig. 4.17: Effect of varying vial size (length and diameter) on thermal conductivity measurements

The fluid sample size or vial size does not seem to have much effect on accuracy level of thermal conductivity measurements. When measured thermal conductivity is compared with its literature standards data at different temperature (20-50°C), the error is found to be within ± 5%, see Fig. 4.17 and Fig. 4.18. It seems that there is no cap on the quantity of fluid sample to be taken for investigations. However, a minimum volume of the nanofluid sample should be prepared for the investigations as per the requirements of a sensor needle. This will bring down the preparation cost of the nanofluid samples. At the same time, the volume should be not too less, otherwise lots of instabilities will be generated in the base fluids/nanofluids samples and which intern might affect the accuracy of the equipment.

whre

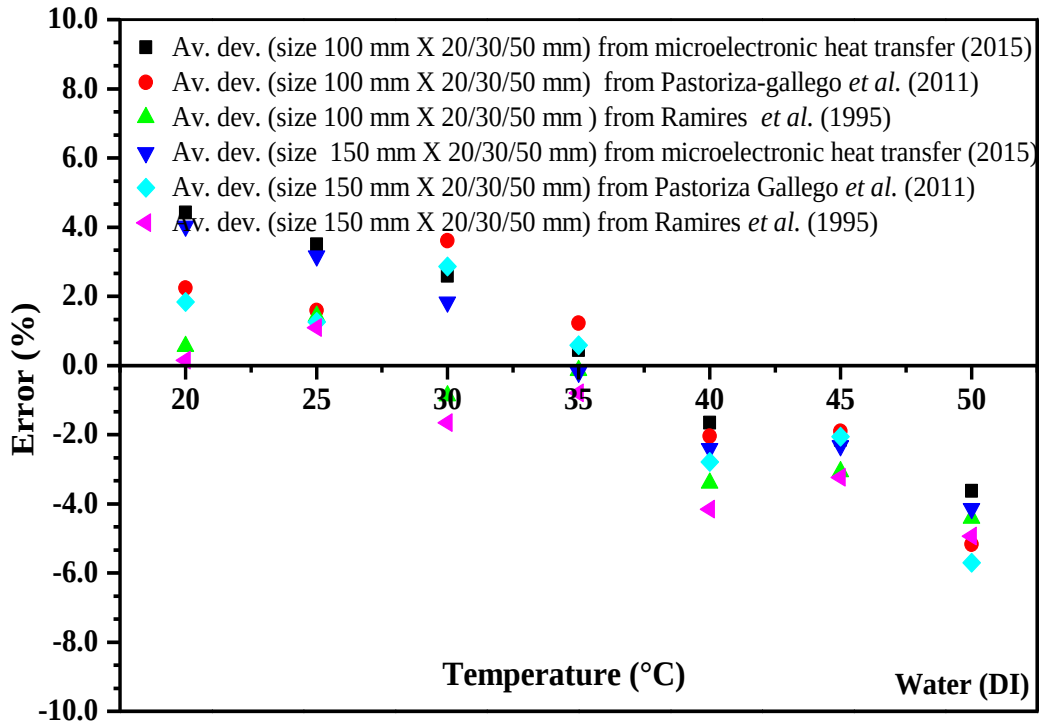

Fig. 4.18: Effect of varying vial size on the thermal conductivity measurements and its deviation from the standard data value

(ii) The position of the needle sensor, i.e., the effect of inclination angle (angle with vertical) on the thermal conductivity measurements

The sensor needle of KD2 Pro is needed to be held vertically while taking the thermal conductivity measurements. The investigations conducted by varying the inclination angle show that the level of accuracy obtained in thermal conductivity measurements is angle dependent. The thermal conductivity of various samples of water (DI) at different temperature (20-50°C) is measured experimentally by setting the sensor needle at different angles (2° to 30°), see Fig. 4.19.

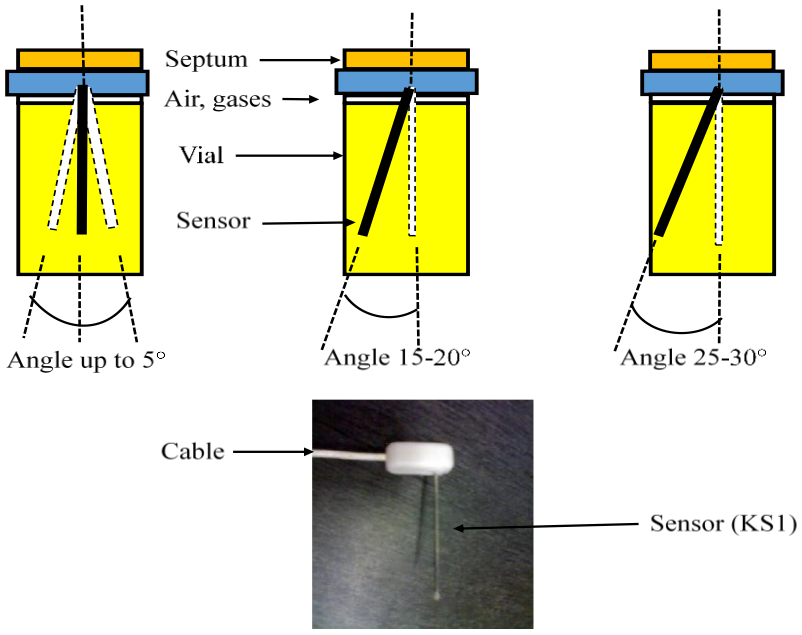

Fig. 4.19: The various angular positions of the sensor needle (with vertical) and thermal conductivity measurements

The obtained results are compared with the standardly available literature. It has also been observed that as the angle is increased, the disturbances in the surrounding fluid too increases. Therefore, the surrounding fluid is no more in a stationary stage, rather than the convection effects start coming up into the picture. At lower temperature range i.e. up to 25°C, these convection effects are not very high and the measurements can be taken with reasonable accuracy, i.e., ± 5%, see Fig. 4.20 and Fig. 4.21. As the temperature increases, these convection effects also increase. The increase in the angle of the sensor needle further inflates the instability level of the fluids, which ultimately decrease the accuracy level of the equipment.

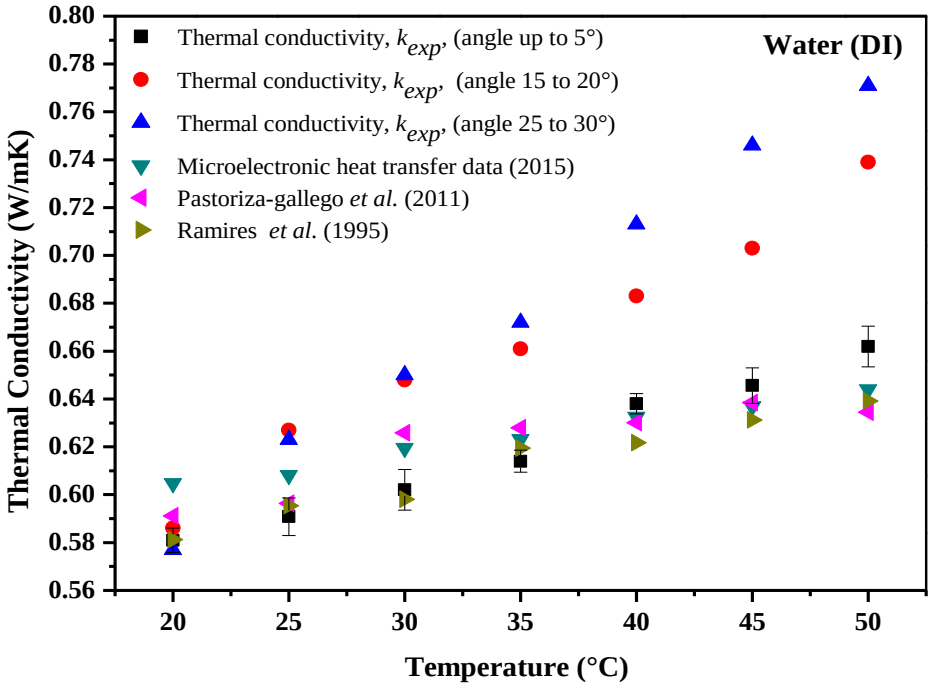

Fig. 4.20: Effect of angle (with vertical) on thermal conductivity measurements

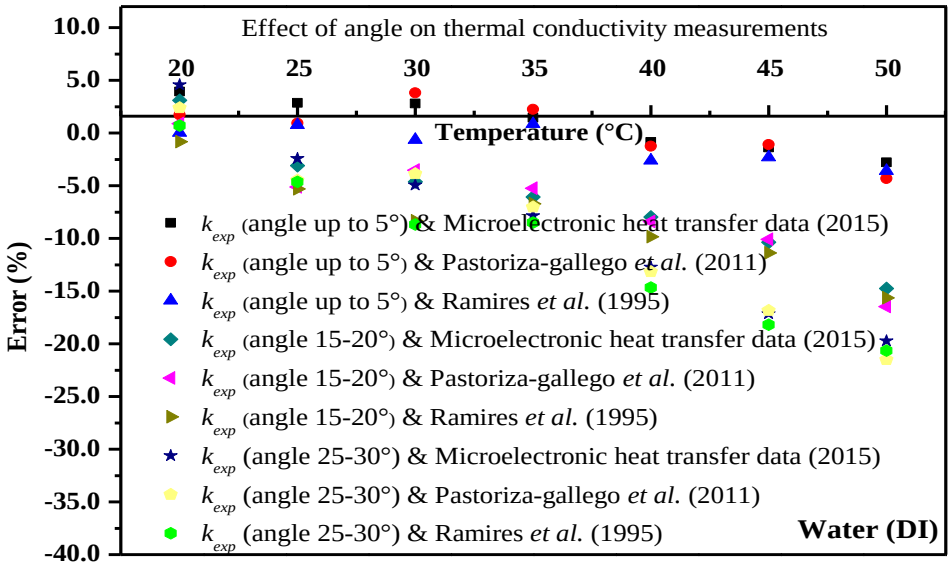

Fig. 4.21: Effect of angle (with vertical) on the thermal conductivity measurements and its deviation from the standard data values

(iii) Inverted position of the sensor needle i.e. effect of sensor position on the thermal conductivity measurements

When the sensor needle of KD2 Pro is kept in normal position while measuring the thermal conductivity, the gases remain on the upper side of the vial, see Fig. 4.22.

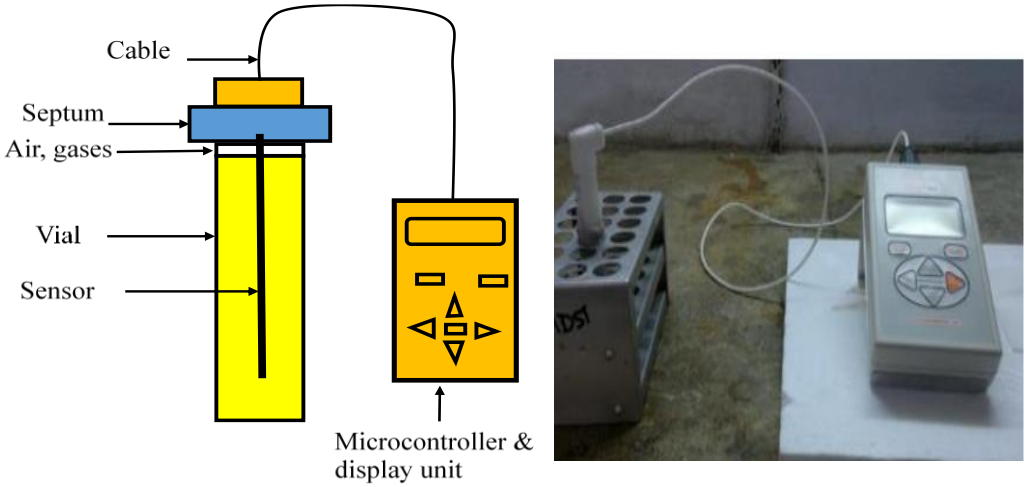

Fig. 4.22: Normal position of sensor needle and thermal conductivity measurements

These gases are in direct contact with the sensor needle. Moreover, the cap equipped with a septum through which the sensor needle is inserted acts as a source of error. Due to this, a particular portion of the total length of sensor needle i.e. 10-15 mm out of 60 mm does not come in contact with the base fluid whose thermal conductivity is to be measured. The accuracy level of the equipment gets more deteriorated at higher temperatures as the hot entrained gases produce more convection effect. This is also quite evident from the Fig. 4.23. To minimize the reported error while measuring the thermal conductivity, a solution is thought off, i.e., to use the sensor needle in the inverted position, see Fig. 4.22. Due to this, the entrapped gases in the vail will not be able to come in contact with the sensor needle. This will also bring down the error in thermal conductivity measurements, see Fig. 4.24. The error produced while measuring the thermal conductivity at different temperatures lies within ± 5% for sensor needle used in an inverted position, see Fig.

4.25. On the other hand, the sensor needle of KD2 Pro used in normal positions introduces a significant error in thermal conductivity measurement. i.e. ± 6% to ± 18%.

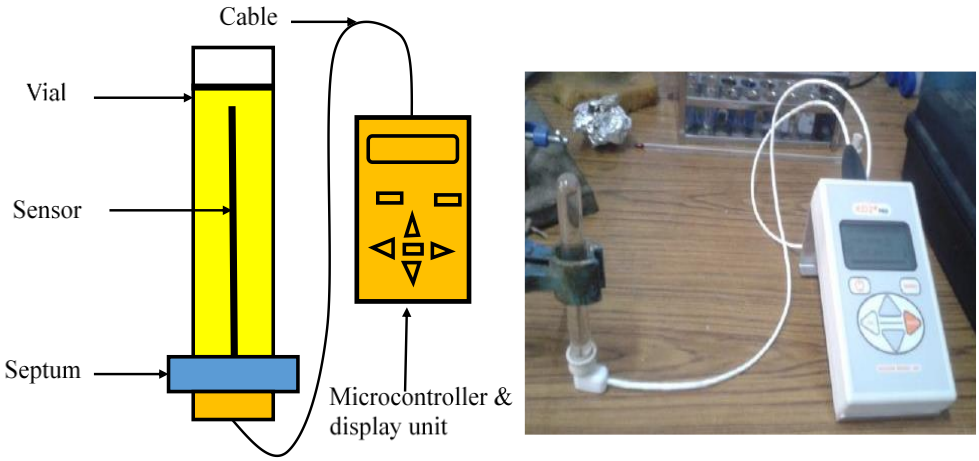

Fig. 4.23: Inverted position of sensor needle and thermal conductivity measurements

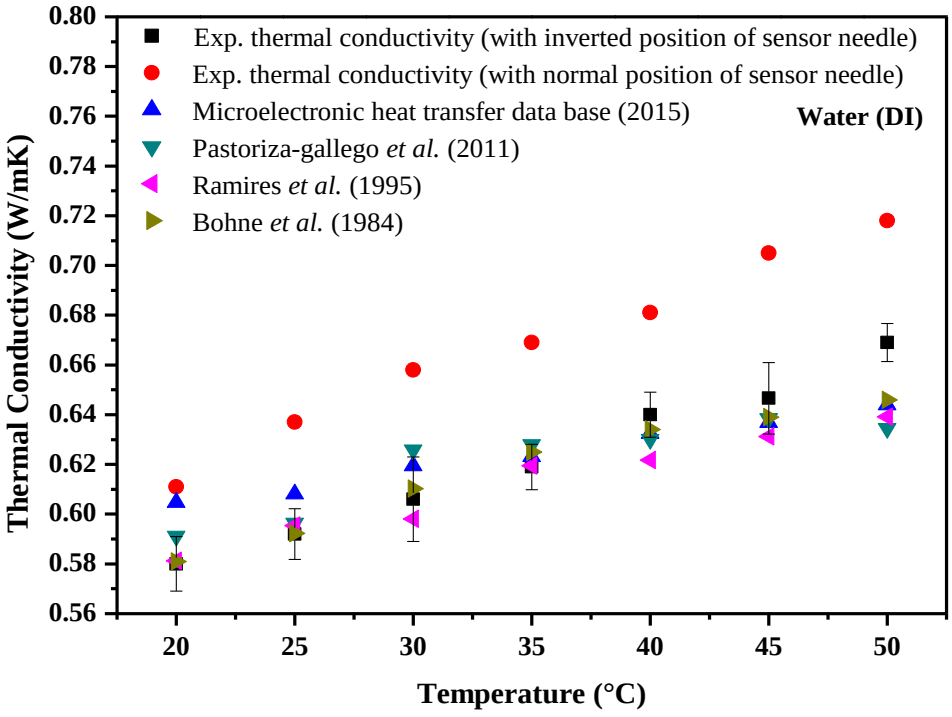

Fig. 4.24: Effect of position of sensor needle (inverted/normal) on thermal conductivity measurements

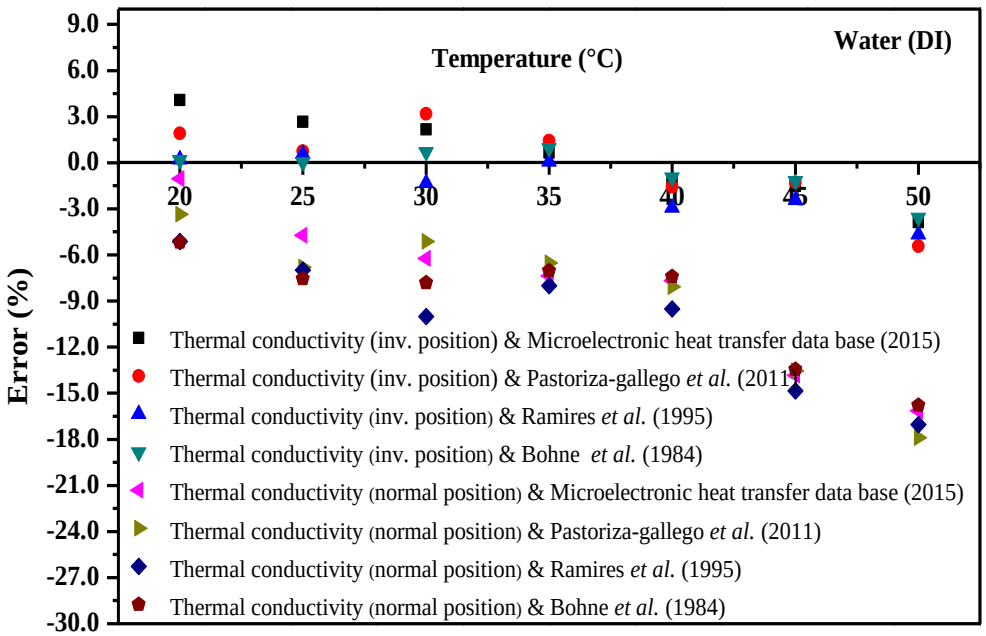

Fig. 4.25: Effect of position of sensor needle (inverted/ normal) on the thermal conductivity measurements and its deviation from the standard data values of thermal conductivity

After conducting the different experiments, following conclusions are drawn regarding the use of KD2 Pro for reasonable accuracy to measure the thermal conductivity of base fluids/ nanofluids.

(i) The needle should be inserted fully into the fluid, oriented vertically and centrally inside the vial without touching the side walls of the vial. It will help in minimizing the errors arising from free convection.

(ii) The vial filled with nanofluid/fluid was turned upside down so that any bubbles in the fluid would float to the top and away from the needle. This will ensure the proper contact between the sensor needle and fluid whose thermal conductivity is to be measured.

(iii) The vial size is found to have a negligible effect on the thermal conductivity measurements. A minimum volume of nanofluid/fluid sample should be used while taking the thermal conductivity measurements. However, too small volume of samples is more prone to the errors produced due to the thermal/mechanical instabilities.

4.3.3 Rheological Study

The viscosity of the various samples of nanofluids is measured using a Brookfield LVDV-III Ultra Viscometer (Cone Spindle CPE-42) supplied by Brookfield Engineering Laboratories of USA (specifications provided in Table 4.2).

Table 4.2: Characteristics of LVDV-III Ultra Viscometer (Cone Spindle, CPE-42)

Model	**Spring Torque (mN/m)**	**Number of Spindle**	**Speed range (rpm)**	**Goss weight**
LVDV-III Ultra (C/P)	0.0673	A spindle wrench, one cone spindle and sample cup Part No. CPE-42	1-250	14.5 kg
Temperature Sensing Range (°C)	Viscosity Accuracy	Viscosity Repeatability	Temperature Accuracy (°C)	Operating Environment (Temp. °C & R.H. %)
- 100 to 300	± 1.0% of full scale range	± 0.2%	± 1.0 (-100 to +150), ± 2.0 (+150 to +300)	0 to 40 °C, 20% to 80%

Before using LVDV-III Ultra Viscometer (Cone Spindle CPE-42), it has been calibrated for its accuracy using standard fluids such as; distilled water (DI) and ethylene glycol (EG). In order to maintain the maximum possible accuracy in the calibration test, viscosity at each temperature is measured at different shear rates and multiple reading were collected. Afterwards, the average value of these measurements is taken as the viscosity of the sample at a particular temperature. The equipment is calibrated by using a water bath maintained at 20-50 ºC. The water (DI) and EG seems to be good options to test the accuracy of the instruments as it involve the testing of

equipment with low and high viscosity fluids. In Fig. 4.26, the variation in the experimentally measured viscosity of water (DI) has been shown against temperature and is also compared with literature standards (Korson *et al.*, 1969; e-Fundamentals., 2011; Fluid Properties, 2011).

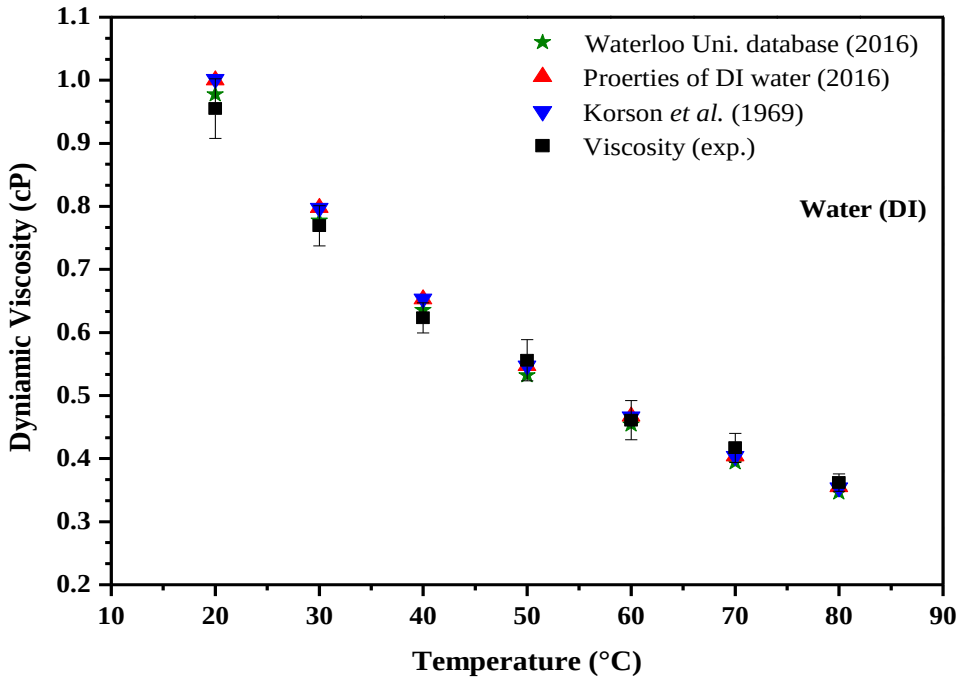

Fig. 4.26: Calibration of LVDV-III Ultra Viscometer Cone Spindle CPE-42, with water (DI)

Similarly, in Fig. 4.27, the viscosity of ethylene glycol (EG) has been compared with the standard data available in the literature (Yang *et al.*, 2003; Fluid Properties, 2011; Pastoriza-gallego *et al.*, 2011; Jamshidi *et al.*, 2012). The plots show that for water (DI) and for ethylene glycol (EG), the accuracy of LVDV-III Ultra Viscometer (Cone Spindle CPE-42) is well within ± 5%, see Fig. 4.28 and Fig. 4.29. However, the magnitude of the average error varies with temperature, shown in Fig. 4.30 and Fig. 4.31. Hence, the calibration of viscometer with certain benchmarked fluids at different temperatures and by comparing literature values with experimental results have helped in evaluating LVDV-III Ultra Viscometer for its accuracy and precision which is found to be well within ± 5%.

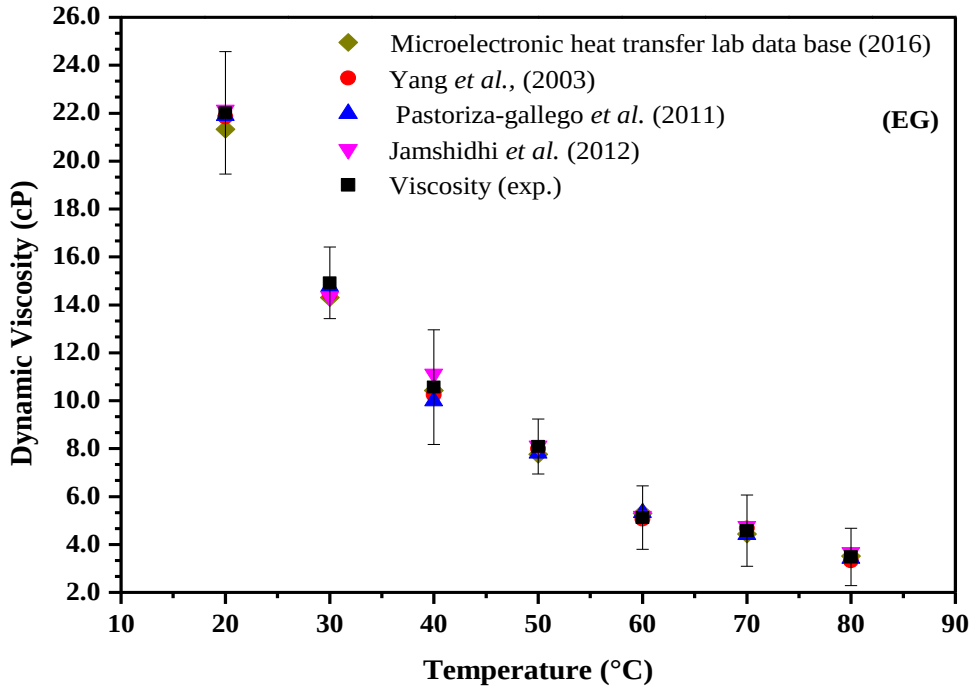

Fig. 4.27: Calibration of LVDV-III Ultra Viscometer Cone Spindle CPE-42, with ethylene glycol (EG)

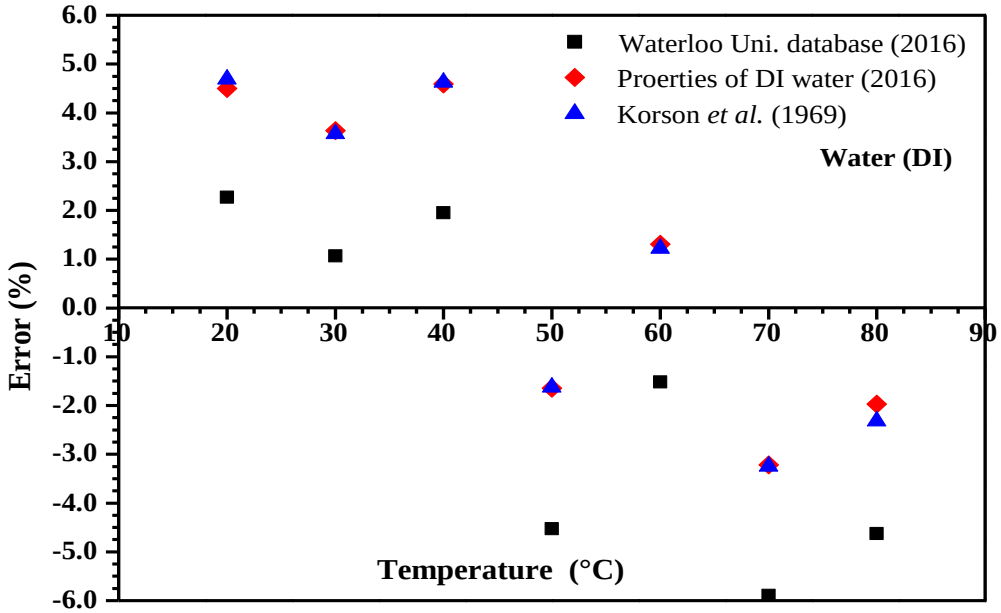

Fig. 4.28: Error analysis of LVDV-III Ultra Viscometer (Cone Spindle CPE-42) with water (DI)

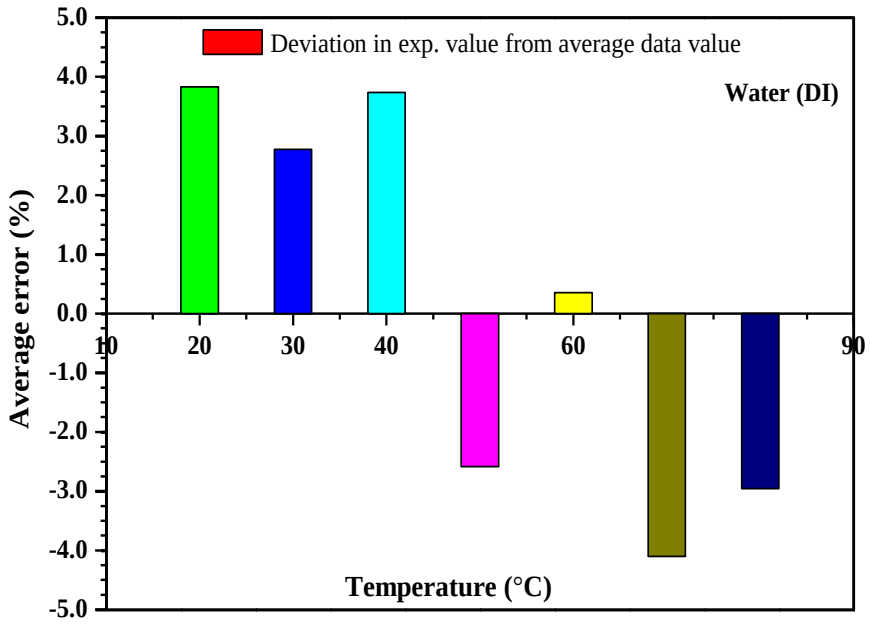

Fig. 4.29: Deviation in the experimental value (LVDV-III Ultra Viscometer, Cone Spindle CPE-42) from the average data value of dynamic viscosity of water (DI)

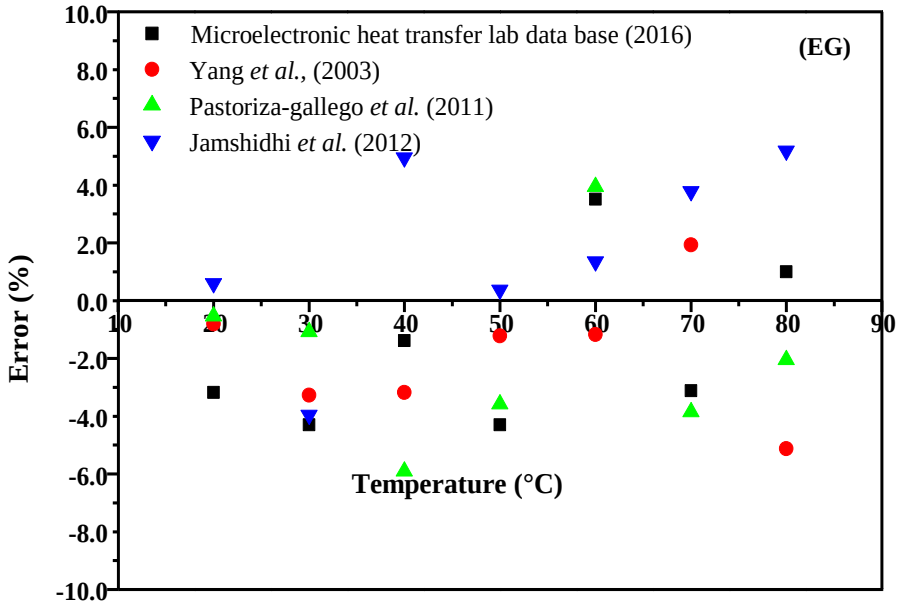

Fig. 4.30: Error analysis of LVDV-III Ultra Viscometer (Cone Spindle CPE-42) with EG

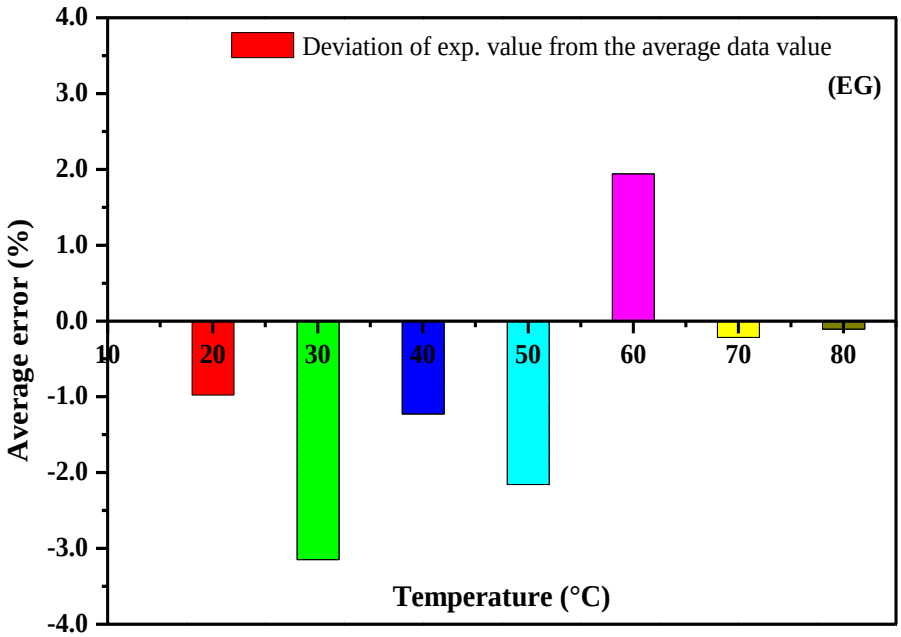

Fig. 4.31: Deviation in the experimental value (LVDV-III Ultra Viscometer (Cone Spindle CPE-42) from the average data value of dynamic viscosity of EG

The distribution and arrangement of the nanoparticles while in suspension affect the thermophysical properties of nanofluids beside other primary parameters, such as the shape and size and volume fraction of nanoparticles. In addition to this, the properties of host fluid such as density, viscosity, specific heat and its own thermal conductivity also play a significant role to determine the thermophysical property of any nanofluid. As far as the viscosity and rheology of the nanofluid are concerned, these do have effects on the suspension quality of nanofluids. Viscosity helps nanoclusters to remain in suspension over longer time period. As a result, this will strengthen the heat transport capacity of nanofluid. Higher the viscosity, longer is the stability of nanofluid. However, selecting the host fluid of higher viscosity will have the negative impact on the overall performance of any nanofluid working as a coolant.

Chapter-5

Modeling Thermal Conductivity through Response Surface Methodology (RSM)

Nanocluster formation is inevitable especially when nanofluids are prepared through Two-Step Method. This fact is found to be proved many times during the experimental investigations. Therefore, it is quite evident that the thermal conductivity of such nanofluids is very much dependent on the formation and the behavior of these nanoclusters. An attempt has been made here to model and optimize the nanocluster based thermal conductivity using a response surface methodology (RSM) technique based on the Design of Experiment (DOE) approach. This method optimizes the required number of experimental runs required to model the thermal conductivity of nanofluid under the given set of affecting parameters.

5.1. Prediction and Optimization of Nanoclusters Based Thermal Conductivity of Nanofluids: Application of Box–Behnken Design (BBD)

5.1.1. Design of experiments and response surface method (RSM)

In spite of potential advantages of the nanofluids, lack of fundamental understanding of the behavior of nanofluids causes inability to reliably model and predict the thermal conductivity enhancements of nanofluids. Researchers have proposed various factors which could be contributing to the thermal conductivity enhancements of nanofluids. In nanofluid suspensions, individual nanoparticles tend to combine with each other to form nanoclusters (Prasher *et al*., 2006). This is a common occurrence observed, when nanofluids are prepared by Two Step Method and where the nanoparticle surfaces are not forming the active bonding with the molecules of the base fluids (Das *et al.*, 2007; Mallick *et al.*, 2013; Mishra *et al.*, 2014). Clustering of nanoparticles occurs more actively in nanofluids possessing a higher volumetric concentration of nanoparticles. As a result of this, the smaller inter-particle distance between the particles increases their probability of agglomeration due to van der Waals attraction (Keblinski *et al.*, 2002; Prasher *et al.*, 2006). This emphasizes the need to study the behavior of nanoclusters in the form of nanoclusters rather than the individual nanoparticles. The modelling and optimization of the nanocluster based thermal conductivity have been achieved through response surface methodology (RSM) technique. The “Design of Experiments” method optimizes the number of experiments required to be performed to achieve a particular objective (Box and Wilson, 1951). An optimization technique

called “Response Surface Methodology (RSM)” which comprises of a statistical method including Box-Behnken design (BBD) has been used for model building and exploitation (Box and Hunter, 1957). The BBD under RSM allows the identification and quantification of interactive effects of various parameters. However, in the knowledge of the authors, there are no reports available in the literature on the optimization of the thermal conductivity of nanofluids and its operating parameters using the above mentioned method. In the presented work, the thermal conductivity of Al_2O_3-H_2O nanofluid has been modeled using BBD under RSM by taking volumetric concentration, temperature and surfactant amount as the contributing factors.

5.1.2. Nanofluid preparation and agglomeration study

Characterization of nanomaterial and samples of Al_2O_3-H_2O nanofluid was done at the room temperature (25ºC) using X-Ray diffraction (XRD), and Dynamic Light Scattering (DLS) technique. In order to study the effect of sonication time on the stability of the suspensions, few samples of Al_2O_3-H_2O nanofluid of volume concernation 0.01, 0.05, and 0.1% were prepared and sonicated continuously for three to six hours without using any surfactant or additive. A significant amount of agglomeration was seen in these samples after sonication was turned-off, see Fig. 5.1 (a), (b).

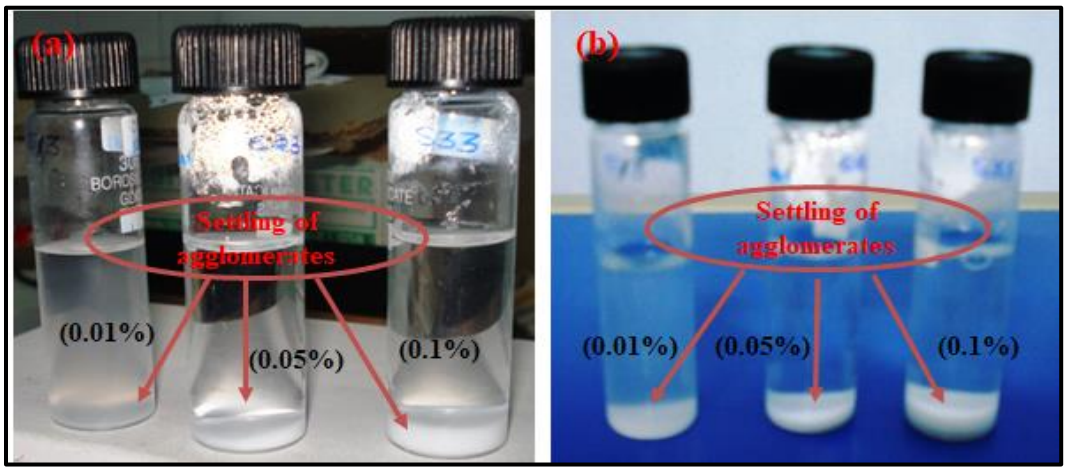

Fig. 5.1: Effect of sonication time on suspension quality of Al_2O_3-H_2O nanofluid after **(a)** three hours of sonication and **(b)** six hours of sonication

After confirming the fact that there is a very high tendency among the nanoparticles to form agglomerates, few more samples of Al_2O_3-H_2O nanofluid were preapred with volume concentartion of 1 to 4%. All these samples were investigated for their particle size distribution using DLS. The DLS results of samples revealed that the hydrodynamic average size of nanoclusters is varying from 900 to 1800 nm for different concentration of Al_2O_3 in DI water, see Fig. 5.2. The nanoparticle clusters of such sizes are prone to agglomerate and also make the suspension highly unstable. The poor dispersion quality is due to the agglomeration and settling of nanoparticles and the interaction between hydroxyl groups present on the surface. This results into trapping of small particles (20 nm) into a large cluster, a high surface-to-volume ratio and a strong van der Waals interaction amongst the particles. The nanofluids with such features are rarely useful for their practical applications unless their stability is improved and the average size of the nanoclusters is reduced.

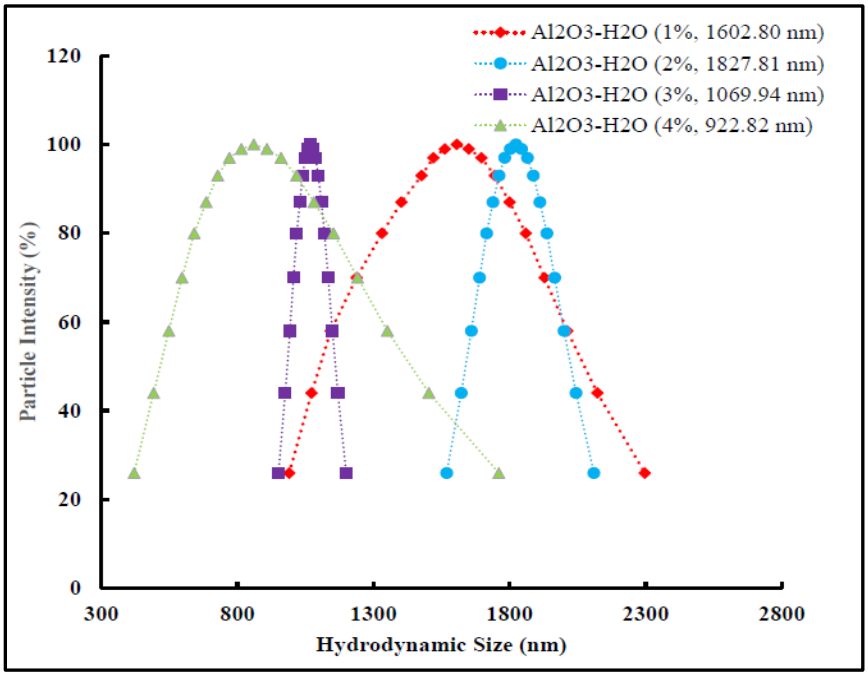

Fig. 5.2: DLS results of Al_2O_3-H_2O nanofluid (without surfactant)

In order to enhance the suspension quality and stability of Al_2O_3-H_2O nanofluid, suitable surfactants are required to be added. To justify the use of a particular type of a surfactant for Al_2O_3-H_2O nanofluid, various surfactants, such as cetyltrimethyl ammonium bromide (CTAB), sodium

dodecyl sulfate (SDS), poly-vinyl pyrrolidone (PVP), triton X100 and oleic acid have been tested. To study the effect of a surfactant on the stability and suspension quality of Al_2O_3-H_2O nanofluid, samples of volume concentration 0.01, 0.5, and 1% were preapred using surfactant, SDS. The suspensions of these samples were found to be stable even after three hours of sonication, see Fig. 5.3 (b). The Fig. 5.3 (a) and (b) have clearly demonstared the effect of using a surafacnat on the stability and suspansion quality of a nanofluid (Al_2O_3-H_2O). Moreover, the nanofluids with such good suspension qualities are considered more useful for their practical applications.

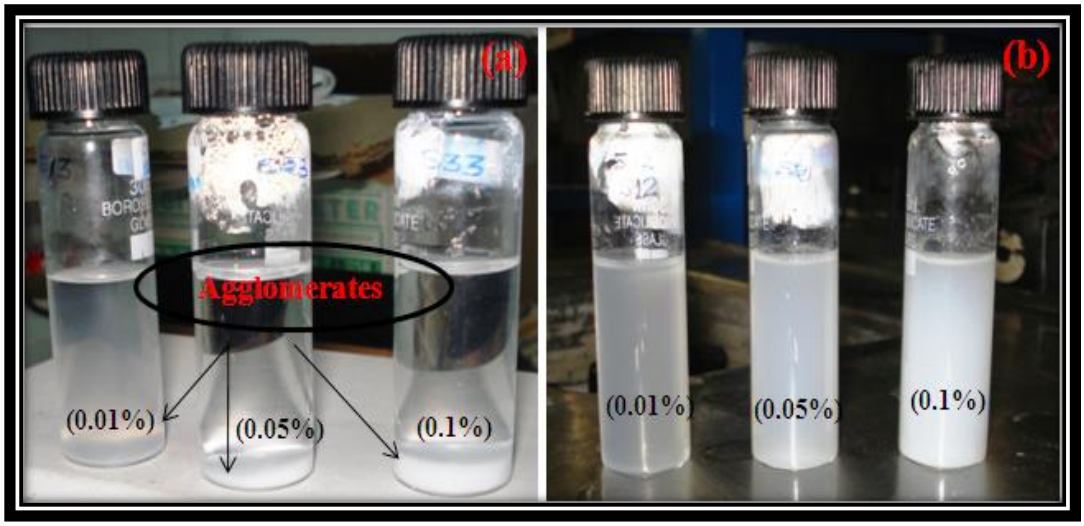

Fig. 5.3: Dispersion quality of Al_2O_3 (γ) in DI water (0.01, 0.05 and 0.1% by volume) **(a)** without surfactant and **(b)** with surfactant (SDS) after three hours of sonication

The indivisual samples of Al_2O_3-H_2O nanofluid (1% and 4% volume concentartion) with each surfactnat were also tested for their thermal conductivity ehnacements. The data on thermal conductivity of Al_2O_3-H_2O nanofluid samples was recoreded using KD2 Pro at different time intervals i.e up to 120 minutes. The following observations are made by analyzing the Fig. 5.4 and Fig. 5.5, (i) Out of various surafcants, SDS is found to have a significant effect on the stability and thermal conductivity enhancement of Al_2O_3-H_2O nanofluid (ii) at higher particle volume concentartion i.e. 4%, the enhancement in the thermal conductivty drops, although the decrease is not very significant. In additon to the above reported facts, the effect of SDS on the nanoparticle size distribution of Al_2O_3-H_2O nanofluid is also studied using DLS where the average size of the

nanoclusters is found to be reduced to less than 200 nm, see Fig. 5.6. Fig. 5.6 also confirms that while in suspension, the nanoparticles of Al_2O_3-H_2O nanofluid are not being reduced to their primary size (20 nm) however, exist in the form of nanoclusters.

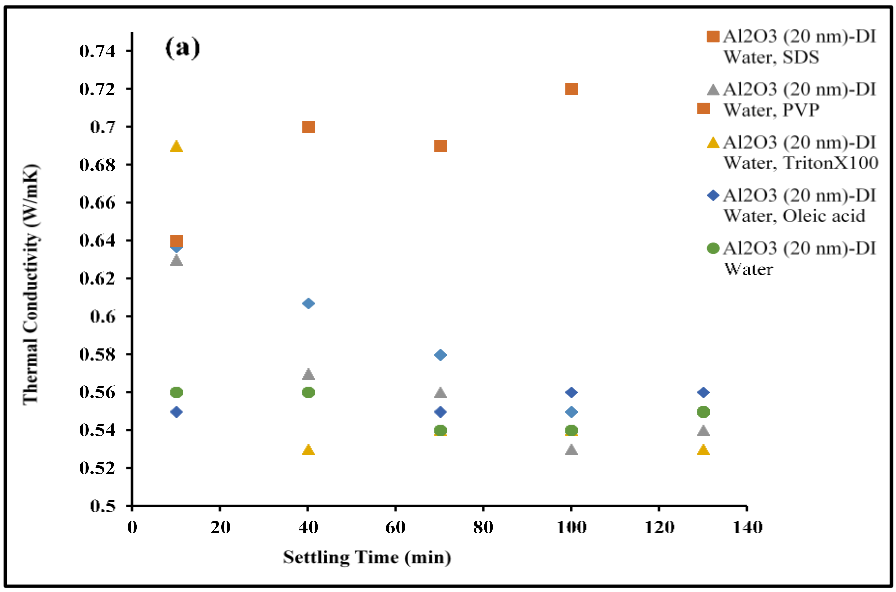

Fig. 5.4: Effect of surfactants on the stability and thermal conductivity of Al_2O_3-H_2O nanofluid at 1% volume concentartion of Al_2O_3 and surfactant

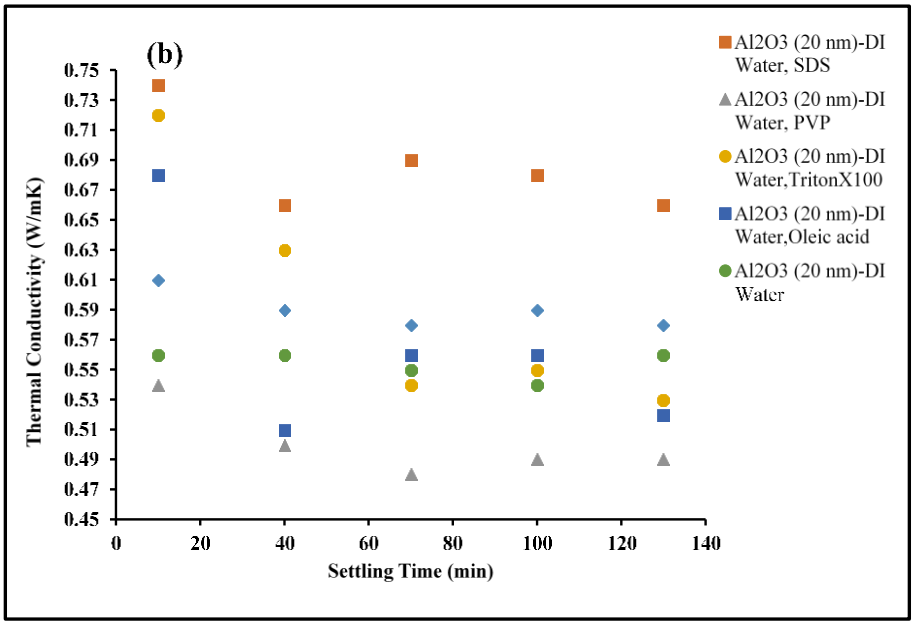

Fig. 5.5: Effect of surfactants on the stability and thermal conductivity of Al_2O_3-H_2O nanofluid at 4% volume concentartion of Al_2O_3 and surfactant

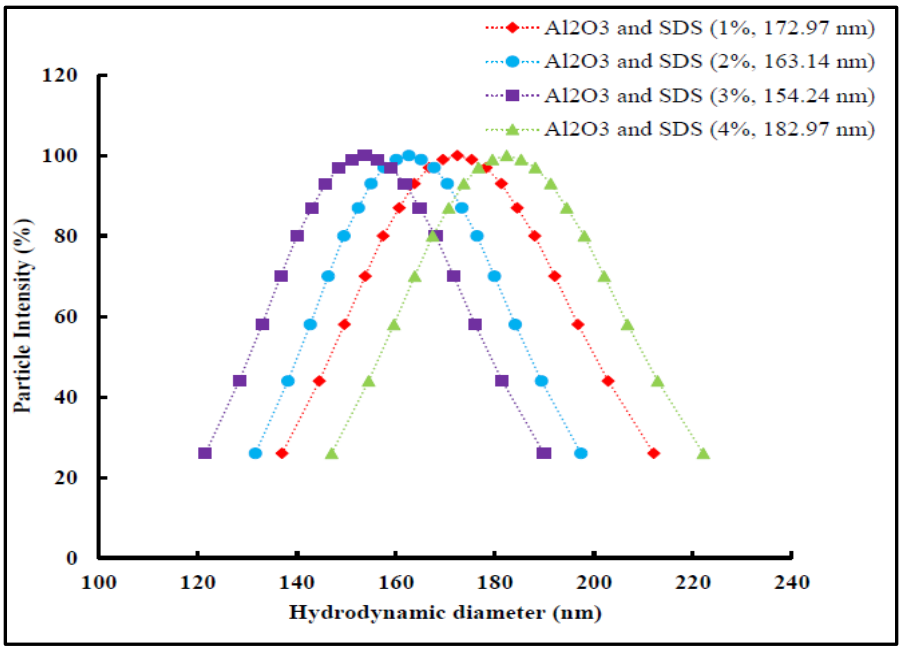

Fig. 5.6: DLS results of Al_2O_3 -H_2O nanofluid (with surfactant, SDS)

In order to get more information about the distribution of nanoclusters, TEM images of few samples of Al_2O_3-H_2O nanofluid are obtained (at 1% of volume concentartion) with and without surfactant, see Fig 5.7 (a)-(d) and Fig 5.8 (a)-(d). These images provide an approximate idea and help to understand that the role of surfactant in nanofluid. It can be observed that the surfactant SDS has resulted into bringing down the size of nanoclusters of Al_2O_3-H_2O nanofluid, see Fig. 5.8 (a)-(d). Moreover, TEM images and DLS results are found to be supporting the role of surfactant SDS in Al_2O_3-H_2O nanofluid. The decrease in cluster size of the nanoparticles while in suspension is due to the structure and composition of adsorbed layers to physic-chemical parameters of the solutions and substrates. Particularly, sodium dodecyl sulfate (SDS) being an anionic surfactant has a wide general interest in the binding of anionic surfactants to interfaces in SDS at Al_2O_3 (γ) surfaces. The SDS hydrolysis of the sulfate group gives rise to significant levels of impurities such as dodecanol and dodecanoic acid and adsorption of anionic surfactants to alumina, which can be controlled by adjusting the pH level of the solution. The sonication time for the required samples of Al_2O_3-H_2O nanofluids has also been optimized through collecting the DLS data. The results showed that a sonication time of about three hours is sufficient to break down the nanoclusters into an average size of the order of less than 200 nm (with SDS) from an average nanocluster size of 1300 nm (without SDS). Thereafter, no significant reduction in the average size of nanoclusters was observed.

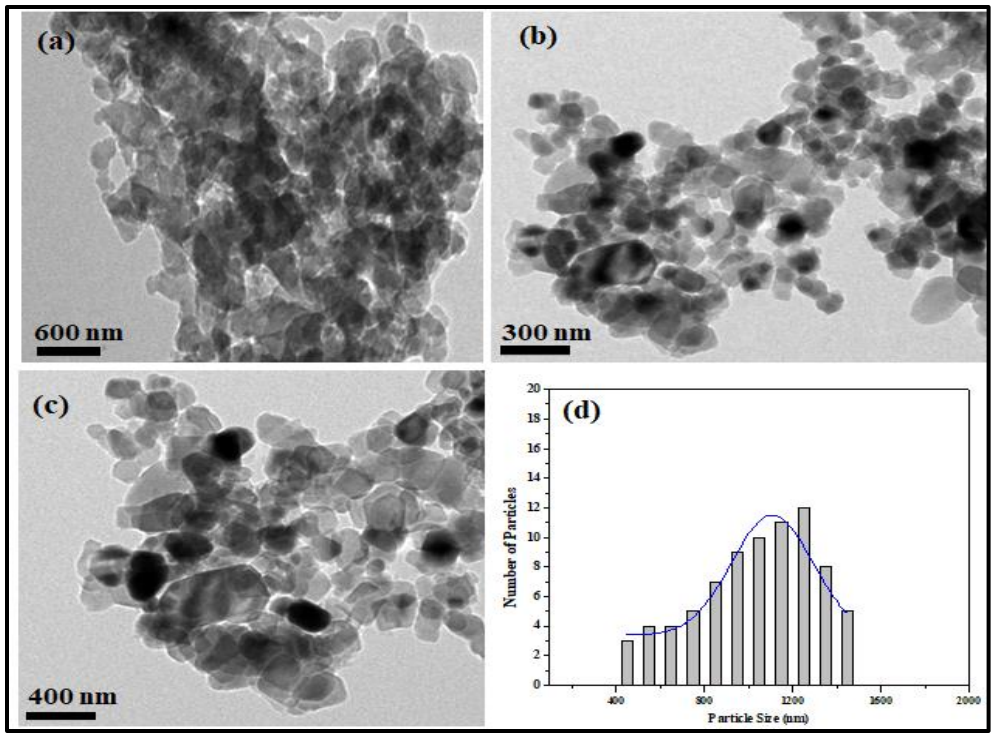

Fig. 5.7: HR-TEM images of Al_2O_3-H_2O nanofluid (**a, b, c**) and size distribution (**d**) without any surfactant

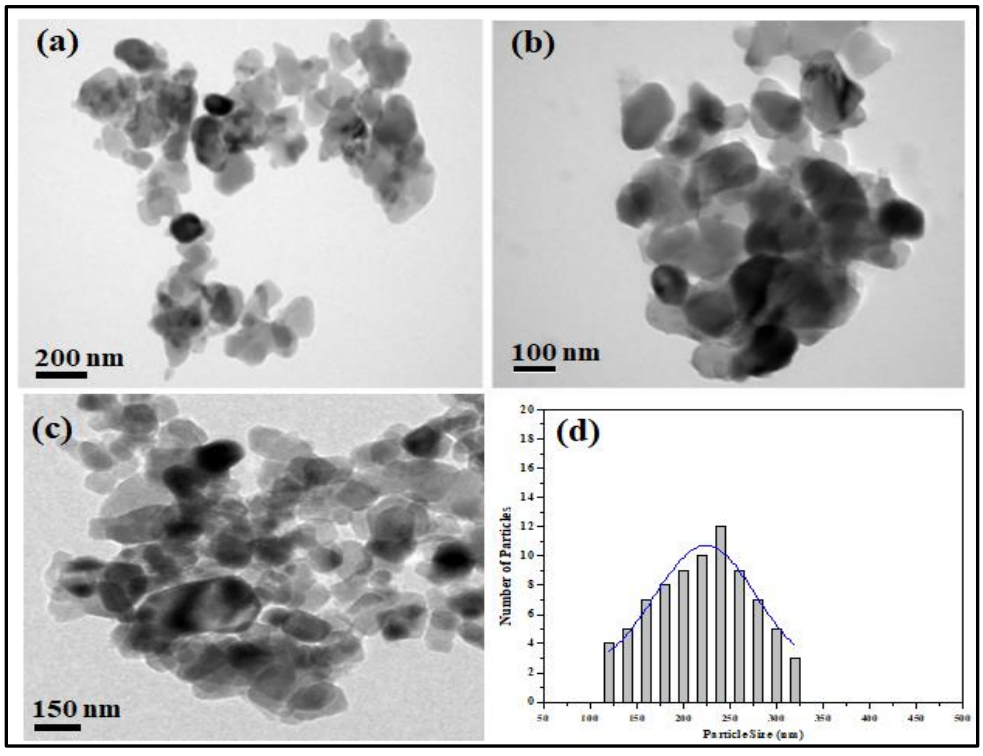

Fig. 5.8: HR-TEM images of Al_2O_3- H_2O nanofluid **(a, b, c)** and size distribution (**d**) with surfactant (SDS)

5.1.3. Design of experiments and optimization

In order to optimize the number of experiments required to predict the nanocluster based thermal conductivity of Al_2O_3-H_2O nanofluid, the method of "Design of Experiments" has been employed. The factors, such as nanoparticles volume concentration, surfactant (SDS) concentration in base fluid (DI water) and the working temperature have been identified and considered as the key parameters for investigation of their effect on the thermal conductivity enhancement of Al_2O_3-H_2O nanofluid.

Box–Behnken design (BBD)

The BBD requires experimental runs according to $N = k^2 + k + C_p$, where, k is the factor number, and C_p is the replicate number of the central point (Box and Hunter, 1957). It is a spherical, revolving design comprising of a central point and the middle points of the edges of the cube circumscribed on the sphere. To analyze a process or a system including a response Y (where Y depends on the input factors: x_1, x_2. . . . x_k), the relationship between the response and the input process parameters is described as:

$$Y = F(x_1, x_2 \dots \dots \dots \dots \dots x_k) \tag{5.1}$$

where, *'F'* is the unknown, but real response function (with its format being unknown) and 'ε*'* is the residual error which describes the differentiation that can be included by the function *'F'*. Considering, all linear terms, square terms and linear by linear interaction terms, the quadratic response model was described as:

$$Y = \beta_0 + \sum_{i=1}^{k} \beta_i x_i + \sum_{i=1}^{k} \beta_{ii} x_i^2 + \sum \tag{5.2}$$

where, β_0 is constant, β_i is the slope or linear effect of input factors, x_i, β_{ij}, is the linear by linear interaction effect between the input factors x_i and x_j, and β_{ii} is the quadratic effect of input factor x_i (Montgomery, 2009). It is important to include the second order model to provide a good prediction throughout the region of interest. The second order response surface design is rotatable,

indicating that the variance of the predicted response is the same at all points. As the location of the optimum is unknown before performing the experiments, it makes sense to use a design that provides equal precisions of estimation in all directions. A three level-three factor BBD was applied to estimate the effect of the parameters on the thermal conductivity. Different values of the parameters have been taken as the input variables. The factor levels were coded as −1 (low), 0 (central point or middle) and 1 (high). The input parameters used in the present work are given in Table 5.1.

Table 5.1: Experimental design levels of selected variables

Variables	**Levels in Box-Behnken design (BBD)**		
Coded level	Low (-1)	Medium (0)	High (+1)
Volume fraction	0.01	0.025	0.04
Temperature (K)	293	308	323
Surfactant concentration (mg)	776	1940	3104

The range of different parameters namely, *'V'* (volumetric fraction of nanoparticles in base fluid), *'T'* (temperature in *K*) and *'S'* (amount of surfactant in base fluid by weight) have been decided based on the information available in the literature, already given in Table 2.1. Therefore, it is quite appropriate to use the volume fraction of nanoparticles in DI water in the lower range, i.e. from 1 to 4%. Also, the amount of surfactant required in a particular type of nanofluid is equal to the weight of the nanoparticles in the base fluid (Gao *et al.*, 2009) i.e. in this particular case, it varies from 776 mg to 3104 mg and the temperature has been varied from 20-50°C.

5.1.4. Experimental data and predicted model

The design matrix of the parameters, volume fraction (*A*), working temperature (*B*) and surfactant (*C*) in the uncoded and coded units by the Box-Behnken design (BBD) is shown in Table 5.2, along with the experimental and predicted values of the response i.e. thermal conductivity ratio (k_{nf}/k_f) of Al_2O_3-H_2O nanofluid. The experimental data for the thermal conductivity has been analyzed by using a statistical Design-Expert version 6.0.6 for regression analysis to fit the equations developed and also to evaluate the statistical significance of the equations. A manual

regression method has been used to fit the second order polynomial (Eq. 5.2) to obtain the data and to identify the relevant model terms.

Table 5.2: Experimental design matrix and response based on the experimental runs and predicted values of thermal conductivity ratio (k_{nf}/k_f) as per BBD

	Independent Variables			**Response**	
	***A* (%)**	***B* (°C)**	***C* (mg)**	**Thermal Conductivity Ratios (k_{nf}/k_f)**	
Run	**Volume Fraction**	**Temperature**	**Surfactant**	**Experimental**	**Predicted**
1	0.04 (+1)	293(-1)	1940(0)	1.225	1.257
2	0.025 (0)	308(0)	1940(0)	2.688	2.81
3	0.025(0)	308(0)	1940(0)	2.706	2.81
4	0.025(0)	308(0)	1940(0)	2.785	2.81
5	0.01(-1)	308(0)	3104(+1)	1.258	1.325
6	0.04(+1)	323(+1)	1940(0)	2.812	3.047
7	0.04(+1)	308(0)	3104(+1)	2.426	2.454
8	0.025(0)	308(0)	1940(0)	2.742	2.81
9	0.01(-1)	323(+1)	1940(0)	1.467	1.56
10	0.025(0)	293(-1)	3104(+1)	1.233	1.271
11	0.025(0)	308(0)	1940(0)	2.571	2.71
12	0.04(+1)	308(0)	776(-1)	2.101	2.158
13	0.025(0)	293(-1)	776(-1)	1.169	1.22
14	0.01(-1)	308(0)	776(-1)	1.296	1.391
15	0.025(0)	323(+1)	776(-1)	2.621	2.607
16	0.025(0)	323(+1)	3104(+1)	2.732	2.746
17	0.01(-1)	293(-1)	1940(0)	1.12	1.029

To decide the adequacy of the model for thermal conductivity, two different tests, the sequential model sum of squares and model summary statistics were performed (Table 5.3). The '*p*' value for the quadratic model values was found to be 0.0001, which means this model with regression coefficient (R^2: 0.9766) is highly recommended for this study (Montgomery, 2009).

Table 5.3: Model selection for thermal conductivity ratio (k_{nf} k_f)

Sequential Model Sum of Squares						
Source	Sum of Squares	DF	Mean Square	F Value	Prob> F	Remarks
Mean	71.86	1	71.86			
Linear	4.47	3	1.49	5.25	0.0136	
2FI	0.42	3	0.14	0.43	0.7392	
Quadratic	*3.08*	*3*	*1.03*	*37.72*	*0.0001*	*Suggested*
Cubic	0.17	3	0.055	8.53	0.0327	Aliased
Residual	0.026	4	6.449E-003			
Total	80.03	17	4.71			
Model Summary Statistics						
Source	Std. Dev.	R-Squared	Adjusted R-Squared	Predicted R-Squared	PRESS	
Linear	0.53	0.5478	0.4434	0.3000	5.72	
2FI	0.57	0.5989	0.3583	-0.0352	8.46	
Quadratic	*0.17*	*0.9766*	*0.9466*	*0.8718*	*2.68*	*Suggested*
Cubic	0.080	0.9968	0.9874	+		Aliased

The ANOVA results for the thermal conductivity ratio (k_{nf}/k_f) of Al_2O_3-H_2O nanofluid, with a model F-value of 32.51 implied that the model is significant (Montgomery, 2009). It is also clear that the all the independent variables are not significant, however, the variables: the volumetric fraction of nanoparticles (V) and temperature (T) are highly significant for the thermal conductivity enhancement. Also, interaction between volume fraction and temperature is more significant for thermal conductivity enhancement compared to any other interaction among the different parameters. In the quadratic model, the values of Prob. > F greater than 0.05 indicates that the model terms are not significant (Table 5.4). The adequate precision of 16.40 (which is more than 4) indicates an adequate signal and the model can be used to navigate the design space (Montgomery, 2009).

Table 5.4: ANOVA for response surface quadratic model of thermal conductivity (k_{nf}/k_f)

Source	**Sum of Squares**	**DF**	**Mean Square**	**F Value**	**Prob> F**	**Remarks**
Quadratic Model	7.98	9	0.89	32.51	< 0.0001	*significant*
A (volume fraction)	1.46	1	1.46	53.72	0.0002	
B (temperature)	2.98	1	2.98	109.41	< 0.0001	*significant*
C (surfactant)	0.027	1	0.027	0.98	0.3555	
A^2 (volume fraction)^2	1.54	1	1.54	56.61	0.0001	*significant*
B^2 (temperature)^2	0.80	1	0.80	29.49	0.0010	*significant*
C^2 (surfactant)^2	0.44	1	0.44	16.08	0.0051	*significant*
AB (volume fraction X temperature)	0.38	1	0.38	14.10	0.0071	*significant*
AC (volume fraction X surfactant)	0.033	1	0.033	1.21	0.3080	*insignificant*
BC (temperature surfactant)	$5.522X10^{-4}$	1	$5.522X10^{-4}$	0.020	0.8908	*insignificant*
Lack of Fit	0.17	3	0.055	8.53	0.0327	*significant*
Pure Error	0.026	4	$6.449X10^{-3}$			
Std. Dev.	0.17	R^2	0.9766	(regression coefficient)		
Mean	2.06	$R^2_{Adj.}$	0.9466			
C.V.	8.03	$R^2_{Pred.}$	0.8718			
PRESS	2.68	A_{deq}. Precision	16.401			

The ANOVA analysis indicates a relationship between the thermal conductivity ratio (k_{nf}/k_f) of Al_2O_3-H_2O nanofluid and affecting variables (*V*, *T*, and *S*). By eliminating the insignificant

interaction terms, an empirical mathematical model for predicting thermal conductivity ratio in terms of actual factors is given as under:

$$\frac{K_{nf}}{K_f} = C_0 + C_1(V) + C_2(T) + C_3(V^2) + C_4(T^2) + C_5(S^2) + C_6(VXT) \qquad (5.3)$$

where, C_0 = -186.19014, C_1 = -271.36944, C_2 = 1.20123, C_3 = -2690.888, C_4 = -1.94 X 10^{-3}, C_5 = -2.38X10^{-7} and C_6 = 1.37778 are constants whose values depend on the type of units used.

The model represents the thermal conductivity enhancement of Al_2O_3-H_2O nanofluid for the nearly spherical size (hydrodynamic diameter) of the nanoclusters in the range from 163-183 nm. In the analysis of the variance, the adequacy of any model can easily be investigated by examination of normal probability plot of studentized residuals or residuals. If an error or residual distribution is normal then the plot will be a straight line (Montgomery, 2009). A normal probability plot and a dot diagram of the residuals are shown in Fig. 5.9 (a) and (b). The data points on this plot lie reasonably close to a straight line, which shows that the variables have been effectively taken into account to study their effect on the thermal conductivity ratio (k_{nf}/k_f). It can be seen that the residuals are in the proximity of the straight diagonal line. The relationship between the actual (experimental) and predicted (model) values of the thermal conductivity ratio (k_{nf}/k_f) of Al_2O_3-H_2O nanofluid has been also shown in the same figure. The actual and the predicted values of thermal conductivity ratio (k_{nf}/k_f) are found to be in good agreement (0.9766).

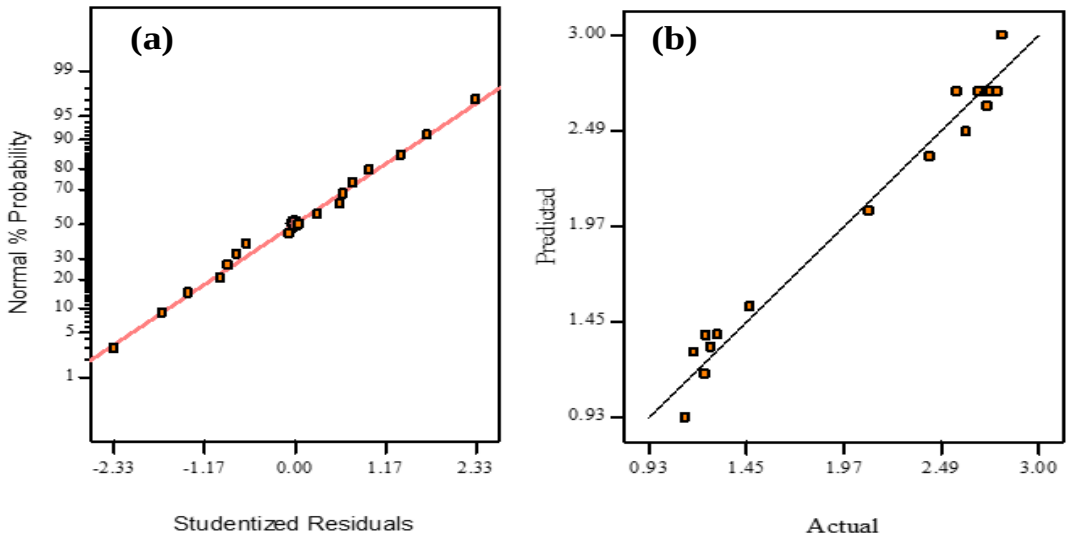

Fig. 5.9: (a) Normal % probability distribution and **(b)** scattered diagram of predicted response versus actual response of thermal conductivity ratio (k_{nf}/k_f)

The effect of nanoparticle volume fraction and surfactant concentration (by weight) on the thermal conductivity ratio (k_{nf}/k_f) is shown in Fig. 5.10. Fig. 5.10 indicates that with an increase in the concentration of Al_2O_3 and surfactant concentration (SDS) in DI water, thermal conductivity of Al_2O_3-H_2O nanofluid increases and the former factor has more prominent effect on its enhancement. The corresponding 2D contour lines express the various combination of the amount of volume fraction and surfactant which can be used to obtain a particular value of thermal conductivity ratio at temperature of 308 K, see Fig 5.11. The 3D response surface representation for the effect of temperature and volume fraction on the thermal conductivity ratio is shown in Fig. 5.12, which shows that with the rise in temperature, the thermal conductivity of Al_2O_3-H_2O nanofluid increases. The enhancement is more at elevated temperature (40-50 ºC) especially, when the volume fraction is high, i.e. around 3 to 4%. The contours lines also explore the different possibilities to choose various combinations of volume fractions and temperature in order to obtain a constant value of thermal conductivity enhancement at 3104 mg of surfactant (SDS), shown in Fig. 5.13. Similarly, 3D plots and contours have been drawn for other factors too, see Fig. 5.14 and Fig. 5.15, respectively.

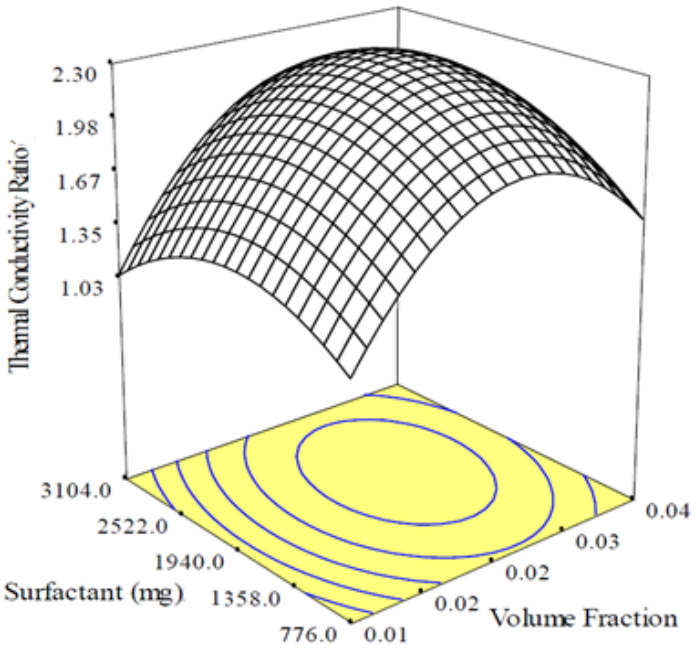

Fig. 5.10: 3D response surface graph of thermal conductivity ratio (k_{nf}/k_f) against surfactant (mg) and volume fraction at 35 ºC

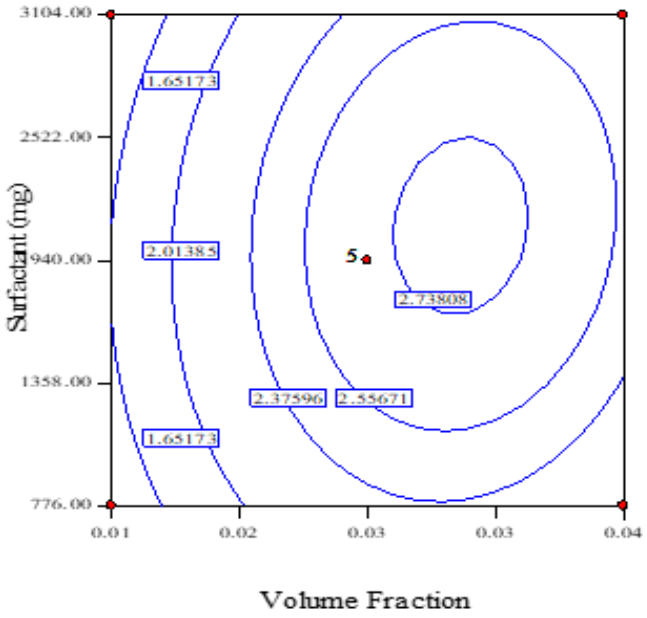

Fig. 5.11: 2D contours lines of thermal conductivity ratio (k_{nf}/k_f) against surfactant (mg) and volume fraction at 35 ºC

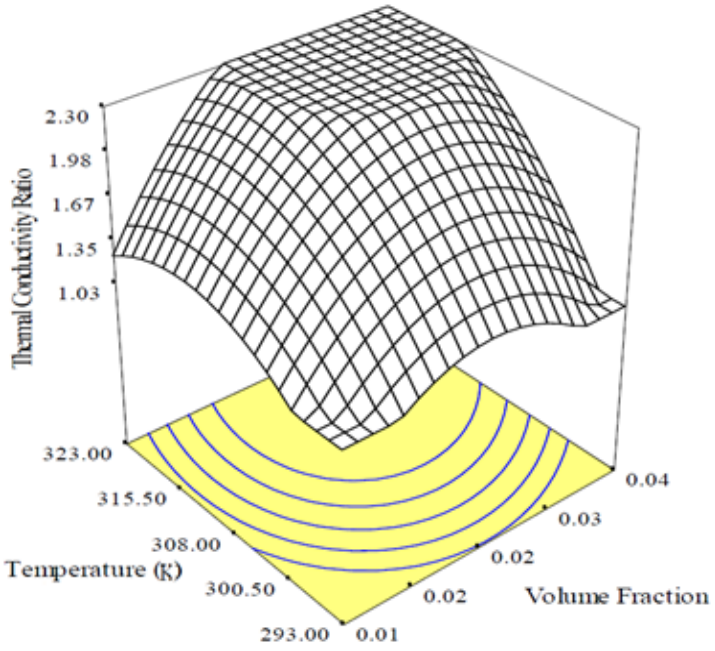

Fig. 5.12: 3D response surface graph of thermal conductivity ratio (k_{nf}/k_f) against volume fraction and temperature at 776 mg (surfactant, SDS)

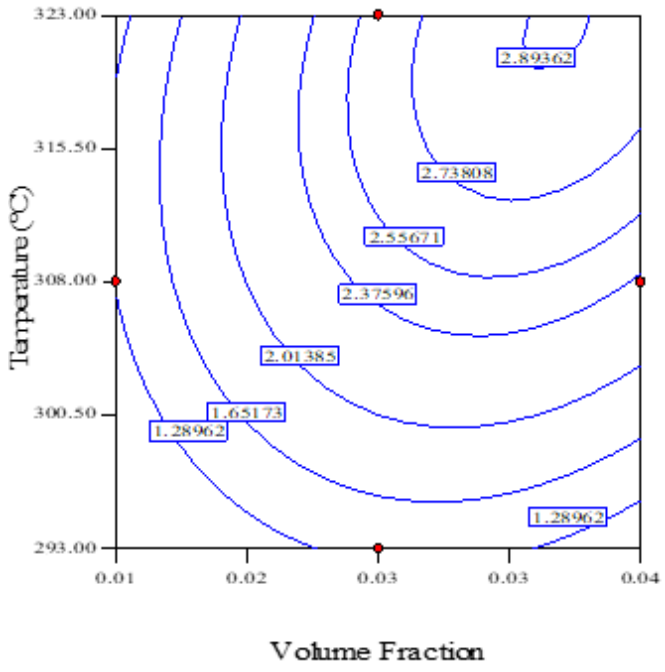

Fig. 5.13: 2D contours graphs of thermal conductivity ratio (k_{nf}/k_f) at different volume fractions and temperature at 3104 mg of surfactant (SDS)

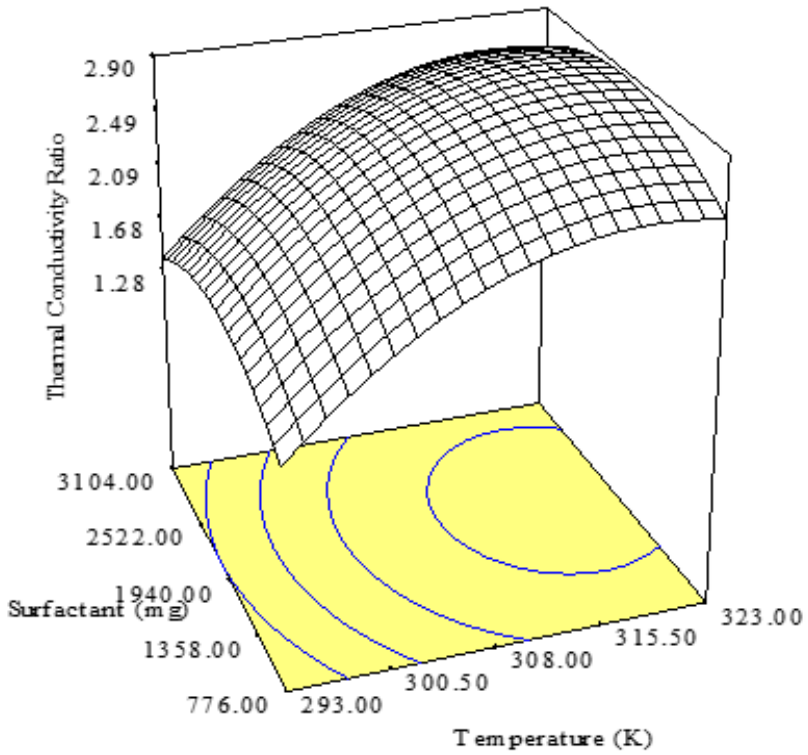

Fig. 5.14: 3D response surface graph of thermal conductivity ratio (k_{nf}/k_f) against surfactant and temperature at 2% of volume fraction

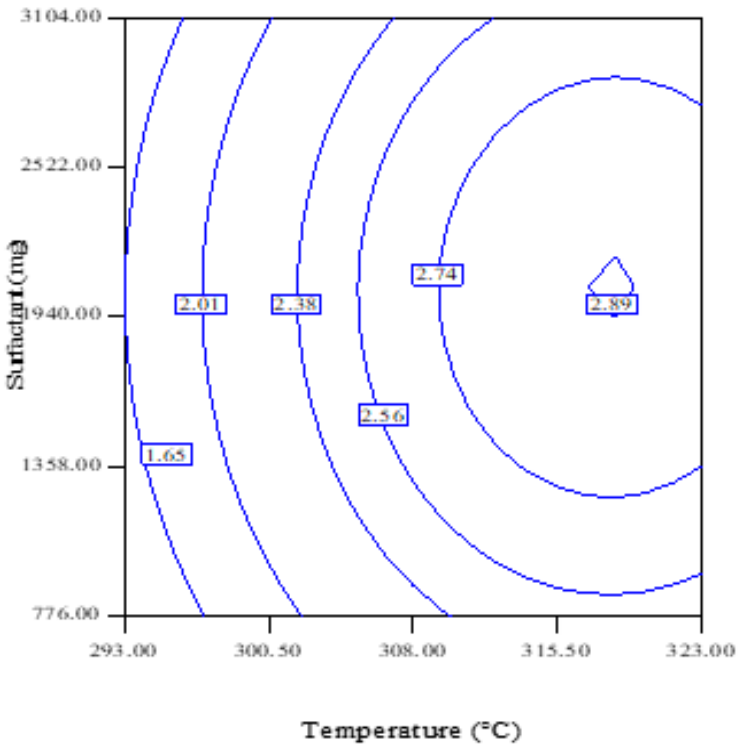

Fig. 5.15: 2D contours graphs of thermal conductivity ratio (k_{nf}/k_f) at different surfactant amount and temperature at 2% volume fraction of Al_2O_3 nanoparticles

To validate the adequacy of the predicted model for thermal conductivity ratio (k_{nf}/k_f) various experimental trials have been re-conducted. The values of the different variables which were affecting the thermal conductivity have been taken to optimize the thermal conductivity ratio (k_{nf}/k_f) of Al_2O_3-H_2O nanofluid. Here, in all the experimental trials, the thermal conductivity ratio has been optimized to its maximum value (2.81 W/mK) for the Al_2O_3-H_2O nanofluid. The predicted and experimental values of thermal conductivity ratio along with selected parameters are shown in Table 5.5. All the experimental and predicted values of thermal conductivity ratio (k_{nf}/k_f) were found to be in good agreement within the accuracy range of ± 8%, which indicates that the model is able to predict the thermal conductivity enhancement successfully with reasonable accuracy.

Table 5.5: The list of the optimized input variables to obtain the maximum gain in thermal conductivity

Variables	**Condition for Optimization**	**Lower Limit**	**Upper Limit**
Volume fraction	is in range	0.01	0.04
Temperature (*K*)	is in range	293	323
Surfactant, *Wt*. (mg)	is in range	776	3104
Thermal Conductivity Ratio (k_{nf}/k_f)	maximize	1.12	2.81

Table 5.6: A comparison between the predicted optimized value of the thermal conductivity ratio (k_{nf}/k_f) and experimental thermal conductivity ratio

S. No.	**Volume Fraction**	**Temperature (K)**	**Surfactant Wt. (mg)**	**Thermal conductivity ratio (k_{nf}/k_f) (Predicted)**	**Thermal conductivity ratio (k_{nf}/k_f) (Experimental)**
1	0.03	322.13	2647.19	3.05	3.12
2	0.04	313.66	2450.72	2.93	3.42
3	0.03	313.74	2370.62	2.93	3.08
4	0.04	320.62	2145.10	3.02	3.12
5	0.03	320.85	2323.19	3.07	3.28

A 3D response surface and 2D contour plots for the optimized thermal conductivity ratio (k_{nf}/k_f) are shown in Fig. 5.16 and Fig 5.17. The response surface and contour represent the condition under which the optimized thermal conductivity ratio (k_{nf}/k_f) can be achieved under the given range of the input variables (given in table 5.5). These figures also represent the conditions under which the different combinations of the two input variables (temperature and volume) and one fixed variable i.e.1000 mg of SDS, can be selected to obtain an optimized value of the thermal conductivity ratio. A variety of 3D response surfaces and contours can be generated for different combinations of input variables. Fig. 5.16 and Fig. 5.17 have been drawn corresponding to 1000 mg of surfactant (SDS).

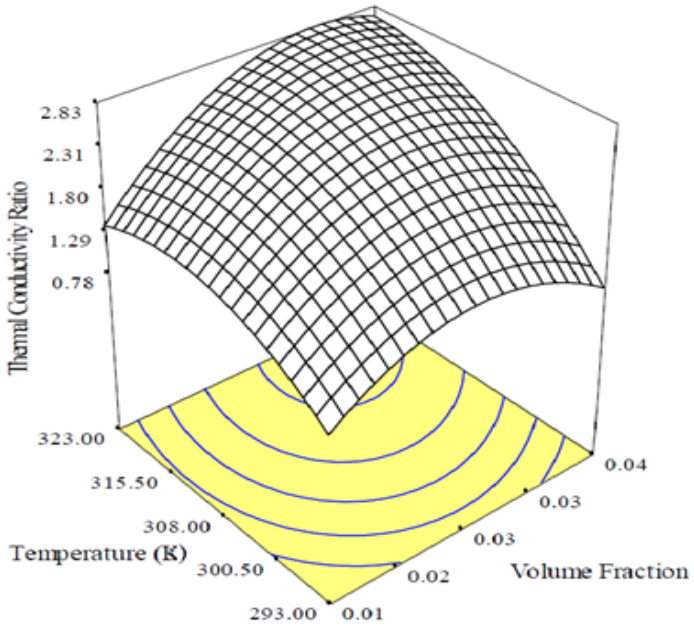

Fig. 5.16: 3D response surface graph of optimized thermal conductivity ratio (k_{nf}/k_f) against volume fraction and temperature at 1000 mg of the surfactant (SDS)

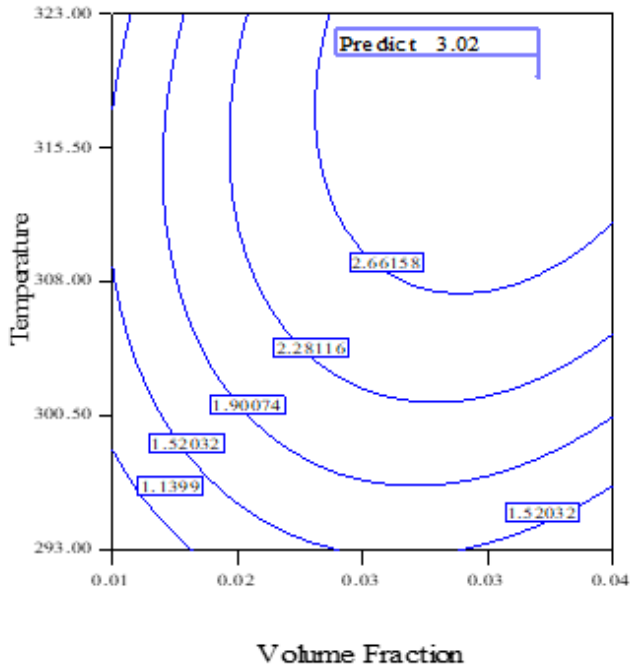

Fig. 5.17: 2D contours graphs of optimized thermal conductivity ratio (k_{nf}/k_f) against volume fraction and temperature at 1000 mg of the surfactant (SDS)

5.1.5. Evaluation of existing models and predicted model

There are many empirical models which have been suggested by various researchers working in the area of nanofluids. Out of these models, few have been used to validate the predicted model, see Fig. 5.18 and 5.19. The following parameters are taken into consideration to evaluate the thermal conductivity of Al_2O_3-H_2O nanofluid, such as; (i) thermal conductivity of Al_2O_3 particles from vary from 39.12 W/mK to 36.10 W/m K in the temperature range from 20-50°C and the thermal conductivity of water vary from from 0.590 W/m K at 20°C to 0.645 W/mK at 50°C (Zhu *et al.*, 2009), (ii) the specific heat and density of water are equal to 4.186 kJ/kg K and 1000 kg/m^3, respectively (iii) molecular diameter of water is 0.3 nm (Bhattacharya *et al*., 2009), (iv) density of Al_2O_3 particles: 3965 kg/m^3 (Zhu *et al.*, 2009), and (v) specific heat of Al_2O_3 is 880 J/kg K (Rea *et al.*, 2009). By taking these inputs parameters, the existing empirical models and developed model have been evaluated for the thermal conductivity enhancement of Al_2O_3-H_2O nanofluid at volume concentration of 1% and 2%. The temperature is made to vary from 20-50°C during these investigations. At 1% of volume concentration of nanoparticles, the prediction of the developed model closely follows the Koo and Kleinstreuer model (Koo and Kleinstreuer, 2005). The developed model follows the measured thermal conductivity ratio (k_{nf}/k_f) with an accuracy of 8 to 10%, see Fig 5.18. Whereas, the other models (Chon *et al.*, 2005; Teng *et al.*, 2010) are able to predict the thermal conductivity enhancements of Al_2O_3-H_2O nanofluid with reasonable accuracy (3-7%) only at lower temperatures i.e. up to 30°C. The error between the measured and predicted values of thermal conductivities increase with rise in temperature and becomes significant (≥20%) at higher temperature i.e. 45 to 50°C.

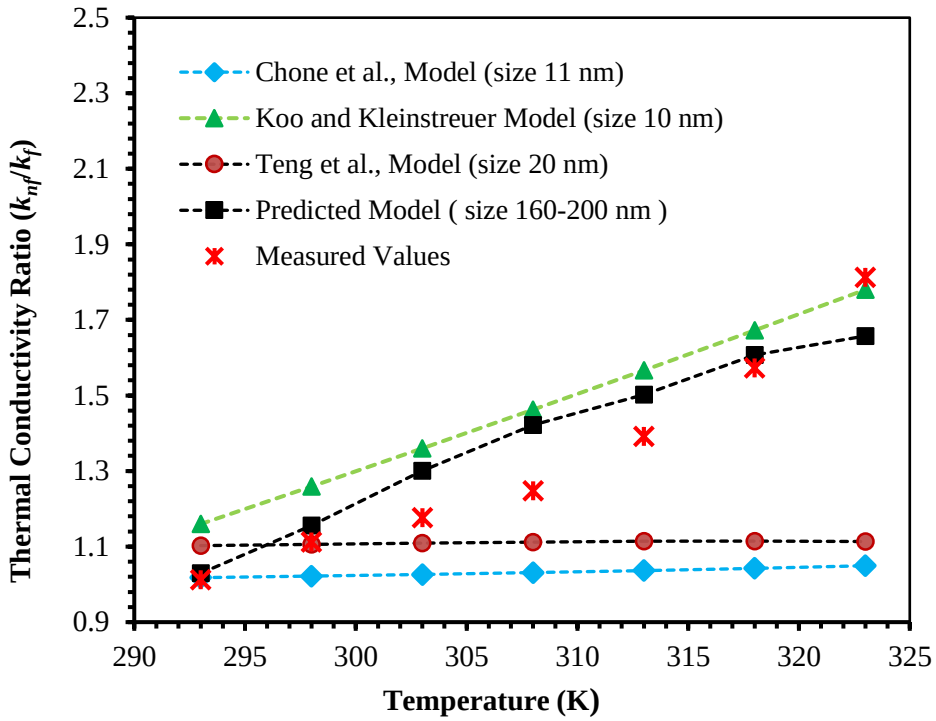

Fig. 5.18: Predicted values of thermal conductivity ratio (k_{nf}/k_f) vs temperature (at 1% volume concentration)

In comparison to other models and under the same temperature variations, the predicted model reports more enhancement in the thermal conductivity of Al_2O_3-H_2O nanofluid at 2% volume concentration of nanoparticles. The developed model seems to be following the measured thermal conductivity ratio with reasonable accuracy (6-9%) at higher temperature, whereas, the error involved at low temperature is comparatively higher i.e. 9-14%, see Fig. 5.19. The differences in the values of the thermal conductivity ratio reported by different models may be attributed due to the varying size of the nanoparticles in Al_2O_3-H_2O nanofluid. Moreover, the results reported on thermal conductivity ratio with smaller size of nanoparticles underestimate the enhancement of thermal conductivity of Al_2O_3-H_2O nanofluid. The results obtained with formation of nanoclusters (size 160-200 nm) are able to make the predictions close to the values of measured thermal conductivity ratio, see Fig. 5.18 and 5.19. Therefore, for the known dispersion quality of nanofluid, this model can be used to predict the thermal conductivity enhancement for a cluster based system. The second merit is that it can be used to predict the thermal conductivity enhancement with varying volume concentration, temperature, and surfactant concentrations.

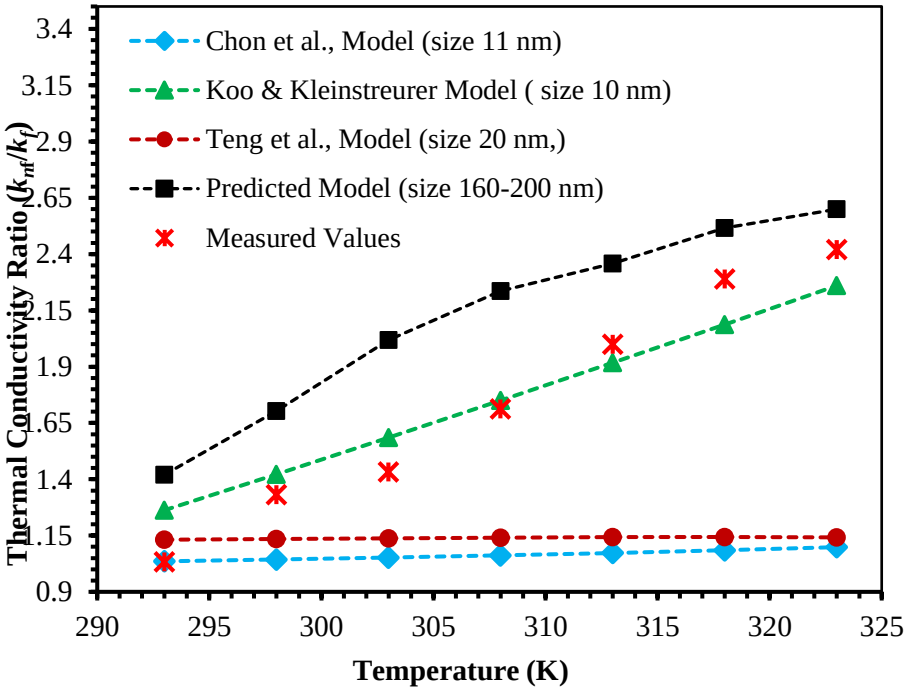

Fig. 5.19: Predicted values of thermal conductivity ratio (k_{nf}/k_f) vs temperature (at 2% volume concentration)

Thus, the predicted model has clearly provided the merits. Firstly, the model is able to predict the thermal conductivity based on the average size of the nanoclusters present in the base fluid. It has been confirmed from the DLS and TEM results of various samples. The enhancement in the thermal conductivity is augmented mainly due to the presence of these nanoclusters. Secondly, the clustering of Al_2O_3 in the base fluid (DI water) has resulted in the formation of a localized particle-rich zone that has lesser thermal resistance to heat flow compared to a particle-free zone. Therefore, the model seems to be tracking the physical mechanism of nanoscale heat transfer and confirming to the practical finding. It seems also justified to note that formation of nanoclusters has resulted in the improvement of thermal conductivity of Al_2O_3 nanofluid. The results confirmed that the model could predict with a high accuracy level (R^2 = 0.9766). The representation of the model and its parameters seems to follow the experimental observations. Furthermore, the model is able to provide various combinations of these parameters (volumetric concentration, surfactant amount and temperature) to achieve a maximum enhancement in the thermal conductivity of Al_2O_3-H_2O nanofluids. The study also emphasizes that dispersion quality/cluster formation as the key factor to predict thermal conductivity enhancement for a particular type of nanofluid.

Chapter-6

Modelling the Morphological Parameters of Nanoclusters

$\mathcal{A}$ significant gap exists between the theoretical and experimental results on the thermal conductivity of a variety of nanofluids (discussed in Chapter 2). To narrow down these differences, the mechanisms responsible for heat transport in nanofluids ought to be re-addressed. The present study focuses on the effect of time, temperature, instantaneous volume fractions and morphological properties of nanoclusters on perikinetic heat conduction and Brownian motion induced micro-convection mechanisms. Moreover, such parameters are required to be involved in the modelling of the thermal conductivity of nanofluids. Two oxide based nanofluids i.e. Al_2O_3-H_2O and TiO_2-H_2O have been investigated to articulate the results of their respective thermal conductivities. In this chapter, governing have been formulated for the thermal conductivity of nanofluids.

6.1 Theoretical Analysis and Morphology of Nanoclusters

The enhancement in thermal conductivity is due to the formation of localized particle-rich zones. On the other hand, nanoclusters are prone to be fast settling and thus creating a "particle-free" zone which may decrease the heat transport capacity of nanofluids, see Fig. 6.1 and Fig. 6.2. The postulations have been made about the structural appearance of the nanoclusters in the form of linear chains and dead-ends (Karthikeyan *et al*., 2008; Mallick *et al*., 2013). Evans *et al.* (2008) emphasized upon the connectivity of nanoparticles in the form of backbones and highlighted their role in the thermal conductivity enhancement. Xuan *et al*. (2003) developed a theoretical model for thermal conductivity by taking into account the structure of the nanoparticles and aggregates. Similarly, a large enhancement is reported in the thermal conductivity due to the presence of uniformly dispersed chain-like aggregates (Philip et al., 2008). It was emphasized that the liquid molecule nanolayer, aggregation and nanoconvection are the important factors which can control the thermal conductivity enhancement in nanofluids (Pang *et al.*, 2016). Some other research groups have also highlighted the effect of the clustering on the thermal conductivity of nanofluids (Longo and Zilio, 2011; Longo *et al.*, 2012). Alipour *et al.* (2014) proposed a theoretical model for measuring the thermal conductivity of nanofluids consisting of two parts; first a statistical model and the second - a dynamic model based on the Brownian motion induced convection of nanoparticles in base fluid along with the effect of interfacial nanolayers among nanoparticles and

base fluid (Alipour *et al.*, 2014). In his own published work, the author has highlighted the nano-clustering phenomenon especially for the nanofluids prepared through the Two-Step Method and have evaluated different models for their accuracy to predict the thermal conductivity enhancement for Al_2O_3 based nanofluids with an error of ± 5% (Mallick, Mishra and Kundan, 2013).

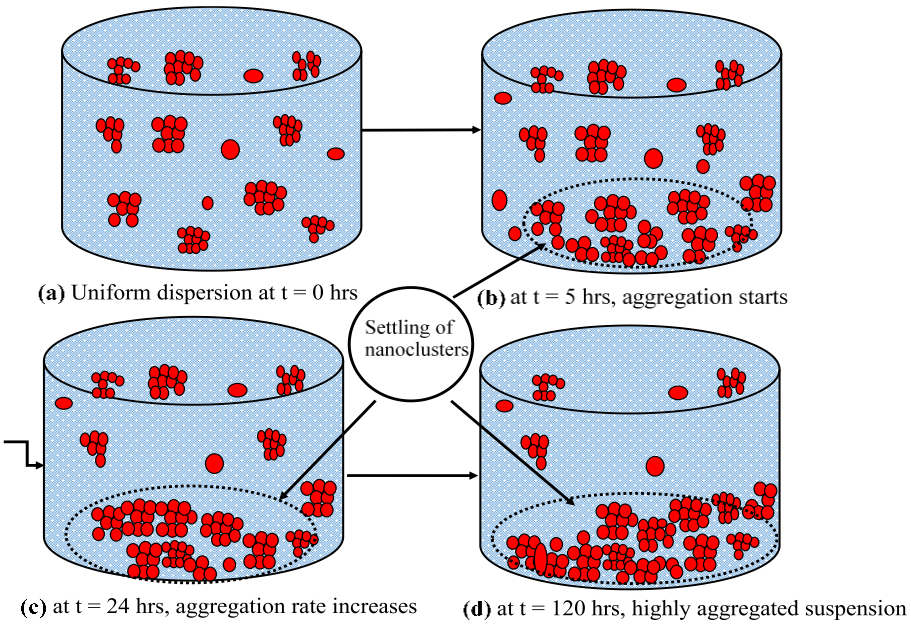

Fig. 6.1: Effect of elapsed time on the suspension quality of nanofluids

There are also fundamental and empirical equations available to predict thermal conductivity enhancement in nanofluids under perikinetic conditions. They take into account the effect of factors, such as nanolayer, interfacial thermal resistance, percolation structure, agglomeration, the surface charge state of nanoparticles, the Brownian motion of nanoparticles etc. (Maxwell, 1873; Hamilton and Crosser, 1962; Hui *et al.*, 1999). It was also postulated that the heat transport through the stationary medium in the host fluids with particle-liquid-particle interactions leads to a faster heat conduction (Jang and Choi, 2004; Koo, 2004; Kumar *et al.*, 2004; Prasher *et al.*, 2006).

The temperature-dependent mathematical models are also available to predict the thermal conductivity enhancement of a variety of nanofluids based on the Brownian motion and kinetic theory. However, there are significant discrepancies exist in the results obtained regarding proper understanding of the scientific basis of these models (Mukherjee *et al.*, 2016).

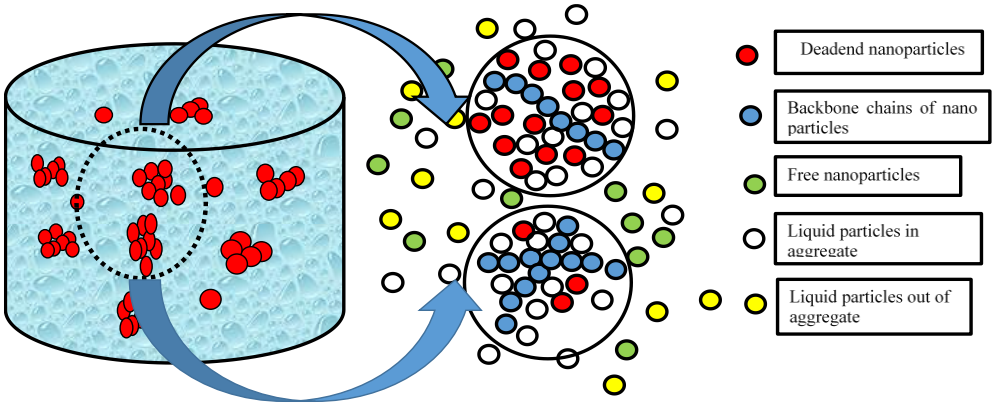

Fig. 6.2: The possible morphological characterization of nanocluster, while in suspension

By the above discussion, it is quite evident that clustering in nanofluids is a common phenomenon and the empirical equations and fundamental models are required to be modified to include the clustering effect. Moreover, these models include the effect of the primary or initial volume concentration of the nanoparticles only, whereas the volume concentration is not constant and it changes with the elapsed time. As a result of this, nanoclusters also grow with the passage of time. The nominal or average diameter of the nanoparticles in dry powder state may not be the accurate representation of particle size in the actual suspension conditions of nanofluid. The existing structural models may also be required to be amended in order to take into account the new morphology of the nanoclusters and their associated effects. Under the favorable conditions, such fractal aggregates lead to a considerable enhancement in the thermal conductivity of nanofluids. This augmentation can be significantly higher than what is predicted by using other models, especially, fundamental models for a well-dispersed colloidal suspension. The adopted fractal morphology of nanoparticle clusters is shown in Fig. 6.3.

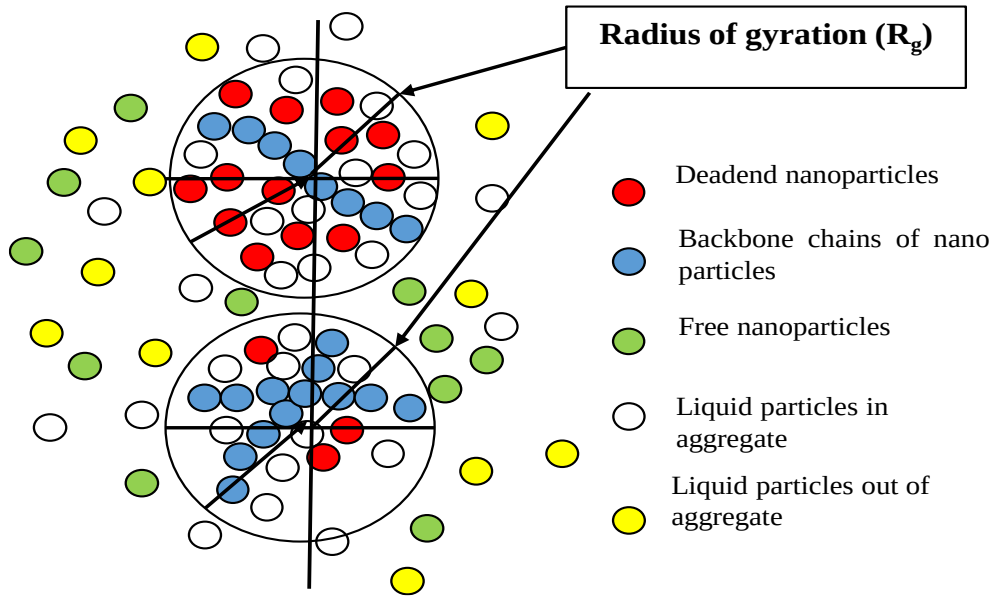

Fig. 6.3: Cluster dispersion morphology in a nanofluid

6.2 Stability Analysis of Nanofluids and Time Dependent Volume Fractions

The perikinetic aggregation with in cluster-cluster aggregation is the key factor responsible for the growth of nanoclusters and leading to a fundamental limiting aggregation regimes, known as diffusion limited aggregation (Hemker and Frank, 1990). The experimental investigations by other researchers revealed that the large Brownian nanoclusters have a fractal structure with measurable dimensions (Lin *et al.*, 1989; Russel *et al.*, 1989). In the present work, cluster structural morphology and the governing empirical equations and models have been modified in terms of the hydrodynamic size of the particle in suspension ($2a$), the fractal (d_f) and chemical (d_l) dimensions of an aggregate instead of considering individual particle size. These fractal aggregates lead to a considerable enhancement in thermal conductivity of nanofluids. As per the fractal morphology of nanoclusters (see, Fig. 6.3), a fractal cluster may be considered embedded within a sphere of radius equal to the radius of gyration (R_g). This cluster is assumed to be composed of a few linear chains, which run through the span of the whole cluster called the backbone of the cluster and the side chains are known as the dead ends (Potanin *et al.*, 1995). The number of particles (N) present in an aggregate, whose radius of gyration is R_g and average radius of nanoparticles is a, is given as (Potanin *et al.*, 1995):

$$N = \left(\frac{R_g}{a}\right)^{d_f} \tag{6.1}$$

where, d_f is the fractal dimension of the cluster/aggregate with $1 \leq d_f \leq 3$ (where, $d_f = 1$, if the nanocluster has only single line structure, i.e., loosely packed and $d_f = 3$ is if the nanocluster is completely compact i.e. spherical aggregate). It has been found that for oxide based colloidal solutions, d_f varies from 1.75 to 2.5 (Russel *et al.*, 1989; Carpineti and Giglio, 1993; Hunter, 2001; Waite *et al.*, 2001). The particle-cluster aggregation leads to a denser aggregate with fractal dimension of about 2.5, whereas, the cluster-cluster aggregation gives a fractal dimension of around 1.8 (Russel *et al.*, 1989). The perikinetic colloidal aggregation is found to be occurring predominately via cluster-cluster aggregation based on the particle sticking probability (Lin *et al.*, 1989, 2002). Wang et al. (2003) showed that in oxide based nanofluids, aggregation is of diffusion-limited colloid aggregation (DLCA) nature. Therefore, $d_f = 2.0$ has been assumed for the current investigation. However, above-mentioned model is valid for all values of d_f. In the diffusion-limited colloid aggregation (DLCA) kinetics, the number density of nanocluster (C) at any time (t) can be correlated by using an approach proposed by Smoluchowski (Russel *et al.*, 1989) where, clusters collision is assumed to be taking place predominately between the nanoclusters of approximately equal size (Russel et al., 1989; Holthoff *et al.*, 1996).

$$N = (1 + \frac{t}{t_p}) = \left(\frac{R_g}{a}\right)^{d_f} \tag{6.2}$$

where, t is the elapsed time, $2a$ is the average hydrodynamic size of the nanoparticles in suspension, R_g is the characteristic dimension and d_f is the fractal dimension of the cluster and t_p is the aggregation time constant, given as:

$$t_p = \pi \mu a^3 W / \varphi_p K_B T \tag{6.3}$$

where, φ_p is volume fraction of the nanoparticles, K_B is the Boltzmann's constant, T is the temperature, μ is the viscosity of the base fluid and W is the stability ratio of the suspension. The volume fraction of the nanoparticles in an aggregate (φ_a) is related to the volume fraction of the primary nanoparticles in base fluid (φ_p) and total volume fraction of the aggregates present in the

base fluid (φ_{at}) by a relation, $\varphi_p = \varphi_a \varphi_{at}$. Potanin *et al.* (1995) gave a correlation where, the volume fraction of the nanoparticles in an aggregate or cluster (φ_a) is related to its radius of gyration (R_g) as given in Eq. (6.4):

$$\varphi_a = \left(\frac{R_g}{a}\right)^{d_f-3} = \left(1+\frac{t}{t_p}\right)^{(d_f-3)/d_f} \quad (6.4)$$

Out of a total number of nanoparticles present in a cluster, the number of particles belonging to the backbone chains is (de Rooij *et al.*, 1993; Potanin *et al.*, 1995):

$$N_b = \left(\frac{R_g}{a}\right)^{d_l} \quad (6.5)$$

where, d_l is known as the chemical dimension given as; $1 \leq d_l \leq d_f$. When, $d_l = 1$, all the nanoparticles in the aggregate form the deadends and if, $d_l = d_f$, all the nanoparticles contribute to form the backbone chains. Generally, DLCA is observed in oxide based nanofluids, and there is a probability of nanoparticles to be present in the form of dead-ends and backbone chains (Wang *et al*. 2003). Therefore, it is appropriate to assume the value of $d_l = 1.5$ for the study undertaken. The volume fraction of backbone particles (φ_{bp}) in an aggregate is given as (de Rooij *et al.*, 1993; Potanin *et al.*, 1995):

$$\varphi_{bp} = \left(\frac{R_g}{a}\right)^{d_l-3} \quad (6.6)$$

The volume fraction of the particles belonging to the dead-ends, φ_{dp}, is expressed as:

$$\varphi_{dp} = \varphi_a - \varphi_{bp} \quad (6.7)$$

The suspension stability of nanofluids mostly depends on the electrostatic repulsion energy (E_R) and the energy due to van der Waals attraction (E_A) present among the nanoparticles while in suspension. The "E_R" between two similar charged particles of the same size is given by Derjaguin-Landau-Verwey- Overbeck (DLVO) theory (Hiemenz, 1977; Bergström, 1997; Kallay and Zalac, 2001):

$$E_R = \frac{\pi \varepsilon_r \varepsilon_0 a^2 \zeta^2 \exp(-\Lambda x)}{a+x} \quad (6.8)$$

where, ε_r and ε_0 are the relative dielectric constant of the liquid and of free space, a is the half of the nanoparticles size in suspension, ζ is the zeta potential, and Λ is the Debye parameter, its value for an aqueous medium is given as:

$$\Lambda = \frac{5.023X\ 10^{11}(I)^{0.5}}{(\varepsilon_r)^2} \quad (6.9)$$

where, I denotes the concentration of ions in aqueous medium, $I = 10^{-pH}$ for pH$\leq$ 7 and $I = 10^{-(14-pH)}$ for pH > 7. The repulsion energy, E_R is proportional to ζ^2, Eq. (6.8). Higher the value of zeta potential, more is the repulsion energy and better is the suspension stability of nanofluid. The attraction energy (E_A) between the same nanoparticles/nanoclusters of same the size is given by the Hamakers' equation (Hunter, 2001):

$$E_A = -\frac{A_{132}}{6x}\left[\frac{2}{s^2-4} + \frac{2}{s^2} + ln\left(\frac{s^2-4}{s^2}\right)\right] \quad (6.10)$$

where, $S = 2\left(1+\frac{x}{a}\right)$ and 'a' is the half of the average size of the particles in suspension, x is the interparticle surface to surface distance and A_{132} is the Hamakers' constant. Its value for metal oxides is typically of the order of 10^{-20}J (Honig *et al.*, 1971; Russel *et al.*, walter, 1989). One of the useful quantitative method to assess the stability of any colloidal dispersion is to measure its stability ratio, W (Hidalgo-alvarez *et al.*, 1996; Hunter, 2001). In the present work, this stability ratio (W) has been used to find out the aggregation time constant (t_p). The nanofluid suspensions having a significant value of W (i.e., $W>>1$) are more stable because of the presence of higher repulsive forces among the nanoclusters whereas, the suspensions with a small value of W (i.e. $W<<1$) signify their least stability. In the study of colloidals, researchers have given the equation to determine the stability ratio (W) for the nanofluid suspensions by modeling the repulsive energy (E_R) and the attractive potential energy (E_A) among the electrostatically stabilized nanoclusters (Hiemenz, 1977; Russel *et al.*, 1989; Hunter, 2001).

$$W = 2a \int_0^{\infty} \frac{\mathrm{B}\,(x)\exp[(E_R + E_A)_{max}\,/K_b\,T\,]}{(2a+x)^2} d_x \qquad (6.11)$$

where, K_B is the Boltzmann constant, T is temperature, '$2a$' is the size of the nanoparticle/nanoclusters and 'x' is the interparticle surface to surface distance. Here, $B\,(x)$ is the parameter, which represents the hydration interaction among the particles, i.e., the amount of energy released when the particles are dissolved in a solvent (Honig *et al.*, 1971; Roebersen and Wiersema, 1971; Hiemenz, 1977; Hunter, 2001).

$$B(x) = \frac{6\left(2\,\frac{x}{a}\right)^2 + 13(x/a) + 2}{6(x/a)^2 + 4\,(x/a)} \qquad (6.12)$$

Eq. (6. 11) shows that stability ratio (W) is a strong function of ζ potential, suspension pH value, ions concentration (I) and interparticle distance (x).

6.3 Improved Models for Thermal Conductivity

In nanofluids, the available models for thermal conductivity take into consideration the effect of various parameters, such as nanolayer, interfacial thermal resistance, percolation structure, agglomeration of particles, cubic arrangement of spherical nanoparticles, surface charge state of nanoparticles and the Brownian motion of nanoparticles. A detailed discussion on perikinetic heat conduction and micro-convection mechanisms based modified models for thermal conductivity of two oxide based nanofluids have been presented in the subsequent sections.

6.3.1. Structural models

There are many structural models available in the literature to predict the thermal conductivity enhancement in a variety of nanofluids (given in chapter 2). Apart from the properties of the nanomaterial and host fluid, these models were developed by assuming that the nanoparticles are stationary or have a negligible bulk movement in base fluid. These models primarily take into

account the individual behavior of nanoparticle and their primary volume concentrations in their respective base fluids.

One of the fundamental models which has been used extensively to predict the thermal conductivity enhancement of variety of nanofluids is the Maxwell Model (Maxwell, 1873), given as:

$$\frac{k_{eff}}{k_l} = \frac{k_p+2k_l+2(k_p-k_l)\varphi_p}{k_p+2k_f-(k_p-k_f)\varphi_p} \tag{6.13}$$

where, k_{eff} is the effective thermal conductivity of nanofluid, k_l and k_p are the thermal conductivities of the base fluid and nanoparticle, respectively, φ_p is the primary particle volume fraction. This model was proposed based on the effective medium field theory for solid-liquid mixture with relatively large particles and conduction through a stationary homogeneous suspension of solid spheres. It has been observed that in many cases, Maxwell Model is not capable of predicting the thermal conductivity enhancement of nanofluids with reasonable accuracy. Similarly, the gaps do exist between the theoretical and experimental values of the thermal conductivities of different nanofluids reported by various researchers (Maxwell, 1873; Hamilton and Crosser, 1962; Das *et al.*, 2003, 2007; Wang *et al*., 2003; Keblinski *et al*., 2005; Xu *et al.*, 2006; Mintsa *et al.*, 2007). In other words, it can be argued that these models still need to be relooked and a thorough understanding of the mechanisms involved to transport heat using nanofluids would be required to be developed. While carrying out the initial investigations on nanofluids, several times it was concluded that agglomeration and stability of nanoparticles in base fluid are challenging issues for the research community working in the area of nanofluids. After peer deliberations on these issues it was decided to reinvestigate the following: (i) clustering phenomenon which is the main reason for agglomeration and settling of nanoparticles while in suspension and (ii) the two most sorted out mechanisms, namely perikinetic conduction and Brownian induced micro-convection responsible for the thermal conductivity enhancement of nanofluids. Two types of oxide based nanofluids, i.e. Al_2O_3-H_2O and TiO_2-H_2O were selected to carry out these investigations. While going through the literature, it is observed that there are few more aspects associated with the morphology of nanoclusters that have not been explored yet. Such characteristics can be incorporated in modelling of the thermal conductivity of nanofluids, given as:

(i) While in suspension, the volume concentration of the nanoparticles (φ_p) is not constant however, changes continuously depending on the chemical and physical properties of nanofluid. At any instant of time, only the actual volume concentration of the nanoparticles (in suspension) will contribute effectively in the thermal conductivity enhancement.
(ii) Nanoparticles form the nanoclusters and behaviour of these nanoclusters determine the thermal conductivity of nanofluid.
(iii) Nanoparticles or nanoclusters which get settled down, do not contribute to any significant enhancement of the thermal conductivity.
(iv) The actual volume fraction of nanoparticles in nanofluid is time and temperature dependent. Therefore, temperature and time dependent volume fraction of nanoparticles should be included in the modelling of thermal conductivity of nanofluids.
(v) While in suspension, the nanoparticles mainly appear in form of nanoclusters. Therefore, instead of using the information of individual nanoparticles, structural information about the nanoclusters should be incorporated in modeling of the thermal conductivity of nanofluids.
(vi) The thermal conductivity of the bulk base fluid (outside to the nanoclusters) is different than the thermal conductivity of base fluid which is close to the nanoparticles or enclosed in a nanocluster. This is because of the fact that base fluid streams pattern near to the solid surfaces is under the influence of boundary layer effect and follow a well-defined shape (Murshed *et al.*, 2006; Verma and Singh, 2016). This effect is assumed to be percolating throughout the entire nanocluster. As a result of this, the thermal conductivity of base fluid present within the characteristic dimension i.e. R_g of a nanocluster is comparatively higher than the thermal conductivity of the bulk base fluid. This increased thermal conductivity is required to be incorporated to develop the equations for overall thermal conductivity enhancement of nanofluids.
(vii) The effect of elapsed time and growth of nanoclusters on the overall thermal conductivity of nanofluid is needed to be investigated.

Therefore, keeping in view the above discussed facts, the thermal conductivity enhancement of the host fluid present in an aggregate is required to be determined first. The base fluid elements of host fluid present in a nanocluster are assumed to be of uniform, size and randomly distributed. The thermal conductivity enhancement of base fluid present within the characteristic dimension (R_g) of a nanocluster has been addressed by using the Bruggemann Model (Bruggeman, 1935; Hui *et al.*, 1999), expressed as:

$$\frac{K_{f1}}{k_f} = \frac{1}{4}\left[(3\varphi_{f1} - 1)\left(\frac{k_f}{k_l}\right) + (2 - 3\varphi_{f1}) + \frac{K_l}{4}\sqrt{A}\right] \quad (6.14)$$

$$\text{where, A} = \left[(3\varphi_{f1} - 1)^2\left(\frac{k_f}{k_l}\right)^2 + (2 - 3\varphi_{f1})^2 + 2(2 + 9\varphi_{f1} - 9\varphi_{f1}{}^2)\left(\frac{k_f}{k_l}\right)\right] \quad (6.15)$$

where, k_l is the thermal conductivity of the bulk fluid, k_f is the thermal conductivity of the fluid elements present in a nanocluster and k_{f1} is the thermal conductivity enhancement in host fluid present in a nanocluster. If $V_a = \frac{4}{3}\pi R_g^3$ is the volume of the nanocluster and $V_{na} = \frac{4}{3}\pi\ a^3 N$ is the volume of the primary nanoparticles in a nanocluster, then volume fraction, φ_{f1} of fluid elements presented in a nanocluster can be expressed as:

$$\varphi_{f1} = \frac{R_g^3 - Na^3}{R_g^3} \quad (6.16)$$

The presence of nanoparticles as dead-ends (those not forming the chain) inside a nanocluster is equivalent to the distribution of the nanoparticles in a liquid (whose thermal conductivity is k_{f1}). The thermal conduction due to these dead-ends nanoparticles can be defined by using the Bruggemann Model (Bruggeman, 1935; Hui *et al.*, 1999). The model is also found suitable to predict the thermal conductivity enhancement of base fluid (whose thermal conductivity is k_{f1}) due to the presence of dead end nanoparticles within the characteristic dimensions of a nanocluster.

$$\frac{k_{dp}}{k_{f1}} = \frac{1}{4}\left[(3\varphi_{dp} - 1)\left(\frac{k_p}{k_{f1}}\right) + (2 - 3\varphi_{dp}) + \frac{k_{f1}}{4}\sqrt{A}\right] \quad (6.17)$$

$$\text{where, A} = \left[(3\varphi_{dp} - 1)^2\left(\frac{k_p}{k_{f1}}\right)^2 + (2 - 3\varphi_{dp})^2 + 2(2 + 9\varphi_{dp} - 9\varphi_{dp}{}^2)\left(\frac{k_p}{k_{f1}}\right)\right] \quad (6.18)$$

where, k_{dp}, is the effective thermal conductivity of a nanocluster sphere due to the presence of dead-end particles and $k_{p,}$ the thermal conductivity of the nanoparticle, k_{f1} the thermal conductivity of base fluid present in an aggregate and φ_{dp} is the volume fraction of the particles belonging to dead-ends.

The thermal conductivity enhancement of a nanocluster due to the presence of backbone chains of nanoparticles is determined by assuming that backbone chains are embedded in a medium whose thermal conductivity is k_{dp}. The backbone chains of nanoparticles are assumed to be of cylindrical shape, randomly oriented and having an aspect ratio greater than unity, i.e., p >1. The Nan Model is an appropriate model to address the thermal conductivity enhancement due to this type of structural arrangements of the nanoparticles and is given in Eq. (6.25) (Clarke *et al.*, 1997). Therefore, the thermal conductivity of a nanocluster due to the combined effect of dead-ends and backbone chains of the nanoparticles in it is given as:

$$\frac{k_{adb}}{k_{dp}} = \left[\frac{3+\varphi_{bp}\,[2\beta_{11}(1-l_{11})+\beta_{33}(1-l_{33})]}{3-\varphi_{bp}[2\beta_{11}\,l_{11}+\beta_{33}l_{33}]}\right] \tag{6.19}$$

where, k_{adb}, is the thermal conductivity of a nanocluster, φ_{bp}, is the volume fraction of the backbone chains of nanoparticles and other parameters are defined as follows:

$$l_{11} = \frac{0.5p^2}{(p^2-1)} - \frac{0.5p\ cosh^{-1}p}{(p^2-1)^{1.5}} \tag{6.20}$$

where, $l_{33} = 1 - 2l_{11}$

$$\beta_{11} = \frac{(K_{11}-k_{f1})}{[K_{f1}+\,l_{11}\,(K_{11}-k_{f1})]} \tag{6.21}$$

$$\beta_{33} = \frac{(K_{33}-\,k_{f1})}{[k_{f1}+l_{33}\,(K_{33}-k_{f1})]} \tag{6.22}$$

where, p is the aspect ratio, which signifies the length of the backbone chain in an aggregate or nanocluster, i.e.$p = \frac{R_g}{a}$

where, $K_{11} = \frac{k_{dp}}{(1+\,r\,l_{11}\;k_{dp}/k_{f1})}$ (6.23)

and $K_{33} = \frac{k_{dp}}{(1+\,r\,l_{33}\;k_{db}/k_{f1})}$ (6.24)

where, $r = \left(2 + \frac{1}{p}\right) R_{BL} \frac{k_{f1}}{d_p}$ for p > 1 (6.25)

The value for R_{BL} varies from 2×10^{-9} m^2 K/W to 2×10^{-8} m^2 (for oxide based nanofluids) (Ge *et al*., 2006; Schmidt *et al.*, 2008), which does not seem to have much influence on the cluster's thermal conductivity. Therefore, for the present work, the accepted value of R_{BL} is of the order of 1×10^{-9} m^2 K/W. Once, the conductivity of the nanocluster (k_{adp}) is calculated by using Eq. (6.19), then the thermal conductivity enhancement for the whole sample of nanofluid can be predicted by using the Maxwell Garnet (M-G) model (Maxwell, 1873), as given below:

$$\frac{\Delta k_{eff}}{K_l} = \left\{\frac{[(k_{adb}+2k_l)+2\varphi_{at}(k_{adb}-k_l)]}{[(k_{adb}+2k_l)-\varphi_{at}(k_{adb}-k_l)]}\right\} \quad (6.26)$$

where, Δk_{eff}, is the effective thermal conductivity of nanofluid considering only the perikinetic heat conduction conditions. The volume fraction of nanoclusters in a given sample of nanofluid is given as:

$$\varphi_{at} = \varphi_p / \varphi_a \quad (6.27)$$

All other terms have their usual meaning.

6.3.2 Brownian Motion (BM) induced micro-convection models

Prasher *et al*. (2005) reported their findings on the thermal conductivity enhancement of Al_2O_3 based nanofluids (diameter: 10 nm, 0.05% volume fraction) and suggested that there could be two aspects responsible for the mode of thermal energy transport in nanofluids; first, the conventional conduction, and second – the Brownian motion induced micro-convection in the base fluid. The dominance of the either effect depends strongly on the size of the particles in suspension and working temperature.

The temperature dependent Brownian movement of the nanoclusters while in suspension causes the induced micro-convection. The velocity (root mean square) of the nanocluster is defined as:

$$v_{nc} = \sqrt{\frac{3K_B T}{m_{nc}}} \tag{6.28}$$

where, m_{nc}, the mass of the nanocluster = $\frac{4}{3}\pi R_g^3 \rho_{nc,}$ and $\rho_{nc} = (1-\varphi_a)\rho_f + \varphi_a \rho_s$, is the density of the nanocluster. For a well-dispersed system, $m_{nc} = m$ (mass of a single particle). However, as the suspension contains nanoparticles in the form of nanoclusters, the mass of nanocluster (after an elapsed time, *t*) is given as: $m_{nc} = Nm$. The Brownian Reynolds Number (R_{eB}) for the equivalent sphere as that of the volume of nanocluster having the characteristic dimension, R_g is given as:

$$R_{eB} = \frac{3\,\rho_{nc}}{\mu_f}\left\{\frac{\left(\frac{K_B T}{\pi \rho_{nc}}\right)^{0.5}}{\left[a\left(1+\frac{t}{t_p}\right)^{1/d_f}\right]^{0.5}}\right\} \tag{6.29}$$

The Eq. (6.29) can be used to investigate the effect of temperature, cluster growth and time on the Brownian Reynolds number (R_{eb}).

The correlation of particle convective heat transfer coefficient (*h*) for all the nanoclusters suspending in the base fluid and contributing for the heat transport is defined by using (Brodkey *et al*., 1991), given as:

$$h = \frac{k_f}{a}(1 + A\ {R_{eB}}^m\ {P_r}^{0.333}\varphi_{at}) \tag{6.30}$$

where, '*A*' and '*m*' are constants and their values depend on the nature of the nanofluid; for metal oxide, A ≈ 5 ×10^4 and, m ≈ 2.5 ± 10% (Prasher *et al.*, 2006), $P_r = \mu\, C_p/k_f$, is the Prandtl's number and, φ_{at} is the actual volume fraction of the nanoclusters in base fluid. In the Stoke's regime, if the spheres of nanoclusters are assumed to be embedded in a semi-infinite medium of thermal conductivity, k_m, then, $h = \frac{k_m}{a}$ (Bergman *et al.*, 1996). Therefore, the equation for the thermal conductivity enhancement due to the Brownian motion induced convection can be expressed as:

$$\frac{k_m}{k_f} = (1 + A\ {R_{eB}}^m\ {P_r}^{0.333}\varphi_{at}) \tag{6.31}$$

Meanwhile, the increase in the thermal conductivity due to the perikinetic conduction part is given as:

$$\frac{\Delta k_{eff}}{k_m} = \left\{\frac{[(k_{adb}+2k_m)+2\varphi_{at}(k_{adb}-k_m)]}{[(k_{adb}+2k_m)-\varphi_{at}\ (k_{adb}-k_m)]}\right\} \tag{6.32}$$

From the above Eqs. (6.31) and (6.32), the final equation for the overall/effective thermal conductivity of a particular nanofluid (include the perikinetic heat condition and Brownian motion induced micro-convection) can be expressed as:

$$\frac{\Delta k_{overall}}{K_f} = \left\{\frac{[(k_{adb}+2k_l)+2\varphi_{at}(k_{adb}-k_l)]}{[(k_{adb}+2k_l)-\varphi_{at}\ (k_{adb}-k_l)]}\right\} \left(1 + A\ {R_{eB}}^m\ {P_r}^{0.333}\varphi_{at}\right) \tag{6.33}$$

where, φ_{at} is the actual volume fraction of the nanoparticles present in the whole base-fluid at any instant of time, *t* and all the terms have their usual meaning as given in the nomenclature.

Chapter-7

Nanoclusters Based Mechanisms of Thermal Heat Transport in Nanofluids

Nanofluid suspension study reveals that the concentration of nanoparticles changes with respect to the elapsed time. This change depends on the morphological properties of the nanoclusters and the thermophysical properties of base fluids. A quantitative analysis of the effect of time and temperature dependent instantaneous volume fraction on perikinetic heat conduction and Brownian motion induced micro-convection mechanisms have been presented for the oxide (Al_2O_3 and TiO_2) based nanofluids. Generally, this aspect is not considered in most of the studies reported on the variety of nanofluids. The structural and Brownian motion based convection models of thermal conductivity for the varying concentration of the nanoparticles in their respective base fluids are being introduced. In addition to the suspensions stability parameters, these models also take into account the effect of nanoclusters growth, temperature, thermal interfacial resistance, and liquid layering. A systematical study to address the above-mentioned issues have been presented in the subsequent sections.

7.1 Perikinetic Heat Transport in Al_2O_3-H_2O and TiO_2-H_2O Nanofluids

The thermal conductivity enhancement of nanofluids depends on the factors affecting their mechanism of heat transport. More insight into the phenomenon of heat conduction in nanofluids has been presented here. The growth of nanoclusters of Al_2O_3 and TiO_2 nanoparticles (size 25-30 nm) in water (DI) as the base fluid has been studied. A comprehensive report is prepared on the size distribution of the particles in their respective nanofluid at different pH values and zeta potential along with the stability of suspensions. A quantitative analysis on the thermal conductivity enhancement and an investigation on the role of nanoparticles present in the form of dead-ends and backbone chains in a nanocluster has been put forward. The effect of nanoclusters under perikinetic heat conduction conditions has been incorporated to address the thermal conductivity enhancement of nanofluids. Moreover, the effect of base fluid layering around the nanoparticles in an aggregate/nanocluster has also been highlighted and considered. The possible and different governing static/structural models which are capable to predict the nanocluster based thermal conductivity enhancement in nanofluids have been investigated and modified. The effect of liquid layering on the thermal conductivity of the water present in an aggregate compared to the bulk water present outside to the nanocluster or an aggregate has been also studied. As already

discussed, the clustering is an important phenomenon responsible for performances and enhancement of their thermal conductivity of nanofluids (Chapter 2). Therefore, clusters size and aspects of their structural arrangement have been incorporated in the modelling of the thermal conductivity of nanofluids rather than the nominal or average diameter of the dry powder state.

7.1.1 Nanofluids' preparation, pH and zeta potential measurements

The commercial nanopowder of Al_2O_3 (γ) and TiO_2 (rutile + anatase), of size 20-30 nm is procured from Intelligent Material Pvt. Ltd. (NANOSHEL, USA). The material characterization is performed with the help of powder X-Ray diffraction (XRD) technique at the room temperature (25ºC). A complete analysis of XRD pattern including lattice parameters and Bragg profiles confirmed the existence of Al_2O_3 (γ) and TiO_2 (rutile + anatase) with 99.99% and 99% purity. This information has already been provided in Chapter 3 (Experimental Section). To carry out the experimental work, the various samples of nanofluids (20 ml each) were prepared by mixing the nanoparticles of 0.05% of volume concentration i.e. 38.80 mg of Al_2O_3 and 41.0 mg of TiO_2 in water (DI). The deionized (DI) water has been chosen as the base fluid for being non-toxic and the most commonly used fluid for many cooling applications. The anionic surfactant Sodium Dodecyl Sulphonate (SDS) has been used to enhance stability the nanofluid suspensions. The effect of pH value on the stability of nanofluid suspensions has been investigated by using hydrochloric acid (HCl) and sodium hydroxide (NaOH) of suitable analytical grades. The surface chemical effects are considered as the key factors affecting the suspension stability of nanofluids and their thermal conductivity. The dispersion quality of Al_2O_3 and TiO_2 nanoparticles in aqueous solution depends on their electro-kinetic properties. A high-quality dispersion can be obtained with nanoparticles having high surface charge density which thereby confirms the presence of strong repulsive forces among the nanoparticles. Therefore, the measurement of the zeta potential is considered to be an important aspect in order to understand the suspension behavior of nanofluids. The measurements of zeta-potential of all the samples have been done by using a Zeta sizer and by repeating the experiments as per the requirement.

7.1.2 Thermal conductivity measurements

The thermal conductivity measurements of different types of nanofluids have been carried out by using a KD2 Pro thermal property analyzer (Decagon Devices, Inc., USA). This method is known to be accurate and a quick way to determine the thermal conductivity of nanofluids (Xie *et al.*, 2002; Das *et al.*, 2003; Jang and Choi, 2004; Wen and Ding, 2004; Zhang *et al.*, 2006). All other detailed information about its calibration has already been provided in Chapter 4.

7.1.3 Interdependency of hydrodynamic size, pH and zeta potential

A Probe Type Ultra Sonicator (Oscar Ultrasonics, 250W, 20 ± 3 kHz) has been used to prepare different samples of Al_2O_3 and TiO_2 based nanofluids under "Two-Step Method." The samples of volume concentration of 0.1% to 0.5% were prepared and subjected to a prolonged sonication up to six hours without using any surfactant or additive. A high settling rate of the nanoparticles is observed in samples just after sonication is turned off. Therefore, the volume fraction of the order of 0.05% has been taken up to carry out the thorough investigations of the nanocluster formation and their associated effects on the thermal conductivity of Al_2O_3-H_2O and TiO_2-H_2O nanofluids. Otherwise, settling rate could have been too fast to observe these effects if higher volume fractions were taken. The stability and adsorptive properties of oxides based nanofluids depend on the various factors, such as crystal structure, surface structure and the presence of surface active sites (Bailar *et al.*, 1973; Patnaik, 2003). Therefore, to achieve a good suspension stability of nanofluids, an anionic surfactant, i.e., sodium dodecyl sulphonate (SDS) has been used, which is found to be suitable especially for oxide based nanofluids (Das *et al.*, 2007; Dongsheng Zhu *et al.*, 2009). The reason to opt for surfactant SDS has already been explained in Chapter 5. The experiments were conducted by using 0.05% volume concentration of alumina (Al_2O_3) and titanium dioxide (TiO_2) individually, along with surfactant, SDS in ratio 1:1 (by weight), respectively. All this was done to measure the Zeta-potential, hydrodynamic size of the nanoparticles, stability ratio, and their effect on the thermal conductivity of the suspensions. The particles size distribution in different samples of nanofluids has been studied by using dynamic light scattering technique (DLS, Brook Haven 7610 Instrument) and the required pH value of the samples was maintained with HCl and NaOH solutions. By following the step wise step procedure, in all the cases 2-4 ml of nanofluid

suspension was transferred into a measuring cell. Then zeta potential values of the nanoparticles were measured by a Malvern ZS Nano S analyzer (Malvern Instrument Inc., London, UK). The measurements were taken at a temperature of 25°C (± 2 °C) with a switch time of t = 50 s. Each experiment was repeated at least three times to get the required parameter i.e. Zeta potential. In the study undertaken, the pH value of the solution has been varied to control the surface charge density and hence the suspension stability of the nanofluids.

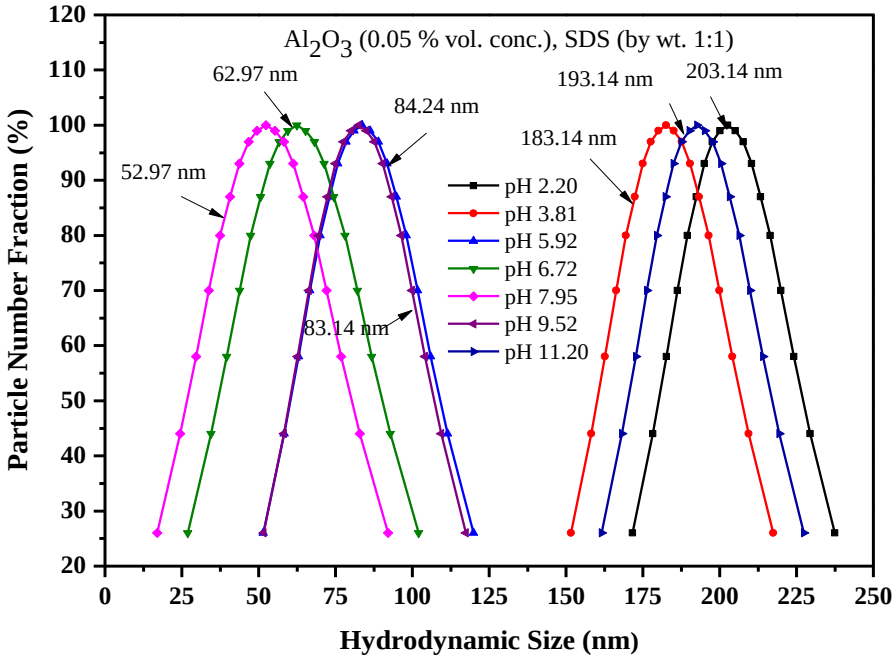

Fig. 7.1: Dispersion quality of Al_2O_3-H_2O nanofluid mixed with SDS (by wt.1:1) at different values of pH (2.20 to 11.20)

The effect of 0.05% volume concentration of nanoparticles (Al_2O_3 and TiO_2) and SDS (by wt. 1:1) on hydrodynamic size of the nanoparticles in suspension has been investigated for suspension stability. These suspensions were also maintained at different pH, i.e. 2.20 to 11.20 for Al_2O_3-H_2O nanofluid and from 2.92 to 11.62 for TiO_2-H_2O nanofluid, respectively. The data for the hydrodynamic size of the Al_2O_3 and TiO_2 nanoparticles while in suspension has been presented in Fig. 7.1 and Fig. 7.2, respectively. These figures reveal that the hydrodynamic size of TiO_2 nanoparticles in suspension is smaller than the Al_2O_3 nanoparticles and it is found to be same at almost all pH values.

Apparently both the suspensions seems to be stable; however, TiO_2-H_2O suspension is finer and comparatively more stable than its counterpart Al_2O_3-H_2O suspension.

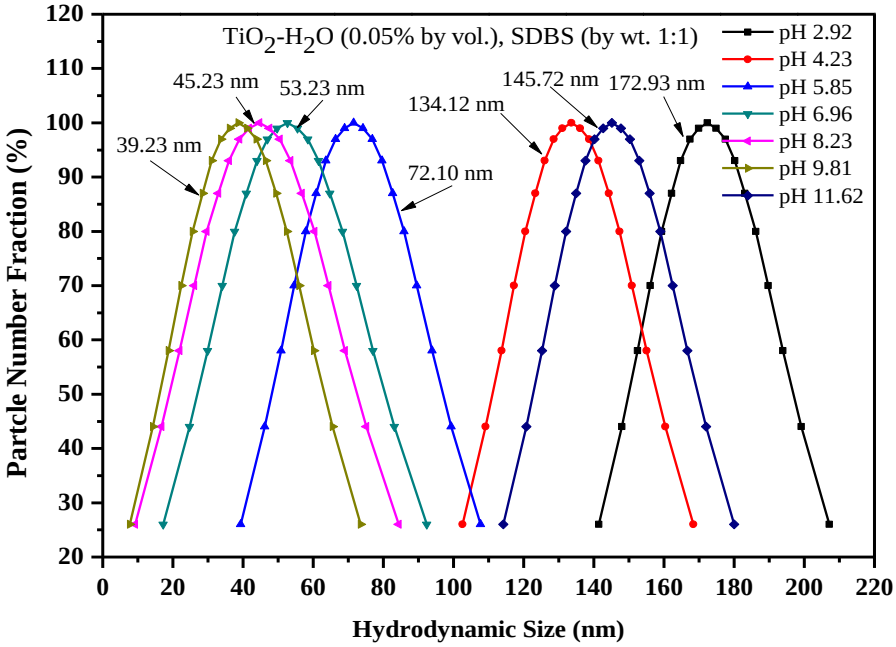

Fig. 7.2: Dispersion quality of TiO_2-H_2O nanofluid mix with SDS (by wt.1:1) at different values of pH (2.92 to 11.62)

The interdependency between zeta-potential, hydrodynamic sizes of nanoparticles and pH for both types of nanofluids have been shown in Fig. 7.3 and Fig. 7.4. Both the nanofluids show almost a similar trend with a change in pH value. The Al_2O_3-H_2O suspension seems to be comparatively more stable at pH equal to 7.3 to 8.2, whereas for TiO_2-H_2O suspension, stability is found to be more at pH of 8.8 to 9.8. The corresponding zeta-potential values for these two nanofluids is maximum around -39.80 mV and -42.93 mV, respectively. Under the same conditions, the minimum average hydrodynamic size of the particles while in suspension is observed to be approximately 52.97 nm for Al_2O_3-H_2O and 39.23 nm for TiO_2-H_2O nanofluid. This significant reduction in their size is augmented due to the presence of surfactant SDS, which is an anionic surfactant. As a result of this, Al_2O_3 and TiO_2 get a negative charge on their surface for the whole pH range, i.e. from 2 to 12. The absolute values of zeta-potential of the particle surfaces (Al_2O_3 and TiO_2) tend to be minimum for pH< 4 or pH>11, thereby enabling the nanoparticles to grow in their size. In this range of pH, the electrostatic repulsion force between particles is just not

sufficient to overcome the attractive force and it leads to a poor dispersion quality. With an increase in pH value, i.e. 4 < pH <11, the zeta-potential also increases and thereby increases the electrostatic repulsion force between nanoparticles which becomes sufficient to overcome the attraction force between particles.

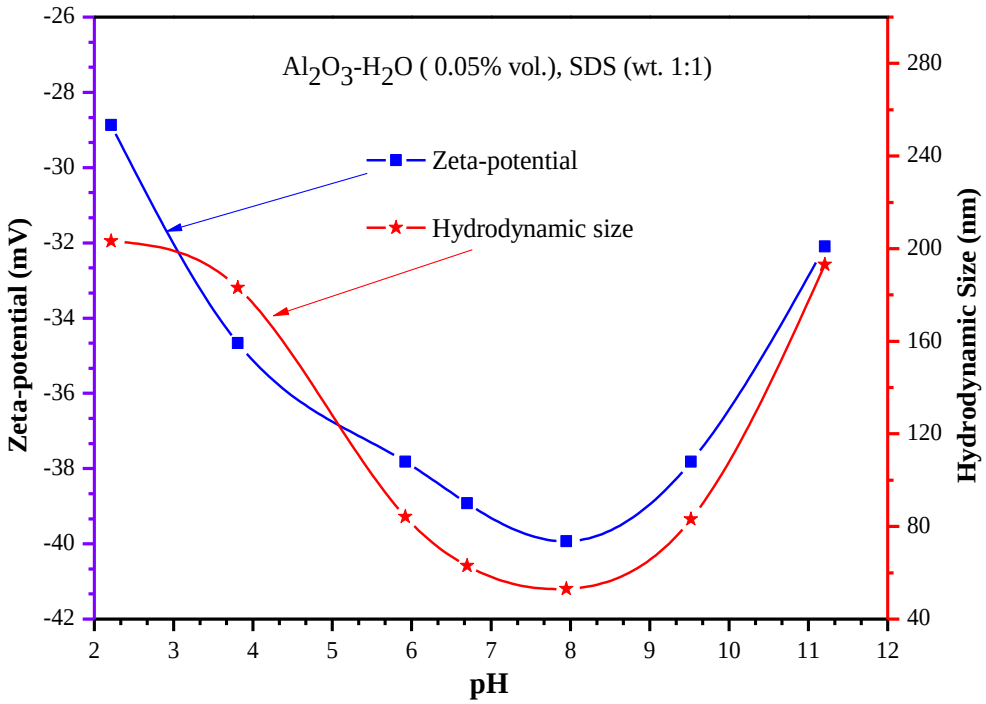

Fig. 7.3: Effect of pH on zeta potential and hydrodynamic size of Al_2O_3-H_2O nanofluid

The large electrostatic force results in freeing more number of particles by increasing the particle-particle distance. This further reduces the probability of particles to coagulate and settle, which ultimately improves the suspensions stability of suspensions. Thus, at pH around 7.95 for Al_2O_3 and 9.81 for TiO_2, the zeta-potential become even higher and the electrostatic repulsion force between particles becomes strong enough to give the best dispersion quality and stability. These experimental investigations confirm the dispersion behavior of Al_2O_3 and TiO_2 based nanofluids in agreement with the DLVO theory (Zhu *et al.*, 2009; Wang *et al.*, 2011).

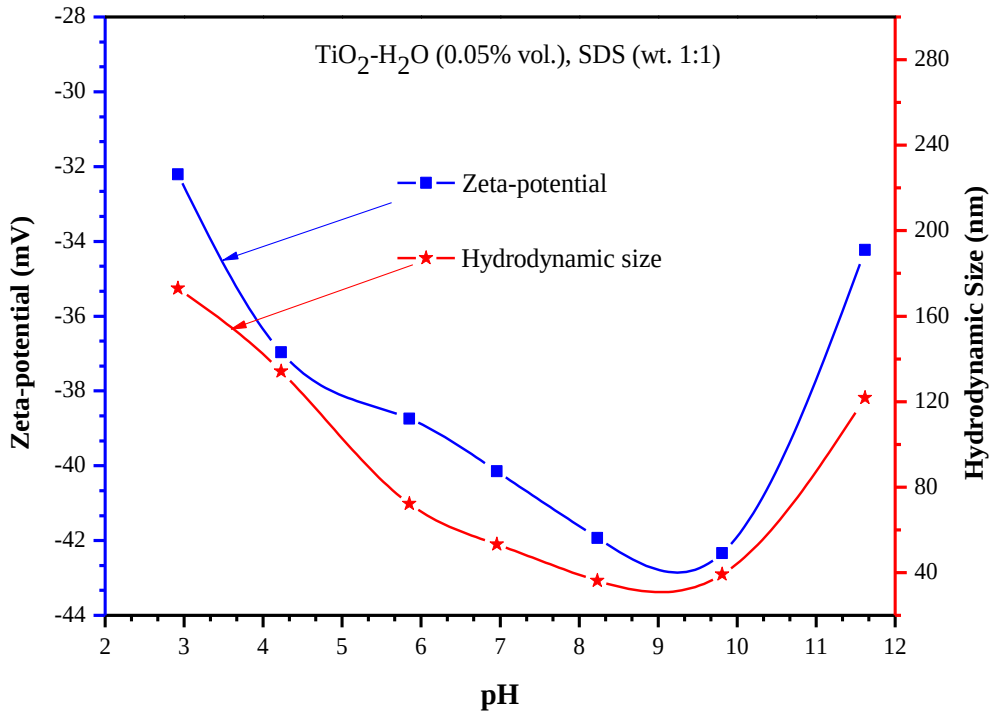

Fig. 7.4: Effect of pH on zeta potential and hydrodynamic size of TiO_2-H_2O nanofluid

7.1.4 Effect of stability ratio and aggregation time constant on the suspension quality

At a loading of nanofluids with 0.05% of volume concentration of Al_2O_3 and TiO_2 and different pH values, the total interaction energy, E_{tot} i.e. $E_R + E_A$ (Eq. 6.8 and 6.10) has been determined for a particle to particle surface distance from x = 5 nm to 100 nm, see Fig. 7.5 and Fig. 7.6. The variation in the level of total interaction energy barriers with distance (x) and pH value of the suspension has been analyzed here. The suspending particles or clusters are required to overcome these energy barriers in order to become agglomerated and thereafter to grow in size. The maximum value of total energy barrier at pH = 7.95 is found to be around 24.5×10^{-20} J for Al_2O_3-H_2O suspension and at a pH = 9.81 it is 27×10^{-20} J for TiO_2-H_2O nanofluid for the particle to particle surface distance around 5 nm. The existence of the relatively strong energy barrier at these optimized pH values helps in keeping away the particles during the suspension and hence makes the suspension more stable.

The values from the locus of the total energy curve have been used as an input to determine the stability ratio of the suspensions at different pH values.

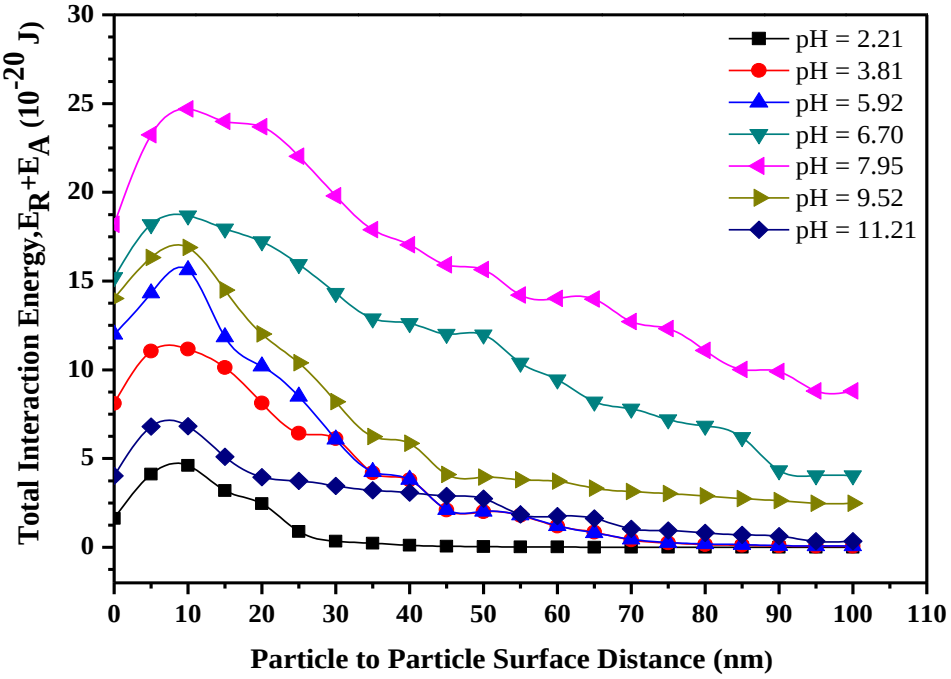

Fig. 7.5: Total interaction energy plots for the Al_2O_3-H_2O nanofluid as a function of surface to surface distance between the particles

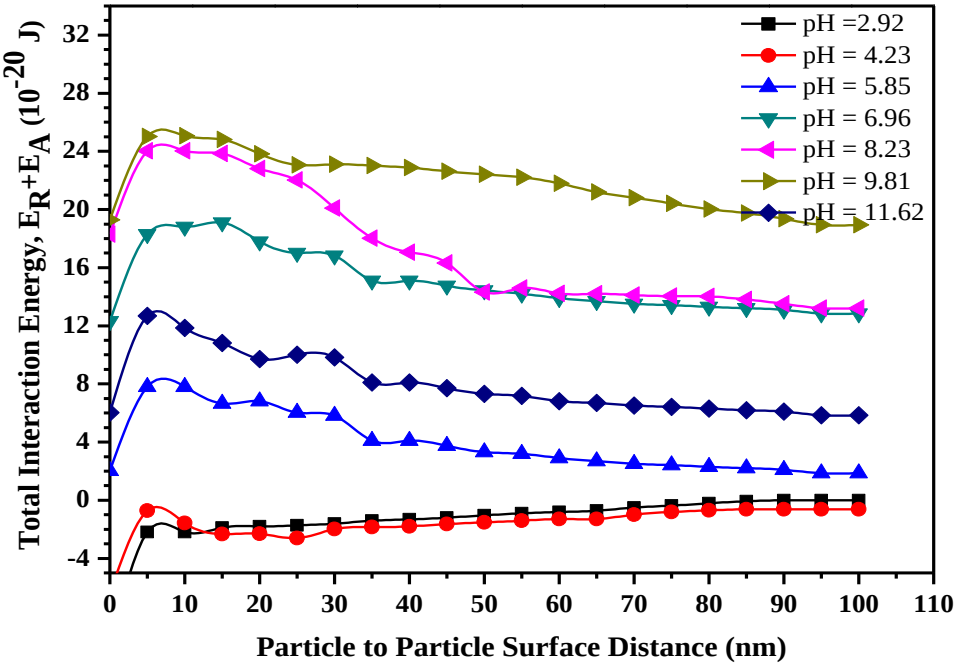

Fig. 7.6: Total interaction energy plots for the TiO_2- H_2O nanofluid as a function of surface to surface distance between the particles

In order to analyze the perikinetic conduction mechanism of nanofluids, the following volume fractions are determined such as (i) volume fraction of the nanoparticles in an aggregate, φ_a (Eq. 6.4) (ii) volume fraction of the primary nanoparticles in base fluid, φ_p (0.05% by volume), (iii) volume fraction of backbone particles in an aggregate, φ_{bp}, (Eq. 6.6), (iv) volume fraction of the particles belonging to dead-ends, φ_{dp}, (Eq. 6.7), (v) volume fraction of fluid elements presented in the aggregate, φ_{f1} (Eq. 6.16) and (vi) volume fraction of the total aggregates present in the base fluid, φ_{at} (Eq. 6.27). The theoretical Eq. (6.8) and (6.10) given for electrostatic repulsion energy (E_R) and attraction energy (E_A) along with Eq. (6.12) for hydration energy have been used to determine the stability ratio (W), given by Eq. (6.11). Calculations have been performed to determine the stability ratio for both types of suspensions. The variations in the stability ratio with variation in pH values and hydrodynamic size of the particles while in suspension have been presented in Fig. 7.7 and Fig. 7.8.

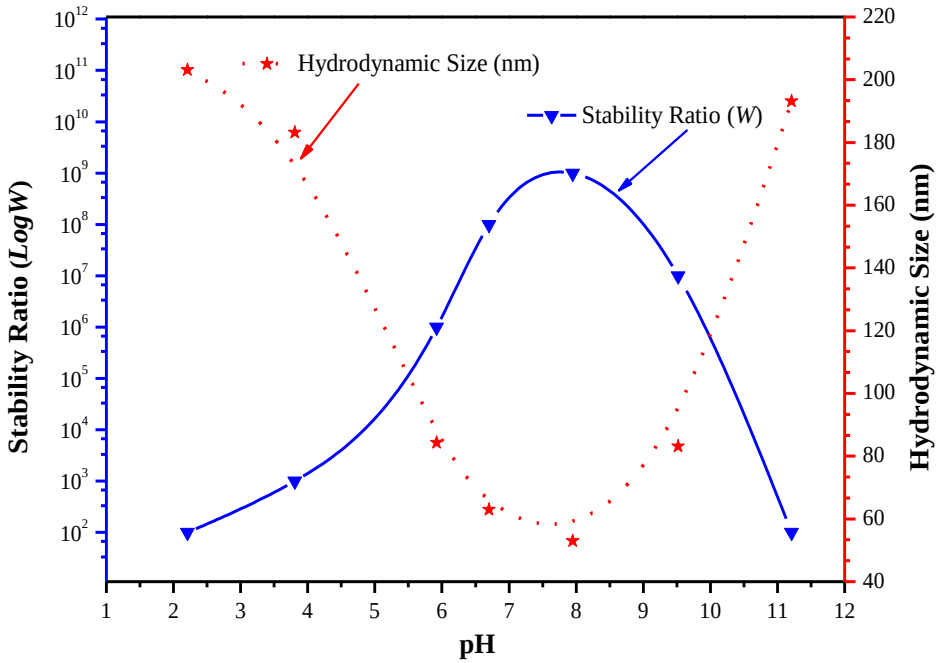

Fig. 7.7: Dispersion quality of Al_2O_3-H_2O (SDS 1:1 by wt.) nanofluid in terms of stability ratio (W)

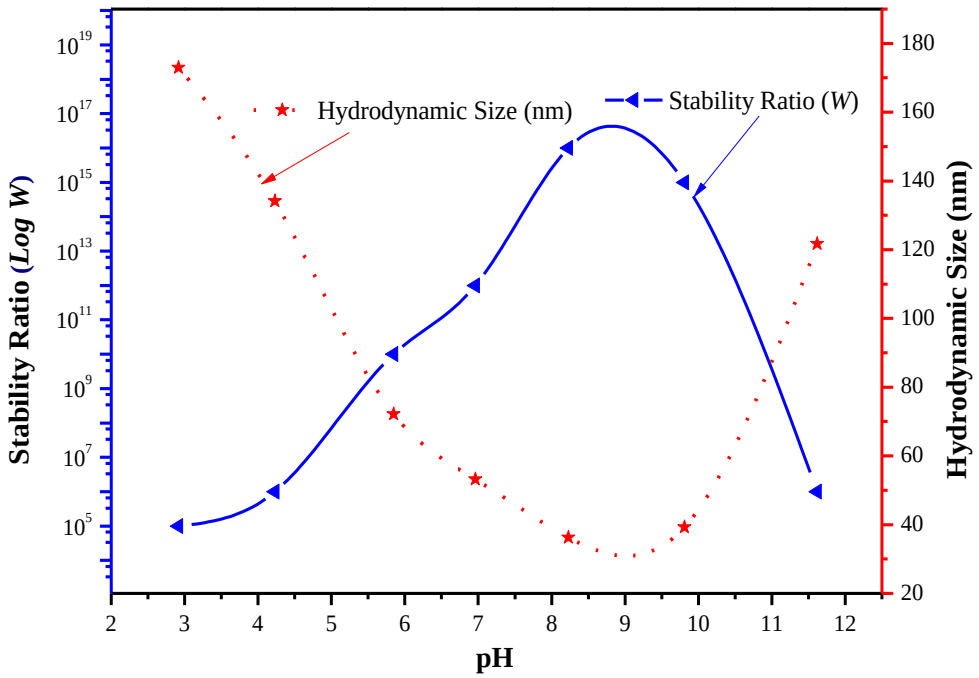

Fig. 7.8: Dispersion quality of TiO_2-H_2O (SDS 1:1 by wt.) nanofluid in terms of stability ratio (*W*)

The stability profiles for both types of nanofluids follow geometrically a similar trend, but differ numerically. The maximum value of *W* is around 10^9 (at pH ≈ 8) for Al_2O_3 based suspension whereas, this value is around 10^{16} (at pH ≈ 9) for TiO_2 based suspension. The corresponding values of the average hydrodynamic size of the particles are approximately 52 nm and 39 nm, respectively.

The behavior of aggregation time constant (t_p) for both types of nanofluids can be investigated by modifying the Eq. 6.3, given as:

$$t_p = \alpha\, a^3\, W \tag{7.1}$$

where, $\alpha = \frac{\pi\,\mu}{K_B\, T \varphi_p}$ is a constant and is equal to 13.58×10^{20} s/m^3, whose value has been determined by taking Boltzmann constant, $K_B = 1.38064852 \times 10^{-23}$ m^2 kg s^{-2} K^{-1} and viscosity of base fluid, $\mu = 0.89$ mPa-s at room temperature of 25 °C (± 2 °C).

The interdependence of aggregation time constant, t_p, (Eq. 7.1) stability ratio, *W* (Eq. 6.11) and hydrodynamic size of the nanoparticles while in suspension (*2a*) have been shown in Fig. 7.9 and

Fig. 7.10. The following important observation can be drawn from this analysis. Firstly, aggregation time constant increases (i) with an increase in stability ratio and (ii) with a decrease in the hydrodynamic size of the nanoparticles for both types of nanofluids. Secondly, TiO_2 nanofluid is found to be possessing a higher value of aggregation time constant (10^{14}) compared to Al_2O_3 nanofluid. Hence, nanoparticles of TiO_2 nanofluid will remain in suspension for a longer time.

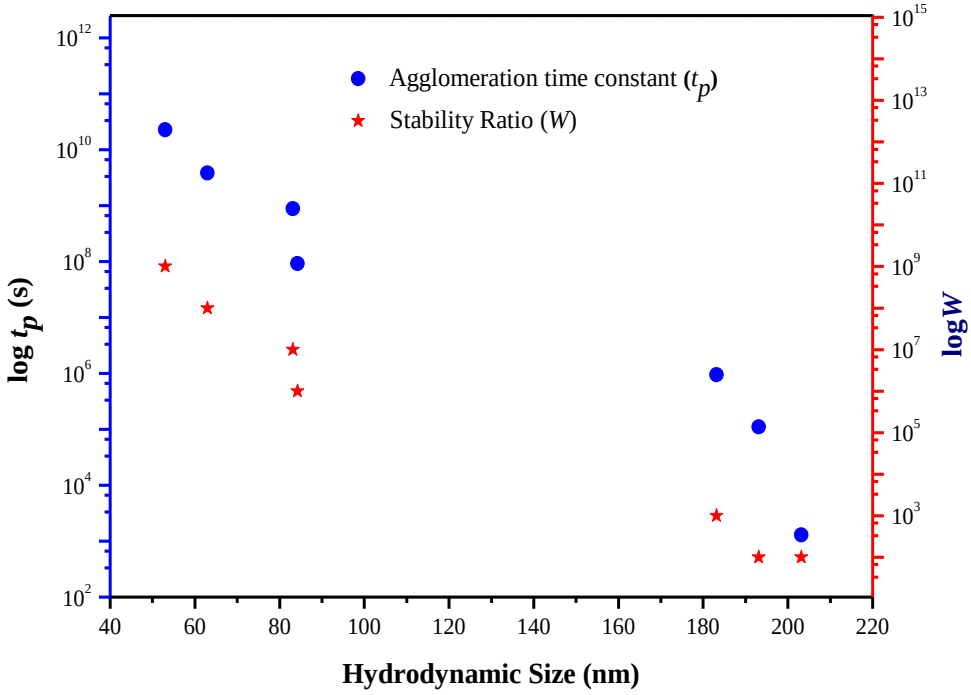

Fig. 7.9: Dependence of agglomeration time constant (t_p) on stability ratio (W) and hydrodynamic size of the nanoparticle for Al_2O_3-H_2O suspension

From the ongoing discussion, it is quite evident that the nanofluid suspensions are comparatively more stable at pH ≈ 7.95 (Al_2O_3) and pH ≈ 9.81 (TiO_2). Thereafter, the investigations were taken further and the parameters of the nanofluid's suspensions were determined only for the pH values which are near to the above mentioned optimized pH values. For a known pH value, the hydrodynamic size ($2a$) and the primary volume concentration of the nanoparticles (φ_p), calculations have been performed for both nanofluids to obtain varying characteristic dimensions (R_g) and the volume fractions. The values of these volume fractions have been obtained with respect to the elapsed time ranging from 1 hour to 240 hours (i.e. up to 10 days). It has been

reported previously in the literature that molecules of the base fluid form a semi-solid layer or a well-defined pattern around the surface of the nanoparticles which may be due to the adsorption of the base fluid molecules on the surface of the nanoparticles. This ordered layering around the nanoparticles possesses a higher thermal conductivity than the rest of the base fluid, which ultimately enhance the effective thermal conductivity of the nanofluid (Keblinski *et al.*, 2002; Yu *et al.*, 2003). Keeping in view the above-mentioned facts, author is of the opinion that the liquid layering may result into an increase in the thermal conductivity of liquid up to 3%. Therefore, for the study presented here, the accepted value for the thermal conductivity enhancement in the cluster is 0.6120 W/mK (increase of 1%) against the 0.6060 W/mK thermal conductivity of water at 25 °C.

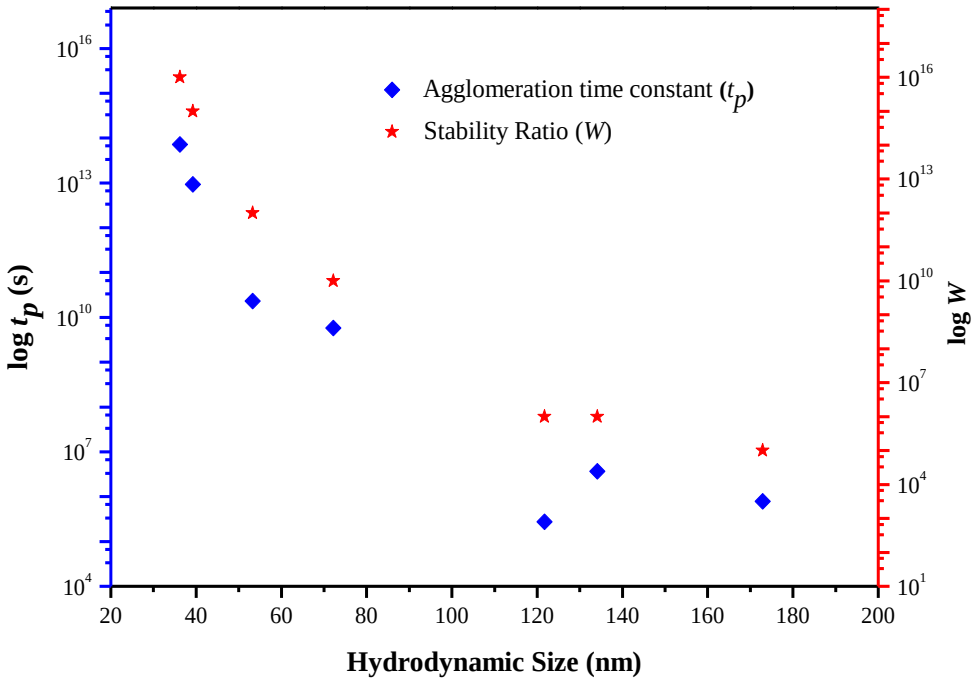

Fig. 7.10: Dependence of agglomeration time constant (t_p) on stability ratio (W) and hydrodynamic size of the nanoparticle for TiO_2-H_2O suspension

7.1.5 Cluster based thermal conductivity and effective thermal conductivity

The values of volume fractions, cluster characteristic dimension and fractal dimensions have been used to predict the different thermal conductivities of nanofluids, such as k_{f1}, k_{dp}, $k_{adb,}$ and Δk_{eff}, given by Eq. (6.14), (6.17), (6.19), and (6.26), respectively. While performing the calculations at a particular instant of time, all the nanoparticles inside a nanocluster are assumed to be of uniform size and spherical in shape. It has also been observed that the number of nanoparticles/nanoclusters increases with elapsed time. The thermal conductivity enhancement due to the back bone chain of nanoparticles embedded in dead-end nanoparticles is represented by k_{adb}, (Eq. 6.19) shown in Fig. 7.11 (a). During the investigations, the nanoparticles forming the back bone chains are found to be in the cylindrical shape with their aspect ratio greater than one, i.e., $p > 1$. These facts were also verified by obtaining the TEM images of the samples collected from time to time, see Fig. 7.11 (b)-(e). Finally, after predicting the thermal conductivity enhancement for a single nanocluster, the effective thermal conductivity enhancement for whole sample of a particular nanofluid, i.e. Δk_{eff}, is determined by using a modified model, Eq. (6.26), see Fig. 7.11 (a). At optimized pH values of nanofluids, the effect of the cluster characteristic dimension (R_g), and elapsed time (t) on the cluster thermal conductivity (k_{adb}) and effective thermal conductivity (Δk_{eff}) have been shown in Fig. 7.11 (a). The characteristic dimension (R_g) is found to be increasing with elapsed time (t), which means that with the passage of time, more and more nanoparticles are coming closer to each other and forming the nanoclusters of bigger and bigger sizes. Both types of thermal conductivities, i.e. k_{adb} and Δk_{eff} are found to be decreasing with an increase in the value of R_g, see Fig. 7.11 (a) and Fig. 7.12 (a). However, the rate at which nanoclusters grow in size is different for Al_2O_3 and TiO_2 based nanofluids. The figures (Fig. 7.11 and 7.12) clearly show that after a particular time interval (time elapsed), TiO_2 based nanofluid shows more enhancement in the effective and nanocluster based thermal conductivity. This can be possible due to the fact that the nanoclusters in TiO_2 based nanofluid are of smaller size compared to the nanocluster's size in Al_2O_3 nanofluid. Nanoclusters with smaller size have tendency to make the nanofluid more homogenous and as a result of this the nanofluid exhibits higher thermal conductivity (Δk_{eff} and k_{adb}). These thermal conductivities are found to be decreasing with elapsed time; however, these are still higher than for water alone if taken as base fluid. Therefore, it can be concluded that the presence of nanocluster has allowed more heat transfer through the nanofluids.

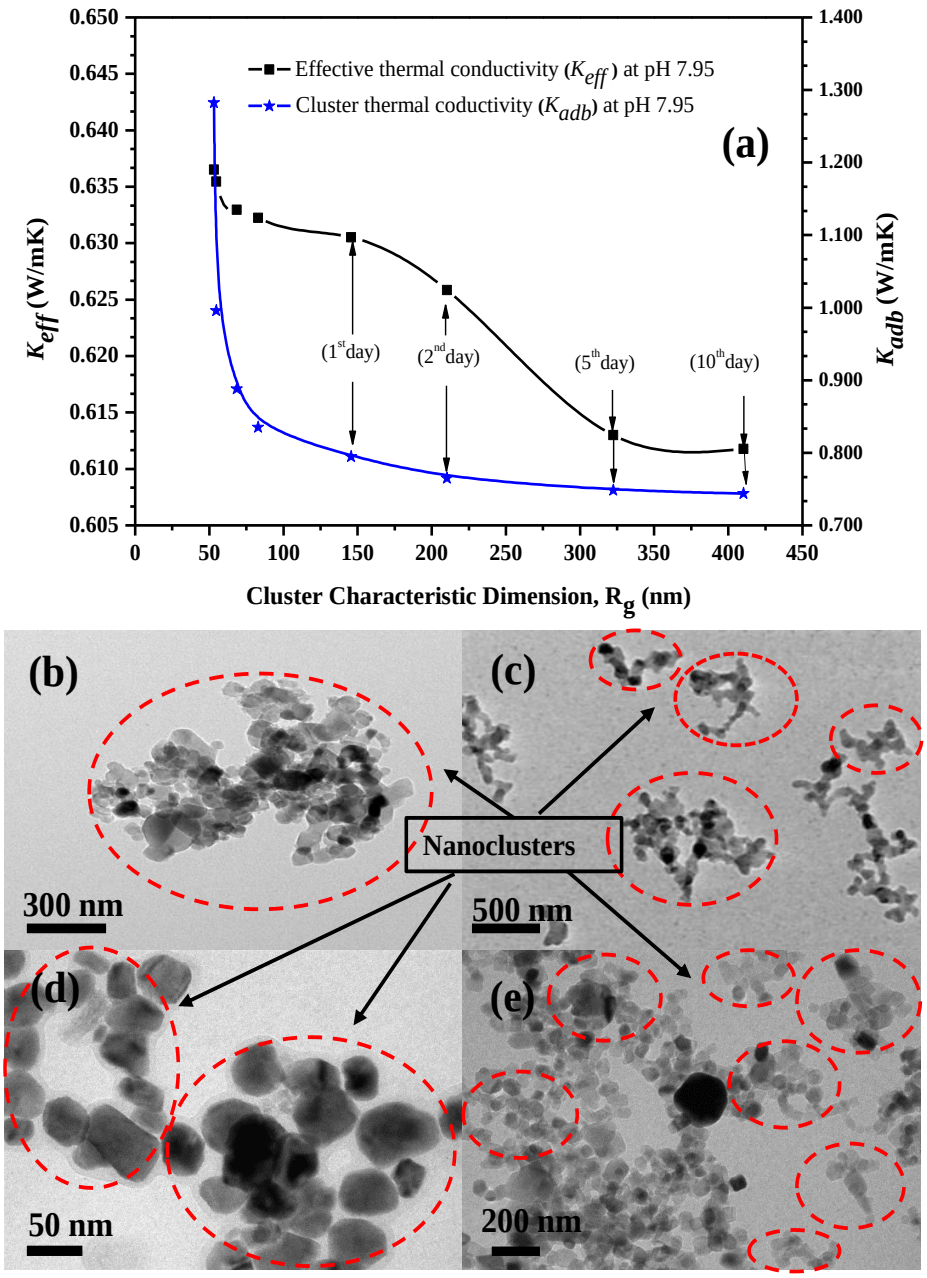

Fig. 7.11: (a) Effect of characteristics dimension (R_g) on the effective thermal conductivity (Δk_{eff}) and cluster thermal conductivity (k_{adb}) of Al_2O_3-H_2O nanofluid and, **(b) to (e)** the corresponding TEM images of the nanoclusters growth in actual suspension

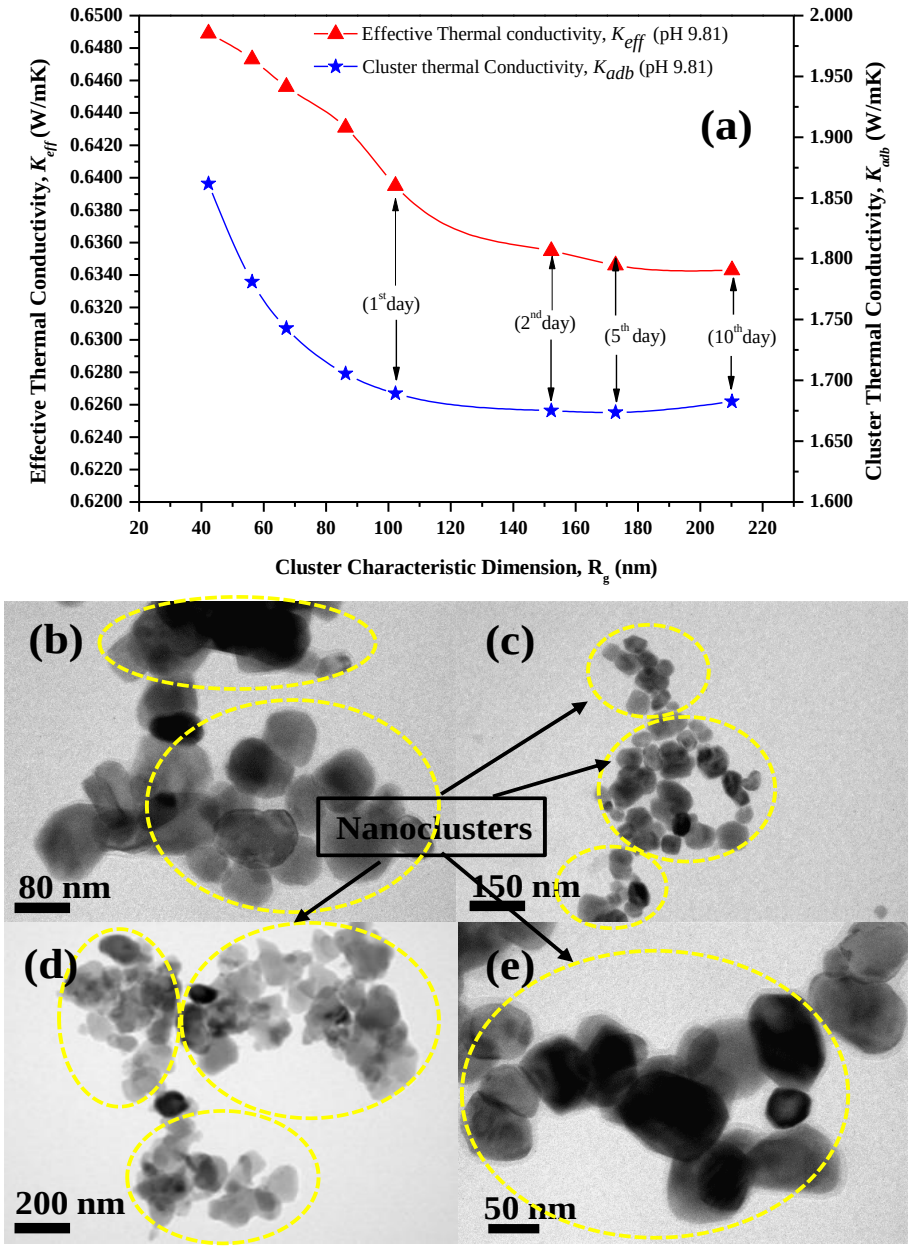

Fig. 7.12: (a) Effect of characteristics dimension (R_g) on the effective thermal conductivity (Δk_{eff}) and on cluster thermal conductivity (k_{adb}) of TiO_2-H_2O nanofluid and **(b) to (e)** the corresponding TEM images of the nanoclusters growth in actual suspension

The enhancement in Δk_{eff} and k_{adb} also depends on the presence of the volume fraction of the nanoparticles in nanocluster (φ_a). The value of φ_a is found to be varying from 45-98% for Al_2O_3-H_2O nanofluid and from 70-100% for TiO_2 -H_2O nanofluid over the time period of ten days. It is

also observed that with increase in the amount of the nanoparticles in a particular nanocluster, the enhancement in thermal conductivities i.e. Δk_{eff} and k_{adb} is also more, see Fig. 7.13 and Fig. 7.14.

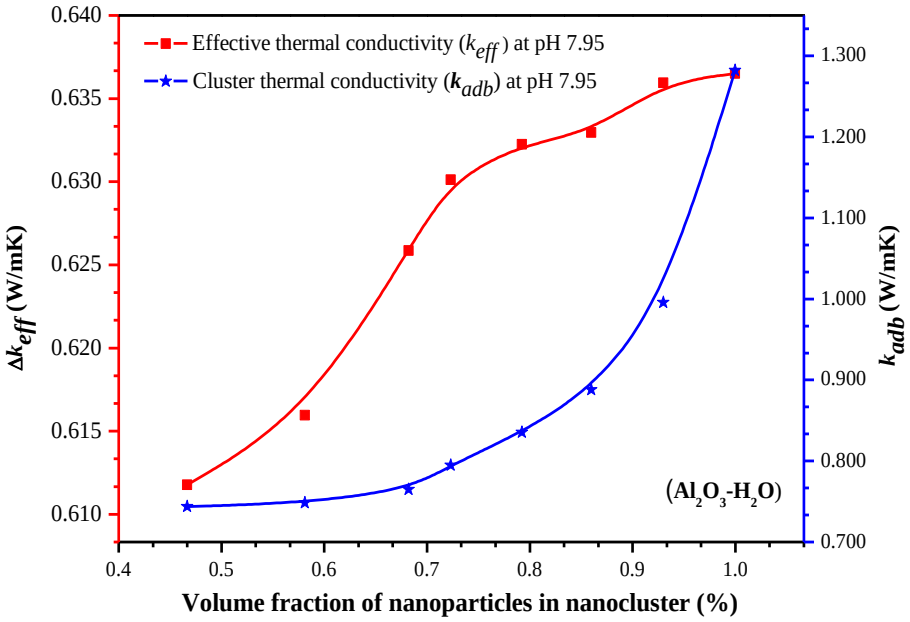

Fig. 7.13: The effect of volume fraction (φ_a) on the effective thermal conductivity (Δk_{eff}) and cluster thermal conductivity (k_{adb}) of Al_2O_3-H_2O nanofluid

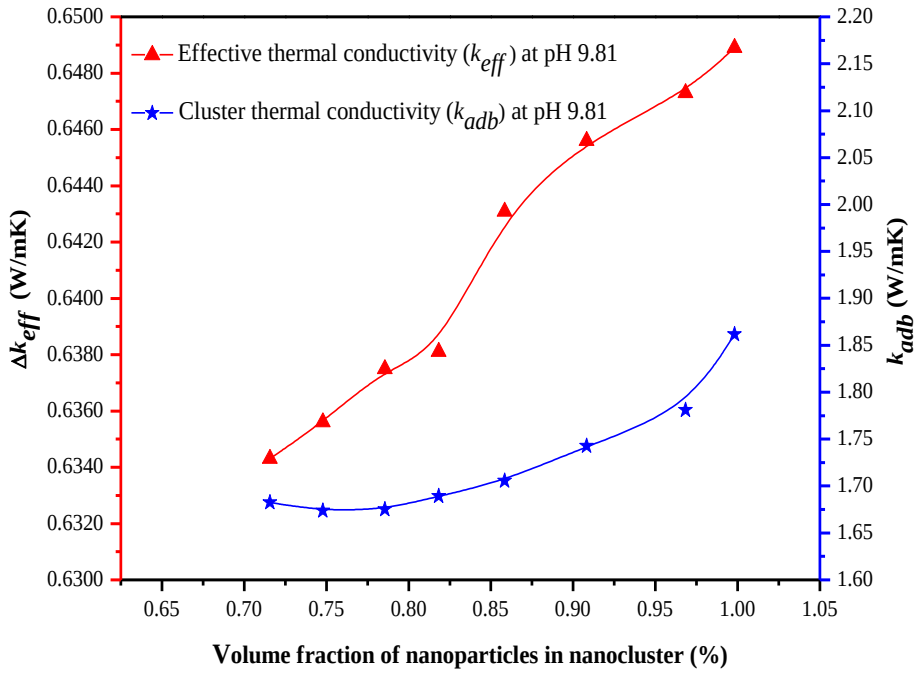

Fig. 7.14: The effect of volume fraction (φ_a) on the effective thermal conductivity (Δk_{eff}) and cluster thermal conductivity (k_{adb}) of TiO_2-H_2O nanofluid

It can be observed for both types of nanofluids that the enhancement in the cluster based thermal conductivity (k_{adb}) is more compared to the enhancement in the effective thermal conductivity (Δk_{eff}). This augmentation is due to the fact that the former represents the thermal conductivity of a single nanocluster whereas, the later represents the thermal conductivity of the whole nanofluid sample. At the extreme and optimized pH values, the variation in the effective thermal conductivities with elapsed time for both the nanofluids is shown in Fig. 7.15 and Fig. 7.16.

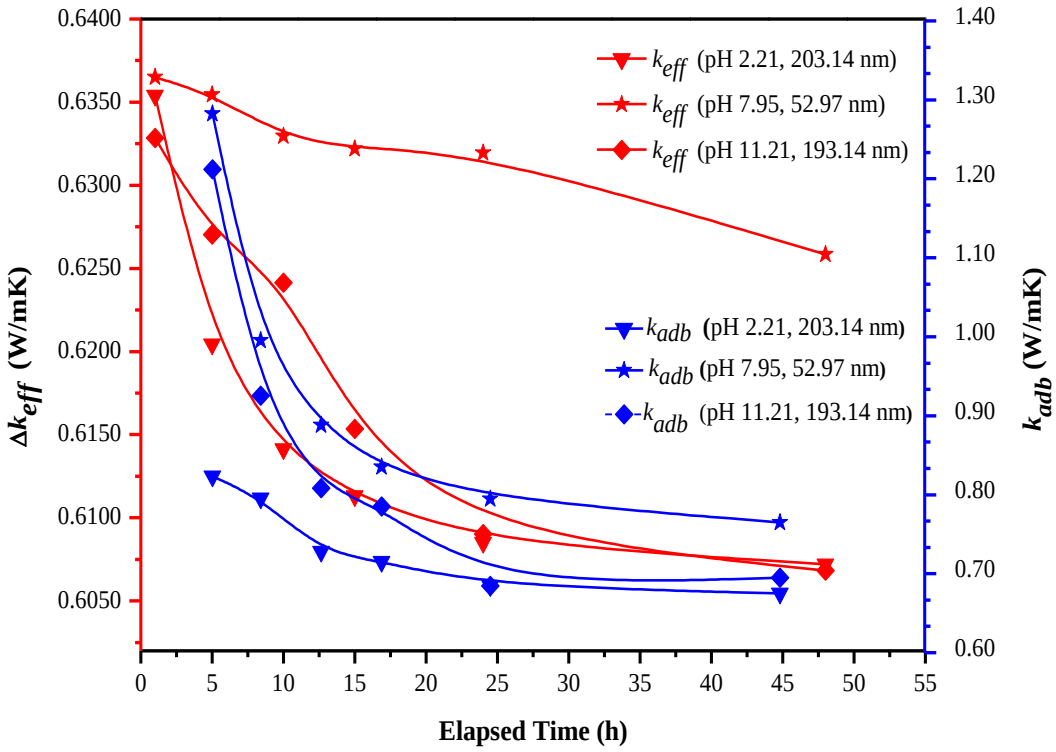

Fig. 7.15: The effect of elapsed time (t) on the effective thermal conductivity (Δk_{eff}) and cluster thermal conductivity (k_{adb}) of Al_2O_3-H_2O nanofluid

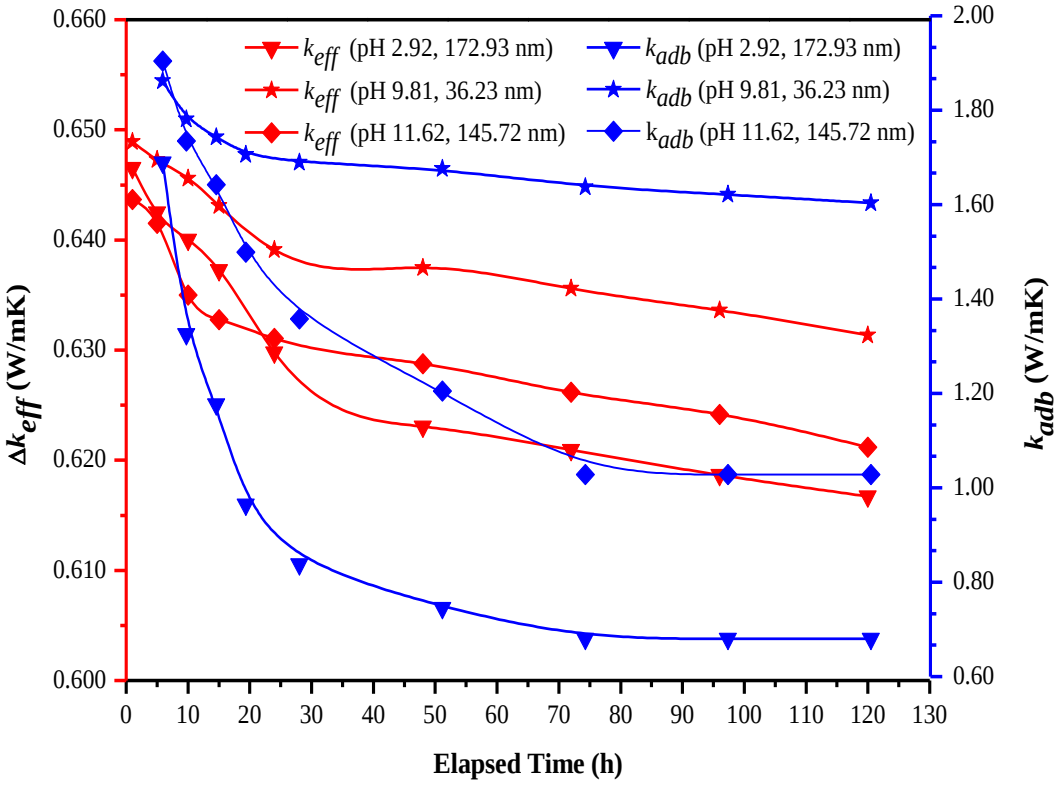

Fig. 7.16: The effect of elapsed time (t) on the effective thermal conductivity (Δk_{eff}) and cluster thermal conductivity (k_{adb}) of TiO_2-H_2O nanofluid

7.1.6 Experimental thermal conductivity (Δk_{exp}) and theoretical thermal conductivity (Δk_{eff})

The effective thermal conductivities of nanofluids have been determined corresponding to the extreme and optimized values of pH for both the nanofluids, i.e. for Al_2O_3-H_2O nanofluid as well as for TiO_2-H_2O nanofluid. As a sample, the different types of thermal conductivities for both the nanofluids at their respective optimized pH values have been given in Appendix A and B. These appendices also give an idea about the level of error involved in comparing the predicted and experimental values for the thermal conductivities. It is found to be varying from 2.5-7.24% for Al_2O_3-H_2O nanofluid and 2.19-6.7% for TiO_2-H_2O nanofluid over the elapsed time of 240 hours at their respective optimized pH values and at room temperature. The experimental values of thermal conductivities are measured using KD2 Pro and found to be higher than the predicted values of the thermal conductivities. The experimentally measured thermal conductivities of the

nanofluids sample at different time intervals have been compared to the predicted thermal conductivities, as shown in Fig. 7.17 and Fig. 7.18.

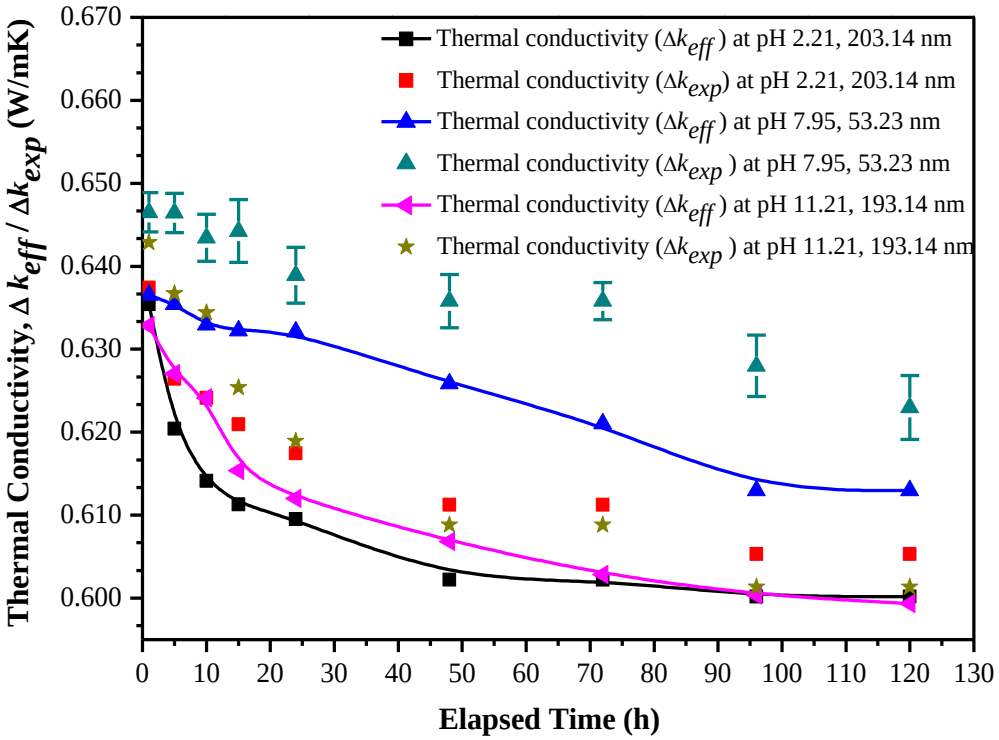

Fig. 7.17: Comparison between the experimental and theoretical or effective thermal conductivities of Al_2O_3-H_2O nanofluid

The Fig. 7.16 and 7.17 reveal that (i) the enhancement in theoretical thermal conductivity is comparatively higher for TiO_2-H_2O nanofluid than Al_2O_3-H_2O nanofluid and (ii) after the same interval of elapsed time, the theoretical values of the thermal conductivities are lower than their corresponding experimental values. The thermal conductivity values for both types of nanofluids are observed to be comparatively high during the initial intervals of the elapsed time i.e. up to 20 h for Al_2O_3-H_2O nanofluid and 40 h for TiO_2-H_2O nanofluid. In the beginning, just after when sonication was turned off, nanoclusters were at their minimum average size, more compact in shape and with more uniform distribution in base fluid. This results in higher thermal conductivity of nanofluids. However, quantity wise the rise in thermal conductivity varies as the size and

distribution of nanoclusters are different for Al_2O_3-H_2O nanofluid and TiO_2-H_2O nanofluid. Over next the 20 to 70 h of elapsed time for Al_2O_3-H_2O nanofluid and 50 to 120 h for TiO_2-H_2O nanofluid, nanoclusters grow in size and comparatively remain stable. Such nanoclusters make loose bonding with the other nanoparticles or nanocluster, and as a result the compactness of the nanoclusters is compromised and at the same time the dispersion quality of the nanofluids grow too weak. This results in lowering down of the thermal conductivities of nanofluids. The breaking and making of the new bonds with other nanoclusters and nanoparticles continued for the extended period of elapsed time. Over the next phase of elapsed time i.e. t > 120 h, the nanoclusters grow to a sufficient large size, which make them prone to settling. Therefore, the thermal conductivity of nanofluids start declining; however, the rate is different in Al_2O_3-H_2O nanofluid than in TiO_2-H_2O nanofluid, see Fig. 7.16 and 7.17. It can also be concluded that the growth rate of nanoclusters and their distribution depend on the nature of surfactant and pH level of nanofluid. Due to these reasons, the enhancement in the thermal conductivity is more when the optimized pH level of nanofluid is maintained.

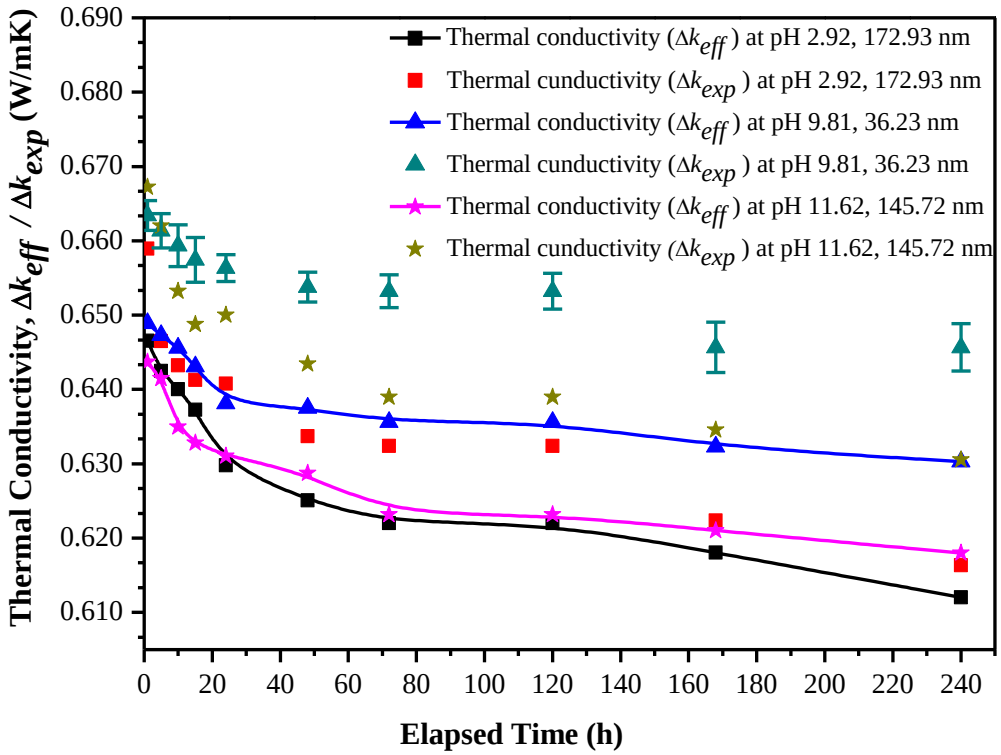

Fig. 7.18: Comparison between the experimental and theoretical or effective thermal conductivities of TiO_2-H_2O nanofluid

7.1.7 Perikinetic heat conduction and thermal conductivity model validation

The validation of the modified model of the thermal conductivity enhancement has been done by comparing existing few fundamental and structural models available for the Al_2O_3-H_2O and TiO_2-H_2O nanofluids, see Fig. 7.19 and Fig. 7.21. While evaluating these models, it is presumed that the nanoparticles do not have bulk movement in their respective base fluids and induced convection effects are negligible. It is also considered that the nanoclusters are isolated in their respective base fluids and possess no interaction amongst themselves. All these models had been developed based on the effective medium theory approach. They take into account the volume concentration of nanoparticles, thermal conductivity of base fluid and that of the nanoparticles as the main contributing parameters affecting the thermal conductivity enhancement of nanofluids. Detailed information of such models has been provided in Appendix C.

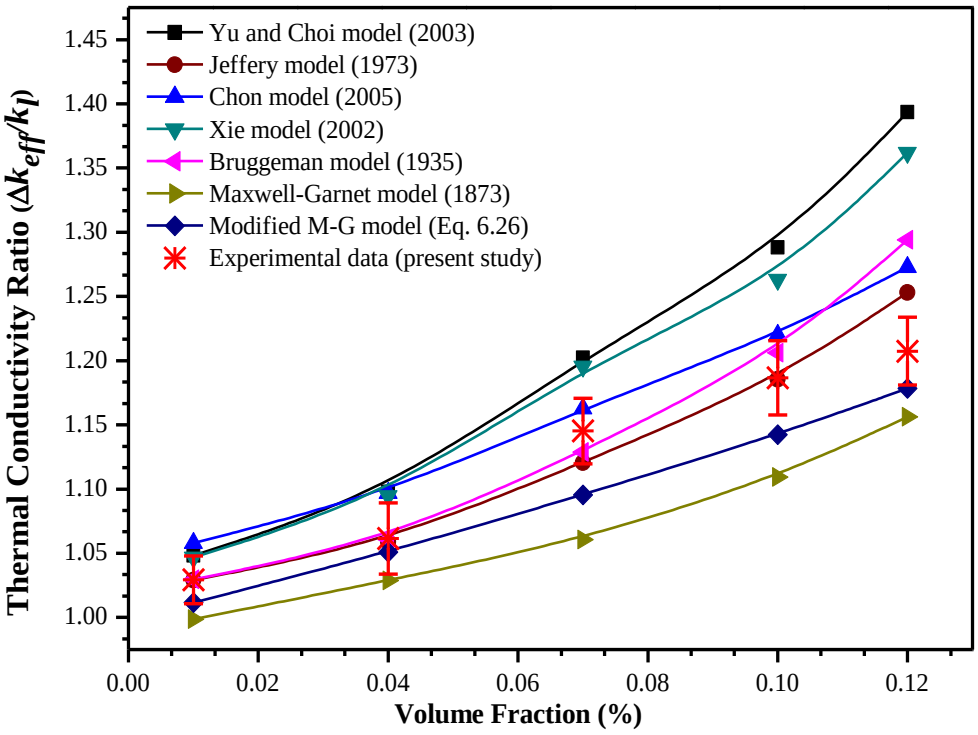

Fig. 7.19: Thermal conductivity enhancement predictions by the developed model and by other existing structural models for Al_2O_3-H_2O nanofluid

The model developed from the present investigations predicts the thermal conductivity enhancements on the basis of parameters, such as instantaneous volume concentration of

nanoparticles, nanoclusters and their morphological parameters, thermal conductivity of the liquid present inside the characteristic dimension of a cluster, instantaneous thermal conductivity of nanocluster, stability ratio, aggregation time constant and pH level of nanofluids. The investigations show that the modified models give a fairly good prediction about the enhancement of the effective thermal conductivities of nanofluids at their optimized pH values although this enhancement decreases with elapsed time. The prediction by the developed model shows that the thermal conductivity ratio of Al_2O_3-H_2O nanofluid increases with an increase in the primary volume fraction (0.01-0.12%), see Fig. 7.19. In the lower range of the primary volume fraction i.e. up to 0.05%, the thermal conductivity predictions of theoretical developed model and other existing models are found to be differing from the experimental predictions with an average error of ± 3%. For all other values of the volume fraction, relative error involved to predict the thermal conductivity of Al_2O_3-H_2O nanofluid is shown in Fig. 7.20.

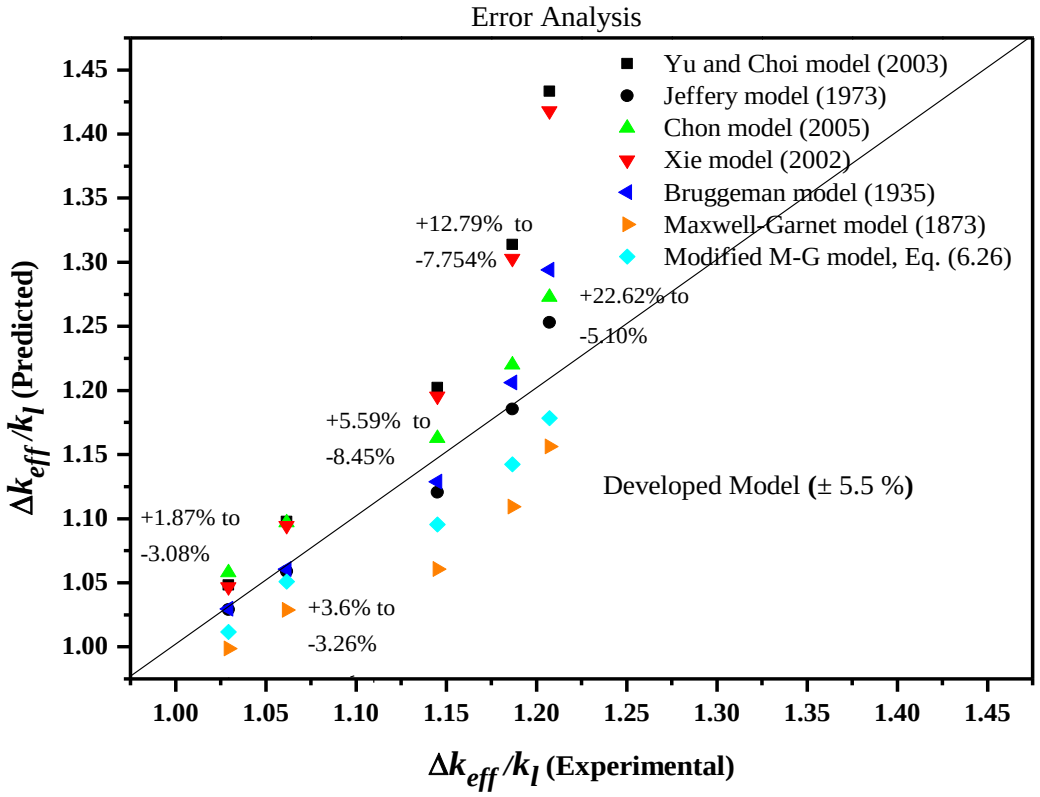

Fig. 7.20: Experimental versus predicted values of thermal conductivity ratio for Al_2O_3-H_2O nanofluid at pH 7.95

The error also increases with an increase in the volume fraction. In the volume fraction range from 0.05-0.10%, this difference increases to a new average value of the error of the order ± 7 to 12% and becomes maximum and significant up to ± 22% at a maximum volume fraction (0.12%), shown in Fig. 7.20. On the other hand, thermal conductivity predictions by the newly developed model closely follow the experimental predictions for Al_2O_3-H_2O nanofluid with an average error of ± 5.5%. Therefore, it can be concluded that over the given range of volume fraction (0.01-0.12%), the developed model can predict the thermal conductivity of Al_2O_3-H_2O nanofluid with higher accuracy compared to other models. The newly developed model has been used to determine the effective thermal conductivity of TiO_2-H_2O nanofluid at its optimized pH values of 9.81. It is quite evident from the Fig. 7.21 that the developed model is also capable to predict the thermal conductivity enhancement close to the experimental thermal conductivity of TiO_2-H_2O nanofluid. The theoretically developed model and other models are found to be under- and over-predicting the thermal conductivities in comparison to the experimental values.

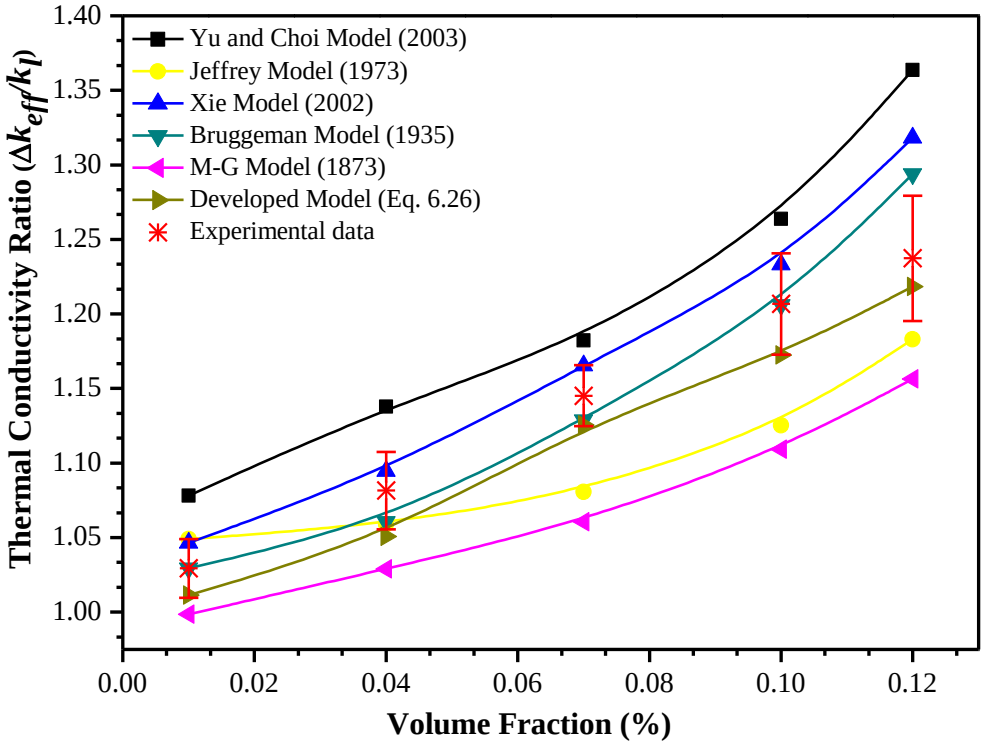

Fig. 7.21: Thermal conductivity enhancement predictions by the developed model and by other existing structural models for TiO_2-H_2O nanofluid

In the lower range of the volume fraction, i.e. at 0.01%, thermal conductivity prediction by the theoretically developed model and other models differ from the experimental predictions by an error ranging from +3% to - 4.87%. In the middle, these error values change from +8.4% to -3.6% and become maximum and significant around +8.10% to -12.62% at the volume fraction of 0.12%; whereas, the thermal conductivity predictions by the newly developed model closely follows the experimental predictions over the other models with an average of ± 6%, see Fig. 7.22.

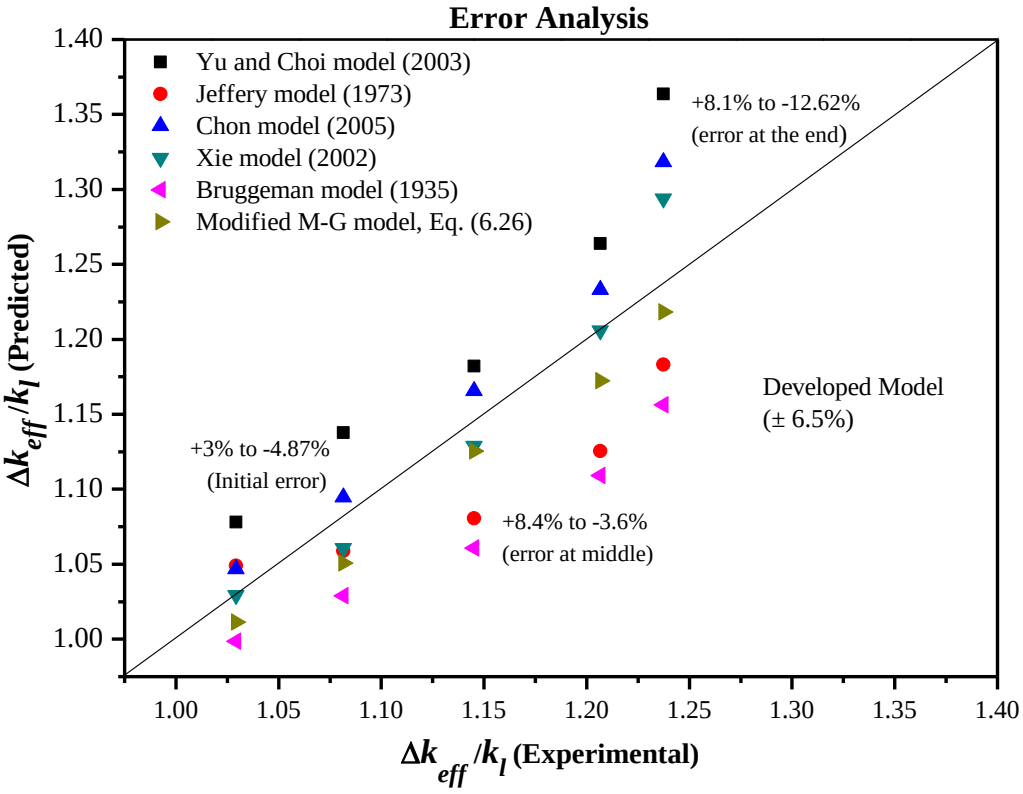

Fig. 7.22: Thermal conductivity enhancement predictions by the developed model and by other existing structural models for TiO_2-H_2O nanofluid

All these experimental and theoretical values of thermal conductivity have been obtained at room temperature (25±2°C). The suspension stability and nanocluster growth are found to be playing a significant role in predicting the effective thermal conductivity of nanofluids. Therefore, in the present work, the morphology and distribution of the nanoclusters and their quantification have helped in a better way to predict the thermal conductivity enhancement of Al_2O_3-H_2O and TiO_2-H_2O nanofluids. The heat transfer through the bulk of liquid present outside the cluster depends upon the nature of the bonding of the molecules of base fluid to each other; but it is quite evident

that the presence of nanoclusters and their distribution in base fluid has acted as the local regions to transfer heat at a faster rate.

7.2 Brownian Motion (BM) Based Induced Micro-Convection

The analysis provided here represents the finding of the effect of time, temperature, and instantaneous volume fraction on the Brownian motion induced micro-convection mechanism for the oxide based nanofluids (Al_2O_3 and TiO_2). The investigations have been extended to estimate the effect of static and dynamic heat transport parameters on the overall thermal conductivity of nanofluids. The Brownian motion based convection model of thermal conductivity for the varying concentration of the nanoparticles have been introduced. In addition to the suspension stability parameters, the model also takes into account the effects of nanoclusters' growth, temperature, thermal interfacial resistance and liquid layering. All these parameters are required to be investigated based on the actual concentration of the nanoparticles presented in a particular nanofluid at a particular time.

7.2.1 Effect of temperature on the stability ratio and aggregation time constant

The stability ratios of both nanofluids i.e. Al_2O_3-H_2O and TiO_2-H_2O are determined at different temperatures and pH values by using Eq. (6.11). The values of total interaction energy have been used to determine these stability ratios at 0.05% of volume fraction (Eqns. 6.8 and 6.10). With rise in temperature (20-50°C), the thermal excitation of nanoclusters increases and as a result of this, the stability of the nanofluid start deteriorating. The stability ratio profiles for both types of nanofluids follow the same trend graphically, but differ numerically, see Fig 7.23 and 7.24. The maximum value of W is around 10^9 (at pH ≈ 7.95) for Al_2O_3 based suspension and 10^{16} (at pH ≈ 9.81) for TiO_2 based suspension at room temperature (25 ± 2°C). These values were found to be decreasing with the rise in temperature. Fig. 7.23, explains the effect of temperature on the pH of Al_2O_3-H_2O nanofluid. The temperature range i.e. 20-50 °C is found to have a marginal effect on pH values of Al_2O_3-H_2O. Same is the case with TiO_2-H_2O nanofluid. Irrespective of rise in

temperature, the stability of nanofluid decreases, at same temperatures and same pH, TiO_2 based nanofluid is comparatively more stable.

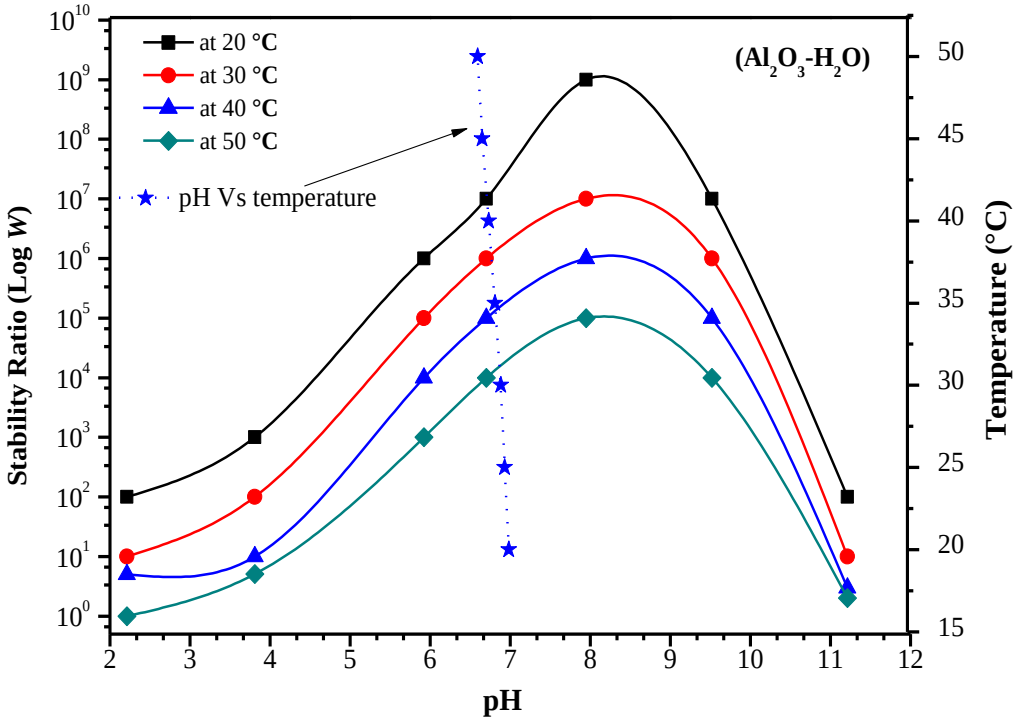

Fig. 7.23: Effect of temperature on the stability ratio and pH of Al_2O_3-H_2O nanofluid

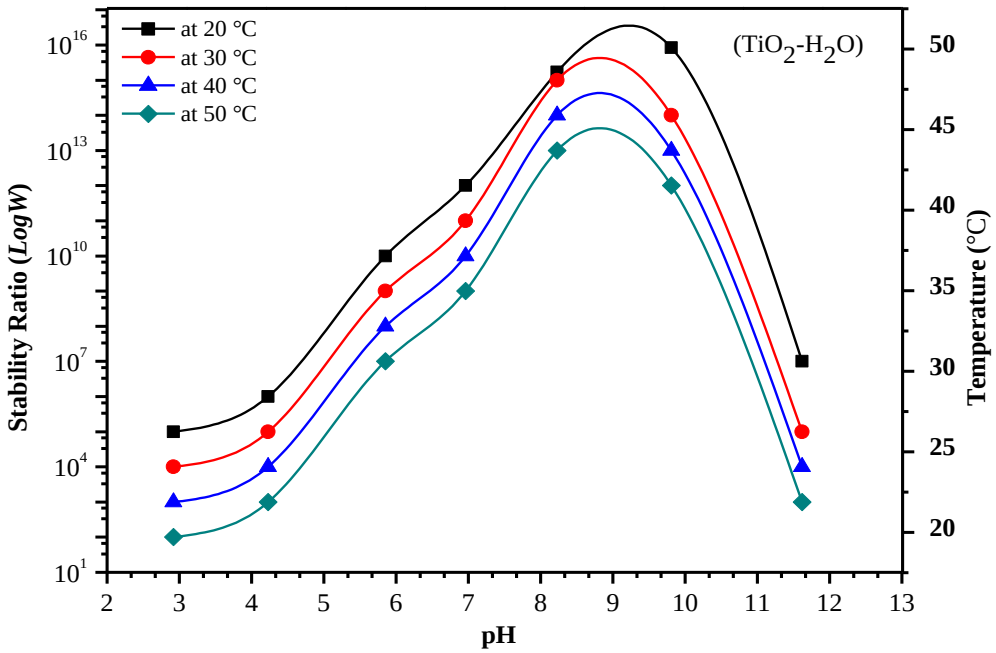

Fig. 7.24: Effect of temperature on the stability ratio and pH of TiO_2-H_2O nanofluid

To carry out investigations further on induced micro-convection, all the volume fractions such as φ_p, φ_a (Eq.6.4), φ_{bp} (Eq.6.6), φ_{dp} (Eq. 6.7), φ_{f1} (Eq. 6.16) and φ_{at} (Eq. 6.27) were determined first. The aggregation time constant (Eq. 6.3) and the stability ratio (Eq. 6.11) for both the nanofluids are found to be decreasing with the rise in temperature, see Fig. 7.25 and Fig. 7.26. The numerical data of these figures show that the TiO_2-H_2O nanofluid is more stable as compared to Al_2O_3-H_2O nanofluid which means its particles will remain in the suspension for a longer time under the given set of conditions.

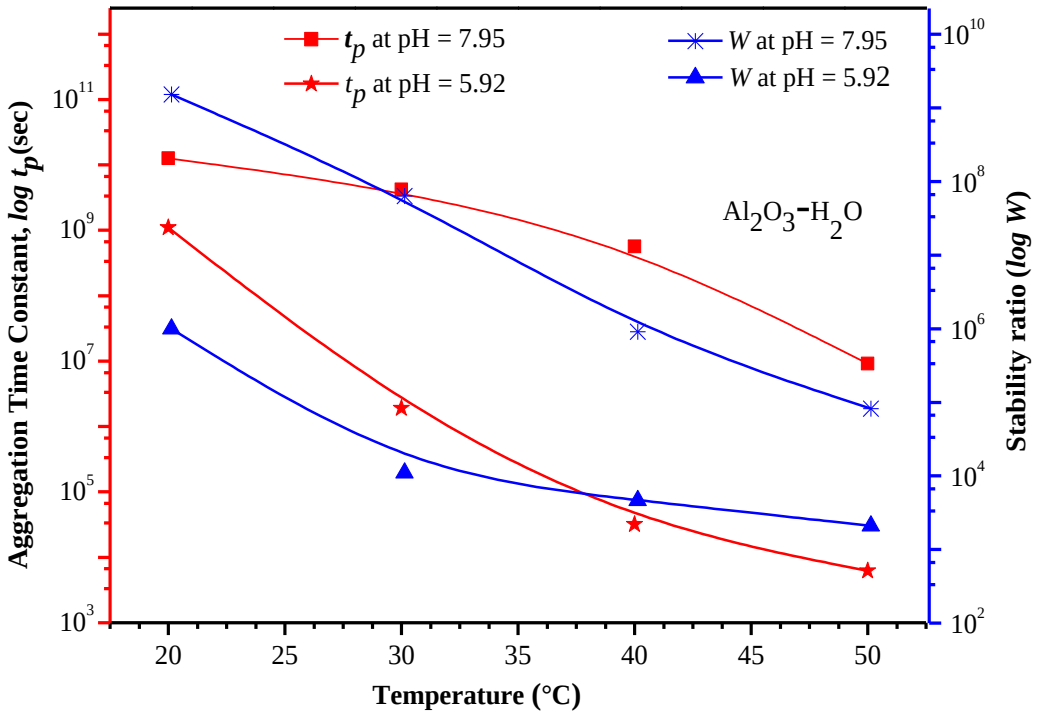

Fig. 7.25: Effect of temperature on stability ratio and aggregation time constant of Al_2O_3-H_2O nanofluid

The results are shown for both the nanofluids for their pH values close to the optimized pH values i.e. 7.95 and 5.92 for Al_2O_3-H_2O nanofluid and 9.81 and 5.85 for TiO_2-H_2O nanofluid. The aggregation time constant (t_p) and stability ratio (W) varies almost linearly with each other. The value of aggregation time constant is more for nanofluids possessing higher stability ratios. The

high value of aggregation time constant and stability ratio are found at low temperatures and optimized pH for the respective nanofluid.

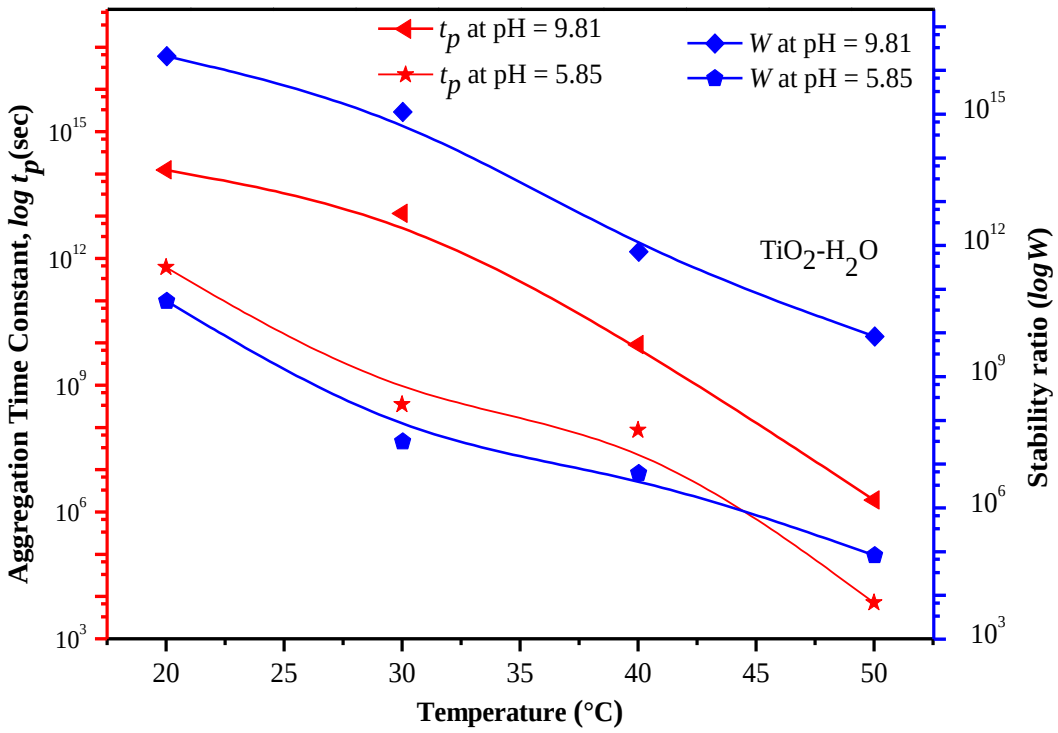

Fig. 7.26: Effect of temperature on stability ratio and aggregation time constant of TiO_2-H_2O nanofluid

7.2.2 Effect of temperature and time on the Brownian Reynolds number

The temperature and time-dependent Brownian motion induced convection plays a crucial role in heat transport of nanofluids. The mathematical modelling based on the morphological parameters of nanoclusters reveals that the Brownian motion induced Reynolds number i.e. Brownian Reynolds number increases with the rise in temperature and decreases with elapsed time and nanocluster growth, Eq. (6.29) see in Fig. 7.27. The investigations show that for both the nanofluids at their optimized pH values i.e. 7.95 for Al_2O_3-H_2O and 9.81 for TiO_2-H_2O nanofluid, the effect of temperature on Brownian Reynolds number is more significant at higher temperatures (i.e. above 35°C). The Brownian motion is found to be more prominent with smaller size

nanoclusters i.e. for varying elapsed time ≤ 24 h. As the size of the nanoclusters increases their Brownian motion decreases or in other words, the particles show high tendency for agglomeration and settling, which can be observed for elapsed time, t ≥ 24 h, see Fig. 7.27.

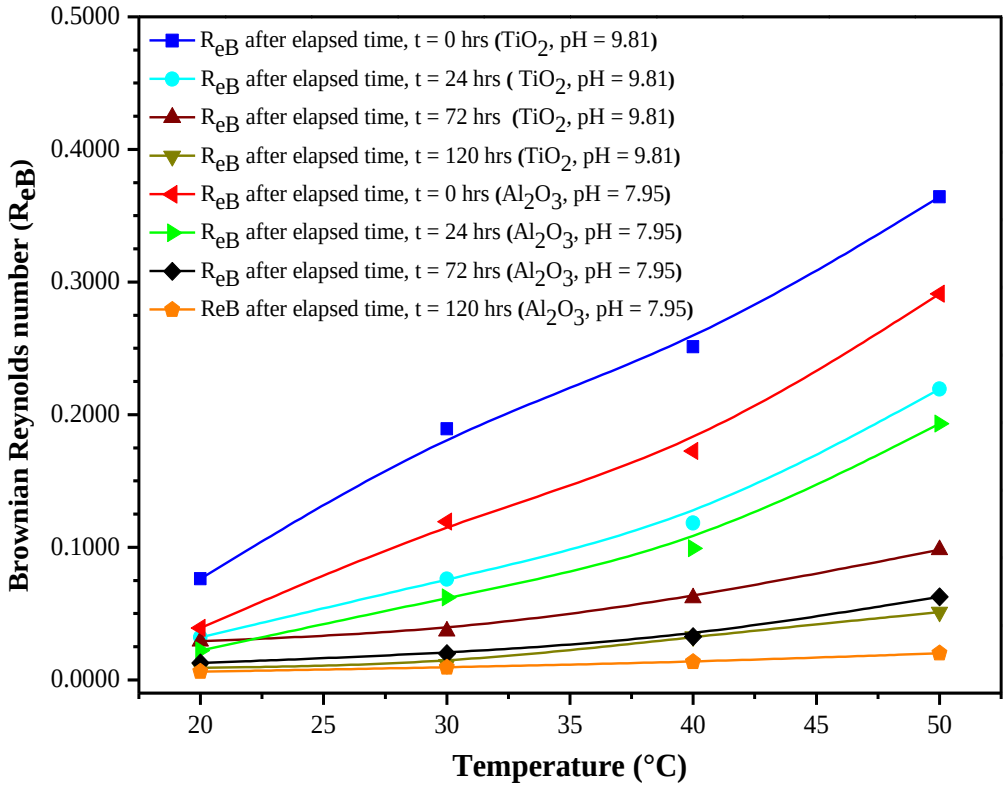

Fig. 7.27: Effect of temperature and time on the Brownian Reynolds number of Al_2O_3-H_2O and TiO_2-H_2O nanofluid

7.2.3 Effect of temperature and time on effective thermal conductivity and Brownian motion based thermal conductivity

Perikinetic effective thermal conductivity, Δk_{eff} (Eq. 6.32) and the Brownian motion based thermal conductivity, k_m (Eq. 6.31) for both the nanofluids are determined using all other required parameters. The thermal conductivities are corresponding to the optimized pH values of the Al_2O_3-H_2O and TiO_2-H_2O nanofluids, shown in Fig. 7.28 and Fig. 7.29. The thermal conductivity

enhancement due to perikinetic conduction (Δk_{eff}) is found to be dominating for both the nanofluids (Al_2O_3-H_2O and TiO_2-H_2O nanofluid), especially in the lower temperature range, i.e. from 20-30°C. At low temperature variations the thermal excitations of the nanoclusters are also weak. Moreover, the magnitude of thermal conductivity enhancement due to the Brownian motion (k_m) is also significantly low. However, as the temperature increases, thermal excitations of the nanoclusters begin to rise and accordingly the Brownian motion based thermal conductivity (k_m) too increases, see Fig. 7.28 and 7.29.

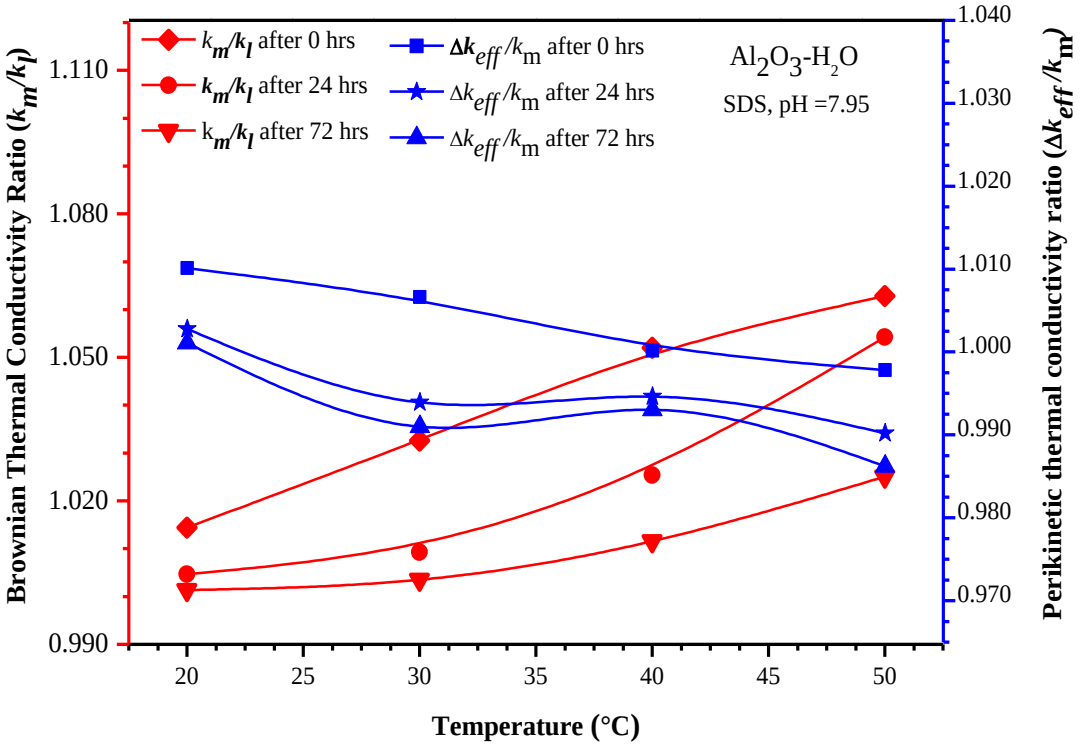

Fig. 7.28: Effect of temperature and time on the Brownian thermal conductivity and perikinetic thermal conductivity of Al_2O_3-H_2O

At any particular temperature (from 20-50 °C), the increase in the Brownian motion based thermal conductivity (k_m) for TiO_2-H_2O nanofluid is more compared to the Al_2O_3-H_2O nanofluid. This behavior is because of the smaller size of nanoclusters of the former nanofluid than the later which leads to more Brownian movement of the nanoclusters and hence the thermal conductivity enhancement.

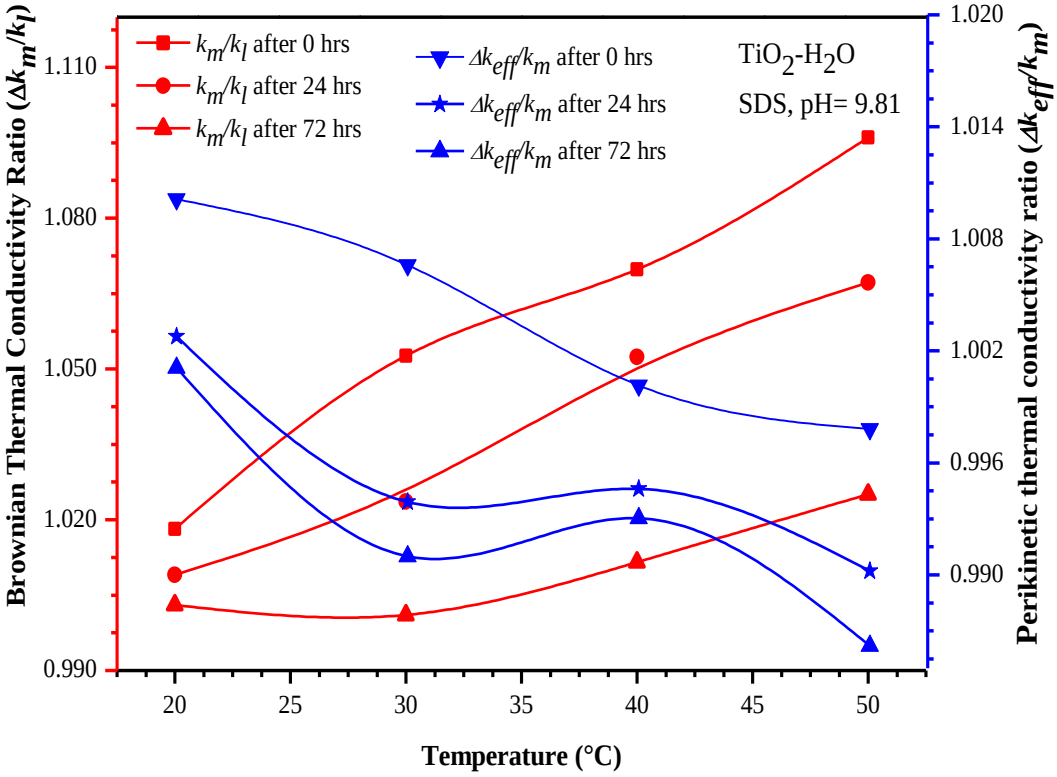

Fig. 7.29: Effect of temperature and time on the Brownian thermal conductivity and perikinetic thermal conductivity of TiO_2-H_2O

On the other hand, the thermal conductivity enhancement due to perikinetic conduction (Δk_{eff}) is found to be decreasing with the rise in temperature. The increase in temperature of nanofluids leads to more thermal excitations of the nanoclusters and hence imparts more energy to them. As a result of this, the probability of the nanoparticles to come close to each other by overcoming the repulsion forces among them also increases significantly. Due to this phenomenon, particles are forced to fuse together and consequently to grow in their shape and size. At the same time, this

also makes the bigger size nanoclusters more prone to settling or to precipitation. With the rise in temperature, bigger size and loosely bounded nanoclusters get to break off and thereby free more number of smaller size nanoparticles into the base fluids. Thus, the phenomenon of breaking off and settling of the nanoclusters goes simultaneously. The smaller size nanoclusters or nanoparticles which are set free into their respective base fluids result into their enhanced Brownian motion and hence affect the Brownian thermal conductivity of nanofluids. Whereas, the nanoparticles which settle down or precipitates with the rise in temperature have the tendency to decrease the thermal conductivity enhancement due to perikinetic conduction.

7.2.4 Time and temperature dependent theoretical and experimental thermal conductivities

The enhancement in the overall thermal conductivity of both the nanofluids under the effect of time, temperature, instantaneous volume fraction, morphological parameters, perikinetic conduction and Brownian induced micro-convection have been shown in Fig. 7.30 and Fig. 7.31. The modelling for the overall thermal conductivity of nanofluid by considering the effect of all these parameters has already been discussed in Chapter 6, Eq. (6.33). In Fig. 7.30 and Fig. 7.31, the effect of elapsed time on the overall thermal conductivity enhancement is shown corresponding to the optimized pH values for the respective nanofluids, i.e. 7.95 for Al_2O_3 and 9.81 for TiO_2 based nanofluids. The enhancement in the theoretical or overall thermal conductivity is observed to be more for TiO_2-H_2O nanofluid compared to Al_2O_3-H_2O nanofluid. This is attributed because TiO_2-H_2O nanofluid suspension is comparatively finer and contain nanoclusters of smaller size. The smaller size nanoclusters are more compact with higher values of the fractal dimension ($\geq$ 2.5). This results into a faster diffusion of heat through the TiO_2-H_2O nanofluid. The theoretical results of overall thermal conductivity enhancement ($\Delta k_{overall}$) for both the nanofluids have been compared with the experimental measured thermal conductivity values (obtained using KD2 Pro). The error involved in experimental and theoretical results of the overall thermal conductivities varies from 8 to 13% for Al_2O_3-H_2O nanofluid and from 4 to 7% for TiO_2-H_2O nanofluid, in the temperature range from 20-50°C. The error is around 9 to 12% for both the nanofluids at a higher temperature (above 40°C), whereas, it remains around 5 to 7% at low temperatures (20-30°C).

This is observed mainly due to the convection effects, which start contributing to the heat transfer with rise in temperatures.

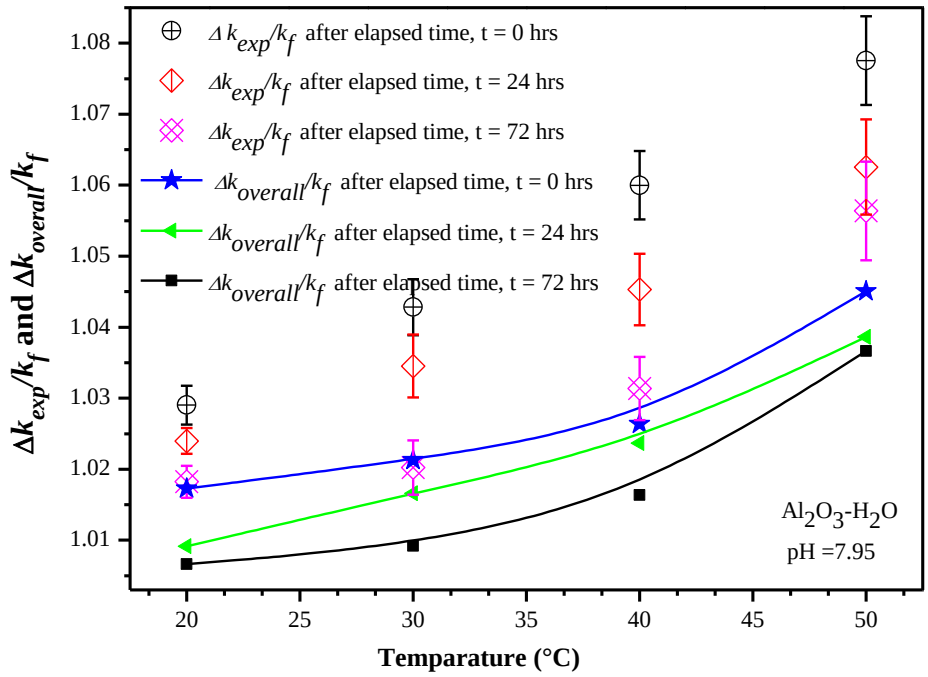

Fig. 7.30: A comparison between the experimental and theoretical values of thermal conductivities of Al_2O_3-H_2O nanofluid at pH =7.95

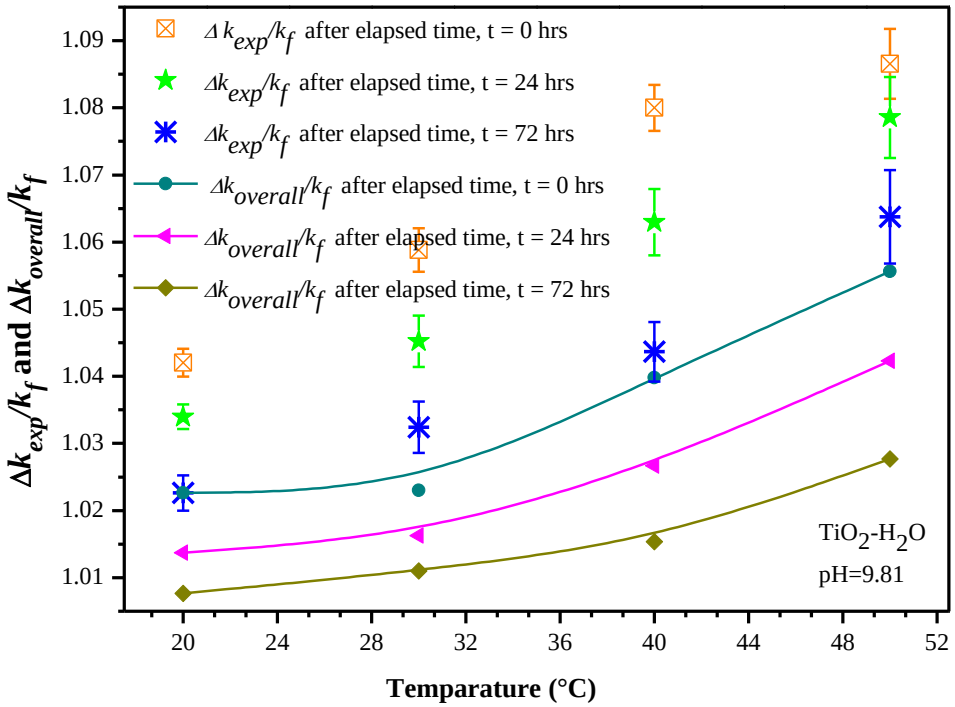

Fig. 7.31: The experimental and theoretical values (model Eq. 6.33) for thermal conductivity for TiO_2-H_2O nanofluid at pH =9.81

The probability to predict the thermal conductivity enhancement of nanofluids would improve significantly if time and temperature dependent instantaneous volume fractions are involved in the analysis. Both the mechanisms, i.e. Perikinetic conduction and Brownian motion induced micro-convection are found to be playing a significant role to increase the heat transport capacity of nanofluids. Also, both the mechanisms are found to be contributing effectively to the overall enhancement in the thermal conductivity of respective nanofluid. However, the magnitude of enhancement of overall thermal conductivity for a particular nanofluid is decided by its internal and external parameters. Therefore, this study represents a new way to look at the heat transport mechanism of the nanofluids under the effect of temperature and varying volumetric concentration of the nanoparticles in nanofluids.

Conclusions

The present work involves the study of mainly two mechanisms i.e. perikinetic heat conduction and Brownian induced micro-convection responsible for the thermal conductivity enhancement of oxide based nanofluids (Al_2O_3-H_2O and TiO_2-H_2O). These mechanisms have been investigated thoroughly by taking into consideration the nanocluster formation and their dynamics instead of the individual nanoparticle behaviour. The role of the nanolayer and its contribution to the thermal conductivity enhancement of nanofluids has also been highlighted and considered. In spite of the higher thermal conductivity of the Al_2O_3 nanoparticles compared to the TiO_2 nanoparticles, the TiO_2-H_2O nanofluid seems to be performing better for heat transportation compared to the Al_2O_3-H_2O nanofluid (20-50°C). Both the mechanisms (perikinetic heat conduction and Brownian motion induced micro convection) are found to be contributing effectively to determine the overall enhancement in the thermal conductivity of nanofluids. However, their scale of magnitude varies with temperature.

An attempt was also made to model the thermal conductivity of Al_2O_3-H_2O nanofluid for the average size of nanoclusters (163-182 nm) using Response Surface Methodology (RSM). Out of various surfactants which were tested, Sodium dodecyl sulfate (SDS) was found to be more effective in improving the stability and thermal conductivity of Al_2O_3-H_2O nanofluid. The average clusters size of nanoclusters is reduced to less than 200 nm from 1602, 1827, 1069 and 922 nm for Al_2O_3-H_2O nanofluid when surfactant (SDS) is used. As a result of this, a consistent enhancement in the thermal conductivity of Al_2O_3-H_2O nanofluid is recorded (i.e. 0.70 W/mK over a period of three hours). The thermal conductivity of Al_2O_3-H_2O nanofluid was modeled using BBD under RSM by taking volumetric concentration, temperature and surfactant amount as the contributing factors. Response Surface Method (RSM) along with Box Behnken Design (BBD) has also been used to generate the 3D response surfaces and contours which represent the variation in the thermal conductivity of Al_2O_3-H_2O nanofluid under given set of constraints i.e. volumetric concentration, temperature and surfactant amount. In comparison to other reported models, the developed model through RSM follows the measured thermal conductivity ratio with an accuracy of 6-14%. Furthermore, it is observed that the dispersion quality, clusters formation and stability are the important factors which decide the thermal conductivity enhancement of a particular type of nanofluid and the formation of nanoclusters in nanofluid is inevitable especially, when nanofluids

are prepared through Two-Step Method. Thus, statistical techniques have been used effectively to study the effect of different parameters on thermal conductivity of Al_2O_3-H_2O nanofluid.

The volume fraction is not constant but its concentration changes continuously and has been studied as a function of time and temperature. All the investigations were based on the size of nanocluster while in suspension, i.e., hydrodynamic size of the particles rather than the particles size of nanopowder. It has been observed that nanoclusters growth enhances the thermal conductivity and hence the heat transfer capability of nanofluids. Zeta potential is found to be proportional to stability ratio and inversely proportional to the hydrodynamic size of the nanoparticles (-42mV for Al_2O_3-H_2O at pH =7.95 and -43mV for TiO_2-H_2O at pH = 9.81). Stability of suspension is found to be decreasing with an increase in the cluster size and temperature (20-50 °C). The tested nanofluids were showing higher suspension quality and thermal conductivity enhancements especially, with anionic surfactants, such as; SDS. The predictions of the effective thermal conductivities by using other existing models are found to be differing from the experimental predictions with an average error varies from ± 3 to 22% at room temperature (25±2 °C). Whereas, the difference between experimentally measured thermal conductivity and modeled effective thermal conductivity is within ± 6%.

Nanocluster based thermal conductivity (k_{adb}) is observed to be higher than the effective thermal conductivity (Δk_{eff}) of nanofluids for perikinetic heat conduction mechanism at temperature varying from 20-50 °C. For the flow within the Stoke's regime, Brownian Reynolds number has been expressed in term of nanocluster geometry, time and temperature and is found to be increasing (up to 0.50) with an increase in temperature (20-50 °C). The heat transport takes place mainly through perikinetic heat conduction mechanism at temperature around 20-30°C, whereas, the induced micro-convection starts dominating as the temperature goes above 30°C. The error involved in experimental and theoretical results of the overall thermal conductivities varies from 8 to 13% for Al_2O_3-H_2O nanofluid and from 4 to 7% for TiO_2-H_2O nanofluid, in the temperature range from 20-50°C. Thus, in the study undertaken the error between the experimental and the theoretical values of the overall thermal conductivities is observed varies from 4-12% at temperature from 20-50 °C. While taking the measurements of the thermal conductivity of nanofluids, it is observed that thermal property analyzer (KD2 Pro) becomes more prone to the convection effects especially, when water is used as working medium beyond 50°C. It gives fairly good results (till 50°C) of thermal conductivity measurements within accuracy and precision of ±5%.

Future Scope and Significance

The preliminary research evidences show that nanofluids have potential to transport heat efficiently and effectively as compared to the conventional fluids. However, the technical breakthroughs in critical issues and in industrial level production of nanofluids are essential to bring nanofluids to their commercialization. The performance capabilities of nanofluids depend upon the fact that how reliably and effectively the fundamental issues about their properties and heat transport mechanisms are addressed? Therefore, the work "*an experimental investigation into clusters formation towards modelling of thermal conductivity of nanofluids*" was undertaken to have a thorough understanding of heat transport mechanisms i.e. perikinteic and induced micro-convection mechanisms of oxide based nanofluids, such as; Al_2O_3-H_2O and TiO_2-H_2O nanofluids. The perikinteic and induced micro-convection mechanisms are found to be addressing well the heat transport of nanofluids thorough nanoclusters. The subsequent discussion highlight the future directions for the existing work.

(i) The thermal conductivity of various other nanofluids can also be predicted by incorporating the time-dependent suspension stability and morphology of dispersed nanoparticles/nanoclusters.

(ii) Limited information was available on the true nature of the thermal conductivity of the liquid layer formed at the sold-liquid interface. Therefore, more investigations are required to be carried out to estimate its value effectively and accurately. Similarly, the role of the Kapitiza resistance (thermal resistance at solid-liquid interface) to determine the thermal conductivity of nanofluids needs more thorough and deeper investigation.

(iii) The influence of convection effects and nanoclusters on the thermal conductivity of Al_2O_3-H_2O and TiO_2-H_2O nanofluids can be investigated beyond Stoke's regime and 50°C.

(iv) The present study revolves around behaviour of overall thermal conductivity of Al_2O_3-H_2O and TiO_2-H_2O nanofluids only however, the same investigation can be used to study other thermophysical properties of nanofluid, such as; viscosity, density and specific heat.

(v) Transient Hot Wire method (THW) based KD2 Pro (A thermal property analyzer) has been used to measure the overall thermal conductivity of nanofluids, experimentally. It is difficult to carry out the measurements with high accuracy and consistency beyond 50°C especially, if water is the base fluid. Therefore, the new equipments working on other principles and suitable to work even at elevated temperature are need to be explored.

References

Akbari, M., Galanis, N. and Behzadmehr, A. (2011) 'A new model for nanofluid conductivity based on the effects of clustering due to Brownian motion', *Heat Transfer—Asian Research*, 40(4), pp. 352–368.

Akoh, H., Tsukasaki, Y., Yatsuya, S. and Tasaki, A. (1978) 'Magnetic properties of ferromagnetic ultrafine particles prepared by vacuum evaporation on running oil substrate', *Journal of Crystal Growth*, 45, pp. 495–500.

Alipour, R., Ghoranneviss, M., Mirzaee, M. and Jafari, A. (2014) 'The direct effect of interfacial nanolayers on thermal conductivity of nanofluids', *Heat Mass Transfer*, 50, pp. 1727–1735.

Amrollahi, A., Hamidi, A. A. and Rashidi, A. M. (2007) 'Preparation of MCM-41 nano fl uid and an investigation of Brownian movement of the nanoparticles on the nano fl uid conductivity', *International Journal of Nanoscience and Nanotechnology*, 3(1), pp. 13–20.

Assael, M. J., Metaxa, I. N., Arvanitidis, J., Christofilos, D. and Lioutas, C. (2005) 'Thermal conductivity enhancement in aqueous suspensions of carbon multi-walled and double-walled nanotubes in the presence of two different dispersants', *International Journal of Thermophysics*, 26(3), pp. 647–664.

Avsec, J. (2008) 'The combined analysis of phonon and electron heat transfer mechanism on thermal conductivity for nanofluids', *International Journal of Heat and Mass Transfer*, 51, pp. 4589–4598.

Bailar, J. C., Emeleus, H. J., Nyholam, S. R. and Trotman-Dickenson, A. F. (1973) *Comprehensive inorganic chemistry*. 1st Ed. Pergamon Press Ltd., Headington Hill Hall, Oxford.

Beck, M. P., Sun, T. and Teja, A. S. (2007) 'The thermal conductivity of alumina nanoparticles dispersed in ethylene glycol', *Fluid Phase Equilibria*, 260, pp. 275–278.

Beck, M. P., Yuan, Y., Warrier, P. and Teja, A. S. (2009) 'The effect of particle size on the thermal conductivity of alumina nanofluids', *Journal of Nanoparticle Research*, 11, pp. 1129–1136.

Bergman, T. L., Lavine, A. S., Incropera, F. P. and DeWitt, D. P. (1996) *Fundamentals of heat and mass transfer*. 6th Ed. John Wiley and Sons Inc. New York.

Bergström, L. (1997) 'Hamaker constants of inorganic materials', *Advances in Colloid and Interface Science*, 70, pp. 125–169.

Bohne, D., Fischer, S. and Obermeier, E. (1984) 'Thermal conductivity, density, viscosity, and Prandtl-numbers of ethylene glycol-water mixtures', *Phys. Chem.*, 88, pp. 739–742.

Box, G. E. P. and Hunter, J. S. (1957) 'Multi-factor experimental designs for exploring response surfaces', *The Annals of Mathematical Statistics*, 28(1), pp. 195–241.

Box, G. E. P. and Wilson, K. B. (1951) 'On the experimental attainment of optimum conditions Title', *Journal of the Royal Statistical Society Series B*, 13(1), pp. 1–45.

Brodkey, R. S., Kim, D. S. and Sidner, W. (1991) 'Fluid to particle heat transfer in a fluidized bed and to single particles', *International Journal of Heat and Mass Transfer*, 34(9), pp. 2327–2337.

Bruggeman, D. A. G. (1935) ‘Berechnung verschiedener physikalischer Konstanten von heterogenen Substanzen. I. Dielektrizitätskonstanten und Leitfähigkeiten der Mischkörper aus isotropen Substanzentle’, *Annalen der Physik*, 416(7), pp. 636–646.

Buongiorno, J. (2005) ‘Convective Transport in Nanofluids’, *J. Heat Transfer*, 128(3), pp. 240–250.

Buongiorno, J., Venerus, D. C., Prabhat, N., McKrell, T., Townsend, J., Christianson, R., Tolmachev, Y. V., Keblinski, P., Hu, L., Alvarado, J. L., Bang, I. C., Bishnoi, S. W., Bonetti, M., Botz, F., Cecere, A., Chang, Y., Chen, G., Chen, H., Chung, S. J., Chyu, M. K., Das, S. K., Paola, R. Di, Ding, Y., Dubois, F., Dzido, G., Eapen, J., Escher, W., Funfschilling, D., Galand, Q., Gao, J., Gharagozloo, P. E., Goodson, K. E., Gutierrez, J. G., Hong, H., Horton, M., Hwang, K. S., Iorio, C. S., Jang, S. P., Jarzebski, A. B., Jiang, Y., Jin, L., Kabelac, S., Kamath, A., Kedzierski, M. A., Kieng, L. G., Kim, C., Kim, J.-H., Kim, S., Lee, S. H., Leong, K. C., Manna, I., Michel, B., Ni, R., Patel, H. E., Philip, J., Poulikakos, D., Reynaud, C., Savino, R., Singh, P. K., Pengxiang Song, Thirumalachari Sundararajan, E. T., Tritcak, T., Turanov, A. N., Vaerenbergh, S. Van, Wen, D., Witharana, S., Yang, C., Yeh, W.-H., Zhao, X.-Z. and Zhou, S.-Q. (2009) ‘A benchmark study on the thermal conductivity of nanofluids’, *Journal of Applied Physics*, 106, p. 94312. Carpineti, M. and Giglio, M. (1993) ‘Aggregation phenomena’, *Advances in Colloid and Interface Science*, 46(C), pp. 73–90.

Challoner A. R. and Powell, R. W. (1956) ‘Thermal conductivities of liquids: new determinations for seven liquids and appraisal of existing values’, *Proc R Soc Lond Ser A*, 238(1212), pp. 90–106.

Chandrasekar, M. and Suresh, S. (2009) ‘A review on the mechanisms of heat transport in nanofluids’, *Heat Transfer Engineering*, 30(14), pp. 1136–1150.

Chandrasekar, M., Suresh, S., Bose, A. and Chandra Bose, A. (2010) ‘Experimental investigations and theoretical determination of thermal conductivity and viscosity of Al_2O_3/water nanofluid’, *Experimental Thermal and Fluid Science*, 34(2), pp. 210–216.

Chien, H. T., Tsai, C. I., Chen, P. H. and Chen, P. Y. (2003) ‘Improvement on thermal performance of a disk-shaped miniature heat pipe with nanofluid’, in *Proc. International Conference on Electronics Packaging Technology , IEEE, Piscataway, NJ*, pp. 389–391.

Chinmay, G., Han, X., To, D., Jallo, L., Gurumurthy, L. and Davé, R. N. (2013) ‘Dispersion of fine and ultrafine powders through surface modification and rapid expansion’, *Chemical Engineering Science*, 85, pp. 11–24.

Choi, S. U. S. and Eastman, J. A. (1995) ‘Enhancing thermal conductivity of fluids with nanoparticles’, in *ASME International Mechanical Engineering Congress and Exposition*, pp. 99–105. doi: 10.1115/1.1532008.

Choi, S. U. S., Zhang, Z. G., Yu, W., Lockwood, F. E. and Grulke, E. A. (2001) ‘Anomalous thermal conductivity enhancement in nanotube suspensions’, *Applied Physics Letters*, 79(14), pp. 2252–2254.

Chon, C. H., Kihm, K. D., Lee, S. P. and Choi, S. U. S. (2005) ‘Empirical correlation finding the role of temperature and particle size for nanofluid (Al2O3) thermal conductivity enhancementitle’, *Physics Letter*, 87, p. 153107.

Chopkar, M., Das, P. K. and Manna, I. (2006) ‘Synthesis and characterization of nanofluid for advanced heat transfer applications’, *Scripta Materialia*, 55, pp. 549–552.

Chopkar, M., Kumar, S., Bhandari, D. R., Das, P. K. and Manna, I. (2007) 'Development and characterization of Al2Cu and Ag2Al nanoparticle dispersed water and ethylene glycol based nanofluid', *Materials Science and Engineering B*, 139, pp. 141–148.

Chopkar, M., Sudarshan, S., Das, P. K. and Manna, I. (2008) 'Effect of particle size on thermal conductivity of nanofluid', *Metallurgical and Materials Transactions A*, 39(7), pp. 1535–1542.

Clarke, D. R., Nan, C. R., Birringer, D. R. and Clarke, H. G. (1997) 'Effective thermal conductivity of particulate composites with interfacial thermal resistance.', *Journal of Applied Physics*, 81(10), pp. 6692–6699.

Codreanu, C., Codreanu, N. and Obreja, V. V. N. (2007) 'Experimental set-up for the measurement of the thermal conductivity of liquids', *Romanian Journal of Information Science and Technology*, 10(3), pp. 215–231.

Das, S. K., Choi, S. U. S., Yu, W. and Pradeep, T. (2007) *Nanofluids: Science and Technology*. 1st Ed. John Wiley and Sons, Inc.

Das, S. K., Putra, N., Thiesen, P. and Roetzel, W. (2003) 'Temperature dependence of thermal conductivity enhancement for nanofluids', *Journal of Heat Transfer*, 125(2003), pp. 567–574.

Deepak Selvakumar, R. and Dhinakaran, S. (2016) 'A multi-level homogenization model for thermal conductivity of nanofluids based on particle size distribution (PSD) analysis', *Powder Technology*, 301, pp. 310–317.

Ding, Y., Alias, H., Wen, D. and Williams, R. A. (2006) 'Heat transfer of aqueous suspensions of carbon nanotubes (CNT nanofluids)', *International Journal of Heat and Mass Transfer*, 49, pp. 240–250.

Duangthongsuk, W. and Wongwises, S. (2009) 'Measurement of temperature-dependent thermal conductivity and viscosity of TiO2-water nanofluids', *Experimental Thermal and Fluid Science*. Elsevier Inc., 33, pp. 706–714.

e-Fundamentals. (2011) *Properties of Distilled Water, http://www.efunda.com. (accessed 2015)*.

Eastman, J. A., Choi, S. U. S., Li, S. and Thompson, L. J. (1997) 'Enhanced thermal conductivity through the development of nanofluids', in *Proc. Mater. Res. Soc. Symp. Materials Res. Soc., Pittsburgh, PA, USA, Boston, MA, USA*, p. 457 (3–11).

Eastman, J. A., Choi, S. U. S., Li, S., Yu, W. and Thompson, L. J. (2001) 'Anomalously increased effective thermal conductivities of ethylene glycol-based nanofluids containing copper nanoparticles', *Applied Physics Letters*, 78(6), pp. 718–720.

Evans, W., Fish, J. and Keblinski, P. (2006) 'Role of Brownian motion hydrodynamics on nanofluid thermal conductivity', *Applied Physics Letters*, 88, pp. 93116-1–3.

Evans, W., Prasher, R., Fish, J., Meakin, P., Phelan, P. and Keblinski, P. (2008) 'Effect of aggregation and interfacial thermal resistance on thermal conductivity of nanocomposites and colloidal nanofluids', *International Journal of Heat and Mass Transfer*, 51, pp. 1431–1438.

Filippos, K., Santipharp, P. and Yunhui, W. (2007) 'Nanosizing — Oral formulation development and biopharmaceutical evaluation', *Advanced Drug Delivery Reviews*, 59(7), pp. 631–644.

Fluid Properties (2011) *Microelectronics Heat Transfer Laboratory*, *http://www.mhtl.uwaterloo.ca (accessed 2015)*.

Fovet, Y., Gal, J. and Toumelin Chemla, F. (2001) 'Influence of pH and fluoride concentration on titanium passivating layer: Stability of titanium dioxide', *Talanta*, 53(5), pp. 1053–1063.

Fu, H. L. and Gao, L. (2012) 'Effect of interfacial nanolayer on thermophoresis in nano fluids', *International Journal of Thermal Sciences*, 61, pp. 61–66.

Ganguly, R., Sen, S. and Puri, I. K. (2004) 'Heat transfer augmentation using a magnetic fluid under the influence of a line dipole', *Journal of Magnetism and Magnetic Materials*, 271(1), pp. 63–73.

Ganguly, S. and Chakraborty, S. (2009) 'Effective viscosity of nanoscale colloidal suspensions Effective viscosity of nanoscale colloidal suspensions', *Journal of Applied Physics*, 124309(1–10).

Gao, J. W., Zheng, R. T., Ohtani, H., Zhu, D. S. and Chen, G. (2009) 'Experimental investigation of heat conduction mechanisms in nanofluids: Clue on clustering.', *Nano Letters*, 9(12), pp. 4128–32.

Ge, Z., Cahill, D. G. and Braun, P. V. (2006) 'Thermal conductance of hydrophilic and hydrophobic interfaces', *Physical Review Letters*. American Physical Society, 96(18), p. 186101.

Ghadimi, A. and Metselaar, I. H. (2013) 'The influence of surfactant and ultrasonic processing on improvement of stability, thermal conductivity and viscosity of titania nanofluid', *Experimental Thermal and Fluid Science*, 51, pp. 1–9.

Ghadimi, A., Saidur, R. and Metselaar, H. S. C. (2011) 'A review of nanofluid stability properties and characterization in stationary conditions', *International Journal of Heat and Mass Transfer*. Elsevier Ltd, 54, pp. 4051–4068.

Gharagozloo, P. E. and Goodson, K. E. (2011) 'Temperature-dependent aggregation and diffusion in nanofluids', *International Journal of Heat and Mass Transfer*, 54, pp. 797–806.

Gleiter, H. (1989) 'Nanocyrstalline materials', *Progress in Materials Science*, 33, pp. 223–315.

Goudarzi, K., Nejati, F., Shojaeizadeh, E. and Asadi Yousef-abad, S. K. (2015) 'Experimental study on the effect of pH variation of nanofluids on the thermal efficiency of a solar collector with helical tube', *Experimental Thermal and Fluid Science*, 60, pp. 20–27.

Granqvist, C. G. and Buhrman, R. A. (1976) 'Ultrafine metal particles', *Journal of Applied Physics*, 47(5), p. 2200.

Gustafsson, S. E. (1990) 'Transient plane source techniques for thermal conductivity and thermal diffusivity measurements of solid materials', *Review of Scientific Instruments*, 62, pp. 797–804.

Haddad, Z., Abu-nada, E., Oztop, H. F. and Mataoui, A. (2012) 'Natural convection in nano fl uids : Are the thermophoresis and Brownian motion effects significant in nanofluid heat transfer enhancement ?', *International Journal of Thermal Sciences*, 57, pp. 152–162.

Hamilton, R. L. and Crosser, O. K. (1962) 'Thermal conductivity of heterogeneous two-component systems.', *Industrial and Engineering Chemistry Fundamentals*, 1(3), pp. 182–91.

Han, X., Ghoroi, C., To, D., Chen, Y. and Davé, R. (2011) 'Simultaneous micronization and surface modification for improvement of flow and dissolution of drug particles', *International Journal of Pharmaceutics*, 415(1–2), pp. 185–195.

Hemker, D. J. and Frank, C. W. (1990) 'Dynamic light-scattering studies of the fractal aggregation of poly (methacrylic acid) and poly (ethylene glycol)', *Macromolecules*, 23(20), pp. 4404–4410.

Hidalgo-alvarez, R., Martln, A., Fernandez, A. and Bastos, D. (1996) 'Electrokinetic properties , colloidal stability and aggregation kinetics of polymer colloids', *Advances in Colloid and Interface Science*, 67, pp. 1–118.

Hiemenz, P. C. (1977) *Principles of colloid and surface chemistry*. New York: Marcel Dekker.

Holthoff, H., Egelhaaf, S. U., Borkovec, M., Schurtenberger, P. and Sticher, H. (1996) 'Coagulation rate measurements of colloidal particles by simultaneous static and dynamic light scattering', *Langmuir*, 12(23), pp. 5541–5549.

Hong, K. S., Hong, T. K. and Yang, H. S. (2006) 'Thermal conductivity of Fe nanofluids depending on the cluster size of nanoparticles', *Applied Physics Letters*, 88(31901), pp. 1–3.

Hong, T. K., Yang, H. S. and Choi, C. J. (2005) 'Study of the enhanced thermal conductivity of Fe nanofluids', *Journal of Applied Physics*, 97, p. 64311.

Honig, E. P., Roebersen, G. J. and Wiersema, P.(1971) 'Effect of hydrodynamic interaction on the coagulation rate of hydrophobic colloids', *Journal of Colloid And Interface Science*, 36(1), pp. 97–109.

Huang, J., Wang, X., Long, Q., Wen, X., Zhou, Y. and Li, L. (2009) 'Influence of pH on the stability characteristics of nanofluids', *Symposium on Photonics and Optoelectronics, (SOPO)*, pp. 2–4.

Hui, P. M., Zhang, X., Markworth, A. J. and Stroud, D. (1999) 'Thermal conductivity of graded composites: numerical simulations and an effective medium approximation', *Journal of Materials Science*, 34(22), pp. 5497–5503.

Hunter, R. J. (2001) *Foundations of colloid science*. New York: Oxford University Press.

Hwang, Y., Lee, J. K., Lee, C. H., Jung, Y. M., Cheong, S. I., Lee, C. G., Ku, B. C. and Jang, S. P. (2007) 'Stability and thermal conductivity characteristics of nanofluids', *Thermochimica Acta*, 455(1–2), pp. 70–74.

Hwang, Y., Lee, J. K., Lee, J. K., Jeong, Y. M., Cheong, S. ir, Ahn, Y. C. and Kim, S. H. (2008) 'Production and dispersion stability of nanoparticles in nanofluids', *Powder Technology*, 186(2), pp. 145–153.

Iris Julie, J. and David Julian, M. (2013) 'Fabrication of biopolymer nanoparticles by antisolvent precipitation and electrostatic deposition: Zein-alginate core/shell nanoparticles', *Trends in Food Science & Technology*, 34, pp. 109–123.

Jamshidi, N., Farhadi, M., Ganji, D. D. and Sedighi, K. (2012) 'Experimental investigation on the viscosity of nanofluids', *IIJE TRANSACTIONS B: Applications*, 25(3), pp. 201–209.

Jang, S. P. and Choi, S. U. S. (2004) 'Role of Brownian motion in the enhanced thermal conductivity of nanofluids', *Applied Physics Letters*, 84(21), pp. 4316–8.

Jang, S. P. and Choi, S. U. S. (2007) 'Effects of Various Parameters on Nanofluid Thermal Conductivity', *Journal of Heat Transfer*, 129, pp. 617–623.

Jang, S. P., Hwang, K. S., Lee, J., Kim, J. H., Lee, B. H. and Choi, S. U. S. (2007) 'Effective thermal conductivities and viscosities of water-based nanofluids containing Al_2O_3 with low concentration', in *Proceedings of the 7th IEEE International Conference on Nanotechnology*, pp. 1011–1014.

Jeffery, D. J. (1973) 'Conduction through a random suspension of spheres.', in *Proceedings of the Royal Society of London Series A*, pp. 355–367.

Jiang, L., Gao, L. and Sun, J. (2003) 'Production of aqueous colloidal dispersions of carbon nanotubes', *Journal of Colloid and Interface Science*, 260(1), pp. 89–94.

Jiang, W., Ding, G. and Peng, H. (2009) 'Measurement and model on thermal conductivities of carbon nanotube nanorefrigerants', *International journal of thermal sciences*, 48(6), pp. 1108–11015.

Jie, X. and Bo-Ming, Y. (2006) 'Effect of clusters on thermal conductivity in nanofluids', *Chinese Physics Letters*, 23(10), pp. 2819–2822.

Jordan, A., Scholz, R., Wust, P., Fahling, H. and Felix, R. (1999) 'Magnetic fluid hyperthermia (MFH): cancer treatment with ac magnetic field induced excitation of biocompatible superparamagnetic nanoparticles', *J. Magn. Magn. Mater.*, 201, pp. 413–419.

Kallay, N. and Zalac, S. (2001) 'Introduction of the surface complexation model into the theory of colloid stability', *Croatica Chemica Acta*, 74(3), pp. 479–497.

Kappiyoor, R., Liangruksa, M., Ganguly, R. and Puri, I. K. (2010) 'The effects of magnetic nanoparticle properties on magnetic fluid hyperthermia', *Journal of Applied Physics*, 108, pp. 1–8.

Karthikeyan, N. R., Philip, J. and Raj, B. (2008) 'Effect of clustering on the thermal conductivity of nanofluids', *Materials Chemistry and Physics*, 109, pp. 50–55.

Keblinski, P., Eastman, J. A. and Cahill, D. G. (2005) 'Nanofluids for thermal transport', *Materials Today*, 8(6), pp. 36–44.

Keblinski, P., Phillpot, S. R., Choi, S. U. S. and Eastman, J. A. (2002) 'Mechanisms of heat flow in suspensions of nano-sized particles (nanofluids)', *International Journal of Heat and Mass Transfer*, 45, pp. 855–863.

Kim, S., Kim, C., Lee, W. H. and Park, S. R. (2011) 'Rheological properties of alumina nanofluids and their implication to the heat transfer enhancement mechanism', *Journal of Applied Physics*, 110, pp. 34316-1–6.

Kim, T. K., Lee, M. N., Lee, S. H., Park, Y. C., Jung, C. K. and Boo, J. (2005) 'Development of surface coating technology of TiO2 powder and improvement of photocatalytic activity by surface modification', *Thin Solid Films*, 475, pp. 171–177.

Kimoto, K., Kamiya, Y., Nonoyama, M. and Uyeda, R. (1963) 'An electron microscope study on fine metal particles prepared by evaporation in Argon gas at low pressure', *Japanese Journal of Applied Physics*, 2(11), pp. 702–713.

Kleinstreuer, C. and Feng, Y. (2011) 'Experimental and theoretical studies of nanofluid thermal conductivity enhancement : a review', *Nanoscale Research Letters*, 6(229), pp. 1–13.

Koo, J. and Kleinstreuer, C. (2005) 'Impact analysis of nanoparticle motion mechanisms on the thermal conductivity of nanofluids B', *International Communications in Heat and Mass Transfer*, 32, pp. 1111–1118.

Koo, J., Kleinstreuer, C. and Koo, J., C. K. (2004) 'A new thermal conductivity model for nanofluids.', *Journal of Nanoparticle Research*, 6, pp. 577–588.

Korson, L., Drost-Hansen, W., Miller, F. J., Korson, L., Drost-Hansen, W., Millero, F. J. and Korson, L., Drost-Hansen, W., & Millero, F. J. (1969) 'Viscosity of water at various temperatures', *Journal of Physical Chemistry*, 73(1), pp. 34–39.

Kreitman, M. M. (1976) 'Thermal comparator measurements on dimethyl sulfite', *Journal of Chemical and Engineering Data*, 21, pp. 11–12.

Kumar, D., Patel, H., Kumar, V., Sundararajan, T., Pradeep, T. and Das, S. K. (2004) 'Model for heat conduction in nanofluids', *Physical Review Letters*, 93(14), pp. 144301-1–3.

Kundan, L., Mallick, S. S. and Pal, B. (2016) 'Prediction and optimization of nanoclusters-based thermal conductivity of nanofluids: Application of Box–Behnken design (BBD)', *Particulate Science and Technology*.

Kurt, H. and Kayfeci, M. (2009) 'Prediction of thermal conductivity of ethylene glycol-water solutions by using artificial neural networks', *Applied Energy*, 86, pp. 2244–2248.

Kwak, K. and Kim, C. (2005) 'Viscosity and thermal conductivity of copper oxide nanofluid dispersed in ethylene glycol', *Korea Australia Rheology Journal*, 17(2), pp. 35–40.

Kwek, D., Crivoi, A. and Duan, F. (2010) 'Effects of temperature and particle size on the thermal property measurements of Al2O3-water nanofluids', *J. Chem. Eng. Data*, 55, pp. 5690–5695.

Lee, D. (2007) 'Thermophysical properties of interfacial layer in nanofluids', *Langmuir*, 23, pp. 6011–6018.

Lee, D., Kim, J.-W., Kim, B. G., Lee, D., Kim, J. W. and Kim, B. G. (2006) 'A new parameter to control heat transport in nanofluids: Surface charge state of the particle in suspension', *J. Phys. Chem. B*, 110, pp. 4323–4328.

Lee, S., S.U.S. Choi and Eastman, J. A. (1999) 'Measuring thermal conductivity of fluids containing oxide nanoparticles', *Journal of Heat Transfer*, 121, pp. 280–289.

Leong, K. C., Yang, C. and Murshed, S. M. S. (2006) 'A model for the thermal conductivity of nanofluids-The effect of interfacial layer', *Journal of Nanoparticle Research*, 8(2), pp. 245–254.

Li, C. H. and Peterson, G. P. (2006) 'Experimental investigation of temperature and volume fraction variations on the effective thermal conductivity of nanoparticle suspensions (nanofluids)', *Journal of Applied Physics*, 99, pp. 84314-1–8.

Li, J. F., Liao, H., Wang, X. Y., Normand, B., Ji, V., Ding, C. X. and Coddet, C. (2004) 'Improvement in

wear resistance of plasma sprayed yttria stabilized zirconia coating using nanostructured powder', *Tribol. Int .*, 37, pp. 77–84.

Li, X. F., Zhu, D. S., Wang, X. J., Wang, N., Gao, J. W. and Li, H. (2008) 'Thermal conductivity enhancement dependent pH and chemical surfactant for Cu-H2O nanofluids', *Thermochimica Acta*, 469(1–2), pp. 98–103.

Li, Y., Yu, Y., Wang, H. and Zhao, F. (2016) 'Effect of process parameters on the recrystallization and size control of puerarin using the supercritical fluid antisolvent process', *Asian Journal of Pharmaceutical Sciences-II*, pp. 281–291.

Li, Y., Zhou, J., Tung, S., Schneider, E. and Xi, S. (2009) 'A review on development of nanofluid preparation and characterization', *Powder Technology*, 196(2), pp. 89–101.

Liang, Z. and Tsai, H. (2011) 'Thermal conductivity of interfacial layers in nanofluids', *Physical Review E*, 41602, pp. 1–8.

Lin, C. Y., Wang, J. C. and Chen, T. C. (2011) 'Analysis of suspension and heat transfer characteristics of Al2O3 nanofluids prepared through ultrasonic vibration.', *Applied Energy*, 88, pp. 4527–4533.

Lin, M. Y., Lindsay, H. M., Weitz, D. A., Ball, R. C., Klein, R. and Meaking, P. (1989) 'Universality in colloid aggregation', *Nature*, 339, pp. 360–362.

Lin, M. Y., Lindsay, H. M., Weitz, D. A., Klein, R., Ball, R. C. and Meakin, P. (2002) 'Universal diffusion-limited colloid aggregation', *Journal of Physics: Condensed Matter*, 2(23), pp. 5283–5283.

Liu, M.-S., I Te, H., Chi-Chuan, W. and Ching-Cheng, Mark, L. (2005) 'Enhancement of thermal conductivity with carbon nanotube for nanofluids', *International Communications in Heat and Mass Transfer*, 32(9), pp. 1202–1210.

Liu, M. S., Lin, M. C. C., Tsai, C. Y. and Wang, C. C. (2006) 'Enhancement of thermal conductivity with Cu for nanofluids using chemical reduction method', *International Journal of Heat and Mass Transfer*, 49(17–18), pp. 3028–3033.

Longo, G. A. and Zilio, C. (2011) 'Experimental measurement of thermophysical properties of oxide-water nano-fluids down to ice-point', *Experimental Thermal and Fluid Science*, 35, pp. 1313–1324.

Longo, G. A., Zilio, C., Ceseracciu, E. and Reggiani., M. (2012) 'Application of artificial neural network (ANN) for the prediction of thermal conductivity of oxide-water nanofluids.', *Nano Energy*, 1, pp. 290–6.

Ma, H. B., Wilson, C., Borgmeyer, B., Park, K., Yu, Q., Choi, S. U. S. and Tirumala, M. (2006) 'Effect of nanofluid on the heat transport capability in an oscillating heat pipe', *Appl. Phys. Lett.*, 88, p. 183116.

Ma, K.-Q. and Liu, J. (2007) 'Nano liquid-metal fluid as ultimate coolant', *Physics Letters, Section A*, 361, pp. 252–256.

Mallick, S. S. S., Mishra, A. and Kundan, L. (2013) 'An investigation into modelling thermal conductivity for alumina-water nanofluids', *Powder Technology*, 233, pp. 234–244.

Malvandi, A. and Ganji, D. D. (2014) 'Brownian motion and thermophoresis effects on slip flow of alumina/water nanofluid inside a circular microchannel in the presence of a magnetic field', *International*

Journal of Thermal Sciences, 84, pp. 196–206.

Matteucci, M. E., Hotze, M. A., Johnston, K. P. and Williams, R. O. (2006) 'Drug nanoparticles by antisolvent precipitation: Mixing energy versus surfactant stabilization', *Langmuir*, 22, pp. 8951–8959.

Maxwell, J. C. (1873) *A treatise on electricity and magnetism*. 2nd Ed. Clarendon Press, Oxford U.K.

Meibodi, M. E., Vafaie-Sefti, M., Rashidi, A. M., Amrollahi, A., Tabasi, M. and Kalal, H. S. (2010) 'The role of different parameters on the stability and thermal conductivity of carbon nanotube/water nanofluids', *International Communications in Heat and Mass Transfer*, 37(3), pp. 319–323.

Mintsa, H. A., Roy, G., Nguyen, C. T. A. M., Mintsa, H. A., Roy, G. and Nguyen, C. T. (2007) 'New temperature dependent thermal conductivity data of water based nanofluids', in *5th IASME/WSEAS international conference on Heat Transfer,Thermal Engineering and Environment, Athens, Greece*, pp. 290–94.

Mintsa, H. A., Roy, G., Nguyen, C. T. and Doucet, D. (2009) 'New temperature dependent thermal conductivity data for water-based nanofluids', *International Journal of Thermal Sciences*, 48, pp. 363–371.

Mishra, A., Kundan, L. and Mallick, S. S. (2014) 'Modeling thermal conductivity for alumina-water nanofluids', *Particulate Science and Technology*, 32(3), pp. 319–326.

Mitra, S. and Chakarborty, S. (2011) *Microfluidics and nanofluidics handbook: fabrication, implementation, and applications*. CRC Press.

Montgomery, D. C. (2009) *Design and analysis of experiments*. 8th Ed. John Wiley and Sons, N.J.

Mostafizur, R. M., Saidur, R., Abdul Aziz, A. R. and Bhuiyan, M. H. U. (2015) 'Thermophysical properties of methanol based Al2O3 nanofluids', *International Journal of Heat and Mass Transfer*, 85, pp. 414–419.

Mukherjee, S., Mishra, P. C., Parashar, S. K. S. and Chaudhuri, P. (2016) 'Role of temperature on thermal conductivity of nanofluids : A brief literature review', *Heat Mass Transfer*, 52, pp. 2575–2585.

Murshed, S. M. S. and Leong, K. C. (2006) 'Thermal conductivity of nanoparticle suspensions (nanofluids)', in *NanoSingapore 2006: IEEE Conference on Emerging Technologies - Nanoelectronics - Proceedings*, pp. 155–158.

Murshed, S. M. S., Leong, K. C. and Yang, C. (2005) 'Enhanced thermal conductivity of TiO2- water based nanofluids', *International Journal of Thermal Sciences*, 44, pp. 367–373.

Murshed, S. M. S., Leong, K. C. and Yang, C. (2008) 'Characterization of electrokinetic properties of nanofluids', *Journal of Nanoscience and Nanotechnology*, 8(11), pp. 5966–5971.

Murshed, S. M. S., Leong, K. C. and Yang, C. (2008) 'Investigations of thermal conductivity and viscosity of nanofluids', *International Journal of Thermal Sciences*, 47, pp. 560–568.

Nagasaka, Y. and Nagashima, A. (1981) 'Absolute measurement of the thermal conductivity of electrically conducting liquids by the transient hot-wire method', *Journal of Physics E: Scientific Instruments*, 14(12), pp. 1435–1440.

Nasiri, A., Shariaty-Niasar, M., Rashidi, A., Amrollahi, A. and Khodafarin, R. (2011) 'Effect of dispersion

method on thermal conductivity and stability of nanofluid', *Experimental Thermal and Fluid Science*, 35(4), pp. 717–723.

Nie, C., Marlow, W. H. and Hassan, Y. A. (2008) 'Discussion of proposed mechanisms of thermal conductivity enhancement in nanofluids', *International Journal of Heat and Mass Transfer*, 51(5–6), pp. 1342–1348.

Nnanna and Agwu, A. G. (2007) 'Experimental Model of Temperature-Driven Nanofluid', *Journal of Heat Transfer*, 129, pp. 697–704.

Nottenburg, R., Rajeshwar, K., Rosenvold, R. and DuBow, J. (1978) 'Measurement of thermal conductivity of Green River oil shales by a thermal comparator technique', *Fuel*, 57, pp. 789–795.

Oh, D. W., Jain, A., Eaton, J. K., Goodson, K. E. and Lee, J. S. (2008) 'Thermal conductivity measurement and sedimentation detection of aluminum oxide nanofluids by using the 3 Omega method', *International Journal of Heat and Fluid Flow*, 29, pp. 1456–1461.

Okhio, C., Hodges, D. and Black, J. (2010) 'Review of literature on nanofluid flow and heat transfer properties', *Cyber Journals: Multidisciplinary Journals in Science and Technology, Journal of Selected Areas in Nanotechnology (JSAN)*, pp. 1–8.

Özerinç, S. S. K. and Yazıcıoğlu, A. G. (2010) 'Enhanced thermal conductivity of nanofluids: A state-of-the-art review.', *Microfluidics and Nanofluidics*, 8, pp. 145–70.

Pak, B. C. and Cho, Y. I. (1998) 'Hydrodynamic and Heat Transfer Study of Dispersed Fluids With Submicron Metallic Oxide Particles', *Experimental Heat Transfer*, 11(2), pp. 151–170.

Palabiyik, I., Musina, Z., Witharana, S. and Ding, Y. (2011) 'Dispersion stability and thermal conductivity of propylene glycol-based nanofluids', *Journal of Nanoparticle Research*, 13(10), pp. 5049–5055.

Palm, S. J., Roy, G. and Nguyen, C. T. (2006) 'Heat transfer enhancement with the use of nanofluids in radial flow cooling systems considering temperature-dependent properties', *Appl. Therm. Eng.*, 26, pp. 2209–2218.

Pang, C., Won, J., Yong, L. and Kang, T. (2016) 'Enhanced thermal conductivity of nanofluids by nanoconvection and percolation network', *Heat and Mass Transfer*. Springer Berlin Heidelberg, 52, pp. 511–520.

Pantzali, M. N., Mouza, A. A. and Paras, S. V. (2009) 'Investigating the efficacy of nanofluids as coolants in plate heat exchangers (PHE)', *Chemical Engineering Science*, 64(14), pp. 3290–3300.

Pastoriza-Gallego, M. J., Casanova, C., Páramo, R., Barḃs, B., Legido, J. L. and Piñeiro, M. M. (2009) 'A study on stability and thermophysical properties (density and viscosity) of Al2O3 in water nanofluid', *Journal of Applied Physics*, 106, pp. 64301-1–8.

Pastoriza-gallego, M. J., Lugo, L., Legido, J. L. and Piñeiro, M. M. (2011) 'Thermal conductivity and viscosity measurements of ethylene glycol-based Al2O3 nanofluids', *Nanoscale Research Letters*, 6(221), pp. 1–11.

Patnaik, P.(2003): ftp://pvictor.homeftp.net/public/Sci_Library/Chem Library/ Handbooks/Patnaik P. Handbook of inorganic chemicals (MGH, 2003) (accessed 2015).

Paul, G., Chopkar, M., Manna, I. and Das, P. K. (2010) 'Techniques for measuring the thermal conductivity of nanofluids: A review', *Renewable and Sustainable Energy Reviews*, 14, pp. 1913–1924.

Philip, J., Shima, P. D. and Raj, B. (2007a) 'Enhancement of thermal conductivity in magnetite based nanofluid due to chainlike structures', *Applied Physics Letters*, 91, pp. 203108-1–3.

Philip, J., Shima, P. D. and Raj, B. (2007b) 'Enhancement of thermal conductivity in magnetite based nanofluid due to chainlike structures', *Applied Physics Letters*, 91(203108-1–3).

Philip, J., Shima, P. D. and Raj, B. (2008) 'Evidence for enhanced thermal conduction through percolating structures in nanofluids.', *Nanotechnology*, 19(305706), pp. 1–7.

Potanin, A. A., Rooij, R. De, Ende, D. V. den and Mellema, J. (1995) 'Microrheological modeling of weakly aggregated dispersions', *J. Chem. Phys.*, 102, p. 5845.

Powell, R. W. (1957) 'Experiments using a simple thermal comparator for measurement of thermal conductivity, surface roughness and thickness of foils or of surface deposits', *Journal of scientific Instruments*, 34, pp. 485–492.

Prasher, R., Bhattacharya, P. and Phelan, P. E. (2005) 'Thermal conductivity of nanoscale colloidal solutions (nanofluids)', *Physical Review Letters*, 94(2), pp. 3–6.

Prasher, R., Bhattacharya, P. and Phelan, P. E. (2006) 'Brownian-Motion-Based Convective-Conductive Model for the Effective Thermal Conductivity of Nanofluids', *Journal of Heat Transfer*, 128(June 2006), pp. 588–595.

Prasher, R., Evans, W., Meakin, P., Fish, J., Phelan, P. and Keblinski, P. (2006) 'Effect of aggregation on thermal conduction in colloidal nanofluids', *Applied Physics Letters*, 89, pp. 143119-1–3.

Prasher, R., Phelan, P. E. and Bhattacharya, P. (2006) 'Effect of aggregation kinetics on the thermal conductivity of nanoscale colloidal solutions (nanofluid)', *Nano Letters*, 6(7), pp. 1529–1534.

Que, Q., Zhang, J. and Zhang, Z. (1997) 'Synthesis, structure and lubricating properties of dialkyldithiophosphate-modified Mo-S compound nanoclusters', *Wear*, 208, pp. 8–12.

Ramires, M. L. V., Castro, C. A. N. de, Nagasaka, Y., Nagashima, A., Assael, M. J. and Wakeham, W. A. (1995) 'Standard references data for thermal conductivity of water', *Journal of Physical and Chemical Reference Data*, pp. 1377–1381.

Rea, U., McKrell, M., Hu, L. W. and Buongiorno, J. (2009) 'Laminar convective heat transfer and viscous pressure loss of alumina-water and zirconia-water nanofluids.', *International Journal of Heat and Mass Transfer*, 52, pp. 2042–8.

Roetzel, W., Prinzen, S. and Xuan, Y. (1990) 'Measurement of thermal diffusivity using temperature oscillations Thermal conductivity', *New York and London: Plenum Press*, 21, pp. 201–208.

de Rooij, R., Potanin, A. A., van den Ende, D. and Mellema, J. (1993) 'Steady shear viscosity of weakly aggregating polystyrene latex dispersions', *The Journal of Chemical Physics*, 99(11), p. 9213.

Russel, W. B., Saville, D. A. and Schowalter, W. R. (1989) *Colloidal dispersions*. Cambridge University Press, New York.

Saterlie, M. S., Sahin, H., Kavlicoglu, B., Liu, Y. and Graeve, O. (2012) 'Surfactant effects on dispersion characteristics of copper-based nanofluids : A dynamic light scattering study', *Chemistry of Materials*, 24, pp. 3299–3306.

Schmidt, A. J., Alper, J. D., Chiesa, M., Chen, G., Das, S. K. and Hamad-Schifferli, K. (2008) 'Probing the gold nanorod-ligand-solvent interface by plasmonic absorption and thermal decay', *Journal of Physical Chemistry C*, 112(35), pp. 13320–13323.

Sheikholeslami, M., Gorji-bandpy, M., Ganji, D. D., Rana, P. and Soleimani, S. (2014) 'Computers and fluids magnetohydrodynamic free convection of Al2O3-water nanofluid considering Thermophoresis and Brownian motion effects', *Computers and Fluids*, 94, pp. 147–160.

Sherif and Mahmoud, N. S. (1966) 'Measurements of thermal conduction and surface finish by the thermal comparator', *J Appl Phys*, 37, pp. 2193–2197.

Shih, W. H., Shih, W. Y., Kim, S.-I., Liu, J. and Aksay, I. A. (1990) 'Scaling behavior of the elastic properties of colloidal gels', *Physical Review A*, 42(8), pp. 4772–4779.

Shukla, R. K. and Dhir, V. K. (2008) 'Effect of Brownian motion on thermal conductivity of nanofluid', *Journal of Heat Transfer*, 130, pp. 42406-1–13.

Sun, X. and Sakai, M. (2016) 'Numerical simulation of twophase flows in complex geometries by using the volumeoffluid/ immersedboundary method', *Chemical Engineering Science*, 139, pp. 221–240.

Sundar, L. S., Ramanathan, S., Sharma, K. V and Babu, P. S. (2007) 'Temperature dependent flow charecteristics of Al2O3 nanofluid', *International Journal of Nanotechnology and Applications*, 1(2), pp. 35–44.

Suslick, K. S., Fang, M. and Hyeon, T. (1996) 'Sonochemical synthesis of iron colloids', *Journal of the American Chemical Society*, 118(47), pp. 11960–11961.

Takabatake, K., Sun, X., Sakai, M., Pavlidis, D., Xiang, J. and Pain, C. C. (2016) 'International Journal of Heat and Mass Transfer Numerical study on a heat transfer model in a Lagrangian fluid dynamics simulation', *International Journal of Heat and Mass Transfer*, 103, pp. 635–645.

Teng, T. P., Hung, Y. H., Teng, T. C., Moa, H. E. and Hsu., H. G. (2010) 'The effect of alumina/water nanofluid particle size on thermal conductivity.', *Journal of Applied Thermal Engineering*, 30, pp. 2213–8.

Tillman, P. and Hill, J. M. (2007) 'Determination of nanolayer thickness for a nanofluid', 34, pp. 399–407.

Timofeeva, E. V., Gavrilov, A. N., McCloskey, J. M., Tolmachev, Y. V., Sprunt, S., Lopatina, L. M. and Selinger, J. V. (2007) 'Thermal conductivity and particle agglomeration in alumina nanofluids: Experiment and theory.', *Journal of Physical Review E*, 76, pp. 61703–1–16.

Tun-ping, T., Hung, Y., Teng, T., Mo, H. and Hsu, H. (2010) 'The effect of alumina/water nano fluid particle size on thermal conductivity', *Applied Thermal Engineering*, 30, pp. 2213–2218.

Tzeng, S. C., Lin, C. W. and Huang, K. D. (2005) 'Heat transfer enhancement of nanofluids in rotary blade coupling of four-wheel-drive vehicles', *Acta Mech.*, 179, pp. 11–23.

Verma, K. and Singh, R. (2016) 'Interfacial layer effect on the thermal conductivity of nanofluids', *Advanced Science, Engineering and Medicine*, 8(1), pp. 36–42.

Verma, S., Gokhale, R. and J.Burgess, D. (2009) 'A comparative study of top-down and bottom-up approaches for the preparation of micro/nanosuspensions', *International Journal of Pharmaceutics*, 380(1), pp. 216–222.

Wagener, M., Murty, B. S. and Gunther, B. (1997) 'Preparation of metal nanosuspensions by high-pressure DC sputtering on running fluids', *S. Komarnenl, J.C. Parker, H.J. Wollenberger (Eds.), Nanocrystalline and Nanocomposite Materials II, Materials Research Society, Pittsburgh, PA*, 457, pp. 149–154.

Wagner, W. and Prub, A. (2002) 'The IAPWS formulation 1995 for the thermodynamic properties of ordinary water substance for general and scientific use', *Journal of Physical and Chemical Reference Data*, 31, p. 387.

Waite, T. D., Cleaver, J. K. and Beattie, J. K. (2001) 'Aggregation kinetics and fractal structure of gamma-alumina assemblages', *Journal of Colloid and Interface Science*, 241(2), pp. 333–339.

Wang, B. X., Zhou, L. and Peng, X. F. (2003) 'A fractal model for predicting the effective thermal conductivity of liquid with suspension of nanoparticles', *International Journal of Heat and Mass Transfer*, 46(14), pp. 2665–2672.

Wang, J.-C., Lin, C.-Y. and Chen, T.-C. (2013) 'Thermal Performance of a Vapor Chamber-Based Plate of High-Power Light-Emitting Diodes Filled with Al2O3 Nanofluid', *Journal of Nanoscience and Nanotechnology*, 13(8), pp. 2871–2878.

Wang, X. J., Li, H., Li, X. F., Wang, Z. F. and Lin, F. (2011) 'Stability of TiO_2 and Al_2O_3 nanofluids', *Chinese Physics Letters*, 28(8), pp. 86601-1–4.

Wang, X. J. and Li, X. F. (2009) 'Influence of pH on nanofluids ' viscosity and thermal conductivity', *CHIN. PHYS. LETT. Vol.*, 26(5), pp. 56601-1–4.

Wang, X. ju, Zhu, D. sheng and Yang, S. (2009) 'Investigation of pH and SDBS on enhancement of thermal conductivity in nanofluids', *Chemical Physics Letters*, 470, pp. 107–111.

Wang, X., Li, X. and Yang, S. (2009) 'Influence of pH and SDBS on the stability and thermal conductivity of nanofluids', *Energy and Fuels*, 23, pp. 2684–89.

Wang, X., Xu, X. and Choi, S. U. S. (1999) 'Thermal conductivity of nanoparticle - Fluid mixture.', *Journal of Thermophysics and Heat Transfer*, 13(4), pp. 474–80.

Wang, Y., Zheng, Y., Zhang, L., Wang, Q. and Zhang, D. (2013) 'Stability of nanosuspensions in drug delivery', *Journal of Controlled Release*, 172(3), pp. 1126–1141.

Wasp, F. J. (1977) *Solid-liquid slurry pipeline transportation, Trans. Tech, Berlin*.

Wei, X., Zhu, H., Kong, T. and Wang, L. (2009) 'Synthesis and thermal conductivity of Cu_2O nanofluids',

International Journal of Heat and Mass Transfer, 52, pp. 4371–4374.

Wen, D. S. and Ding, Y. L. (2004) 'Experimental investigation into convective heat transfer of nanofluids at the entrance region under laminar flow conditions.', *International Journal of Heat and Mass Transfer*, 47(24), pp. 5181–88.

Wena, D., Linb, G., Vafaeia, S. and Zhangc, K. (2009) 'Review of nanofluids for heat transfer applications', *Particuology*, 7(2), pp. 141–150.

Wu, C., Cho, T. J., Xu, J., Lee, D., Yang, B. and Zachariah, M. R. (2010) 'Effect of nanoparticle clustering on the effective thermal conductivity of concentrated silica colloids', *Physical Review E*, 81(11406), pp. 11406-1–7.

Xie, H., Fujii, M., Zhang, X., Xie, H., Fujii, M. and Zhang, X. (2005) 'Effect of interfacial nanolayer on the effective thermal conductivity of nanoparticle-fluid mixture', *Heat and Mass Transfer*, 48(14), pp. 2926–32.

Xie, H., Gu, H., Fujii, M. and Zhang, X. (2006) 'Short hot wire technique for measuring thermal conductivity and thermal diffusivity of various materials', *Measurement Science and Technology*, 17, pp. 208–214.

Xie, H., Lee, H., Youn, W. and Choi, M. (2003) 'Nanofluids containing multiwalled carbon nanotubes and their enhanced thermal conductivities', *Journal of Applied Physics*, 94(8), pp. 4967–4971. doi: 10.1063/1.1613374.

Xie, H. Q., Wang, J. C., Xi, T. G., Liu, Y., Ai, F. and Wu, Q. R. (2002) 'Thermal conductivity enhancement of suspensions containing nanosized alumia particles', *Journal of Applied Physics*, 91(7), pp. 4568–4572.

Xie, H., Wang, J., Xi, T. and Liu, Y. (2002) 'Thermal conductivity of suspensions containing nanosized SiC particles', *International Journal of Thermophysics*, 23(2), pp. 571–580.

Xie, H., Wang, J., Xi, T., Liu, Y., Ai, F. and Wu, Q. (2002) 'Thermal conductivity enhancement of suspensions containing nanosized alumina particles', *Journal of Applied Physics*, 91(7), pp. 4568–4572.

Xu, J., Boming, U., Zou, M. and Xu, P. (2006) 'A new model for heat conduction of nanofluids based on fractal distributions of nanoparticles', *Journal of Physics D: Applied Physics*, 39, pp. 4486–4490.

Xuan, Y. and Li, Q. (2000) 'Heat transfer enhancement of nanofluids', *Int. J. Heat Fluid Flow*, 21(1), pp. 58–64.

Xuan, Y., Li, Q. and Hu, W. (2003) 'Aggregation structure and thermal conductivity of nanofluids', *AIChE Journal*, 49(4), pp. 1038–1043.

Xue, Q. and Xu, W. (2005) 'A model of thermal conductivity of nanofluids with interfacial shells', *Materials Chemistry and Physics*, 90, pp. 298–301.

Yang, C., Ma, P., Jing, F. and Tang, D. (2003) 'Excess molar volumes , viscosities , and heat capacities for the mixtures of ethylene glycol + water from 273.15 K to 353.15 K', *J. Chem. Eng. Data*, 48, pp. 836–840.

Ying, Y., Grulke, E. A., Zhang, Z. G. and Wu, G. (2006) 'Thermal and rheological properties of carbon nanotube-in-oil dispersions', *Journal of Applied Physics*, 99(114307), pp. 1–8.

Yoo, D.-H., Hong, K. S. and Yang, H.-S. (2007) 'Study of thermal conductivity of nanofluids for the application of heat transfer fluids', *Thermochimica Acta*, 455(1), pp. 66–69.

Yu, W., Choi, S. U. S. and Drobnik, J. (2007) 'Temperature and concentration dependence of effective thermal conductivities of alumina-oil based nanofluids', in *ECI Conference on Nanofluids: Fundamental and Applications*, pp. 16–20.

Yu, W., Choi, S. U. S., Yu, W. and Choi, S. U. S. (2003) 'The role of interfacial layers in the enhanced thermal conductivity of nanofluids: A renovated Maxwell model.', *Journal of Nanoparticle Research*, 5, pp. 167–71.

Yu, W., Xie, H., Chen, L. and Li, Y. (2009) 'Investigation of thermal conductivity and viscosity of ethylene glycol based ZnO nanofluid', *Thermochimica Acta*, 491, pp. 92–96.

Yu, W., Xie, H., Chen, L. and Li, Y. (2010) 'Enhancement of thermal conductivity of kerosene-based Fe3O4 nanofluids prepared via phase-transfer method', *Colloids and Surfaces A: Physicochemical and Engineering Aspects*, 355(1–3), pp. 109–113.

Yu, W., Xie, H., Li, Y. and Chen, L. (2011) 'Experimental investigation on thermal conductivity and viscosity of aluminum nitride nanofluid', *Particuology*, 9(2), pp. 187–191.

Zhang, X., Gu, H. and Fujii, M. (2006) 'Effective thermal conductivity and thermal diffusivity of nanofluids containing spherical and cylindrical nanoparticles.', *Journal of Applied Physics*, 100(4), pp. 44325–5.

Zhang, X., Gu, H. and Fujii, M. (2007) 'Effective thermal conductivity and thermal diffusivity of nanofluids containing spherical and cylindrical nanoparticles', *Experimental Thermal and Fluid Science*, 31, pp. 593–599.

Zhang, Z. (2010) *Experimental Evaluation of Heat Transfer Characteristics of Silica Nanofluid*. Massachusetts Institute of Technology.

Zhou, D. W. (2004) 'Heat transfer enhancement of copper nanofluid with acoustic cavitation', *Int. J. Heat Mass Transfer*, 47, pp. 3109–3117.

Zhou, D. and Wu, H. (2014) 'A thermal conductivity model of nanofluids based on particle size distribution analysis', *Applied Physics Letters*, 105(8), p. 83117.

Zhu, D., Li, X., Wang, N., Wang, X., Gao, J. and Li, H. (2009) 'Dispersion behavior and thermal conductivity characteristics of Al2O3-H2O nanofluids', *Current Applied Physics*, 9(1), pp. 131–139.

Zhu, D., Li, X., Wang, N., Wang, X., Gao, J. and Li, H. (2009) 'Dispersion behavior and thermal conductivity characteristics of Al2O3–H2O nanofluids.', *Current Applied Physics*, 9, pp. 131–139.

Zhu, H. T., Zhang, C. Y., Tang, Y. M. and Wang, J. X. (2007) 'Novel Synthesis and Thermal Conductivity of CuO Nanofluid', *The Journal of Physical Chemistry C*, 111(4), pp. 1646–1650.

Appendix A

Theoretical thermal conductivity calculations and comparison with experimental thermal conductivity for Al_2O_3-H_2O nanofluid (at optimized pH = 7.95)

S. No.	pH	Particle size (nm)	Elapsed Time (h)	*Rg* (nm)	Thermal Conductivity enhancement in base fluid (k_{fl})	Thermal Conductivity enhancement due to dead end partoicles (k_{dp})	Thermal Conductivity enhancement due to dead end and backbone particles (k_{adb})	Effective Thermal Conductivity enhancement in nanofluid (Δk_{eff})	Experimental Thermal Conductivity (Δk_{exp})	Base fluid thermal conductivity at 25 °C degree (k_l)	$\Delta k_{eff}/k_l$ (thermal conductivity gain)	$(\Delta k_{exp}-\Delta k_{eff})/\Delta k_{exp}$	% age error
1	7.95	52.97	1	53.23	0.6060	0.6077	1.2822	0.63651	0.64651	0.6060	1.0668	0.0155	3.5468
2	7.95	52.97	5	54.64	0.6060	0.6081	0.9955	0.63544	0.64844	0.6060	1.0700	0.0200	2.8048
3	7.95	52.97	10	68.45	0.6060	0.6088	0.8880	0.63295	0.64295	0.6060	1.0610	0.0156	2.5553
4	7.95	52.97	15	82.98	0.6069	0.7267	0.8352	0.63225	0.64425	0.6060	1.0631	0.0186	3.8626
5	7.95	52.97	24	145.6	0.6081	0.6829	0.7946	0.63212	0.6389	0.6060	1.0543	0.0106	4.0612
6	7.95	52.97	48	210.2	0.6086	0.7262	0.7649	0.62585	0.6358	0.6060	1.0492	0.0156	3.5650
7	7.95	52.97	72	273.3	0.6086	0.7205	0.75295	0.62105	0.6325	0.6060	1.0238	0.0181	6.810
8	7.95	52.97	96	296.4	0.6085	0.7153	0.75120	0.61625	0.62903	0.6060	1.01590	0.0203	4.03
9	7.95	52.97	120	322.5	0.6098	0.6688	0.7481	0.61299	0.62799	0.6060	1.0363	0.0239	5.3886
10	7.95	52.97	240	410.2	0.6107	0.6156	0.7438	0.60897	0.62285	0.6060	1.0278	0.0223	7.2285

Appendix B

Theoretical thermal conductivity calculations and comparison with experimental thermal conductivity for TiO_2-H_2O nanofluid (at optimized pH = 9.81)

S. No.	pH	Particle size (nm)	Elapsed Time (h)	*Rg* (nm)	Thermal Conductivity enhancement in base fluid (k_{f1})	Thermal Conductivity enhancement due to dead end partoicles (k_{dp})	Thermal Conductivity enhancement due to dead end and backbone particles (k_{adb})	Effective Thermal Conductivity enhancement in nanofluid (Δk_{eff})	Experimental Thermal Conductivity (Δk_{xp})	Thermal conductivity of base fluid (k_l)	$\Delta k_{eff}/k_l$ (thermal conductivity gain)	$(\Delta k_{exp}$-$\Delta k_{eff})/\Delta k_{exp}$	% age error
1	9.81	36.23	1	36.23	0.6061	0.6256	1.8616	0.6489	0.6634	0.6060	1.0708	0.0219	2.190
2	9.81	36.23	5	36.23	0.6062	0.6330	1.7809	0.6473	0.6613	0.6060	1.0682	0.0212	3.122
3	9.81	36.23	10	40.25	0.6065	0.6387	1.7427	0.6456	0.6593	0.6060	1.0653	0.0058	5.576
4	9.81	36.23	15	56.37	0.6066	0.6349	1.7055	0.6431	0.6574	0.6060	1.0612	0.0067	4.670
5	9.81	36.23	24	65.34	0.6067	0.6368	1.6893	0.6391	0.6563	0.6060	1.0530	0.0128	3.275
6	9.81	36.23	48	72.23	0.6068	0.6445	1.6765	0.6375	0.6538	0.6060	1.0520	0.0097	4.974
7	9.81	36.23	72	136.23	0.6070	0.6454	1.6373	0.6356	0.6542	0.6060	1.0488	0.0284	3.841
8	9.81	36.23	96	164.56	0.6070	0.6471	1.6212	0.6316	0.6566	0.6060	1.0422	0.0308	3.080
9	9.81	36.23	120	180.12	0.6070	0.6486	1.6087	0.6313	0.6559	0.6060	1.0488	0.0270	5.697
10	9.81	36.23	240	240.34	0.6072	0.6529	1.6026	0.63031	0.6452	0.6060	1.0467	0.0176	6.758

Appendix C

Classical/ Structural Models for thermal conductivity enhancements of nanofluids

Model	Mathematical expression	Affecting parameters and mechanism of heat transfer
Yu and Choi Model (Yu *et al.*, 2003)	$\frac{\Delta k_{eff}}{k_l} = 1 + \frac{n\varphi_p A}{1-\varphi_p A}$ Where, $A = \frac{1}{3}\sum_{i=a,b,c} \frac{k_{pj} - k_l}{k_{pj} + (n-1)k_j}$	Affecting parameters: thermal conductivity of base fluid, thermal conductivity of nanoparticles, primary volume concentration of the nanoparticles and particle size around 10 nm and nanolayer thickness is assumed as 1 nm are the main contributing factors. This include the interfacial layer and the superposition principle concept of parallel and series thermal conductivity have been used. Modified Maxwell model and thermal conductivity of equivalent and individual particles are taken into account.
Xie Model (H. Q. Xie *et al.*, 2002)	$\frac{k_{nf} - k_f}{k_l} = 3\Theta\,\varphi_T + \frac{3\Theta^2\varphi_T^2}{1-\Theta\Phi_T}$ Where, Θ, B_{lf}, B_{pl}, B_{fl}, K_l, Φ and M are defined by: $\Theta = \frac{B_{lf}\left[(1+\Upsilon)^3 - \frac{B_{pl}}{B_{fl}}\right]}{(1+\Upsilon)^3 + 2B_{pl}B_{lf}}$; $B_{pl} = \frac{k_p - kl}{K_p + 2K_l}$; $B_{fl} = \frac{k_f - k_l}{k_f + 2k_l}$; $B_{lf} = \frac{k_l - k_f}{k_l + 2k_f}$ $K_l = \frac{K_f M^2}{(M-\Upsilon)\ln(1+M) + \Upsilon M}$; $\phi_r = \varphi(1+\Upsilon)^3$: $\Upsilon = \frac{\delta}{r_p}$; $M = \alpha(1+\Upsilon) - 1$	Main affecting parameters are: thermal conductivity of base fluid, thermal conductivity of nanoparticles, primary volume concentration of the nanoparticles and particle size. Model takes into account the thermal conductivity of nanofluids by taking into account the effect of interfacial nano-layer at the solid–liquid interface, where the thermal conductivity distribution is assumed to be linear.
Bruggeman Model (Bruggeman, 1935)	$\frac{\Delta k_{eff}}{k_l} = \frac{\left(3\varphi_p - 1\right)\frac{k_p}{k_l} + \left\{3\left(1-\varphi_p\right) - 1\right\} + \sqrt{A}}{4}$ $A = \left[\left(3\varphi_p - 1\right)\frac{k_p}{k_l} + \left\{3\left(1-\varphi_p\right) - 1\right\}\right]^2 + 8\frac{k_p}{k_l}$	Contributing factors: thermal conductivity of base fluid, thermal conductivity of nanoparticles, primary volume concentration of the nanoparticles and particle size and room temperature. This model has been defined for the binary mixture of homogeneous and random distributed nanoparticles. Individual nanoparticle's parameters are used to study the rise in thermal conductivity of nanofluids.

Jeffery Model (Jeffery, 1973)	$\frac{\Delta k_{eff}}{k_l} = 1 + 3\eta\varphi_{\mathrm{p}} + \varphi_p^2\left(3\eta^2 + \frac{3\eta^2}{4} + \frac{9\eta^3\,(K+2)}{16\,(2K+3)}\right) + \cdots$ Where, $K = \frac{k_p}{k_l}$, $\eta = \frac{k-1}{k+2}$	Parameters: volume concentration of nanoparticles, base fluid thermal conductivity and thermal conductivity of nanoparticles. This model addresses the conduction through a solution of stationary spheres of nanoparticles, where high order terms of model represent pair interactions of randomly dispersed spherical particles.
Maxwell Garnet (M-G) Model (Maxwell, 1873)	$\frac{\Delta k_{eff}}{k_l} = \left\{\frac{\left[\left(k_p + 2k_l\right) + 2\varphi_p\left(k_p - k_l\right)\right]}{\left[\left(k_p + 2k_l\right) - \varphi_p\left(k_p - k_l\right)\right]}\right\}$	Parameters: volume concentration of nanoparticles, thermal conductivity of base fluid and thermal conductivity of nanoparticles. This model is based on the effective mean theory (EMT) and particles interaction is not taken into account. This assume the particles are uniformly and individually distributed in the base fluids.
Hamilton Crosser Model (Hamilton and Crosser, 1962)	$\frac{\Delta k_{eff}}{k_l} = \frac{k_p + (n-1)k_l + (n-1)\varphi_{\mathrm{p}}(k_p - k_l)}{k_p + (n-1)k_l - \varphi_{\mathrm{p}}(k_p - k_l)}$	A fundamental and a primary model applicable for spherical and cylindrical particles with uniform distribution, where the shape factor has been used. The volume concentration of nanoparticles, thermal conductivity of base fluid and thermal conductivity of nanoparticles are the main contributing factors.
Xuan *et al*. (2003) Model	$\frac{\Delta k_{eff}}{k_l} = \frac{k_p + 2k_l + 2\varphi_{\mathrm{p}}(k_p - k_l)}{k_p + 2k_l - \varphi_{\mathrm{p}}(k_p - k_l)}$	Assumed the shape factor is unity and valid for other geometries other than the spherical particles. Primary effecting parameters are the same i.e. volume concentration of nanoparticles, thermal conductivity of base fluid and thermal conductivity of nanoparticles.
Pak and Cho (1998) Model	$\frac{\Delta k_{eff}}{k_l} = 1 + 7.47\varphi_{\mathrm{p}}$	This model is quite simple and based on assumption that the dispersion of suspended nanoparticles causes the enhancement of thermal conductivity and primary volume concentration of the nanoparticles is responsible for the rise in the thermal conductivity of nanofluids. Nothing is mentioned about the aggregation kinetics. Only the volume concentration of nanoparticles has been considered to effect the rise in thermal conductivity of alumina-water based nanofluids.

Prasher *et al.* (2006) Model	$\frac{\Delta k_{eff}}{k_l} = \varphi_p \frac{k_p}{k_l} + (1 - \varphi_{\mathrm{p}})$	Inclusion of combined base fluids and nanoparticle thermal conductivities. Volume concentration of nanoparticles, thermal conductivity of base fluid and thermal conductivity of nanoparticles are the main contributing factors.
Li and Peterson (2006) Model	$\frac{\Delta k_{eff}}{k_l} = 1 + 0.76448\varphi_{\mathrm{p}} + 0.01868867T - 0.46214175$	Temperature and primary volume concentration of nanoparticle dependent model. Assumes no aggregation of nanoparticle.
Timofeeva *et al.* (2007) Model	$\frac{\Delta k_{eff}}{k_l} = 1 + 3\varphi_{\mathrm{p}}$	Based on EMT for Al_2O_3 nanofluids with the effect of agglomeration.
Teng *et al.* (2010) Model	$\frac{K_{nf}}{k_l} = C_0 + C_1(100\omega) + C_2(T - 273.15) + C_3 d_p + c_4(100\omega)^2 + C_5(T - 273.15)^2 + C_6 d_p^2 + C_7 + C_8(T - 273.15)^3$ Where: $C_0 = 0.991$, $C_1 = 0.253$, $C_2 = -0.001$, $C_3 = -0.002$, $C_4 = -0.189$, $C_5 = 6.19\times 10^{-5}$, $C_6 = 1.317\times 10^{-5}$, $C_7 = 0.049$, $C_8 = -7.66\times 10^{-7}$.	This empirical model was developed by considering the effect of temperature, nanoparticles size and weight fraction on thermal conductivity ratio of Al_2O_3–water nanofluids. The experiments were performed with 20, 50 and 100 nm size of nanoparticles in the temperature range of 10–50°C with volume fraction up to 2% by volume.
Developed Models (current investigation)	$\frac{\Delta k_{eff}}{k_l} = \left\{\frac{[(k_{adb} + 2k_l) + 2\varphi_{\mathrm{at}}(k_{adb} - k_l)]}{[(k_{adb} + 2k_l) - \varphi_{\mathrm{at}}(k_{adb} - k_l)]}\right\}$ (Eq. 6.26, Chapter 6) $\frac{\Delta K_{overall}}{K_f} = \left\{\frac{[(k_{adb} + 2k_l) + 2\varphi_{\mathrm{at}}(k_{adb} - k_l)]}{[(k_{adb} + 2k_l) - \varphi_{\mathrm{at}}(k_{adb} - k_l)]}\right\} \left(1 + A\ {R_{eB}}^m\ {P_r}^{0.333}\varphi_{\mathrm{at}}\right)$ (Eq. 6.33, Chapter 6)	This model predicts the thermal conductivity rise on the basis of following parameters (i) instantaneous volume concentration of nanoparticles and their cluster formation tendency in the solution at a particular time (ii) takes into account the thermal conductivity of the liquid present inside the cluster (iii) takes into account the instantaneous thermal conductivity of the nanoclusters rather than the particle thermal conductivity. Where, k_{eff} is the overall or effective thermal conductivity of the nanofluid sample and $\varphi_{at} = \varphi_p / \varphi_a$ is the volume fraction of the aggregates in a given sample of a nanofluid.